

UC Irvine

UC Irvine Electronic Theses and Dissertations

Title

Modulation of LEF/TCFs and Wnt Signaling in Colon Cancer

Permalink

<https://escholarship.org/uc/item/6391x60p>

Author

Tanio, Stephanie Sprowl

Publication Date

2016

Peer reviewed|Thesis/dissertation

UNIVERSITY OF CALIFORNIA,
IRVINE

Modulation of LEF/TCFs and Wnt Signaling in Colon Cancer

DISSERTATION

submitted in partial satisfaction of the requirements
for the degree of

DOCTOR OF PHILOSOPHY

in Biomedical Sciences

by

Stephanie Sprowl Tanio

Dissertation Committee:
Professor Marian L. Waterman, Chair
Professor Emiliana Borrelli
Professor Manuela Raffatellu

2016

© 2016 Stephanie Sprowl Tanio

DEDICATION

This dissertation is dedicated to

my husband,
Christopher Tanio

and

my sister,
Sara Sprowl

in recognition of their constant love, support and encouragement.

TABLE OF CONTENTS

	Page
LIST OF FIGURES	v
ACKNOWLEDGEMENTS	viii
CURRICULUM VITAE.....	x
ABSTRACT OF THE DISSERTATION	xiv
CHAPTER 1: Introduction	
Wnt Signaling	1
LEF/TCF Structure	6
LEF/TCFs and Wnt in the Intestine	9
Wnt Signaling in Colon Cancer	11
Cancer and Metabolism	17
Chapter Guide	19
CHAPTER 2: Wnt Signaling Directs a Metabolic Program of Glycolysis and Angiogenesis in Colon Cancer	
Introduction.....	20
Results	
Blocking Wnt alters the expression of metabolism-linked genes	21
dnLEF-1 and dnTCF-1mut do not alter the cell cycle or proliferation <i>in vitro</i>	23
Blocking Wnt alters the metabolic program of colon cancer cells	24
Blocking Wnt reduces PDK1 levels via regulation of transcription.....	34
PDK1 overexpression rescues the altered metabolic phenotype induced by blocking Wnt.....	39
Blocking Wnt reduces <i>in vivo</i> tumor growth	47
Blocking Wnt reduces tumor vessel density, while reintroduction of PDK1 restores it.....	51
Discussion.....	54
CHAPTER 3: Lactate Transporter MCT-1 is a Wnt Target Gene and Confers Sensitivity to 3-bromopyruvate in Colon Cancer	
Introduction.....	62
Results	
MCT-1 is regulated by Wnt signaling	66
MCT-1 is a direct target of Wnt signaling	71
Wnt signaling inhibition increases colon cancer cell resistance to	

3-bromopyruvate.....	79
Discussion.....	85
CHAPTER 4: A uniform human Wnt expression library reveals a shared secretory pathway and unique signaling activities	
Introduction.....	89
Results	
Human Wnt cloning.....	91
Wnt ligand production and secretion profile	92
Wnt activation of the β -catenin-dependent pathway	97
Wnt-dependent phosphorylation of LRP6 and stabilization of β -catenin.....	105
Analysis of the core Wnt modification and secretion pathway	107
Discussion.....	112
CHAPTER 5: Discussion	
Functions of LEF/TCFs and Wnts in Colon Cancer.....	118
Considerations for Clinical Therapeutics of Colon Cancer	133
REFERENCES	144
APPENDIX A: Predicting mechanism of biphasic growth factor action on tumor growth using a multi-species model with feedback control	158
APPENDIX B: Materials and Methods	182

LIST OF FIGURES

	Page
Figure 1.1. Schematic representation of the β -catenin dependent Wnt signaling pathway	3
Figure 1.2 β -catenin-dependent and β -catenin-independent Wnt signaling pathways	5
Figure 1.3. Schematic representation of the LEF/TCF family of transcription factors	7
Figure 1.4. TCF-1 localization in normal colon and colon cancer	10
Figure 1.5. Common mutations of the Wnt signaling pathway in colon cancer.....	13
Figure 2.1. Blocking Wnt alters the expression of metabolism-linked genes	22
Figure 2.2. dnLEF-1 and dnTCF-1mut do not alter the cell cycle or proliferation <i>in vitro</i>	25
Figure 2.3. Blocking Wnt alters the metabolic program of SW480 and DLD-1 colon cancer cells	28
Figure 2.4. Blocking Wnt alters the metabolic program of SW620, LS174T, HCT116 and HT-29 colon cancer cells	29
Figure 2.5. Fluorescence lifetime analysis of NADH reveals shifts in glycolysis upon expression of dnLEF/TCF.....	32
Figure 2.6. FLIM analysis of colon cancer cell cultures.....	35
Figure 2.7. Blocking Wnt directly reduces PDK1 levels via regulation of transcription	37
Figure 2.8. <i>PDK1</i> transcription is directly regulated by LEF/TCFs and Wnt signaling.....	40
Figure 2.9. PDK1 overexpression rescues the altered metabolic phenotype induced by blocking Wnt.....	42
Figure 2.10. PDK1 overexpression rescues the altered metabolic phenotype induced by blocking dnLEF-1	45
Figure 2.11. Blocking Wnt reduces <i>in vivo</i> tumor growth.....	48
Figure 2.12. Fluorescence Lifetime Imaging (FLIM) of live xenograft tumors	50
Figure 2.13. Blocking Wnt alters the metabolic program of colon cancer cells <i>in vivo</i>	52

Figure 2.14.	Blocking Wnt reduces tumor vessel density, while reintroduction of PDK1 restores it.....	53
Figure 2.15.	β -catenin-dependent Wnt signaling is not coupled to mTORC2 activity.....	56
Figure 2.16.	TCF-4 occupies the <i>PDK</i> and <i>MCT1</i> promoters	59
Figure 3.1.	Blocking Wnt with dnLEF-1 reduces MCT-1 but not MCT-4 levels.....	67
Figure 3.2.	Wnt signaling levels and expression of MCT-1 in colon cancer cell lines.....	70
Figure 3.3.	Wnt directly targets the MCT-1/ <i>SLC16A1</i> promoter for regulation.....	72
Figure 3.4.	<i>SLC16A1</i> transcription is directly regulated by LEF/TCFs and Wnt signaling.....	74
Figure 3.5.	Identification of a Wnt responsive region in the <i>SLC16A1</i> promoter region	77
Figure 3.6.	XAV939 affects colon cancer cell sensitivity to 3-bromopyruvate	81
Figure 3.7.	XAV939 promotes colon cancer cell recovery from 3-bromopyruvate	83
Figure 4.1.	Wnt cloning scheme using WNT1 as an example.....	93
Figure 4.2.	Analysis of FLAG-tagged Wnts.....	94
Figure 4.3.	V5-tagged Wnt expression.....	96
Figure 4.4.	WNT mRNA levels in HEK293 cells.....	98
Figure 4.5.	Wnt activation of the β -catenin-dependent pathway	100
Figure 4.6.	Wnt activation of the β -catenin-dependent pathway	103
Figure 4.7.	Wnt-dependent phosphorylation of LRP6 and stabilization of β -catenin.....	106
Figure 4.8.	Wnts require PORCN for activity	109
Figure 4.9.	All tested Wnts bind WLS in a PORCN-dependent manner	110
Figure 4.10.	Wnt signaling requires WLS	111
Figure 5.1.	Wnt signaling promotes aerobic glycolysis through PDK1 and MCT-1	120
Figure 5.2.	MCT-1 and MCT-4 expression in colon adenocarcinoma samples.....	122
Figure 5.3.	Wnt signaling promotes aerobic glycolysis through PDK1	125

Figure 5.4.	Bioinformatic analysis of Wnt and glycolysis gene signatures.....	126
Figure 5.5.	PDK1 staining in xenograft tumors.....	130
Figure 5.6.	WNT1 and WNT5A induce TCF-1 export in SW480 cells.....	134
Figure 5.7.	WNT1, 2, and WNT5A induce TCF-1 export in RKO cells.....	135
Figure 5.8.	The role of endocytosis in TCF-1 export.....	138
Figure 5.9.	Wnt signaling influences cancer metabolism through regulation of <i>SLC16A1</i> / MCT-1.....	139
Figure A1.	A multispecies model of tumor signaling.....	170
Figure A2.	Dose response curve of original system.....	171
Figure A3.	Dose response curve of quasi-steady state system.....	172
Figure A4.	Dynamics of stem cell, terminal cell, W and T concentrations in the original model for linear and cubic g and at $H = 10$	173
Figure A5.	Dynamics of stem cell, terminal cell, W and T concentrations in the original model for linear and cubic g and at concentrations of $H = 0$, $H = 20$, and $H = 100$	174
Figure A6.	Phase planes of stem and terminal cell dynamics for the quasi-steady state system at $H = 0$, $H = 20$, with linear cubic $g(H)$, and $H = 100$, with linear cubic $g(H)$...175	
Figure A7.	Stem cell fraction at $t = 9$ and $20 \leq H \leq 100$ for the quasi-steady state system at linear and cubic $g(H)$	176
Figure A8.	Example of a linear dose-response curve.....	177
Figure A9.	Examples of non-linear dose-response curves.....	178
Figure A10.	Summary of parameter values for Eqs. (1)-(7).....	179

ACKNOWLEDGEMENTS

I am overwhelmed with gratitude for those around me, both in academia and in my personal life, who have supported me in the pursuit of my graduate studies. I came across one of my favorite quotes at the beginning of graduate school; on the home page of the Google Scholar website it states, “We stand on the shoulders of giants”. While this largely applies to building upon previous discoveries to continue exploration of scientific unknowns, I also envision being hoisted onto the shoulders of those that love and support me in order to reach for and achieve my dreams. I have a wonderful support system that I believe has enabled my success. Words cannot express how thankful I am for the amazing support from both my husband, Chris, and my sister, Sara. You both mean the world to me, and earning this doctorate is as much your celebration as it is mine. I am also so thankful for all of the support from my parents, Walter, Wendy, and Kellie. To my grandparents, Artie, Kathy, Ann, and Ron, and to my Aunt Diane I thank for always looking out for me and being my biggest fans; Maine has never felt far away with all the encouragement you send my way.

I am indebted to Dr. Marian Waterman, and truly grateful for all of the hours (so, so many hours) spent with me- not only as a mentor, but even as a life coach and counselor- she is a prime example of “doing it all, and doing it well”. While I haven’t actually seen it, I am certain Marian wears a super hero cape under her clothes. She is an exemplary scientist and human being; kind, and professional to a fault. I am fortunate she chose me to conduct my graduate studies in her lab, and all of the whole milk lattes in the world aren’t enough to express my thanks.

I would also like to thank all of the members of the Waterman lab I have had the privilege to work with over the years. The Waterman lab has a reputation for being tight-knit; I enjoyed spending time with my colleagues outside the lab as well, beyond the bench, where I made lasting friendships. In particular I would like to thank Drs. Kira Pate, Becky Tsai, Beibei Wu, Rani Najdi, Noriko Yokoyama and Nate Hoverter, as well as Amber Habowski and George Chen. Each one of these individuals is unique, special, and has mentored me in the lab to some capacity. To members of the Donovan lab, I thank for the scientific assistance I have received in lab meetings and over coffee. I especially thank Dr. Peter Donovan and Dr. Stanbridge for going above and beyond to advise me on my project and to promote and engage me toward better scientific understanding. To other members of the Department of Microbiology and Molecular Genetics (MMG), I thank for their assistance with various techniques and providing reagents. To the MMG staff, especially Mike Vo and Janet Horwitz, I thank for all their help and support- administrative and otherwise.

I especially would like to thank my collaborators. I have engaged in many wonderful collaborations over the years with individuals from a variety of scientific fields and backgrounds. For the metabolism and Wnt projects: To Dr. Robert Edwards and Dr. Kehui Wang, thank you for the help with all of the mice work for both the xenograft experiments, FLIM analysis of the mouse xenograft tumors, and also Immunohistochemical staining of tumor samples. Thank you to Enrico Gratton and Dr. Chiara Stringari from the Laboratory for Fluorescent Dynamics for their contribution to the project through all of the FLIM experiments. To Dr. Anand Ganesan and Rolando Ruiz I thank for their assistance with techniques and for generously sharing their

shRNA library. For the Wnt Open Source project: thank you to Dr. David Virshup, Dr. Kyle Proffitt, and other members of the Virshup lab for their contribution to the project on all Wnt secretion experiments, as well as their expertise on Wnt ligands. For the Mathematical Modeling Project: I am grateful to Dr. John Lowengrub and Dr. Anna Konstorum for their mathematical expertise, and passion and desire for math-biology collaboration. It's been eye-opening and exciting to see what cross-discipline collaboration allows us to explore and accomplish.

I lastly want to thank the members of my dissertation committee, Dr. Marian Waterman, Dr. Manuela Raffatellu and Dr. Emiliana Borrelli for all of their encouragement, critical advice, and suggestions for my project. It has been an honor to work with such passionate, successful scientists, and I have learned a great deal through all of our interactions.

Curriculum Vitae

STEPHANIE SPROWL TANIO

EDUCATION

University of California, Irvine (UCI) 2009 - 2016
Doctor of Philosophy, Microbiology and Molecular Genetics

California State University, Fullerton (CSUF) 2003 - 2009
Bachelor of Science, Biological Science Minor, Chemistry

RESEARCH EXPERIENCE

Graduate Student Researcher, UC Irvine, Irvine CA 2010 - Present
Advisor: Marian L. Waterman, Ph.D., Department of Microbiology and Molecular Genetics

Undergraduate Student Researcher, Cal State Fullerton, Fullerton CA 2005 - 2009
Advisor: Chandra Srinivasan, Ph.D., Department of Chemistry and Biochemistry

- **NSF-REU Summer Researcher**, Cal State Fullerton, Fullerton CA 2006

Summer Research Intern, Stanford University School of Medicine 2007 - 2008
and VA Palo Alto Health Care System, Palo Alto, CA
Advisor: Ting-Ting Huang, Ph.D., Department of Neurology and Neurological Sciences

Undergraduate Education Researcher, Cal State Fullerton, Fullerton CA 2007 - 2008
Advisor: Barbara Gonzalez, Ph.D., Department of Chemistry and Biochemistry

PUBLICATIONS

Stephanie Sprowl-Tanio, Kira T. Pate, Marian L. Waterman. *Submitted*
Lactate Transporter MCT-1 is a direct Wnt target gene and confers sensitivity to 3-bromopyruvate in colon cancer

Kira T. Pate, Chiara Stringari, **Stephanie Sprowl-Tanio**, Kehui Wang, Tara TeSlaa, 2014
Nate Hoverter, Miriam McQuade, Chad Garner, Michael Teitell, Robert A. Edwards,
Enrico Gratton, Marian L. Waterman. **Wnt Signaling Directs a Metabolic Program of Glycolysis and Angiogenesis in Colon Cancer** EMBO. 33(13):1454-73

- Anna Konstorum, **Stephanie Sprowl**, Marian L. Waterman, Arthur D. Lander, and John Lowengrub. **Predicting mechanism of biphasic growth factor action on tumor growth using a multi-species model with feedback control.** J. Coupled Syst. Multiscale Dyn. 1(4):459-467 2013
- Stephanie Sprowl** and Marian L. Waterman. **Past visits present: TCF/LEFs partner with ATFs for β -catenin-independent activity.** PLOS Genet. 9(8):e1003745 2013
- Rani Najdi, Kyle Proffitt, **Stephanie Sprowl**, Simran Kaur, Jia Yu, Tracey M. Covey, David M. Virshup, and Marian L. Waterman. **A uniform human Wnt expression library reveals a shared secretory pathway and unique signaling activities.** Differentiation 84:203-213 2012
- Noriko N. Yokoyama, Kira T. Pate, **Stephanie Sprowl**, and Marian L. Waterman. **A role for YY1 in the repression of dominant negative LEF-1 in colon cancer.** Nucl. Acids Res. 38(19):6375-6388 2010

TEACHING EXPERIENCE

- Laboratory Instructor-** Applied Human Anatomy (Bio Sci D170), UC Irvine, Irvine CA 2014
- Teaching Assistant-** Biology and Chemistry of Cooking (Bio Sci 9B), UC Irvine, Irvine CA 2014
- Teaching Assistant-** Stem Cell Biology (Bio Sci D121), UC Irvine, Irvine CA 2011
- Discussion Instructor-** DNA to Organisms (Bio Sci 93), UC Irvine, Irvine CA 2010
- Laboratory Instructor-** Survey of Chemistry Lab (Chem 100), Cal State Fullerton, Fullerton CA 2008
- Laboratory Instructor-** General Chemistry Lab (Chem 120A), Cal State Fullerton, Fullerton CA 2008
- Laboratory Instructor-** Chemistry for Nursing and Allied Professionals Lab (Chem 200), Cal State Fullerton, Fullerton CA 2007

RELATED TEACHING EXPERIENCE

- Guest Lecturer-** Cell and Molecular Biology (Biol G180) Golden West College, Huntington Beach CA 2016
- Guest Lecturer-** Applied Human Anatomy (Bio Sci D170), UC Irvine, Irvine CA 2014
- Guest Lecturer-** Biology and Chemistry of Cooking (Bio Sci 9B), UC Irvine, Irvine CA 2014

LEADERSHIP EXPERIENCE

Graduate Student Program Leader , UCI Cancer Research Institute Youth Fellows Mentorship Program, UC Irvine, Irvine CA	2011 - 2015
Graduate Student Representative , Microbiology and Molecular Genetics, UC Irvine, Irvine CA	2013 - 2014
Student Seminar Committee Leader , UC Irvine, Irvine CA	2012
Associated Students (ASI) Board Director , Cal State Fullerton, Fullerton CA Representing the College of Natural Sciences and Mathematics	2005 - 2007
Treasurer, Flying Samaritans International, CSUF-UCR Clinic , Cal State Fullerton, Fullerton CA	2006 - 2007
Treasurer, Chemistry and Biochemistry Club , Cal State Fullerton, Fullerton CA	2006

SCIENTIFIC PRESENTATIONS

Poster Presentation , Cancer Research Institute May Symposium, UC Irvine Role of Wnt Signaling in Colon Cancer Cell Metabolism <i>Runner-Up for Best Poster Presentation</i>	2016
Poster Presentation , Experimental Biology Conference, San Diego CA Role of Wnt Signaling in Colon Cancer Cell Metabolism	2016
Oral Presentation , Cancer Biology Journal Club, UC Irvine, Irvine CA Role of Wnt Signaling in Colon Cancer Cell Metabolism- Focus on Monocarboxylate Transporter MCT-1	2016
Oral Presentations , Microbiology and Molecular Genetics, UC Irvine, Irvine CA	
• HGF/c-Met Crosstalk to Wnt Signaling in Colon Cancer Metabolism and Wnt Signaling in Colon Cancer	2015 2014
• Tumor Microenvironment Crosstalk to Wnt Signaling in Colon Cancer	2013
• Tumor Microenvironment Crosstalk to Wnt Signaling in Colon Cancer	2012
Poster Presentation , Wnt Meeting, Egmond aan Zee, Netherlands Crosstalk Interactions Between HGF/SF-MET and Wnt Signaling in Colon Cancer Cells	2012
Poster Presentation , Wnt Meeting, Los Angeles Negative Crosstalk Interactions Between the Tumor Microenvironment and Wnt Signaling in Colon Cancer	2011
Poster Presentation , Experimental Biology Conference, San Diego CA	2008

- The Effect of SOD-1 Deficiency and Manganese Supplementation on Oxidative Stress Resistance in *Caenorhabditis elegans*
- Poster Presentation**, CSU Biotechnology Symposium (CSUPERB), Oakland, CA 2008
The Effect of SOD-1 Deficiency and Manganese Supplementation on Oxidative Stress Resistance in *Caenorhabditis elegans*
- Poster Presentation**, Experimental Biology Conference, Washington D.C. 2007
Using Gel Electrophoresis Methodology for the Measurement of Superoxide Dismutase Enzyme Activity in *Caenorhabditis elegans*
- Poster Presentation**, CSU Biotechnology Symposium (CSUPERB), Oakland, CA 2007
Using Gel Electrophoresis Methodology for the Measurement of Superoxide Dismutase Enzyme Activity in *Caenorhabditis elegans*
- Poster Presentation**, West Coast Biological Sciences Undergraduate Research Conference (WCBSURC), San Diego CA 2006
Methodology Development for the Measurement of Superoxide Dismutase Enzyme Activity in *Caenorhabditis elegans* Using Native Gel Electrophoresis

CERTIFICATES, AWARDS AND FELLOWSHIPS

- Certificate in Course Design**, Center for Engaged Instruction, UC Irvine, Irvine CA 2016
- UCI President's Dissertation Year Fellowship**, UC Irvine, Irvine CA 2015 - 2016
- HHMI-UCI Graduate Fellowship**, UC Irvine, Irvine CA 2010
- Crellin Pauling Student Teaching Award**, CSU Biotechnology Symposium, Los Angeles CA 2009
- Commencement Speaker**, College of Natural Sciences and Mathematics, Cal State Fullerton, Fullerton CA 2009
- Biotechnology Travel Award**, Experimental Biology Conference, Washington D.C. 2007
- Lyle Wallace Service Award**, Department of Chemistry and Biochemistry, Cal State Fullerton, Fullerton CA 2007
- Outstanding Poster Presentation Award**, West Coast Biological Sciences Undergraduate Research Conference (WCBSURC), San Diego CA 2006

ABSTRACT OF THE DISSERTATION

Modulation of LEF/TCFs and Wnt Signaling in Colon Cancer

By

Stephanie Sprowl Tanio

Doctor of Philosophy in Biomedical Sciences

University of California, Irvine, 2016

Professor Marian L. Waterman, Chair

Oncogenic Wnt signaling is implicated as the major driving force in colon cancer. Actions of misregulated Wnt signaling rely on the upregulation of Lymphoid Enhancer Factor/T-cell Factor (LEF/TCF) transcription factor-dependent Wnt target genes. In colon cancer, Wnt-activating, full-length LEF/TCFs are expressed, while their dominant negative, Wnt-suppressing counterparts (dnLEF/TCFs) are not. Therefore, full-length isoforms act unopposed, leading to overactive, inappropriate expression of target genes. We use re-expression of dnLEF/TCFs as a tool to modulate Wnt signaling in colon cancer and discover what cancer phenotypes and gene programs are contributing to the oncogenic drive to cell transformation. Using expression of dnLEF-1 and dnTCF-1, this thesis illustrates how Wnt/ β -catenin signaling directs Warburg metabolism. We identify Pyruvate dehydrogenase kinase 1 (PDK1) - a kinase that directs the conversion of pyruvate to lactate, and *SLC16A1/MCT-1* - a transporter of small metabolites such as lactate, as important direct targets within a larger gene program for metabolism. Given recent preclinical development of small molecules that target Wnt signaling and metabolism, and given interest in developing new combination therapies for cancer treatment, we tested how Wnt inhibition affects the ability of 3-bromopyruvate to kill cancer cells *in vitro*. We report that this

toxic molecule kills colon cancer cells, but that Wnt signaling inhibition lowers its efficacy. We conclude that both PDK1 and MCT-1 are part of a core Wnt gene program for glycolysis in colon cancer and that modulation of this program could play an important role in shaping sensitivity to drugs that target cancer metabolism.

Wnt ligands are secreted morphogens that control multiple developmental processes during embryogenesis and adult homeostasis. A diverse set of receptors and signals have been linked to individual Wnts, but the lack of tools for comparative analysis has limited the ability to determine which of these signals are general for the entire Wnt family, and which define subsets of differently acting ligands. We have created a versatile Gateway expression library of clones for all 19 human Wnts. An analysis comparing epitope-tagged and untagged versions of each ligand shows that despite their similar expression at the mRNA level, Wnts exhibit considerable variation in stability, processing and secretion. This comprehensive toolkit provides critical tools and new insights into human Wnt gene expression and function.

CHAPTER ONE

Introduction

Wnt Signaling

Wnt signaling is necessary for many normal cellular processes, including tissue development and homeostasis, as well as cell fate, proliferation and survival activities. While there is one Wnt signaling cascade that directs β -catenin to the nucleus for transcriptional activation of Wnt-driven gene programs, Wnt signaling is more complex in that additional pathways modulate cell phenotypes without β -catenin. In general, these two types of signals are commonly defined as canonical, or β -catenin-dependent signaling and non-canonical, or β -catenin-independent signaling. Both types of signaling are present in normal developmental and cellular processes. There are, however, several instances where both canonical and non-canonical components are used together in ways that defy traditional signal categorization^{1,2} How these signals are propagated and what Wnt receptor complex triggers them are basic unknowns in the field. Chapters 2 and 3 focus largely on the “traditional” way we currently understand the canonical Wnt signaling pathway, specifically in the disease context of colon carcinogenesis. These chapters describe the discovery that canonical Wnt signaling drives Warburg metabolism. Chapter 4 highlights the development of a Wnt ligand expression plasmid library and its use as a tool to study both canonical and non-canonical Wnt signaling pathways. The inspiration for development of the library was to make discovery and study of unconventional Wnt signaling more feasible. Finally, implications and speculation about Wnt signaling in the context of colon cancer as a whole will be discussed in Chapter 5.

In normal tissue, canonical/ β -catenin-dependent Wnt signaling regulates the fate and activities of cells through the actions of β -catenin, a nuclear-localizing mediator that can activate the transcription of Wnt target genes important in cell growth and proliferation. β -catenin activates target gene expression via direct binding to Lymphoid Enhancer Factor/ T-cell Factor (LEF/TCF) transcription factors, a family of four DNA binding proteins that upregulate specific target genes (and collectively, gene programs) that contribute to the phenotypes and functions of cells (see *LEF/TCF Structure* for additional details about these transcription factors). β -catenin levels are controlled by upstream steps in the pathway beginning with Wnt ligands interacting with a Lrp5/6:Frizzled co-receptor complex at the cell surface. Canonical/ β -catenin-dependent Wnt signaling requires the binding of a Wnt ligand to the LRP5/6 co-receptor component to promote β -catenin accumulation and downstream interaction with LEF/TCF transcription factors to promote gene activation. When Wnt ligands are absent and the co-receptor complex is unoccupied (Fig. 1.1, “OFF”), a destruction complex, comprised of the scaffold protein Axin and Adenomatous Polyposis Coli (APC), Casein Kinase 1 α (CK1 α), Glycogen Synthase Kinase 3 β (GSK3 β) and other proteins, act to phosphorylate β -catenin, promoting its ubiquitination and subsequent degradation by the proteasome¹⁻⁶. When a Wnt ligand binds to the Lrp5/6:Frizzled co-receptor complex (Fig. 1.1, “ON”), a series of signal transduction steps are triggered and the destruction complex is disrupted in its function. A disrupted destruction complex allows β -catenin to avoid complex-associated ubiquitination and degradation which therefore enables it to accumulate and translocate to the nucleus to activate the transcription of Wnt target genes³⁻⁶.

Studies in the field of Wnt signaling have been largely focused on the canonical/ β -catenin-dependent Wnt signaling pathway because it plays an important role not only in development and degenerative diseases, but also in the transformation of the normal colon

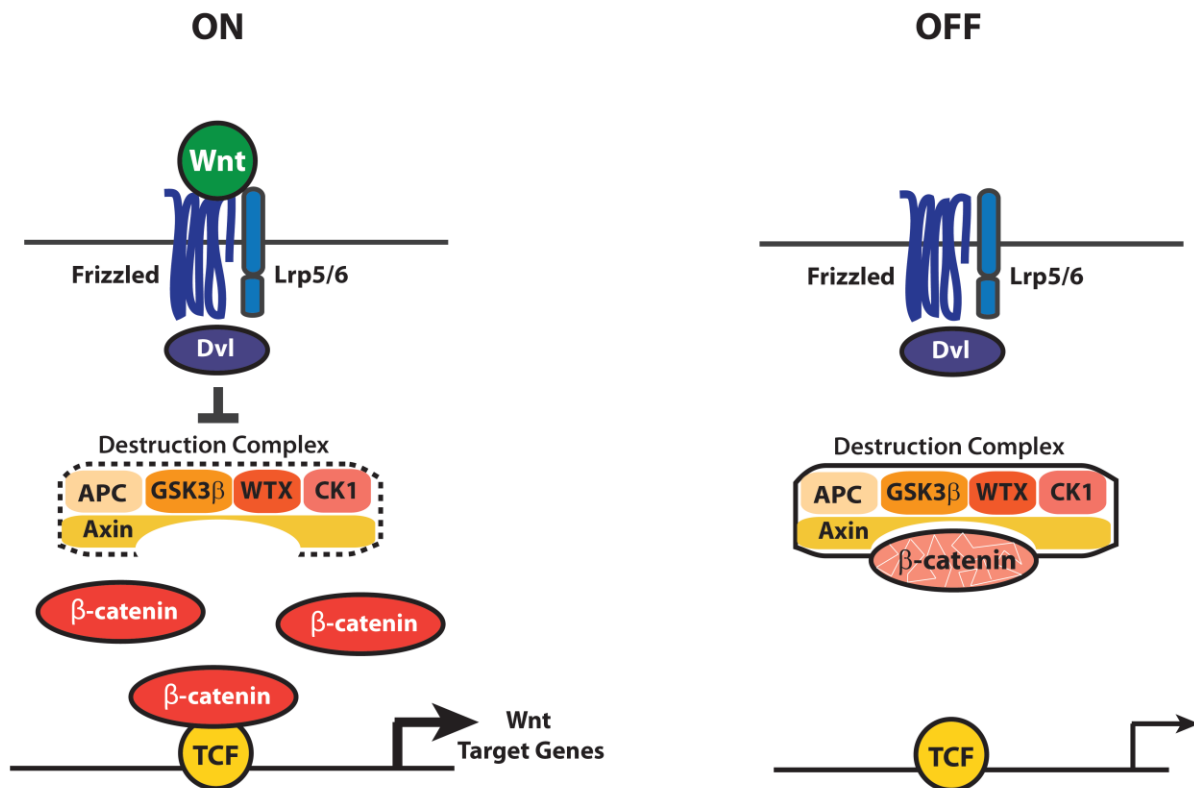


Figure 1.1. Schematic representation of the β -catenin dependent Wnt signaling pathway. In the absence of Wnt, the destruction complex, composed of several proteins including Adenomatous Polyposis Coli (APC), Glycogen Synthase Kinase 3 β (GSK3 β), Wilms tumor gene on the X chromosome (WTX), Casein Kinase 1alpha (CK1), and Axin, phosphorylate β -catenin, targeting it for degradation via the ubiquitin-proteasome pathway. In this state, LEF/TCF transcription factors are bound to Wnt target genes, but recruit transcription co-repressors, such as Groucho which keep Wnt target gene transcription in an off-mode. Upon the binding of Wnt to the Frizzled/LRP receptor, Wnt signaling is activated, resulting in the release of β -catenin from the destruction complex. This results in the accumulation of β -catenin, which translocates into the nucleus and interacts with the LEF/TCFs, displacing Groucho/repression complexes to activate Wnt target genes. (*Figure modified from Najdi, et al., 2009*⁷)

epithelium to cancer (See section *Wnt Signaling in Colon Cancer*). However, the less studied non-canonical/ β -catenin-independent Wnt signaling pathways also play an important role in cell motility, adhesion, and they have been associated with cancer cell migration and metastasis. Alternative to β -catenin-driven upregulation of Wnt target genes, non-canonical Wnt signaling regulates cell activities through activation of calcium signals and kinase cascades. These alternative pathways have previously been defined by the receptor context with which Wnt ligands bind⁸ (Figure 1.2). For example, the Planar Cell Polarity Pathway (PCP) is mediated by Frizzled (Fz) receptor and Disheveled (Dvl); Lrp 5/6 co-receptors, β -catenin, and LEF/TCFs are not involved. These types of Wnt-Frizzled interactions activate c-Jun-N-terminal kinase (JNK) and Rho-associated kinase (Rho-kinase) to govern cell polarity (hence its namesake). That Wnt ligands are involved in directing these activities is due in part to genetic experiments that specifically inactivate Wnts. For example, expression of the Wnt inhibitors secreted Frizzled-related proteins 1 and 3 (sFRP1 and sFRP3) and Wnt inhibitory factor 1 (WIF1) disrupt PCP in the neurosensory epithelium of mice⁹⁻¹¹. Which of the 19 Wnt ligands are capable of triggering PCP is not completely known, but several ligands have been linked to this pathway. For example, knockout of Wnt5A and Wnt11 in zebrafish lead specifically to defects in convergent extension¹²⁻¹⁵. Despite these kinds of evidence implicating some Wnt ligands in PCP and other β -catenin-independent activities, many experimental approaches have not used a Wnt ligand to authentically stimulate signaling from the co-receptor complex on the cell surface – meaning that we have a limited understanding of the effect of many of the individual 19 Wnt ligands. The Wnt Open Source project and expression plasmid library (discussed in Chapter 4) can be used to address these experimental unknowns.

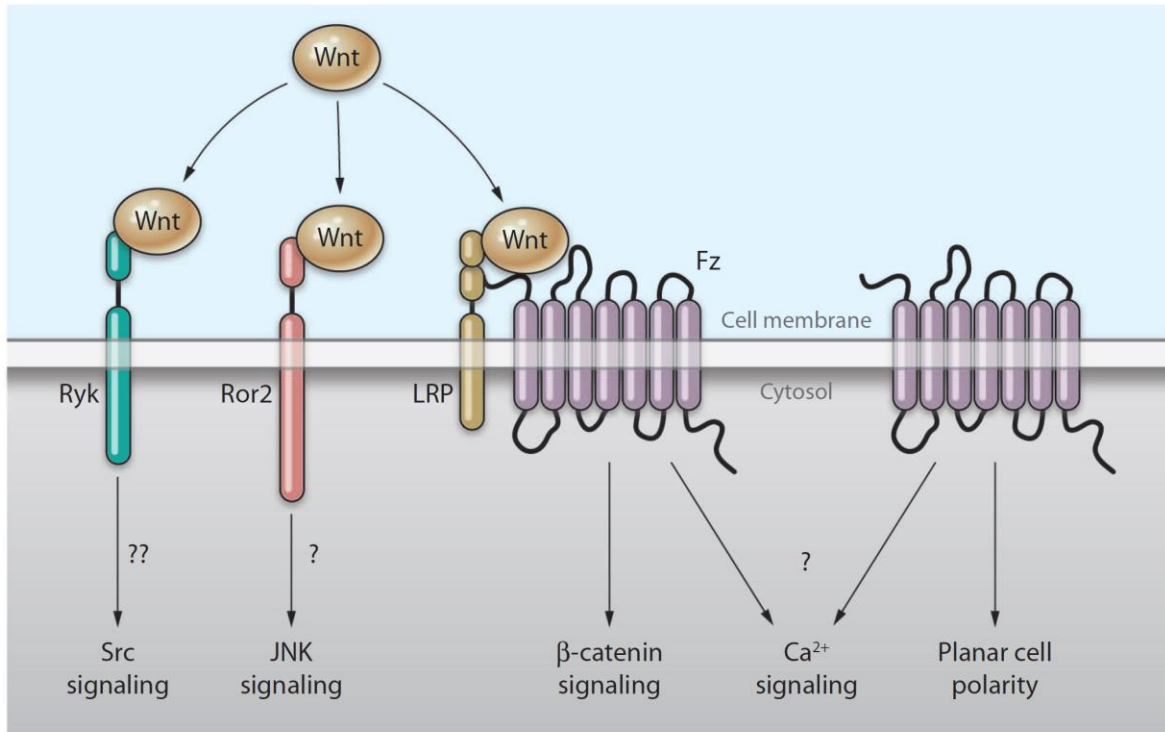


Figure 1.2. β -catenin-dependent and β -catenin-independent Wnt signaling pathways.

Wnt signaling pathway activation is determined by the receptors available on the cell surface. The β -catenin-dependent pathway is activated by Wnt ligands binding to Frizzled (Fz)/ Lipoprotein Receptor-related protein (LRP) co-receptors. Signaling through Frizzled alone results in the activation of the calcium or the Planar Cell Polarity (PCP) pathway. Signaling through receptor tyrosine kinases such as Receptor tyrosine-like kinase (RYK) and Receptor tyrosine-like Orphan Receptor 2 (Ror2) activate Sarcoma (Src) and c-Jun Terminal Kinase (JNK) signaling, respectively. (Figure adapted from van Amerongen, et al., 2008⁸)

Wnts can also bind to Frizzled to activate the Wnt/Calcium pathway, which can stimulate an increase in intracellular calcium levels which in turn activate G proteins and transcription factors like nuclear factor associated with T cells (NFAT). Alternative to the Frizzled receptor, Wnts can bind receptor tyrosine kinases such as Ryk to induce Src signaling, or bind to Ror2 to promote JNK signaling¹⁶⁻¹⁸. Wnt5A-Ryk signaling in *Drosophila* has been shown to control axon guidance and salivary gland migration (likely through Src), while Wnt-Ror2 receptor interactions result in convergence and extension movements in *Xenopus* and mouse cell lines, likely through JNK^{8,19}. Even though we know that Wnt plays a key role in these pathways, there is much to be learned about these β -catenin independent Wnt signaling actions in other translational model systems and contexts.

LEF/TCF Structure

Downstream of Wnt-ligand interaction and the destruction complex, LEF/TCF transcription factors control the transcriptional output of canonical Wnt signaling in the nucleus. The LEF/TCF family is comprised of four members: LEF-1 (*LEF1*), TCF-1 (*TCF7*), TCF-3 (*TCF7L1*) and TCF-4 (*TCF7L2*)^{20,21} (protein domain schematic, Figure 1.3). All four proteins share two highly conserved regions: a C-terminal High Mobility Group (HMG) DNA binding domain, and an N-terminal β -catenin binding domain. The HMG DNA binding domain contains a Nuclear Localization Signal (NLS) and together these two domains recognize Wnt Response Elements (WREs- characterized by the sequence YCTTTGWW^{22,23}) on Wnt target genes with relatively high affinity ($K_d \sim 1 \times 10^{-9} M$). The β -catenin binding domain on the N-terminus of LEF/TCF proteins allows for recruitment of β -catenin by WRE-bound LEF/TCFs to form complexes that can activate target genes^{4,24}. Less conserved protein domains in the LEF/TCF

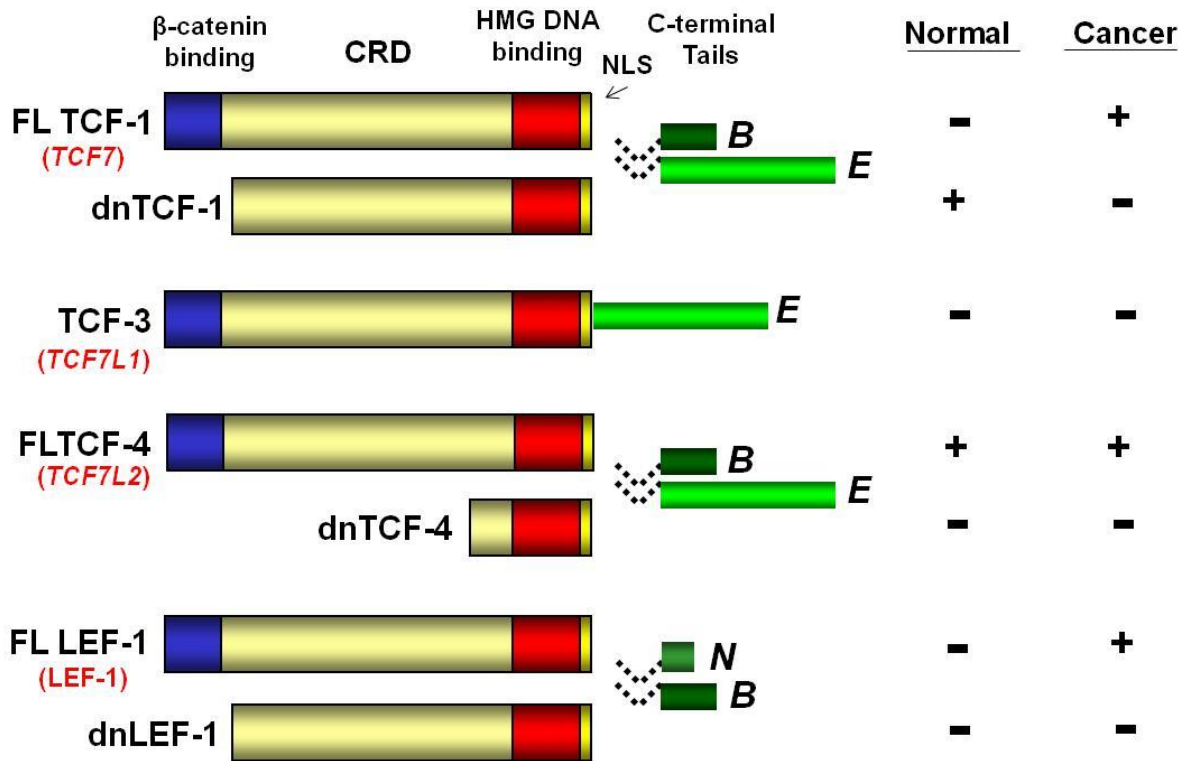


Figure 1.3. Schematic representation of LEF/TCF family of transcription factors.

All four full-length proteins share the highly conserved N-terminal β -catenin binding domain (blue), as well as the high-mobility group (HMG) DNA binding domain (red). Alternative splicing produces alternative exons within the context-dependent regulatory domain (CRD) (yellow), as well in the C-terminal tail (green). Dominant negative isoforms dnTCF-1, dnTCF-4 and dnLEF-1 are produced from alternative promoter usage and the protein products lack the β -catenin binding domain. The table on the right summarizes the expression pattern of LEF/TCF proteins, showing if the isoforms are absent (-) or present (+) in normal colon and colon cancer²⁷. (Figure adapted from Dr. Kira Pate)

family dictate differences in the overall function among its members. One example of this is the Context-dependent Regulatory Domain (CRD) which is poorly conserved among LEF/TCFs, and can serve as a scaffold for transcription co-repressors such as Groucho^{25,26}. Another example of diversity in the family is the various C-terminal tails that result from alternative splicing; the Waterman lab has shown that one of these tails contains an additional DNA binding domain that influences recognition of weaker Wnt Response Elements. Specifically, alternative splicing produces TCF-1, and TCF-4 protein products with a C-terminal tail that contains a cysteine-rich region called the “C-clamp”. The Waterman lab has previously shown that the C-clamp enables TCF-1 and TCF-4 to occupy specific target genes that regulate cell proliferation through the cell cycle^{28,29}.

Alternative to DNA binding characteristics, differences in β -catenin binding capabilities arise from the activity of different promoters for transcription. *LEF1*, *TCF7*, and *TCF7L2* gene loci produce truncated isoforms that lack the β -catenin binding domain³⁰⁻³². Since they still retain DNA-binding activity and the CRD with capabilities to recruit corepressors, they are considered dominant negative (dn) versions of the proteins (named dnLEF-1, dnTCF-1 and dnTCF-4). Dominant negative LEF/TCFs, when expressed, compete with their full-length, β -catenin binding-counterparts to bind and silence transcription of target genes^{33,34}. We exploit this dominant negative action by using dnLEF-1 and dnTCF-1 protein expression as a tool to modulate Wnt signaling in colon cancer. The main discovery from these studies is the identification of a novel Wnt-driven gene program, which is outlined in Chapters 2 and 3.

LEF/TCFs and Wnt in the Intestine

Expression of the LEF/TCF isoforms has been studied in the intestine. The isoforms present in normal intestinal tissue include TCF-1 and TCF-4, while LEF-1 and TCF-3 are absent (Figure 1.4). More specifically, the Waterman Lab discovered that the predominant forms in the normal intestine are full-length TCF-4, and a dominant negative isoform of TCF-1 (dnTCF-1) (Figure 1.3) – both of which carry the C-clamp DNA binding domain³⁵. Differences in protein structure were determined only after the observation that while TCF-1 and TCF-4 have overlapping expression patterns in the small intestine of mice, they have opposing knockout phenotypes. Knockout of TCF-4 leads to a loss of the stem cell compartment and breakdown of intestinal tissue^{31,36}. On the contrary, the TCF-1 knockout caused an increase in growth and adenomatous polyp formation in adult mice³⁷. This finding suggests that the isoforms serve different functions based on their β -catenin binding capacity; while TCF-4 is growth-promoting, TCF-1 (now known to be dnTCF-1) is growth-suppressing in the normal mouse intestine. While knockout of full-length TCF-4 opposes activation of Wnt target genes, knockout of dnTCF-1 relieves repression of Wnt target genes. Clearly, TCF isoforms are expressed to maintain proper levels of Wnt signaling such that the stem cell population at the base of the crypt is maintained and normal intestinal organization is homeostatic and over- or under-growth does not occur. Colon cancer cells exhibit differential expression patterns of the LEF/TCFs such that activating forms are more dominant, therefore it would seem that LEF/TCF activities and expression play a key role in colon cell transformation (see *Wnt signaling and Colon Cancer*)^{38,39}.

As mentioned above, Wnt ligand expression is crucial for maintenance of the stem cell compartment in the colon crypt. For example in the stem cell niche, stem cell-neighboring Paneth cells and supporting myofibroblasts express Wnt3 and Wnt11, and in organoid cultures

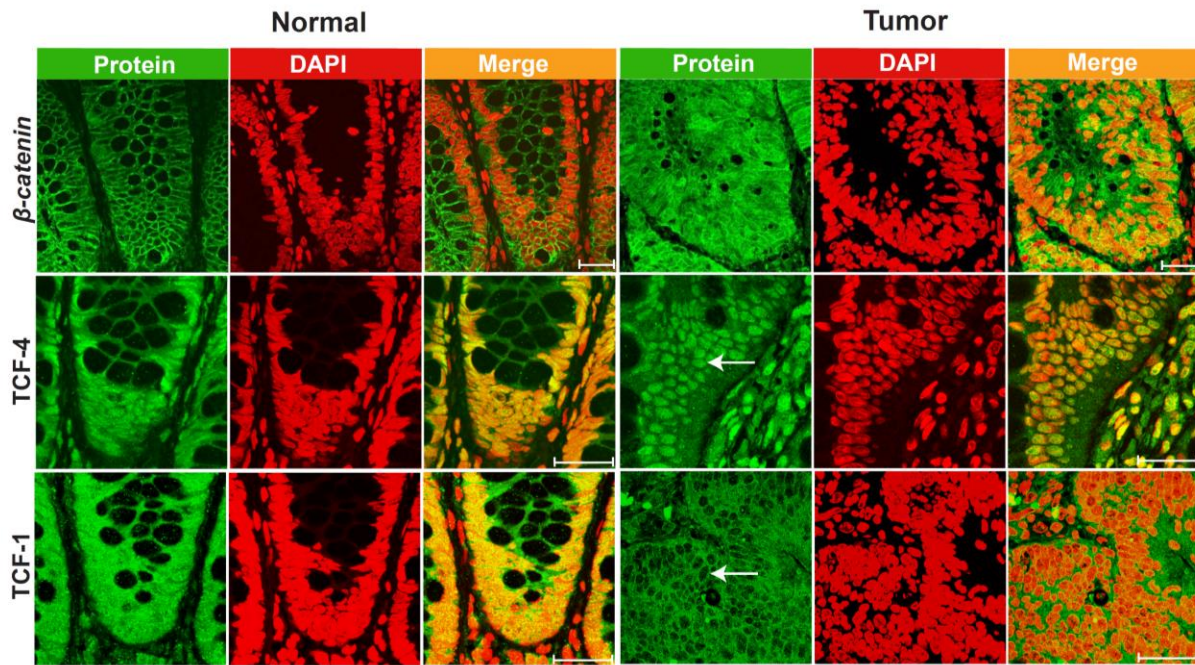


Figure 1.4. TCF-1 localization in normal colon and colon cancer.

Immunofluorescent detection of TCF-1 and TCF-4 in paraffin-embedded sections of tumor and normal matched human colon tissue. Antibody staining of TCF or β -catenin is green. Nuclei are stained with DAPI (false colored here as red to allow visualization). In the merged images, co-localization of antibody and DAPI is yellow. Scale bar is 20 μ m. Control experiments show that in normal colon tissues β -catenin is cytoplasmic. In colon cancer, β -catenin is nuclear and cytoplasmic thus validating the tissue integrity for these studies and confirming elevated Wnt signaling in the tumor. TCF-4 is predominantly nuclear in both normal and colon cancer tissues. TCF-1 is both nuclear and cytoplasmic in normal colon tissues, but TCF-1 is cytoplasmic and absent from nuclei in colon cancer. (Figure from Najdi et al, 2009³⁵)

the absence of these two cell types can be overcome by supplementing with Wnt3A⁴⁰. Expression of Wnt3A in mouse embryonic stem cells (ESCs) promotes self-renewal, while Wnt inhibition with Wnt secretion inhibitor IWP2 leads to differentiation^{41,42}. There are 19 human Wnt ligands, all with differences in signaling capabilities depending on the ligand and receptor context (See *Wnt Signaling*), so defining the expression patterns of the Wnts in the normal intestine may provide insight into pathway modulation in disease and cancer. Early studies using antisense RNA *in situ* hybridization in human tissues by the Waterman lab and others examined expression patterns for a subset of Wnt ligands. Wnt 1, 4, 5A, 5B, 6, 7B, 10B were found to be expressed in normal colon mucosa samples, whereas Wnt 2 and 7A were absent⁴³. Questions remain as to the levels of expression for the entire 19 human Wnt family, however, and importantly, a lack of understanding of the spectrum of Wnt signaling properties that are possible with each Wnt ligand has emphasized the requirement for a full standardized set of Wnt expression plasmids in the same backbone, which would allow a direct side-by-side comparison of Wnt processing, secretion and signaling. For this reason, we started the “Open Source Wnt” plasmid depository and cloned open reading frame sequences for all 19 human Wnts as cassettes into the same plasmid backbone for mammalian expression. This effort and initial findings using the plasmid expression library are discussed in Chapter 4.

Wnt signaling in Colon Cancer

While Wnt signaling is necessary for development and maintenance of normal tissue, aberrant activation of the pathway has been associated with several cancers, including colon, breast, prostate, thyroid, ovarian, melanoma and hepatocellular carcinoma⁴⁴⁻⁴⁷. Mutations of the Wnt signaling pathway cooperate with mutations in *SMAD4*, *KRAS* and p53(*TP53*) to promote

transformation of normal colon epithelium to carcinoma^{48–50}. The most common mutations of the Wnt signaling pathway are loss-of-function mutations in destruction complex-associated APC, and gain-of-function, stabilizing mutations in β -catenin. The large majority (over 80%) of colon cancers arise from tumor suppressor APC loss-of-heterozygosity which damages the ability of the Destruction Complex to degrade β -catenin⁵¹. Alternatively, mutation of β -catenin contributes to a subset of colon cancers, wherein loss of a specific serine residue necessary for GSK3 β -mediated phosphorylation thwarts β -catenin degradation via the ubiquitin-proteasome-mediated pathway⁵². Mutations in these two components have differential effects on the ability to make Wnt signaling activity strongly constitutive in cancer cells (see Figure 1.5 for schematic of common Wnt signaling mutations in colon cancer and associated cell lines). Recent mouse modeling studies restoring APC show tumor regression and subsequent restoration of normal gut homeostasis, highlighting the importance of aberrant Wnt signaling in the progression and maintenance of colorectal cancer, as well as validation of the Wnt signaling pathway as a target for therapy⁵³.

Both APC and β -catenin mutations result in aberrant accumulation of β -catenin which in turn results in an unregulated increase in the functional output of the pathway. Increased Wnt signaling is now widely recognized as the main driver activity that results in unregulated growth and colon carcinogenesis. This unregulated growth is due to the constitutive upregulation of target genes such as c-Myc (*MYC*), *CCND1* (cyclin D1), *SP5* and *VEGF*, resulting in expression of proteins that contribute to Wnt-driven gene programs such as cell cycle, angiogenesis and cell growth^{54–62}. Wnt ligands and extracellular growth factors can crosstalk to unregulated Wnt signaling downstream of APC and β -catenin to modulate target gene transcription. For example, the Hepatocyte Growth Factor (HGF)-Met signaling pathway is known to crosstalk to oncogenic

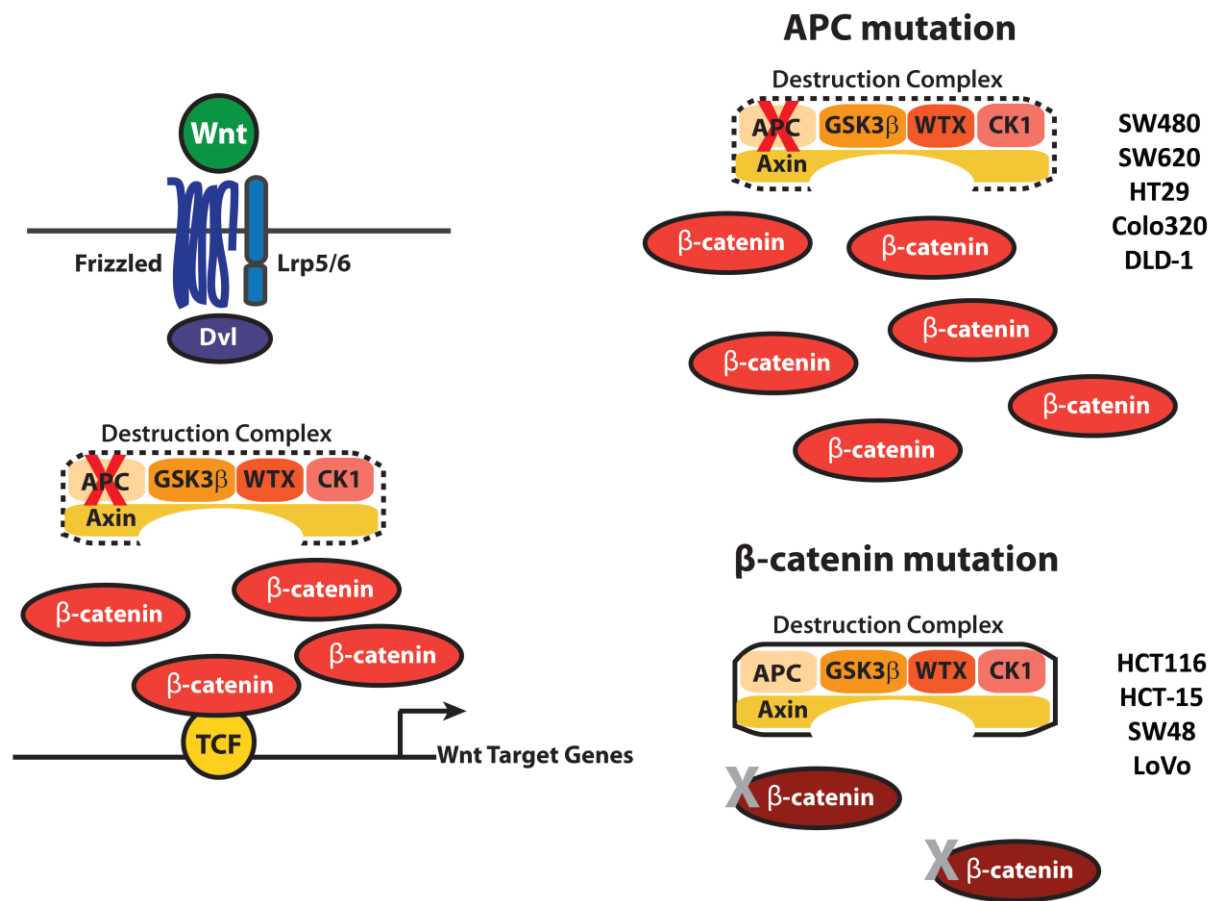


Figure 1.5. Common mutations of the Wnt signaling pathway in colon cancer.

The most common mutations of the Wnt signaling pathway are loss-of-function mutations in destruction complex-associated APC, present in over 80% of colon cancer (above, right), and gain-of-function, stabilizing mutations in β -catenin (below, right). Specifically, mutations in tumor suppressor APC result in loss-of-heterozygosity⁵¹. Alternatively, β -catenin mutations prevent β -catenin degradation through loss of serine residues necessary for GSK3 β -mediated phosphorylation – such mutations generally result in lower levels of accumulated β -catenin in colon cancer cells. Several colon cancer cell culture lines (listed, far right) are available through ATCC (www.atcc.org) for studying cancer phenotypes that arise from these different mutational backgrounds. (Figure modified from Najdi, et al., 2009⁷)

Wnt signaling to activate transcription of Wnt target genes which promote a cancer stem cell phenotype. Specifically, HGF, which derives from HGF-secreting stromal cells, stabilizes and increases levels of nuclear localized β -catenin in the transformed colon epithelia. This crosstalk appears to upregulate a group of genes associated with stemness. That HGF comes from the tumor microenvironment, means that HGF crosstalk occurs most strongly at the tumor/stroma interface – which therefore promotes tumor cell heterogeneity. Immunohistochemical staining of human colon tumor tissue reveals upregulated levels of nuclear β -catenin on the edges of transformed epithelial tissue neighboring HGF-secreting cancer-associated fibroblasts⁶³. In addition, HGF-Met signaling directly activates *LEF1* transcription through Phosphatidylinositol-4,5-bisphosphate 3-kinase (PI3K)/Akt and nuclear factor kappa-light-chain-enhancer of activated B cells (NF κ B) signaling⁶⁴. Wnt ligands are also capable of circumventing the destruction complex and modulating the pathway at the level of LEF/TCFs and β -catenin. For example, WNT5A inhibits β -catenin dependent Wnt signaling through Ror2 receptor binding and subsequent pathway activation. On the other hand, WNT5A activates β -catenin-dependent signaling signals through interaction with co-receptors Fz4 and LRP5⁶⁵. Separately, our group recently showed that a kinase signaling cascade triggered by Wnt ligand activation regulates TCF-1 export in colon cancer cells³⁵. We will further discuss what ligands trigger this export response, how other ligands other than Wnt5A work in this pathway, and their inhibitory activities in Chapters 4 and 5.

Downstream of the destruction complex, LEF/TCFs govern β -catenin interaction with target genes - meaning that the types of isoforms (activating vs inhibiting) and their relative concentrations determine how much access β -catenin has for target gene activation. The evidence is overwhelmingly in favor of granting β -catenin access. For example, while LEF-1 is

not expressed in normal colon tissue, its expression is activated in colon cancer^{6,31}. Even more, while the full-length form of LEF-1 is expressed, the dominant negative form, with potential to provide functional balance, is not expressed in colon cancer^{6,31}. Previous studies by the Waterman lab show that expression of full-length LEF-1 isoforms is due, in part, to aberrant transcriptional activation of *LEF1* promoter 1 which contains Wnt response elements near the transcription start site; *LEF1* is therefore positively regulated by the pathway because it is a Wnt target gene. In addition, the Waterman lab determined that promoter 2, which produces inhibitory dnLEF-1 isoforms, is actively repressed at the transcription level by repressive elements that include YY1, a transcriptional repressor protein⁶⁶. As for TCF-1, only the silencing dominant negative isoform is expressed in the normal colon, but a switch to the full length TCF-1 isoform occurs in colon cancer, the mechanisms have not been defined. Full length TCF-4 is expressed in both normal and colon cancer, and TCF-3 is not expressed in either setting^{6,31,35,36,67} (See Figure 1.4). Taken together, full length LEF-1, TCF-1 and TCF-4 are turned on or remain expressed in colon cancer, while their dominant negative counterparts are turned off or remain off, contributing to overactive Wnt target gene transcription in colon carcinogenesis, a pattern that is very likely to enhance the escape from normal cell cycle regulation.

The presence of full length isoforms in colon cancer cells, and an absence of their dominant negative counterparts, provides a window of opportunity for understanding the functional outputs and gene programs that are misregulated by Wnt signaling. Clearly, full-length LEF/TCFS facilitate transformation of colon epithelial cells because they can recruit β -catenin to target genes. The opportunity we exploited was to challenge the action of full-length LEF/TCFs by expressing dnLEF/TCFs in these cancer cells. Controlled, overexpression of individual dnLEF/TCFs revealed distinct capabilities and targeting specificities for each of the

isoforms. For example, overexpression of isoforms of dnTCF-1 or dnTCF-4 that contained an E-tail compared to isoforms without an E-tail, revealed the role of C-clamp in regulation of the cell cycle and proliferation (see *Wnt signaling*). Expression of dnTCF-1E or dnTCF-4E led to a stall in the G1 phase of the cell cycle causing a halt in cell proliferation. Isoforms that were missing the C-clamp, or mutants that had an inactivated C-clamp had no effect on cell cycle progression. Global gene expression studies in colon cancer cells expressing these various isoforms showed that regulation of the cell cycle occurs through transcriptional repression of p21 by Wnt target genes, the most important of which is the SP5 transcription repressor⁵⁶. In contrast, other groups showed that expression of dnTCF-4 with an N-tail in colon cancer cells (an alternatively spliced version different from the E tail) did not have an effect on cell cycling, but instead restored epithelial cell polarity⁶⁸. In summary of our current understanding in the field, oncogenic Wnt signaling promotes cell cycle misregulation and disruption of normal epithelial polarity. Other isoforms such as TCF-1B and LEF-1N, which lack the C-terminal E-tail in colon cancer^{31,35}, have largely uncharacterized roles in colon cancer and it is unknown how they contribute to the cancer phenotype, even though we know they are expressed. Through expression of dnLEF-1N and dnTCF-1 isoforms that are missing a bona fide C-clamp, we discovered the role of Wnt signaling in regulation of colon cancer cell metabolism. Chapter 2 will discuss the initial discovery of metabolism as a Wnt-driven gene program and the role of Wnt target gene Pyruvate Dehydrogenase Kinase 1 (PDK1) in glycolysis. I solidify the connection between Wnt signaling and glycolytic metabolism in Chapter 3 by showing that the lactate transporter MCT-1 is also a direct Wnt target gene. Since MCT-1 lies downstream of PDK1 action (exports the metabolic waste product lactate that PDK1 activity promotes), the discovery emphasizes how important

this pathway is Wnt-directed actions in cancer, and this finding suggests that Wnt normally promotes this form of metabolism in normal colon crypts.

Cancer and Metabolism

Otto Warburg paved the way for scientific inquiry into cancer cell metabolism with his observation in the 1930's that cancer cells preferentially perform glycolysis, even in normoxia (termed Warburg metabolism, or aerobic glycolysis)^{69,70}. Since then, many researchers have sought to understand the mechanisms by which cancer manipulates the normal metabolic program in cells, with ever-increasing interest in its therapeutic relevance and potential. With no oxygen limitation, why do cancer cells prefer to utilize glucose for glycolysis and fermentation to lactate over oxidative phosphorylation? One well-established explanation is the need to produce large quantities of biointermediates for rapid cell proliferation⁷¹. In order to acquire biomass, cancer cells must increase their glucose consumption and perform several adaptations to facilitate and support alternative metabolic pathways. For example, an increased reliance on glucose requires upregulation of glucose transporters and glycolytic enzymes; oncogenes such as c-Myc and the protein kinase B (Akt) pathway promote these coordinated efforts. Importantly, an increase in lactate secretion as a result of fermentation requires an upregulation of lactate/monocarboxylate transporters to maintain intracellular pH levels, otherwise, cells will die. Furthermore, cancer cells increase their dependency on the pentose phosphate pathway and NADPH for nucleotide synthesis and lipid synthesis, respectively⁷². Cancer cells also adapt an increased use of glutaminolysis, which facilitates lipid synthesis, amino acid, and nucleotide synthesis through glutamine catabolism to α -ketoglutarate flux⁷³. Cancer cells may also prefer aerobic glycolysis as a method of glucose utilization because they wish to limit reactive oxygen

species (ROS) produced by oxidation phosphorylation⁷¹. By limiting ROS production, cancer cells can protect themselves from DNA damage and modification that may lead to apoptosis.

Oncogenic signaling pathways themselves can be major regulators of Warburg metabolism. As alluded to above, the Akt pathway has been implicated in supporting the metabolic program of cancer. Specifically, the PI3K/Akt pathway can both drive tumor proliferation and the metabolism needed to support it⁷⁴⁻⁷⁶. While AMP activated protein kinase (AMPK) signaling generally functions as a metabolic checkpoint in cells by inhibiting mTOR, oncogenic mutations in cancer can suppress it^{77,78}. Although Wnt plays a well-known role in homeostatic liver metabolism⁷⁹ and can crosstalk with metabolic pathways in normal cells such as differentiating osteoblasts^{80,81}, there is little data implicating Wnt directly in the metabolic reprogramming of cancer. The overall impact of our work therefore, as discussed in Chapters 2 and 3, presents evidence of a novel, direct connection between oncogenic Wnt signaling and colon cancer cell metabolism. The implication is that cellular metabolism is a normal program influenced by Wnt signaling, and the challenge for colon cancer therapy lies in exploiting this connection.

Chapter Guide

The remainder of this thesis will address the modulation of Wnt signaling by LEF/TCFs and Wnt ligands, and the resulting insights into Wnt signaling regulation and output. Chapter 2 reveals a novel role of Wnt signaling in regulating colon cancer cell metabolism and identifies a new key target gene that mediates this function, PDK1 (pyruvate dehydrogenase kinase 1). Chapter 3 expands on the knowledge of Wnt signaling regulation of colon cancer cell metabolism to identify a second Wnt target gene that supports this oncogenic phenotype, lactate transporter MCT-1 (monocarboxylate transporter 1). Chapter 4 describes the Open Source Wnt expression library, a necessary tool for the Wnt signaling community, and preliminary findings using this new tool to probe unknowns of the Wnt signaling pathway.

CHAPTER TWO

Wnt Signaling Directs a Metabolic Program of Glycolysis and Angiogenesis in Colon Cancer

Introduction

Cancer metabolism is quickly regaining a forefront position in research as its role in epigenetics, proliferation, and survival are understood to be fundamentally connected. Otto Warburg first recognized that cancer cells ferment much of their glucose supply into lactate regardless of the presence of oxygen, a phenomenon termed the Warburg effect, or aerobic glycolysis⁷⁰. It is now appreciated that cancer cells have different metabolic demands than normal cells and they therefore modify their use of metabolites to meet those demands. Instead of a dominant program for efficient production of ATP, proliferating tumor cells rely on a metabolic program of glycolysis to support anabolic production of biomass^{71,72}. An emphasis on glycolysis is thought to be driven not only from exposure to hypoxic conditions (mostly through stabilized HIF1 α ⁸²) but also by oncogenic signaling pathways, such as PI3K/AKT^{74,76}. Although Wnt plays a well known role in homeostatic liver metabolism⁷⁹ and can crosstalk with metabolic pathways in normal cells such as differentiating osteoblasts^{80,81}, there is little data implicating Wnt directly in the metabolic reprogramming of cancer.

In this chapter we probe the contribution of LEF/TCF/ β -catenin activity to the metabolic programming of cancer cells. We block the downstream activity of Wnt through disruption of β -catenin/LEF/TCF complexes by overexpressing dominant negative (dn)LEF/TCF isoforms that lack the β -catenin binding domain. We utilize both standard metabolomics analyses and a state-of-the-art microscopy technique for monitoring changes in the metabolism of living cells and tissues. The microscopy technique, called the phasor approach to fluorescence lifetime imaging

microscopy (FLIM), utilizes two-photon microscopy for label free detection of intrinsically autofluorescent molecules^{83,84}. In this study, we used FLIM to monitor the metabolic coenzyme nicotinamide adenine dinucleotide (NADH), the principle electron acceptor in glycolysis and electron donor in oxidative phosphorylation. NADH FLIM is especially powerful as it provides a non-invasive, rapid and sensitive readout of the metabolic status of single cells within their native microenvironment. FLIM analysis was used to discover that stem cells at the base of intestinal crypts are highly glycolytic, and that a metabolic trajectory of glycolysis-to-oxidative phosphorylation tracks with a gradient of strong-to-weak Wnt signaling in intestinal crypts⁸⁵. FLIM detection of free and bound NADH *in vitro* in living cancer cells and *in vivo* in living perfused tumors shows that blocking Wnt alters the metabolic program of cancer cells and leads to reduced use of aerobic glycolysis. We identify pyruvate dehydrogenase kinase (PDK1) as a novel Wnt target gene that promotes this effect, and we note that a cell-extrinsic effect of PDK1-driven glycolysis is enhanced tumor angiogenesis.

Results

Blocking Wnt alters the expression of metabolism-linked genes

Although multiple roles of Wnt signaling in colon cancer have been well studied, such as proliferation via regulation of the G1 phase of the cell cycle⁸⁶, there are other functions that have yet to be identified. To reveal new roles of Wnt in colon cancer, we performed Gene Ontology analysis of our recently published microarray data set²⁹. This dataset reflected the change in global gene expression when three different dominant negative (dn) LEF/TCF isoforms were individually and rapidly induced with doxycycline in DLD-1 colon cancer cells (Fig. 2.1A). Induction of dnLEF/TCFs reduces Wnt signaling through interference with endogenous β -catenin/TCF and β -catenin/LEF complexes, and we therefore focused our analysis on genes that

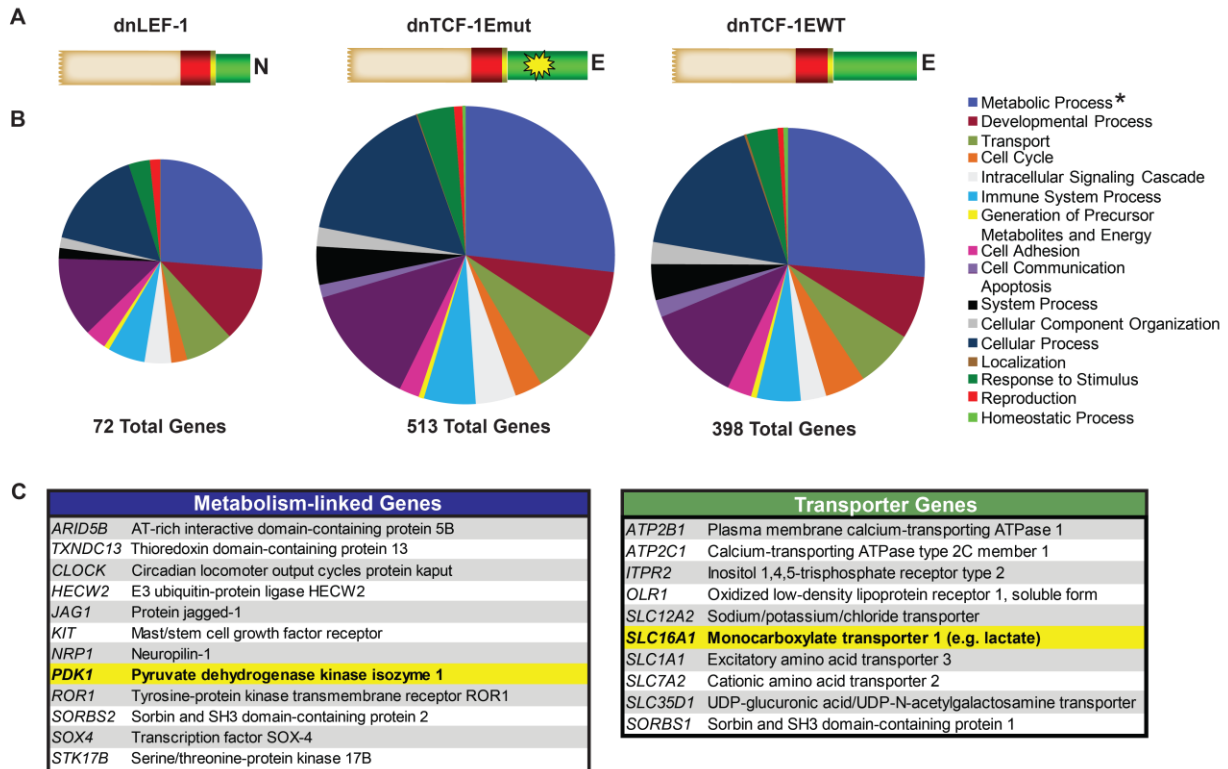


Figure 2.1. Blocking Wnt alters the expression of metabolism-linked genes.

Panther Gene Ontology analysis of microarray data from DLD-1 cells overexpressing either dnLEF-1 (23h), dnTCF-1Emut (8h), or dnTCF-1EWT (8h). **(A)** Schematic of dnLEF/TCF isoforms expressed (Beige box = context-dependent regulatory domain; Red box = HMG DNA binding domain; Yellow box = nuclear localization signal; Green box = alternatively spliced C-terminal tails; Yellow star = mutation in E-tail). **(B)** Ontology analysis of dnLEF/TCF downregulated genes reveals a large category of genes linked to metabolism. PANTHER binomial statistical analysis determined statistically-significant overrepresentation of regulated genes within each category compared to representation in the human genome (*p-value <0.01) **(C)** List of metabolism-linked genes downregulated by all three dnLEF/TCF isoforms. List of transporter genes regulated by at least 2 dnLEF/TCF isoforms. For all genes on the list changes are p < 0.05, and range of fold changes is -1.3 to -6.0. (Figure adapted from Figure 1 of Pate, Stringari, Sprowl-Tanio et al., 2014).

were down-regulated within 8 and 22 hours after induction. The ontology analysis was carried out using PANTHER software which classified the down-regulated genes into different categories of biological processes^{87,88}. A consistently large subset of regulated genes fell under the category of metabolism (Fig. 2.1B,C). In fact, Panther binomial statistical analysis revealed that Wnt target genes connected to metabolism were the most highly overrepresented category compared to baseline representation of these genes in the human genome. These data, along with the notable downregulation of two key genes critical to cancer metabolism, pyruvate dehydrogenase kinase (*PDKI*) and the lactate transporter, MCT-1 (*SLC16A1*), led us to hypothesize that Wnt specifically and directly regulates a program of cellular metabolism in colon cancer cells.

dnLEF-1 and dnTCF-1Emut do not alter the cell cycle or proliferation *in vitro*

To test this hypothesis we used dnLEF/TCF overexpression to block Wnt target gene regulation in colon cancer cell lines and examined resultant changes in metabolism. Knowing that overexpression of the potent dnTCF-1E or dnTCF-4E isoforms halts cell cycle progression and cell proliferation⁸⁶, while isoforms lacking the alternatively spliced C-terminal E-tail avoid this stall^{28,68}, we induced the expression of dnLEF-1N which naturally lacks E-tail sequences. In parallel, we also induced the expression of dnTCF-1Emut, a mutated form of dnTCF-1E with a five amino acid substitution in the auxiliary C-clamp DNA binding domain in the E-tail that eliminates control of proliferation²⁸. Use of these less potent dominant negative isoforms enabled an uncoupling of our test for effects on cell metabolism from effects on cycle progression. We utilized two different expression systems in two different colon cancer cell lines. In two independent clonal lines of DLD-1 colon cancer cells, we used a stably integrated doxycycline

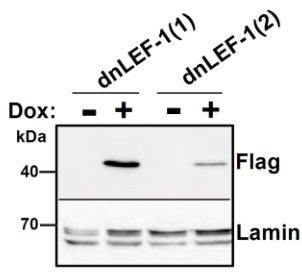
inducible system to express Flag-tagged dnLEF-1(dnLEF-1(1) and dnLEF-1(2)). In a second cell line (SW480), we used a lentiviral system to express physiological levels of Flag-dnLEF-1 or Flag-dnTCF-1Emut. In all cases, transgene expression was assessed by Western Blot (Fig. 2.2A,E), and functional disruption of Wnt activity confirmed by repression of the luciferase reporter Super TOPFlash (STOP) (Fig. 2.2B,F). We also confirmed that dnLEF-1 and dnTCF-1Emut had no impact on cell proliferation (Fig. 2.2C,G) or any parameter of the cell cycle profile (Fig. 2.2D,H). Cell cycle analysis performed at even longer timepoints of dnLEF/TCF expression also showed no change in the profile (data not shown). Overall these data show that dnLEF-1N and dnTCF-1Emut expression have no effect on the cell cycle or the intrinsic ability of the cells to proliferate and can therefore reveal phenotypes of blocking Wnt that are uncoupled from these functions.

Blocking Wnt alters the metabolic program of colon cancer cells

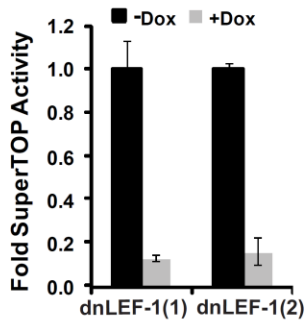
One of the most recognized hallmarks of cancer is Warburg metabolism, or, a tendency for cancer cells to utilize glycolysis rather than oxidative phosphorylation regardless of the availability of oxygen⁷⁰. We tested whether blocking Wnt alters carbohydrate metabolism by testing for changes in lactate (a byproduct of glycolysis) and ATP production (most efficiently produced via oxidative phosphorylation). A measure of lactate levels in the media of mock-infected SW480 cells compared to cells infected with lentivirus expressing dnLEF-1 or dnTCF-1Emut, revealed a significant decrease in lactate production (Fig. 2.3A,B). This was true for both 2D conventional cultures and 3D suspension cultures in soft agar which were accompanied by a visual color change of the media (due to secretion of excess lactic acid; Fig. 2.3B). The drop in lactate production occurred independently of cell number, which was not significantly altered

DLD-1:

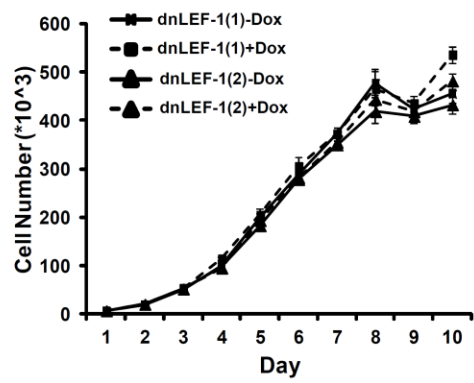
A



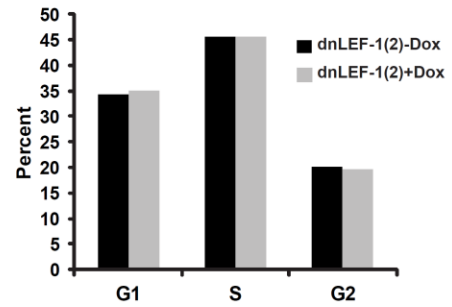
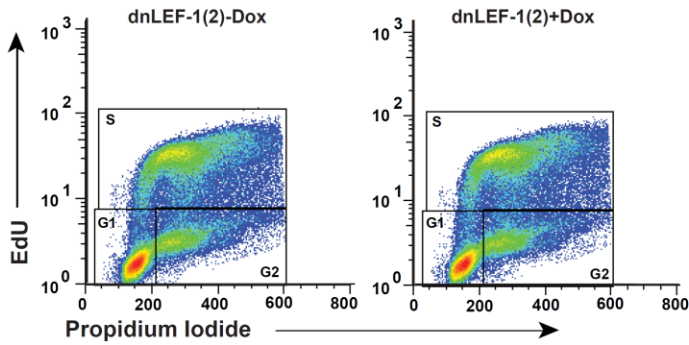
B



C

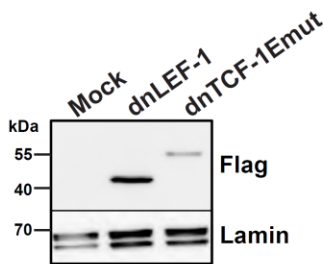


D

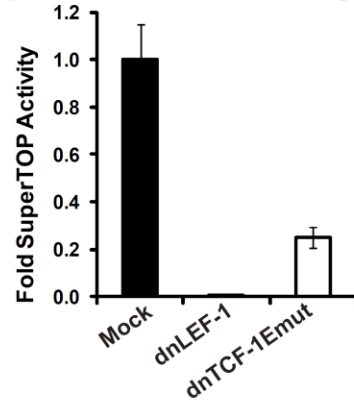


SW480:

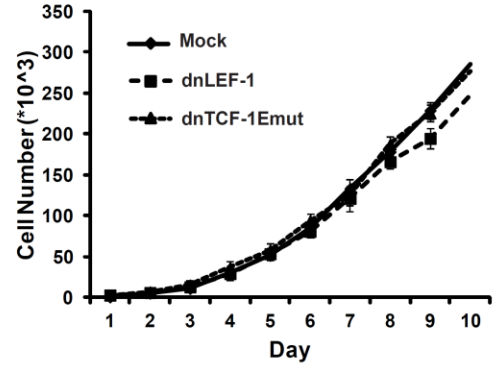
E



F



G



H

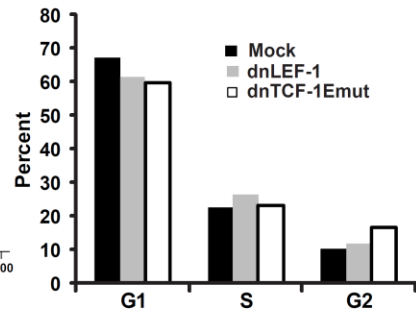
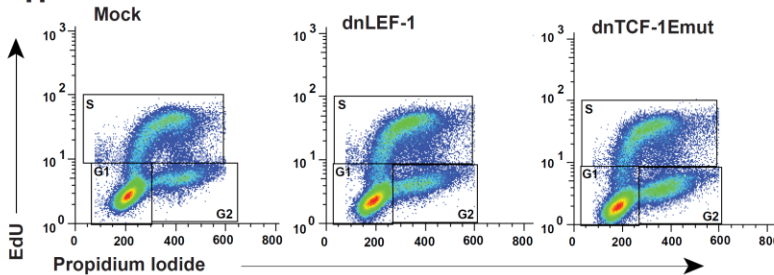


Figure 2.2. dnLEF-1 and dnTCF-1Emut do not alter the cell cycle or proliferation *in vitro*.

(A-D) Analysis of two clonal DLD-1 cell lines (dnLEF-1(1) and dnLEF-1(2)) with stably integrated doxycycline-inducible expression of flag-tagged dnLEF-1. **(E-H)** Analysis of SW480 cells infected with lentivirus carrying flag-tagged dnLEF-1 or dnTCF-1Emut. **(A,E)** Western blot analysis of flag-tagged transgenes after five days of doxycycline treatment (A) or six days post transduction (E). **(B,F)** Luciferase reporter assays show that dnLEF/TCF expression (B: 24h doxycycline; F: six days post transduction) reduces activity of the Wnt reporter, SuperTOPFlash. Graphs shown are representative of three replicates. Error bars represent the spread between duplicates. **(C,G)** A colorimetric-based growth curve assay shows little to no difference in proliferation rate over ten days of dnLEF/TCF expression. Graphs shown are representative of at least three replicates. Error bars depict the standard deviation of eight internal replicates. **(D,H)** FACS scatter profiles (left) and quantitation (right) show no change in cell cycle after 24h of doxycycline treatment (D) or three days after lentiviral infection (H). (*Figure adapted from Figure S1 of Pate, Stringari, Sprowl-Tanio et al., 2014*).

because of the lack of any effect of dnLEF/TCF expression on proliferation (Fig. 2.3A). Similar analyses were performed in four different colon cancer cell lines (Fig. 2.4). We also interfered with Wnt by application of the drug XAV939. This small molecule inhibitor targets poly-ADP-ribosyltransferases Tankyrase1, 2 to destabilize β -catenin, an action that works even in colon cancer cells where its destruction complex components are defective⁸⁹. We observed similar decreases in lactate production upon XAV939 application, a change consistent with a decrease in Warburg-type metabolism (Fig. 2.3C). Another hallmark of Warburg is less efficient production of ATP (since oxidative phosphorylation produces more ATP per molecule of glucose than glycolysis). We therefore measured changes in ATP levels in SW480 cells infected with dnLEF/TCF-expressing lentivirus. We observed that any interference with Wnt signaling triggered increases in ATP production suggesting an increased utilization of oxidative phosphorylation vs. glycolysis (Fig. 2.3D). We also tested for rates of glucose consumption, and as expected, rates were lower when either dnLEF/TCFs or XAV939 were used to disrupt Wnt signaling (Fig. 2.3E-G). For more precise measurements we used Seahorse technologies to measure the glycolytic flux (Extracellular Acidification Rate or ECAR) and mitochondrial respiration (Oxygen Consumption Rate or OCR) of colon cancer cells subjected to our conditions. We observed that expression of dnLEF/dnTCF in SW480 cells lowered the rate of glycolysis but did not significantly affect the rates of respiration (Fig. 2.3H, I). XAV939 treatment induced a similar effect, which we report as a 30%-40% increase in the rates of oxidative phosphorylation relative to glycolysis (OCR:ECAR ratio; Fig. 2.3J).

While the above technologies are quantitative, they are single end-point measurements of an entire population of cells. Recognizing that cancer metabolism can be heterogeneous and is best evaluated in living cells, we utilized the phasor approach to fluorescence lifetime imaging

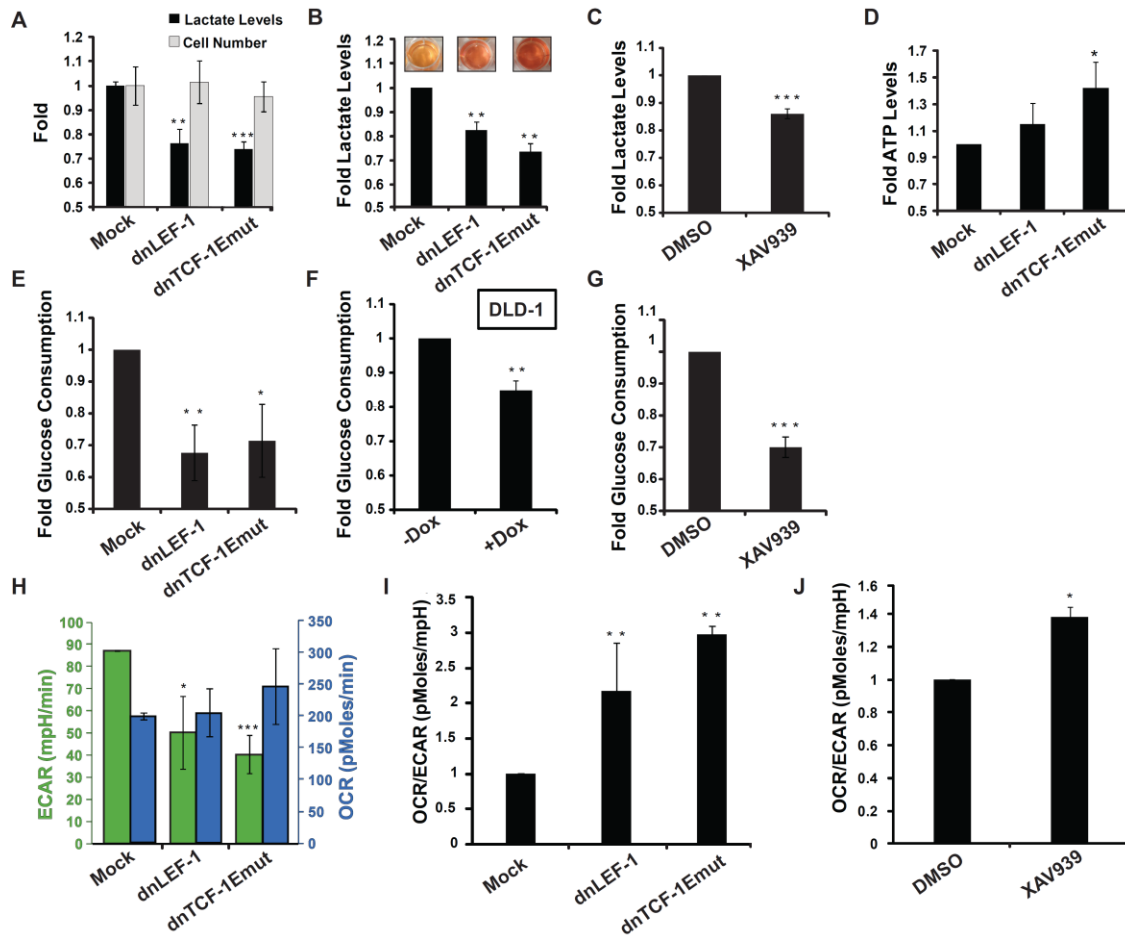
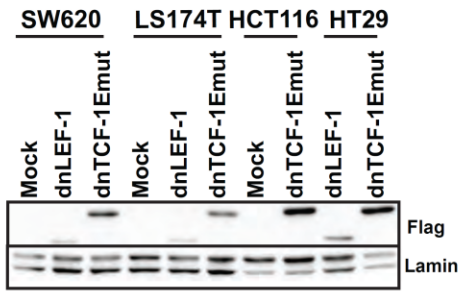


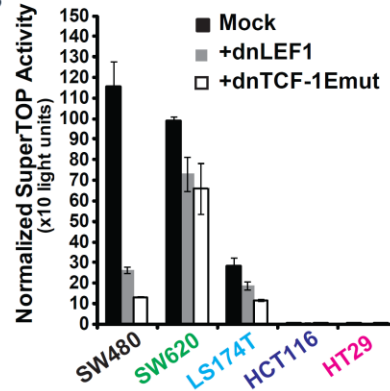
Figure 2.3. Blocking Wnt alters the metabolic program of colon cancer cells.

(A) Lactate levels are reduced with lentiviral transduction of dnLEF-1 or dnTCF-1Emut in SW480 cells growing under standard culture conditions for 10 days. Representative graph of three replicates is shown with error bars representing the S.E.M. between three internal replicates (B) Fold change of lactate levels produced in 3D cultures. Images are of representative wells for each condition. Measurements performed on media collected from SW480 cells grown in soft agar after 22 days. Representative graph of three replicates is shown with error bars representing the S.E.M. between three internal replicates. (C) Fold change in lactate levels of SW480 cells treated with Wnt inhibitor XAV939 (10 μ M) for a minimum of four days. Data represent the average of six independent trials (+/- S.E.M.). (D) ATP levels in SW480 cells collected seven days post transduction. Data represent the average of three independent trials (+/- S.E.M.). (E) Fold changes in glucose consumption in SW480 cells expressing dnLEF/TCFs, (F) DLD-1 cells (dnLEF-1(2)) treated with doxycycline to induce dnLEF-1 expression, and (G) SW480 cells treated with XAV939 (10 μ M). Data represent the average of four trials (+/- S.E.M.) (H) Extracellular acidification rate (ECAR) and oxygen consumption rate (OCR) in SW480 cells transduced with MOCK, dnLEF-1 or dnTCF-1Emut virus. (I) Data from panel H represented as an OCR/ECAR ratio. (J) OCR/ECAR ratio of SW480 cells treated with XAV939 (10 μ M). Data in H-J represent the average of three independent trials (+/- S.D.). (*p-value<0.05; **p-value<0.01; ***p-value<0.001) (Figure is adapted from Figure 2 of Pate, Stringari, Sprowl-Tanio et al., 2014).

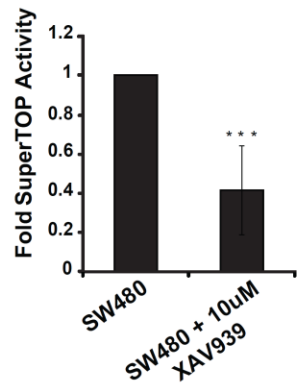
A



B



C



D

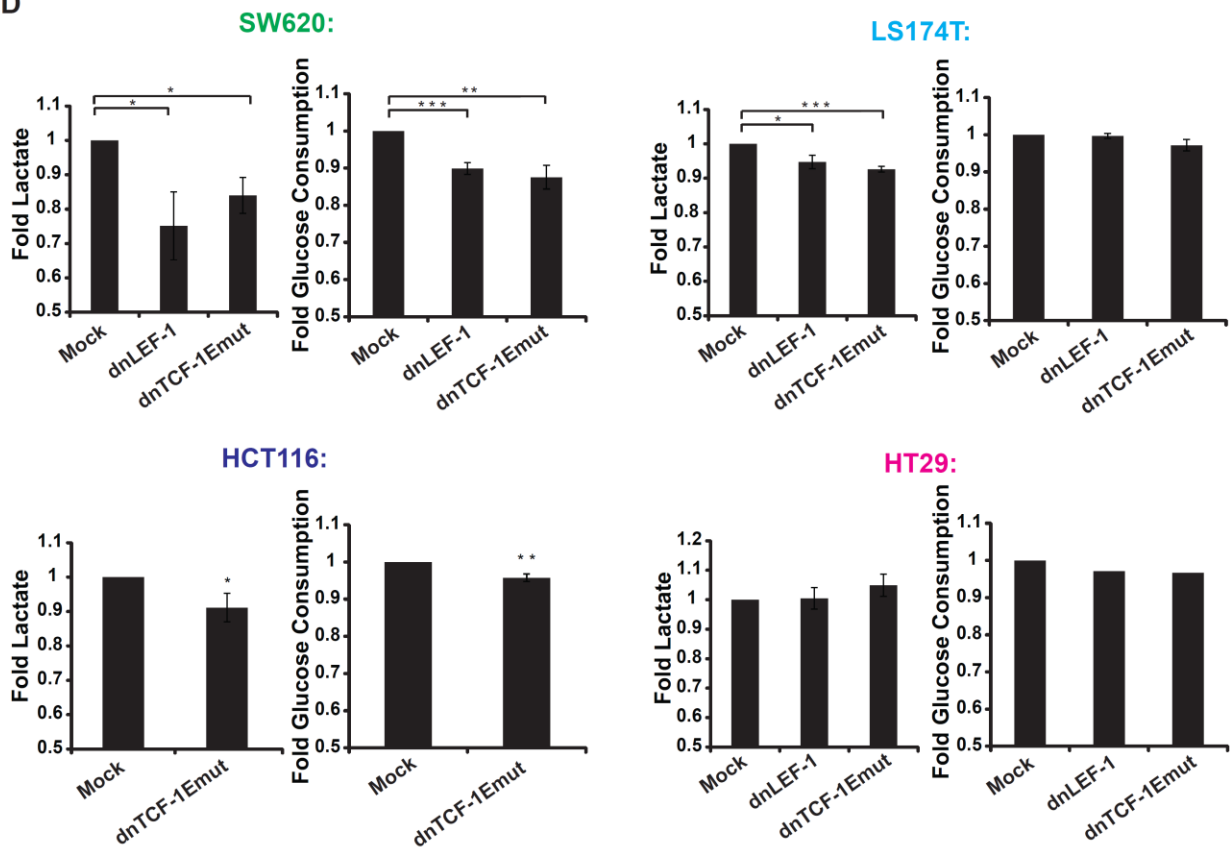


Figure 2.4. Blocking Wnt alters the metabolic program of colon cancer cells.

(A) Western blot analysis of lentiviral transduction and expression of FLAG-tagged dnLEF-1 and dnTCF-1Emut in SW620, LS 174T, HCT116 and HT-29 colon cancer cells. **(B)** SuperTOP Wnt reporter assay in colon cancer cell lines with or without co-expression of dnLEF-1 or dnTCF-1Emut. Normalized luciferase activity from SuperTOP (to a co-transfected CMV- β -galactosidase control) shows both the relative levels of Wnt signaling in each cell line and the magnitude of interference by dnLEF-1/dnTCF-1Emut. Graph shown is representative of three replicates. Error bars represent the spread between duplicates. **(C)** SuperTOP luciferase reporter assay in SW480 cells treated with the XAV939 inhibitor (10 μ M). Graph shown represents the average of five trials (\pm S.D.). **(D)** Lactate production and glucose consumption assays in four colon cancer cell lines in the presence/absence of dnLEF-1 or dnTCF-1Emut. Note that cell lines with low levels of tonic Wnt activity (see panel B) show little or no response in lactate and glucose when dnLEF-1 or dnTCF-1Emut are expressed. With the exception of the glucose consumption data in HT-29 cells (which is representative of two replicates), the data shown represents the average fold values from four independent trials (\pm S.E.M.). (*p-value<0.05; **p-value<0.01; ***p-value<0.001). (Figure adapted from Figure S2 of Pate, Stringari, Sprowl-Tanio et al., 2014).

microscopy (FLIM) to evaluate metabolism. Specifically, we used FLIM to monitor dynamic shifts in patterns of aerobic glycolysis vs. oxidative phosphorylation by following the signature of the metabolic and autofluorescent cofactor NADH. NADH autofluorescence can be excited at a specific wavelength (740 nm), and the pattern of the decay of this fluorescence differs depending on its bound or unbound state⁹⁰. Glycolytic cells have a predominance of free, unbound NADH. Respiring cells have high rates of oxidative phosphorylation and a predominance of bound NADH (e.g. NADH bound to mitochondrial enzymes)^{91,92}. The signature of fluorescence decay of NADH can be graphically represented on a 2D phasor plot where the decay rates for the pure free or bound species of NADH occupy very different positions^{83,84,93,94}. In a complex cellular environment where combinations of free and bound NADH co-exist, fluorescence signatures of decay map to experimental points between the extreme phasor plot positions of the pure free and bound species (Fig. 2.5A). In other words, experimental positions on the phasor plot indicate the relative ratio of free:bound NADH and therefore the relative levels of glycolysis and oxidative phosphorylation. In our analysis, increases in the free:bound NADH ratio (rightward and downward shift of experimental points in the phasor plot), indicate more glycolysis and an overall cancer-type of metabolism⁹⁵⁻⁹⁸.

To demonstrate the relationship between a phasor shift and a change in metabolism, cells were treated with potassium cyanide (KCN) for 1 minute to block mitochondrial respiration and trigger an increase in reduced, free NADH. FLIM analysis (using two photon microscopy at 740 nm to excite bound and free NADH) before and after KCN treatment moved the phasor distribution closer to the pure free NADH position, indicating a release of NADH from mitochondria and an increase in the ratio of free:bound NADH (Fig. 2.5A). This result is also visually confirmed through a false-color mapping of free:bound NADH overlaid pixel-by-pixel

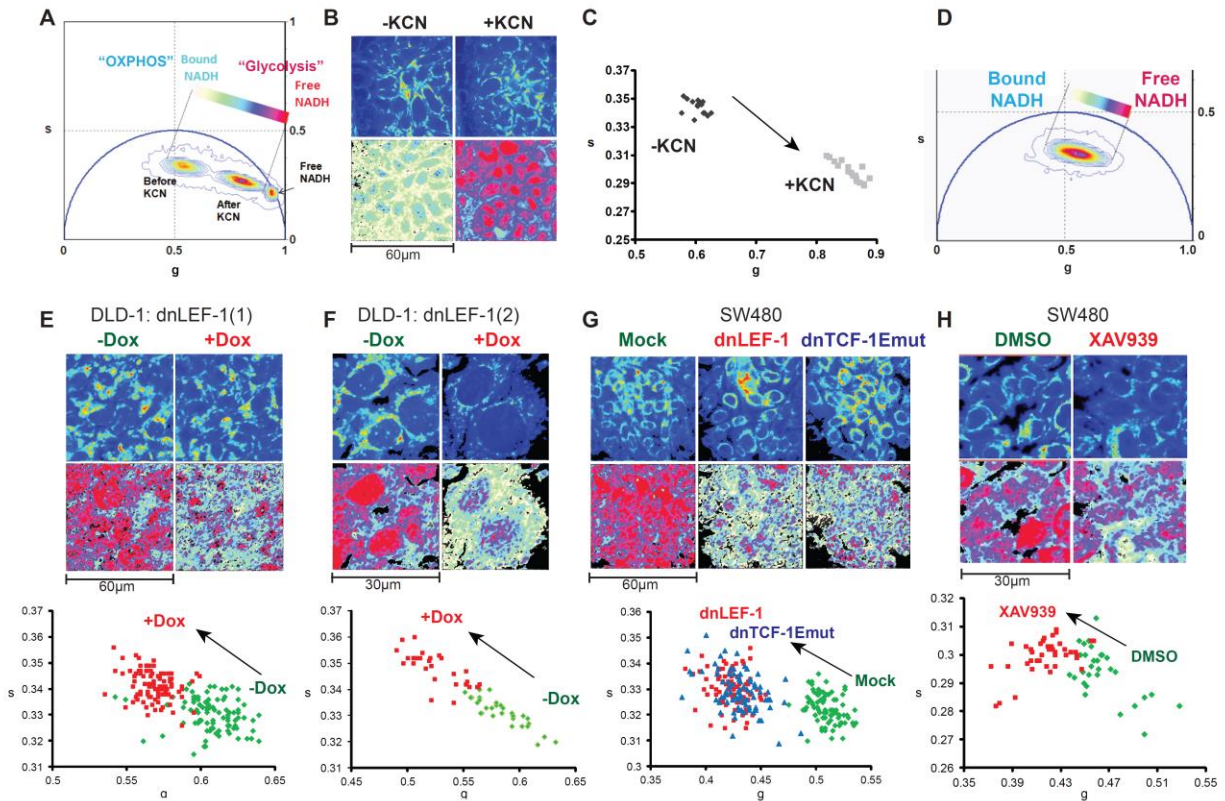


Figure 2.5. Fluorescence Lifetime Analysis of NADH Reveals Shifts in Glycolysis Upon Expression of dnLEF/TCF.

(A) Phasor plot of a FLIM analysis showing DLD-1 cells before and after a 1 minute treatment with 4 mM Potassium Cyanide (KCN). The phasor position of pure free NADH is also shown. (B) Top panel of images shows the autofluorescent intensity at 740 nm. Bottom panels correspond to the free:bound NADH coloring of the same field of cells according to the color map shown on the phasor plot in (A). Changes indicate an increase in free:bound NADH after KCN treatment. This is also shown in (C), a scatterplot analysis of average phasor positions of individual cells before and after KCN treatment. (D) Phasor position of DLD-1: dnLEF-1(1) cells, and a color map to represent the gradient of relative levels of free and bound NADH. (E-H) The top row of images show two-photon fluorescence intensity images excited at 740nm for two clones of DLD-1 dnLEF-1 stable cells (dnLEF-1(1) and dnLEF-1(2)), and SW480 cells. The bottom row shows free:bound NADH color mapping as indicated by the color map in panel D. The bottom panels show scatter plots where each point represents the average phasor position from one cell. Induction of dnLEF-1 or dnTCF-1Emut expression, or treatment with the Wnt inhibitor XAV939 results in a phasor shift toward bound NADH. All images and measurements were taken five days after seeding under confluent conditions. Representative data from single trials are shown from among at least three replicate experiments for each cell line. Each treatment resulted in a population on the scatterplot distinct from mock cells with $p < 0.0001$. (Figure adapted from Figure 3 of Pate, Stringari, Sprowl-Tanio et al., 2014).

on the original images taken of the cells, where pink/red and blue/white represents, respectively, higher and lower concentrations of free NADH relative to bound NADH (Fig. 2.5B). A scatterplot display of the data enables a comparison of the average position of individual cells for each set of conditions and therefore reveals the spread of the data between replicates of the same conditions as well as between different experimental conditions. In this case, the phasor positions of each pixel within one cell is averaged and plotted as a single point (Fig 2.5C).

To assess the impact of blocking Wnt target gene activation on the ratio of free:bound NADH, we performed FLIM analysis on normoxic cells expressing dnLEF/TCFs or cells treated with the XAV939 inhibitor. Doxycycline induction of dnLEF-1N in two different clonal DLD-1 cell lines caused the average phasor position to shift away from free NADH to the upper left of the scatterplot, toward bound NADH (Fig. 2.5D,E,F). This shift represents a decrease in free:bound NADH, a change that was also evident in the color mapping of NADH states in the DLD-1 cells. Parental DLD-1 cells treated with the same concentration of doxycycline showed no significant change in the phasor positions indicating that doxycycline alone does not alter the metabolic signature (Fig. 2.6D). To confirm this result in other colon cancer cells we performed FLIM analysis on SW480 cells infected with empty virus or lentivirus carrying dnLEF-1N or dnTCF-1Emut expression cassettes (Fig. 2.5G; additional dnTCF isoforms Fig. 2.6A,B,C), as well as analysis of cells treated overnight with XAV939, the Wnt signaling inhibitor (Fig. 2.5H). We also tested four other colon cancer cell lines that varied with respect to their endogenous level of Wnt signaling (Fig. 2.6C). Shifts in metabolism correlated directly with the ability to reduce Wnt signaling. These data suggest that blocking Wnt signaling in colon cancer cells results in a decrease in the ratio of free:bound NADH which indicates a decrease in glycolysis. Taken together, our assessment of lactate production, ATP production, ECAR, OCR, Glucose

consumption, and FLIM signatures of NADH all indicate that oncogenic Wnt signaling promotes a glycolytic form of metabolism.

Blocking Wnt reduces PDK1 levels via regulation of transcription

We next asked whether the changes in metabolism induced by blocking Wnt could be attributed to any of the metabolism-linked target genes identified in the DLD-1 microarray experiments. One common target gene downregulated by all of the dnLEF/TCF proteins was pyruvate dehydrogenase kinase (PDK1). This kinase phosphorylates and inhibits the pyruvate dehydrogenase (PDH) complex in mitochondria⁹⁹. Inhibition of PDH, in turn, reduces the conversion of pyruvate to acetyl-CoA for entry into the TCA cycle and oxidative phosphorylation. Therefore, PDK1 plays an important modulatory role in the promotion of a glycolytic phenotype, and is therefore, not surprisingly found to be upregulated in a number of cancers¹⁰⁰⁻¹⁰².

To validate the microarray data and test whether PDK1 levels are modulated by β -catenin and LEF/TCFs, Western blot analysis was performed for both DLD-1 and SW480 cells expressing dnLEF-1 or dnTCF-1Emut. PDK1 protein levels were reduced 50-75% for all cell lines (Fig. 4a). To confirm that this reduction is evident at the mRNA level, qRT-PCR analysis of *PDK1* mRNA was performed for doxycycline-treated dnLEF-1 DLD-1 cells after 24 hours or 120 hours of expression. At both time points *PDK1* mRNA levels were reduced to 60%, similar to the reduction observed at the protein level (Fig. 2.7B,C). Since there are four members of the PDK family (PDK1-4), we asked whether any of the additional PDK family members were also downregulated after blocking Wnt. RT-qPCR analysis of *PDK2-4* levels in DLD-1 cells expressing dnLEF-1 indicates that neither *PDK2* nor *PDK3* levels were altered, while *PDK4*

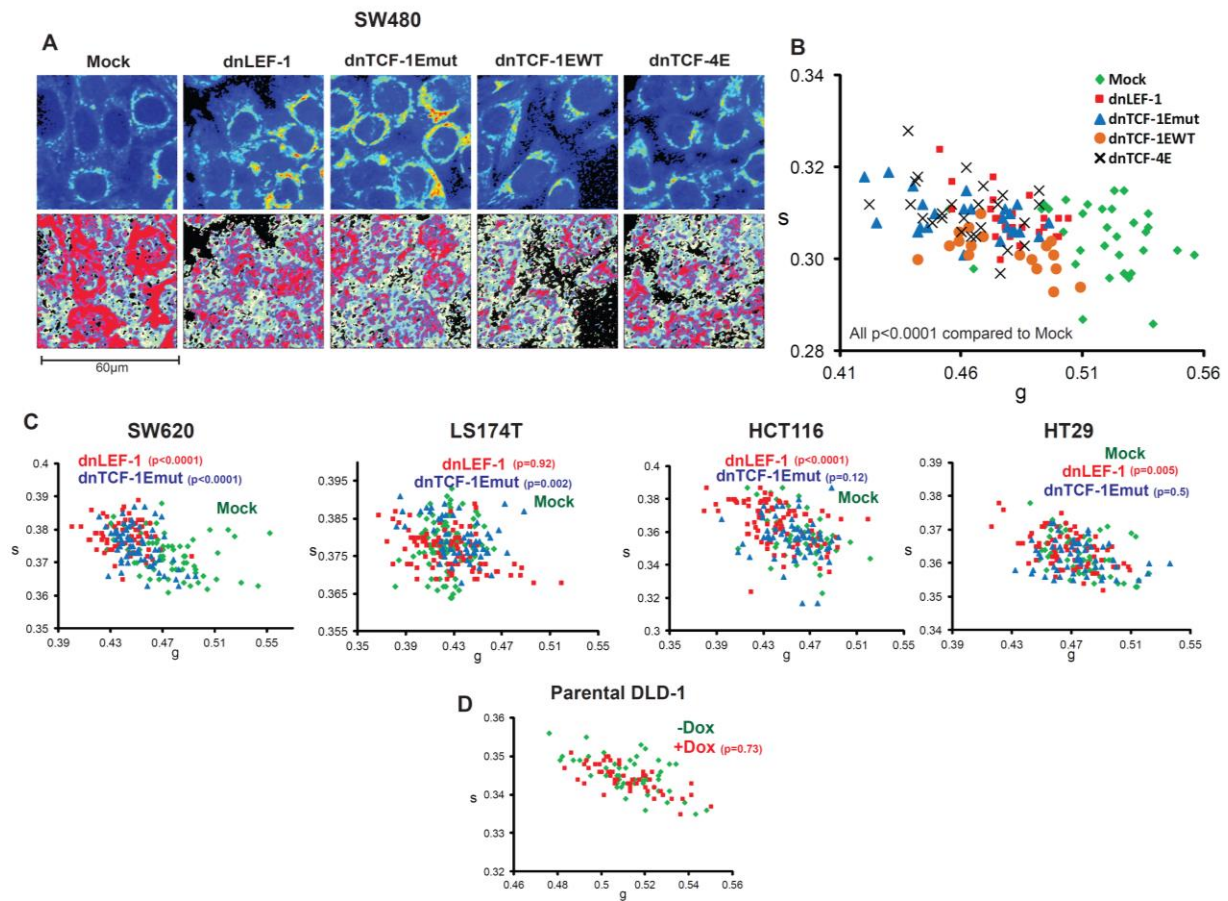


Figure 2.6. FLIM analysis of colon cancer cell cultures.

(A) Top panel of images shows the autofluorescent intensity of SW480 cells excited at 740 nm. Bottom panels correspond to the free:bound NADH color map of the same field of cells according to the color map depicted in the phasor plot in Figure 3D. (B) Scatter plot summary of FLIM analysis (for NADH) of SW480 cells transduced with different lentiviral transductions to express four different dnLEF/dnTCFs. (C) Additional FLIM analyses of four different colon cancer cell cultures transduced with the indicated lentiviral expression constructs. (D) Scatter plot analysis shows that DLD-1 parental cells do not respond to 0.01 $\mu\text{g/ml}$ doxycycline alone (compare to shifts in the phasor towards bound NADH when DLD-1 clonal cells are induced to express dnLEF-1 (Figure 2.5E, 2.5F). (Figure adapted from Figure S3 of Pate, Stringari, Sprowl-Tanio et al., 2014).

showed a modest, but significant decrease from its already low basal level (Fig. 2.7B). Overall, these data suggest that PDK1 and possibly PDK4 are regulated by Wnt/ β -catenin signaling in colon cancer cells.

A possible connection between Wnt and metabolism occurs through the Wnt target gene, c-Myc, and in fact, previous reports suggest that under certain conditions, c-Myc can potentiate the upregulation of PDK1 levels¹⁰³. We examined c-Myc levels after expression of dnLEF/TCF. With the exception of a slight decrease in c-Myc protein after 96 hours of dnLEF-1 expression in DLD-1 cells (Fig. 2.7A), there is little to no difference in c-Myc mRNA or protein levels even after 120 hours (Fig. 2.7A,C). This result also matches the previously published microarray, which showed no change in c-Myc mRNA after expression of dnLEF-1. Therefore, the change in PDK1 levels observed is independent of Wnt regulation of c-Myc.

To determine the kinetics of PDK1 transcription upon disruption of Wnt signaling, we used a 4-thiouridine labeling procedure to identify actively transcribed mRNAs¹⁰⁴. After induction of dnTCF-1Emut for 2 hours, DLD-1 cells were incubated with a pulse of 4-thiouridine for 30 minutes to incorporate the nucleotide label into nascently transcribed RNA. After the pulse, cells were harvested and labeled RNA was purified via a biotinylation/streptavidin pull-down procedure¹⁰⁴. Semi-quantitative RT-PCR for *PDK1* mRNA demonstrated that transcription of the *PDK1* locus was immediately reduced upon induction of dnTCF1E-mut expression (Fig. 2.7D). The known Wnt target gene *AXIN2* served as a positive control and constitutive, ubiquitous *UBA52* served as a negative control. Induction of dnTCF-1Emut reduced transcription by at least 50% for both *PDK1* and *AXIN2*, demonstrating that *PDK1* is likely to be a direct Wnt target gene. We have also performed a genome-wide ChIP-seq study of dnTCF-1E binding¹⁰⁵, and discovered in the genome dataset that TCF-1 binds to distal

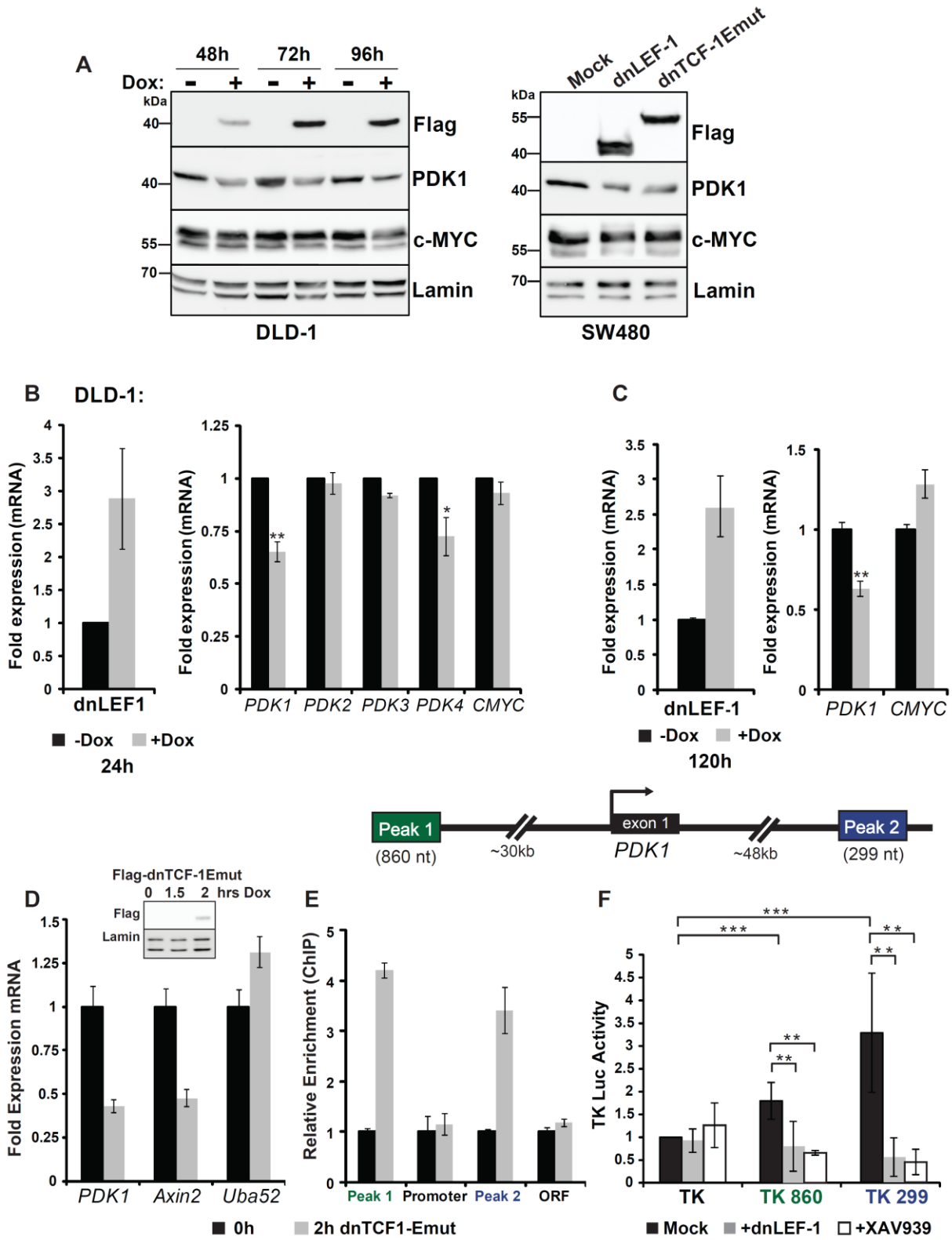


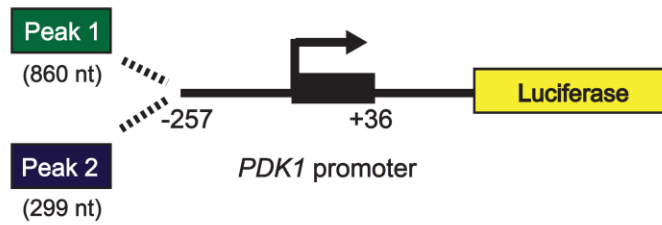
Figure 2.7. Blocking Wnt directly reduces PDK1 levels via regulation of transcription.

(A) Whole cell lysates from DLD-1 dnLEF-1(1) cells were collected 48h, 72h, and 96h after 0.01 μ g/ml doxycycline treatment and were probed with the antibodies shown. SW480 cells were harvested 48h post transduction. (B, C) RT-qPCR analysis was performed on RNA collected from DLD-1 dnLEF-1(2) cells harvested 24h (B) or 120h (C) after the addition of doxycycline. Graphs shown represent the average of three trials (+/- S.E.M.). (D) RT-qPCR analysis was performed on 4-thiouridine-labelled RNA isolated from a 30 minute pulse in the presence/absence of dnTCF-1Emut, induced by 2 h doxycycline treatment in DLD-1 cells. Known Wnt target gene *Axin2* and *Uba52* were used as positive and negative controls respectively. A representative graph is shown of two replicates, with error bars representing the S.D. among three internal replicates. (E) RT-qPCR analysis of chromatin immunoprecipitated from DLD-1 cells with or without induction of FLAG-dnTCF-1Emut, using anti-FLAG antibody. PCR primers designed to detect the indicated *PDK1* genomic regions show that dnTCF-1Emut associates with distal regions that flank the *PDK1* locus. A representative graph is shown of two replicates, with error bars representing the S.D. among three internal replicates. (F) Luciferase reporter activity in SW480 cells shows that Peak1 and Peak2 regions confer elevated transcription activity to the heterologous thymidine kinase (TK) promoter. Expression of transduced dnLEF-1, or treatment with the Wnt inhibitor XAV939 (10 μ M) eliminates the regulatory activity of these fragments. Graph shown represents the average of three independent replicates (+/- S.D.). (*p-value<0.05; **p-value<0.01; ***p-value<0.001) (Figure adapted from Figure 4 of Pate, Stringari, Sprowl-Tanio et al., 2014).

upstream (“Peak 1”) and downstream (“Peak 2”) sites surrounding the *PDK1* locus (Fig. 2.7E). Each genomic region of TCF-1 occupancy contains three putative Wnt Response Elements (Fig. 2.8). We designed PCR primers specific to these two regions as well as the *PDK1* promoter and an internal site in the locus as a negative control. Using chromatin immunoprecipitation procedures we determined that TCF-1 directly binds to the distal sites but not the promoter (Fig. 2.7E). To test whether these sites confer transcription regulation in colon cancer cells, we subcloned each distal region next to the heterologous thymidine kinase promoter and luciferase open reading frame. Transient transfection assays showed that both fragments increased promoter activity in SW480 colon cancer cells and induction of either dnLEF-1 or treatment with XAV939 eliminated this regulation (Fig. 2.7F). We also tested these fragments for their ability to regulate the PDK1 promoter (Fig. 2.8). While both regions conferred a distinct, modest level of activation, the PDK1 promoter itself was markedly sensitive to downregulation by dnLEF-1 (Fig. 2.8). These data demonstrate that PDK1 is a direct Wnt target gene and that regulation occurs through distal regulatory sites upstream and downstream of the locus.

PDK1 overexpression rescues the altered metabolic phenotype induced by blocking Wnt

To determine how much of the Wnt-driven metabolic signature depends on PDK1, we asked whether restored expression could rescue the metabolic shift induced by dnLEF-1. We used lentiviral infection of DLD-1 cells to restore physiological levels of PDK1. As shown in Figure 2.9A, dnLEF-1 expression alone led to a decrease in endogenous PDK1 levels and a decrease in glycolysis (a shift in the FLIM phasor position away from free NADH). In contrast, lentiviral restoration of normal PDK1 levels rescued the FLIM signature of glycolysis (a return of the phasor position back to that of cells not expressing dnLEF-1; Fig. 2.9A). This rescue is



Peak 1: Chr2 173390266-173391125

CTGGGCACTCTGAAAAGGAACAGGATAACAGCGATTTTCAGGGAACAAGGGAGATAACCATAAGGTCTGACTGCCTGTGGGGCTGGGCAGAAC
 AGAGTCATATTTTTCTTTTTACAGAAAGCAAATAGGAGAAATATCACTGAATTCCTTTCCAGCAAGGAATAACCCAGGGAAAGGACTGCATTCC
 CAGGGGAGGTCTACGGACTGCCACTCTGGGAGTGTCTGCCTATGCGATTGAAGACAAGGGATGAAATACGCCCTGGTCTCCCGCAGTGCCC
 TCAGGCTTGCTAGGATTAGGAAATCCAGCCTGGTGAATTCTAGTCAGACAGGTTGTCAGCTCTCAAACCCCTGTTTCCTGTTAAGATGTTTACCA
 ATGACAATGCATGCCAGTGGGACATGGAACCTTATCAGTAATTCTAATTCGCCCCTGGCCTTGATCTTGCTCTGCCTCTCTGCCTTGTGAT
 CTTTTATTGCCCTTTGAAATGCATGTGATCTTTGTGACTTACTCCCTGCTCGTACCCCTCTCCCTTTTGAAATTCCTAATAAAAAACATGCTGTTTT
 GCGGCTCACAGGGCATCACGGAACCTGCCAATATGTGATGCACCCCGGAGGCCTAGCTGTAATAATTTCTCTCTTTCTCTTTATT
 TCTCAGACCCGCCGATACTTAGGGAAAACAGAAAGGACCTACGTTGAAATATTGGGGGCTGGTTCCCCCACTATAAACAGCATATTAACAGCA
 GCTGCAGGCATACAAGAGGGATTGAGGTATCCCCCACTGCCACATAGCACCTTATAACCACCCTCCCAAAGTGGATTCTGGAACATGCGTTC
 CCACTCTTGAT

Peak 2: Chr2 173469007-173469305

GCCACCTCAAGGGATCCACCTGCCTTGGCCTCCCAAAGTCTGGGATTTATAAGCGTGAGTCACCGTACCTGGCCAGACATAGCATATATCTTC
 CTTTACATAGATTGCCTTTGATTTCTTTCAATTGTTACTTTGATGTTTTCAGCTTACAGATTCCGCGCATATTTTGTAGACTTAAATCTAAGTATTG
 CTTTTTTTTAACTTACAAATTTTTTAAAAAACGTTTTTCTCTCCAATGTTCAATTGCTAATACATTTACGTTTGAATCTCCAGTTCAGAAAAATC
 ATGGCCTC

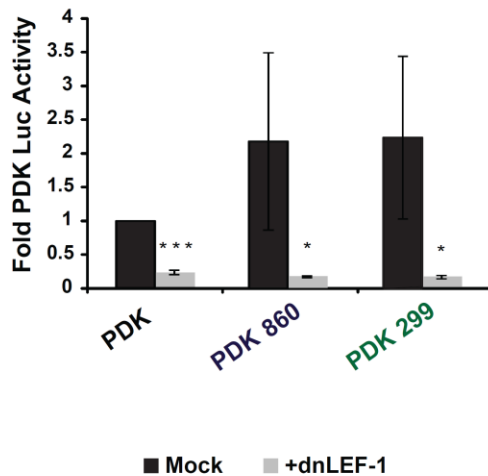


Figure 2.8. *PDK1* transcription is directly regulated by LEF/TCFs and Wnt signaling.

Two distal regulatory regions located approximately 30kb upstream and 48kb downstream from the *PDK1* transcription start site (+1) that are occupied by dnTCF-1E contain three putative Wnt Response Elements (highlighted in red). Each region (schema in top panel) was subcloned 5' of the *PDK1* promoter (-257, +36) and luciferase open reading frame. Transient transfection analysis of more than three independent experiments in SW480 cells show that each fragment increases transcription by two-fold and that co-expression of dnLEF-1 reduces activity of these promoter constructs to below the baseline activity of the *PDK1* promoter. Graph shown represents the average of three trials (+/- S.D.; *p-value<0.05; ***p-value<0.001). (Figure is adapted from Figure S4 of Pate, Stringari, Sprowl-Tanio et al., 2014).

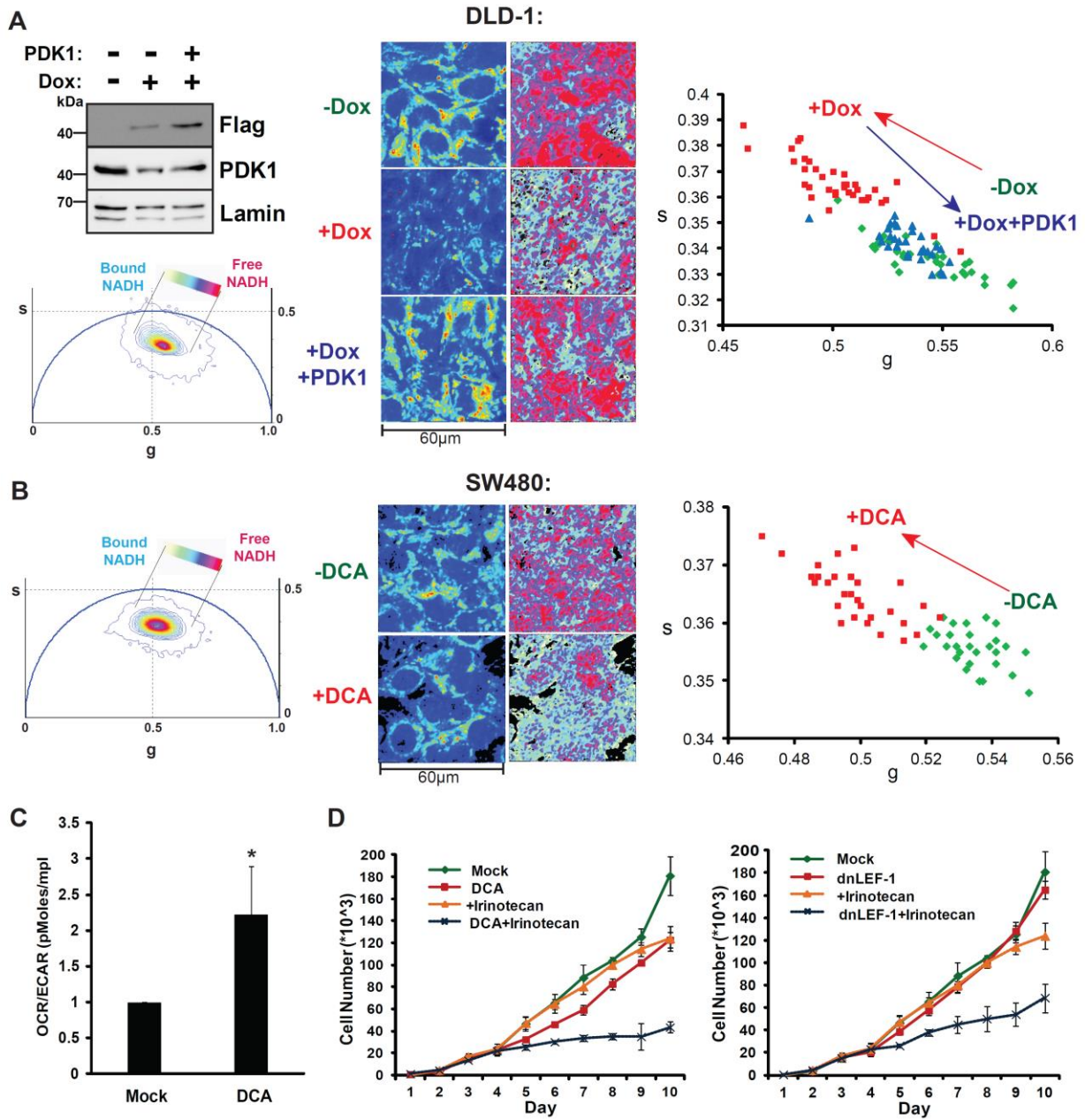


Figure 2.9. PDK1 overexpression rescues the altered metabolic phenotype induced by blocking Wnt.

(A) Western blot analysis of lysates collected from DLD-1 dnLEF-1(2) cells treated with or without 0.01 μ g/ml doxycycline for 24h and with or without PDK1 lentivirus for 72h. FLIM imaging was performed at confluency (96h doxycycline and 7 days post transduction). Intensity images are shown on the left. FLIM results, shown through the free:bound NADH color mapping (right), as well as the scatterplot, show that doxycycline induction of dnLEF-1 shifted the phasor toward bound NADH, while PDK1 rescue shifted it back to its original position ($p < 0.0001$ comparing -Dox to +Dox and comparing +Dox to +Dox+PDK1). (B) FLIM analysis of SW480 cells treated with 50mM DCA for 48h shows a phasor shift toward bound NADH ($p < 0.0001$ comparing +DCA to mock). (C) OCR/ECAR ratio of DCA (10 mM) treated SW480 cells shows that blocking PDK1 activity doubles the oxygen consumption rate (mitochondrial activity) relative to the extracellular acidification rate (glycolysis-produced lactate). Data shown represents the average of three independent trials (\pm S.D.; * p -value <0.05). (D) Sulforhodamine B proliferation assay of SW480 cells treated with or without 2.5 μ M Irinotecan, 20 mM DCA, and dnLEF-1 lentivirus shows an increased sensitivity to Irinotecan when treated with DCA or dnLEF-1. A representative graph of two trials is shown. Error bars represent the standard deviation between eight internal replicates. (*Figure adapted from Figure 5 of Pate, Stringari, Sprowl-Tanio et al., 2014*).

also evident in the free:bound NADH color mapping of the cells, showing similar levels of free:bound NADH in cells without doxycycline compared to cells with doxycycline and PDK1. When repeated in the second DLD-1 clonal line expressing dnLEF-1, a rescue of the FLIM signature was similar, indicating at least a partial rescue in the metabolic shift (Fig. 2.10). Taken together these results suggest that reduction of PDK1 could be a major reason for the metabolic shift triggered by dnLEF/TCF interference with Wnt/ β -catenin signaling.

Given that we propose PDK1 expression as a major Wnt target for glycolysis, we compared the effects of dnLEF/TCF to dichloroacetate (DCA), a well-known small molecule inhibitor of PDK1¹⁰⁶. A 48 hour treatment of DCA led to the same characteristic shift in the phasor plot toward bound NADH that was seen with expression of dnLEF/TCF, again indicating a decrease in a glycolytic phenotype (Fig. 2.9B). The FLIM shift corresponded to an increase in the ratio of oxygen consumption (oxidative phosphorylation) relative to the extracellular acidification rate (OCR/ECAR, Fig. 2.9C). These changes in metabolic metrics match previous reports that DCA treatment decreases lactate excretion¹⁰⁷ and increases ATP levels¹⁰⁸ similar to our measurements with dnLEF/TCF expression. Another reported phenotype of DCA treatment in cancer cells is an increase in sensitivity to chemotherapy treatment¹⁰⁹⁻¹¹¹. Therefore, we examined whether dnLEF-1 forced similar increases in sensitivity to the chemotherapeutic agent Irinotecan. We treated SW480 cells with DCA alone, dnLEF-1 alone, DCA with Irinotecan or dnLEF-1 with Irinotecan. Neither 2.5 μ M Irinotecan nor dnLEF-1 alone had much effect on cell proliferation and 20 mM DCA had only a very slight impact. In contrast, both DCA and dnLEF-1 greatly enhanced the sensitivity of the cells to Irinotecan, showing a synergistic decrease in the proliferation rate (Fig. 2.9D). These data suggest that dnLEF/TCF inhibition of PDK1 in many ways mimics the effects of DCA. However, while there was congruence between dnLEF/TCF

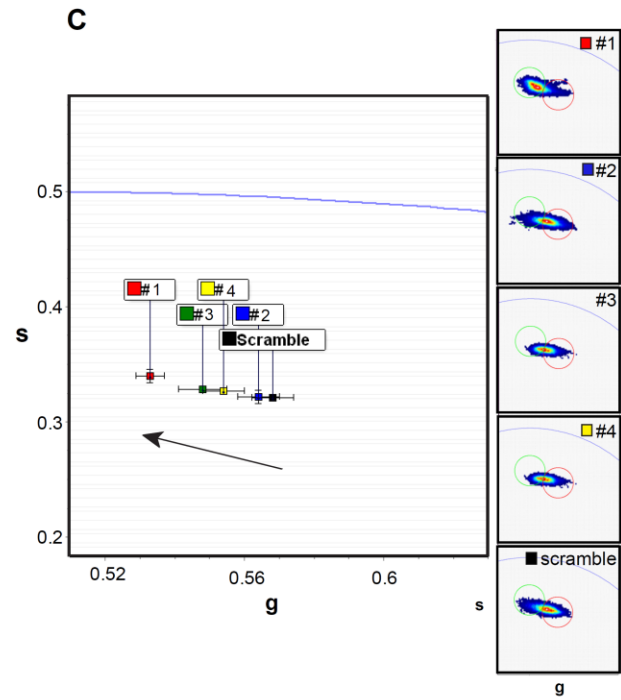
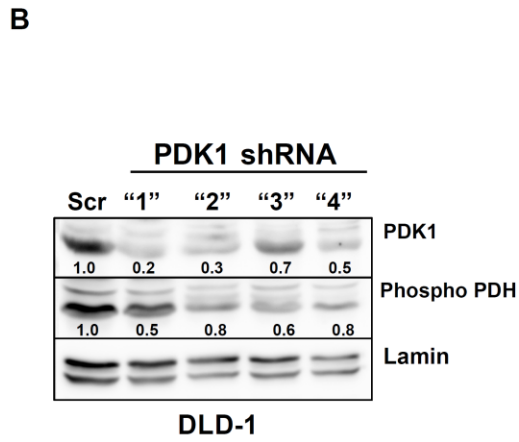
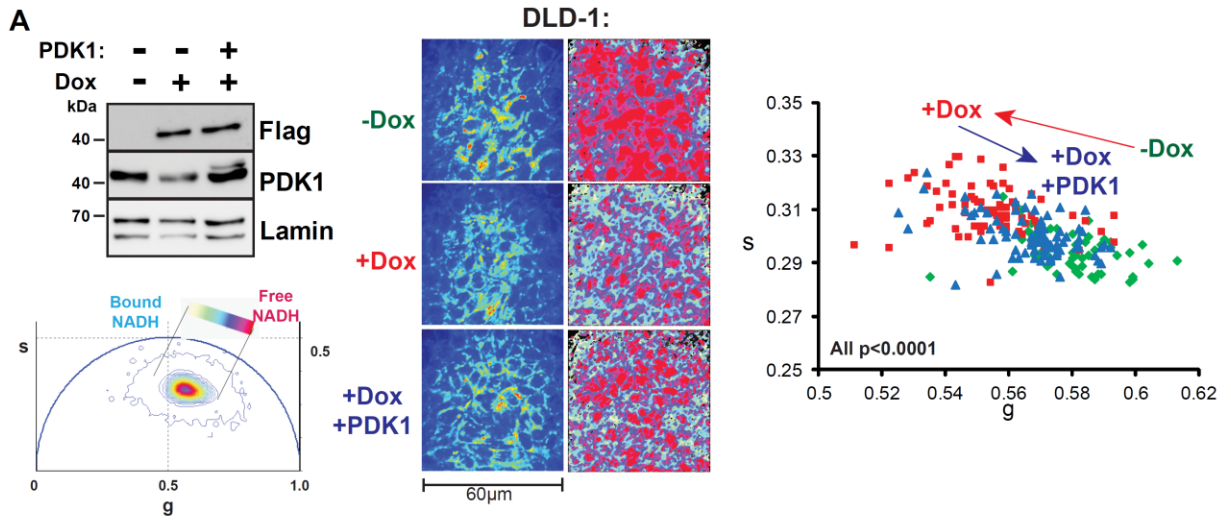


Figure 2.10. PDK1 overexpression rescues the altered metabolic phenotype induced by dnLEF-1.

(A) Western blot analysis of lysates collected from DLD-1 dnLEF-1(1) cells treated with or without 0.01 $\mu\text{g/ml}$ doxycycline for 24h and with or without PDK1-expressing lentivirus for 72h. FLIM imaging was performed at confluency (96h doxycycline and 7 days post transduction). Intensity images are shown on the left column of panels. FLIM results, shown through the free:bound NADH color mapping on the right-hand column of panels. A scatterplot summarizes multiple cells in multiples images and shows that doxycycline induction of dnLEF-1 shifted the phasor toward bound NADH, while PDK1 rescue shifted it back to its original position (p-value < 0.0001 comparing +Dox to -Dox and comparing +Dox+PDK1 to +Dox).

(B) Western blot analysis of lysates collected from DLD-1 cells stably selected for lentiviral expression of either scramble or PDK1-specific shRNAs (#1, #2, #3, #4). The indicated antibodies probe for PDK1 protein and phosphorylation of Pyruvate Dehydrogenase (ser293). Numbers represent fold over scramble after signal in each lane was normalized to the loading control (lamin). (C) FLIM analyses of NADH in shRNA-expressing cultures show that knockdown of PDK1 shifts the average phasor position toward greater bound NADH compared to scramble shRNA cultures. Error bars represent the standard deviation of each phasor position in each culture (all cytosol pixels in N=4-6 regions). Thumbnail phasor histograms show the phasor position for all cytosolic pixels in all regions. The green and red circles are drawn in the same position on each plot so that changes in the location of the phasor histogram can be easily discerned. (Figure adapted from Figure S5 of Pate, Stringari, Sprowl-Tanio et al., 2014).

and the DCA phenotypes, DCA targets all four members of the PDK family, not just PDK1. We therefore used lentiviral shRNA knockdown to test for the specific significance of PDK1 (Fig. 2.10B,C). Western blot analysis of multiple knockdown lines revealed reduced PDK1 protein levels and significant reduction of phosphorylation of its main substrate, mitochondrial Pyruvate Dehydrogenase (PDH_{pSer293}, Fig.2.10B). FLIM analysis of each knockdown cell line revealed significant shifts in the free:bound NADH signature that mimic the decrease in glycolysis observed with dnLEF1 or dnTCF1 expression or DCA treatment (Fig. 2.10C). These results indicate that PDK1 is an important Wnt target gene and that it contributes major activities to glycolysis. However, we also observed the knockdown cultures to revert to a glycolysis mode of metabolism several days later. Western blot analysis of the reverted cultures showed that while PDK1 protein levels remained low, phosphorylation of the target substrate Pyruvate Dehydrogenase had recovered, a sign of compensatory rescue via other PDK family members or other kinases (*data not shown*). Thus, the more stable shift in metabolism observed with DCA treatment or dnLEF1/dnTCF expression suggests that total cellular PDK activity is targeted by Wnt signaling beyond single, selective regulation of PDK1. We conclude that PDK1 is a major Wnt target gene, but that it is coordinately regulated within an entire gene program for glycolysis.

Blocking Wnt reduces *in vivo* tumor growth

Since growing cells *in vitro* (on plastic) does not accurately mimic the metabolic demands of an *in vivo* tumor, we tested the impact of dnLEF/TCF expression on cancer cells in a xenograft tumor model. As shown in Figure 2.11A, expression of dnLEF-1 or dnTCF-1Emut in SW480 cells injected into immune-deficient-NOG mice drastically decreased tumor growth by

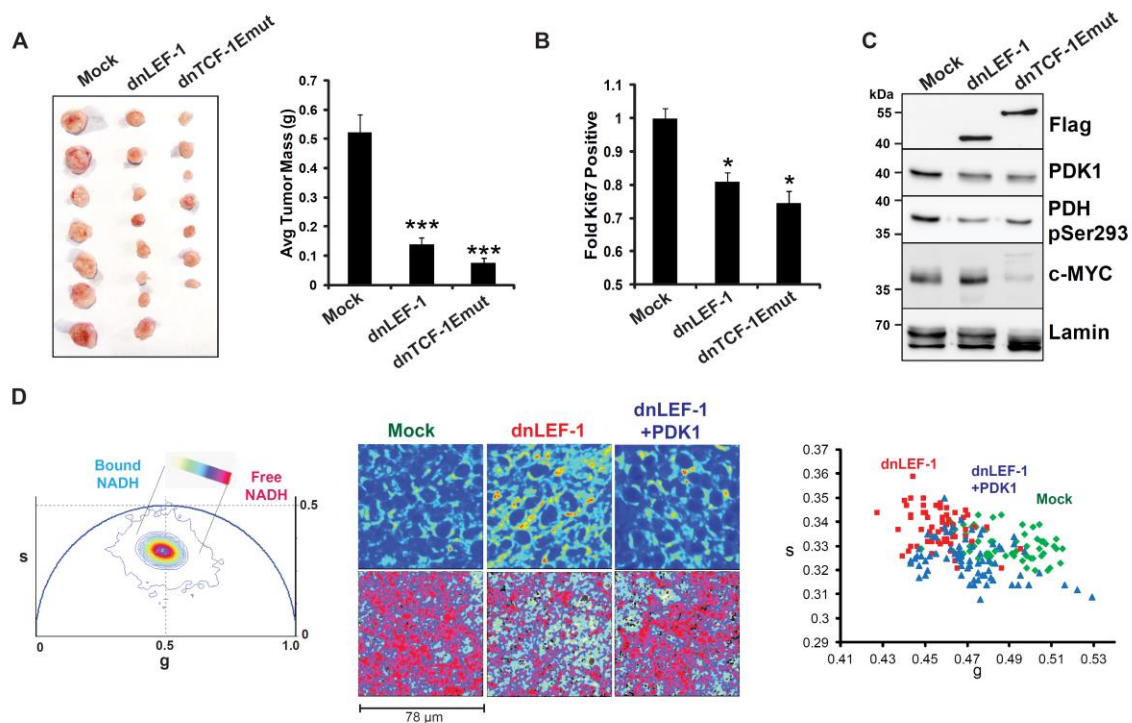


Figure 2.11. Blocking Wnt reduces *in vivo* tumor growth.

(A) Expression of dnLEF-1 or dnTCF-1Emut in SW480 cells results in smaller xenograft tumors. Images of tumors are shown with quantification of the tumor mass and volume at the time of harvest. Data includes measurements of eight tumors for each condition. Error bars represent the S.E.M. among eight replicates (** p -value<0.001). (B) Ki67 staining of paraffin-embedded sections from xenograft tumors shows fewer Ki67-positive cells with dnLEF-1/dnTCF-Emut expression. Data shown represent the average of counts from at least eight fields. Error bars represent the S.E.M. among at least eight replicates (* p -value<0.05). (C) Western blot was performed on protein lysates prepared from freshly-extracted xenograft tumors. Western blot analysis of endogenous PDK1 and its target, Pyruvate DeHydrogenase (pSer293-PDH) shows decreases when dnLEF-1 or dnTCF-1Emut are expressed. cMYC expression shows variable levels of expression. (D) Phasor plot representation for the color mapping of *in vivo* tumor FLIM analysis, fluorescence intensity (top image panels), FLIM color mapping (bottom panels) and scatter plot analysis are as described in Figure 2.9 except that these analyses were performed on living, surgically exposed, yet still actively perfused, xenograft tumors. Both the free:bound NADH color mapping (bottom row) and scatter plot (average phasor position of individual cells within each tumor) show a shift in the phasor position toward bound NADH with dnLEF-1 expression and a return to free NADH with PDK1 overexpression (p <0.0001 comparing dnLEF-1 to Mock and comparing dnLEF-1+PDK1 to dnLEF-1). A minimum of three fields of view per tumor were analyzed. Data shown is from one mouse representative of eight replicates (additional tumor analysis in Figure 2.13). (Figure adapted from Figure 6 of Pate, Stringari, Sprowl-Tanio et al., 2014).

up to 90%. The tumors created from cells expressing dnLEF/TCF had 20%-30% fewer proliferating cells as measured by Ki67 staining (Fig. 2.11B). To compare the changes in protein expression *in vivo* with the previous results *in vitro*, we used Western Blot analysis to examine levels of PDK1 and c-Myc. PDK1 protein was reduced in both dnLEF/TCF tumor types. Levels of c-Myc protein were variable but overall similar between the dnLEF-1 expressing tumors compared to mock, while c-Myc protein was significantly reduced in the dnTCF-1Emut tumors (Fig. 2.11C). These results are consistent with the previously described microarray which showed a decrease in c-MYC RNA levels with dnTCF-1Emut, but not dnLEF-1²⁹. Western blot analysis also revealed stable reduction of pyruvate dehydrogenase phosphorylation in both dnLEF/TCF tumor types (PDHpSer293; Fig. 2.11C). Overall, the tumor analysis suggests that while tumors expressing dnLEF/TCF show similar reductions in PDK1 as cells *in vitro*, the expression of dnLEF/TCF has a much different effect on cell growth: no change *in vitro* but a strong, negative effect on growth *in vivo*.

To test whether the same change in metabolism that we detected *in vitro* by FLIM analysis is also detected *in vivo*, we adapted FLIM analysis for living, actively-perfused xenograft tumors. For all tumors, tail vein injection of fluorescent dextran (FITC-dextran) was used to continuously image live blood cell flow through the vasculature of the tumor. Mice were anesthetized and intact xenograft tumors were exposed (with feeder vessels preserved) followed by immediate stabilization of the mice over the microscope objective in a temperature-controlled environment. Non-invasive, confocal FLIM imaging was performed at depths between 50 μm to 200 μm around the sub-capsular region of the tumors (schematic of *in vivo* FLIM Fig. 2.12). A similar metabolic response to Wnt signaling inhibition was observed with these analyses. That is, dnLEF/dnTCF1 expressing tumors were less glycolytic (phasor position shifted towards bound

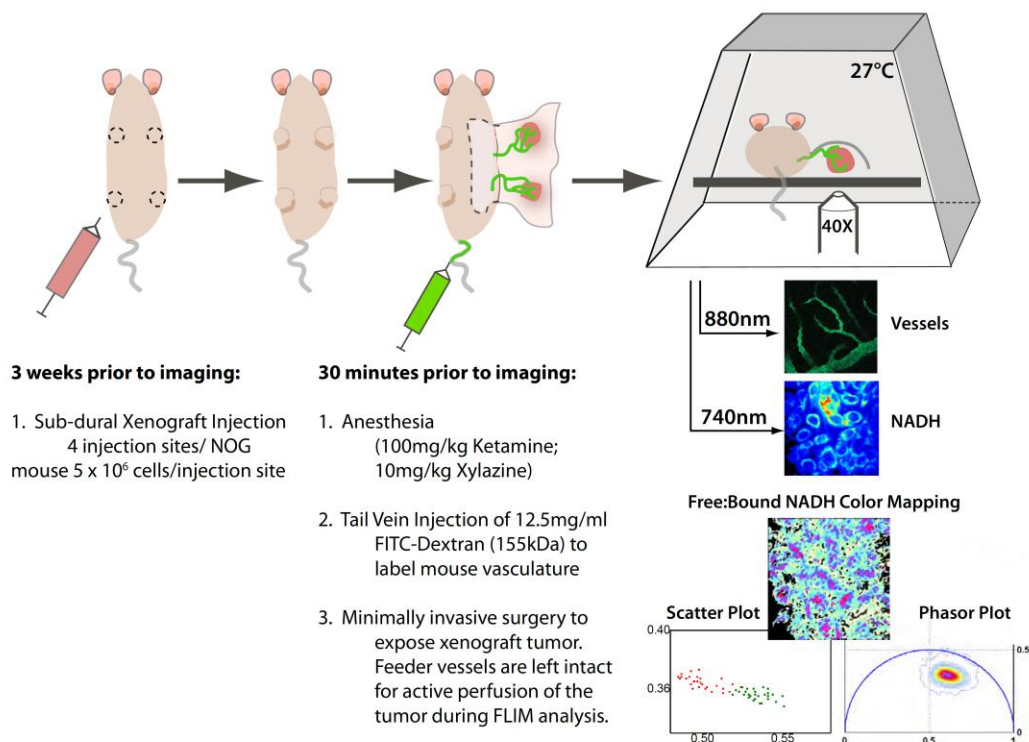


Figure 2.12. Fluorescence Lifetime Imaging (FLIM) of live xenograft tumors.

Xenograft tumors were grown for 3-4 weeks in NOG mice before imaging. The schematic shows how tumors are exposed on the day of imaging. A temperature controlled environment was constructed for the microscope stage and continuous monitoring of blood flow through FITC-labeled vessels ensured that xenograft tumors were actively perfused throughout the imaging session. Tumors (four per mouse) were successively exposed via surgery (with feeder vessels to the tumor preserved for adequate perfusion) immediately prior to imaging. Multiple image fields were captured at depths that ranged from 50 μ m to 200 μ m over a 30 minute to 1hour period. (Figure adapted from Figure S6 of Pate, Stringari, Sprowl-Tanio et al., 2014).

NADH; Fig. 2.11D). A notable difference compared to cells grown in monoculture *in vitro* was that xenograft tumors had a greater degree of variability in FLIM profile, reflecting the existence of a more complex tumor microenvironment (additional replicates shown in Fig. 2.13). To test whether PDK1 expression could rescue this effect, we imaged xenograft tumors of dnLEF-1 cells that had been lentivirally transduced with a PDK1 expression vector prior to injection into the mice. PDK1 expression rescued the metabolic signature, shifting the phasor plot back toward the free NADH position (Fig. 2.11D, 2.13).

Blocking Wnt reduces tumor vessel density, while reintroduction of PDK1 restores it

Much of the cost and benefit analysis of glycolytic metabolism has focused on intracellular changes in metabolites and biosynthetic intermediates. However, imaging live tumors highlighted a striking extrinsic benefit of glycolytic metabolism on the tumor microenvironment. FITC dextran labeling of the vasculature revealed that the density of blood vessels was greatly diminished in dnLEF/TCF expressing tumors (Fig. 2.14A). Thus, one important reason these dnLEF/dnTCF-expressing tumors were reduced in size was because of poor nutrient delivery. Interestingly, re-expression of PDK1 strictly in the injected tumor cells appeared to restore vessel density to levels equivalent to that of the mock tumors (Fig. 2.14A). To quantitate these changes, we stained tumor sections for the endothelial marker CD31 and counted vessel density in the same sub-capsular region where the FLIM analysis was performed. Vessel density was greatly diminished in the tumors expressing dnLEF-1 or dnTCF-1Emut, but, rescue-expression of PDK1 returned vessel density back to the original level observed in the mock tumors (Fig. 2.14B). A few studies have shown that enhanced glycolysis can promote angiogenesis through stabilization of HIF1 α ¹¹²⁻¹¹⁴. We therefore evaluated HIF1 α protein levels

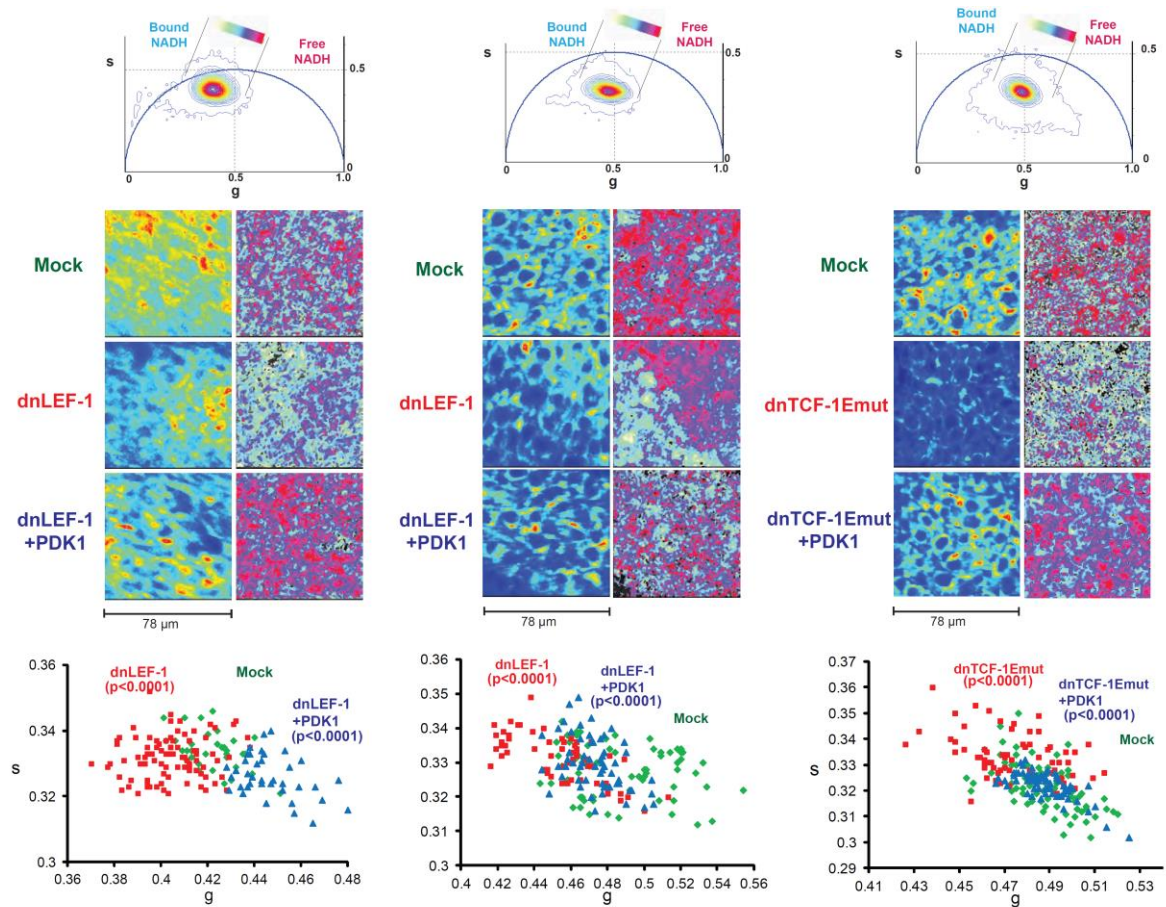


Figure 2.13. Blocking Wnt alters the metabolic program of colon cancer cells *in vivo*. FLIM analysis was performed on actively-perfused xenograft tumors within live mice. Both the free:bound NADH color mapping (images on right) and scatter plot (which show the average phasor position of cells within each tumor) show a shift in the phasor position toward bound NADH with dnLEF-1 expression and back toward free NADH with PDK1 overexpression. At least three fields of view per tumor were analyzed for the scatterplot analysis. Each column of data was generated from a different mouse, representative of a total of eight mice analyzed. (Figure adapted from Figure S7 of Pate, Stringari, Sprowl-Tanio et al., 2014).

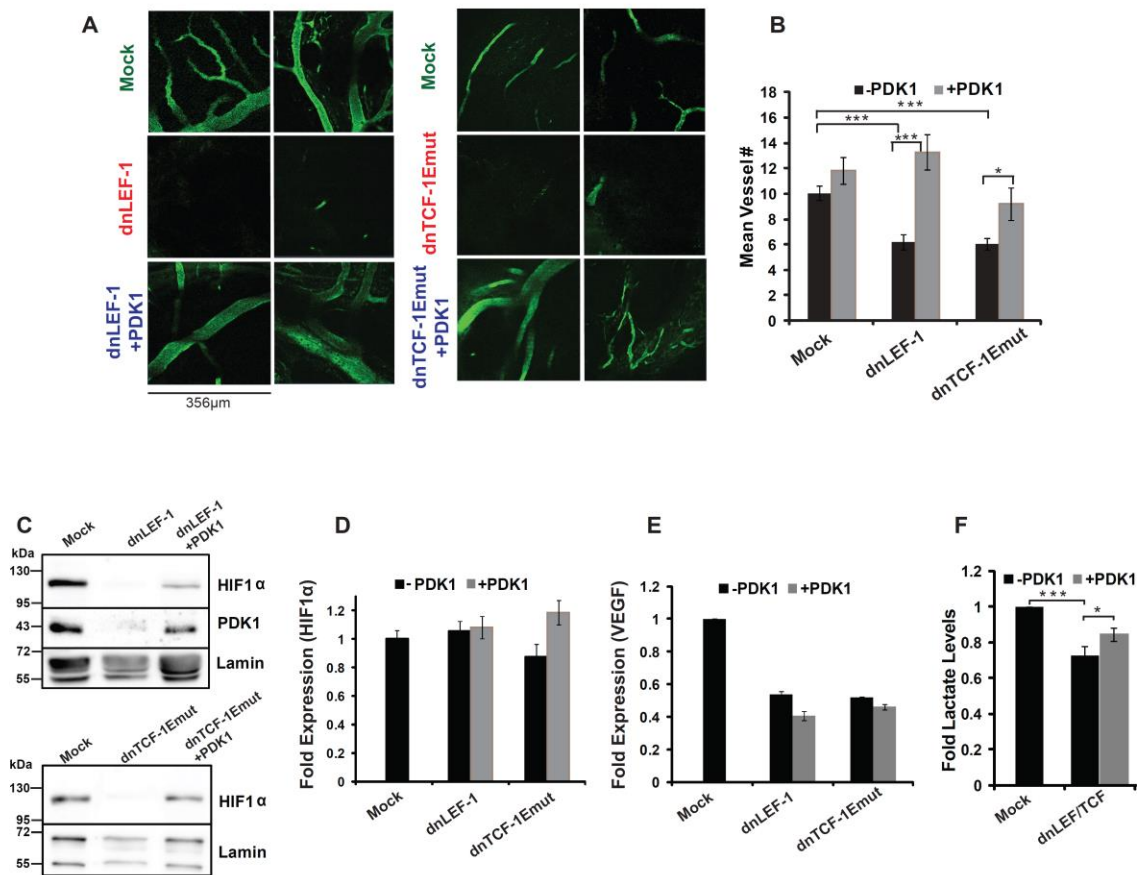


Figure 2.14. Blocking Wnt reduces tumor vessel density, while reintroduction of PDK1 restores it.

(A) Tumor vessel density within the sub-capsular region is greatly diminished with dnLEF/TCF but is restored with PDK1 expression. Images show FITC dextran labeled vasculature in the xenograft tumors (~50-200 μm deep). (B) Quantification of vessel density derived from the CD31 staining of paraffin-embedded sections of each tumor. For quantification, the number of vessels per field of view (40x objective) were averaged from every cross section (at least 20 for each condition) within the subcapsular region for each tumor. Error bars represent the S.E.M. among at least 20 replicate fields. (C) Western blot analysis was performed on protein lysates prepared from freshly-extracted xenograft tumors. (D) RT-qPCR analysis of *HIF-1 α* and (E) *VEGF* expression in xenograft tumor RNA. *HIF-1 α* mRNA levels do not change among the various tumors (normalized to *GAPDH*), but *VEGF* expression levels are down in the dnLEF-1 and dnTCF-1Emut tumors. However, PDK1 rescue expression does not change the levels of either *HIF-1 α* or *VEGF* mRNA. RT-qPCR data shown are representative of four replicate tumor sets. Error bars represent the standard error between three internal replicates. (F) Lactate levels in dnLEF/TCF expression tumors are reduced compared to MOCK levels and are partially restored with PDK1 rescue expression. Data shows the average fold lactate levels (compared to mock) in five tumors for each condition, with error bars representing the S.E.M. (*p-value<0.05; ***p-value<0.001). (Figure adapted from Figure 7 of Pate, Stringari, Sprowl-Tanio et al., 2014).

in the xenograft tumors. Interestingly, HIF1 α protein levels were reduced upon dnLEF/TCF expression, and levels were at least partially restored with reintroduction of PDK1 (Fig. 2.14C). HIF1 α mRNA levels were unaffected and stable in all conditions (Fig. 2.14D), suggesting that regulation occurs at a post-transcriptional step. We also note that while the well known angiogenic factor VEGF was downregulated in the dnLEF/TCF expressing tumors. Addition of PDK1 did not restore these levels (Fig. 2.14E), suggesting that the PDK1 rescue of angiogenesis is VEGF-independent. Overall, dnLEF/TCF expression *in vivo* reduced tumor growth, reduced PDK1 levels, reduced the glycolytic metabolic signature (including tumor lactate levels, Fig. 2.14F), and reduced the density of blood vessels feeding the tumor. Restoration of PDK1 expression rescued both the change in metabolism as well as the reduction in vessel density, a striking demonstration of cell-autonomous and non-autonomous effects of a metabolic enzyme.

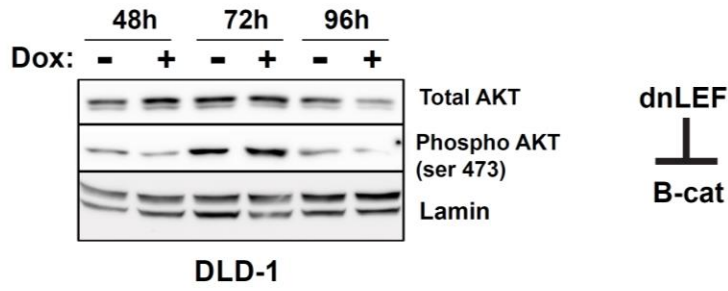
Discussion

We report that Wnt/ β -catenin signaling directs a metabolic program of glycolysis in colon cancer cells, a common cancer phenotype known as the Warburg effect. This metabolic change is accompanied by non-autonomous effects on the microenvironment in the form of increased vessel development. A direct Wnt target gene, PDK1, is identified to participate in both of these Wnt-driven, cancer-supporting phenotypes (model in Fig. 5.1A). We also describe for the first time the use of FLIM imaging to detect metabolic changes in living, actively-perfused xenograft tumors. We suggest that effects on metabolism are a common, core function of all LEF/TCF family members and isoforms, even those isoforms previously understudied due to their lack of regulation of proliferation and the cell cycle.

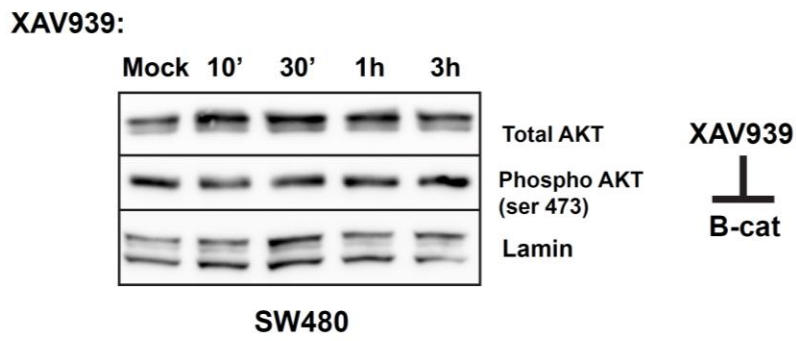
A prevailing theme in the field of cancer metabolism is that the same oncogenic pathways that drive transformation must also favor metabolic pathways that support this process⁷⁴. In fact, given that Wnt signaling plays a critical involvement in embryonic development, tissue remodeling and cancer biology, and given that the success of these processes depend on tight coordination with the metabolic pathways that support them, it has been suggested that Wnt is a prime candidate for directing this coordination⁸⁰. Our study supports this paradigm as we demonstrate that blocking Wnt target gene activation alters cancer cell metabolism by reducing aerobic glycolysis. Two recent studies also support this conclusion. One study in breast cancer cells found that activation of Wnt signaling enhanced glycolysis through indirect actions of the transcriptional repressor Snail on cytochrome c oxidase, a component of the electron transport chain¹¹⁵. A second, more recent study found that Wnt stimulates a fast-acting, short-term Wnt-Lrp5-Rac1-mTORC2-Akt signal to upregulate protein and activity levels of glycolytic enzymes, including PDK1⁸¹. Regulation occurred within 10-20 minutes of Wnt stimulation and was independent of β -catenin, LEF/TCFs and transcription. Our findings contrast with this system because we find that β -catenin and LEF/TCF are required to directly target *PDK1* transcription. Indeed our test for a connection to mTORC2 was negative as inhibition of β -catenin with either dnLEF/TCF expression or XAV939 treatment for as long as three hours had no effect on mTORC2 activity in DLD-1 and SW480 cells, and inhibition of mTORC2 for 24 hours with the specific mTOR inhibitor PP242 had no effect on *PDK1* mRNA levels (Fig. 2.15).

We propose that Wnt signals have short-term and long-term modes of metabolic regulation. Short-term modes trigger an mTOR kinase cascade that affects protein stability of glycolytic enzymes. Long-term modes use β -catenin to change gene expression of at least some of these enzymes as well as other metabolically relevant components (Fig. 2.1C). This latter

A



B



C

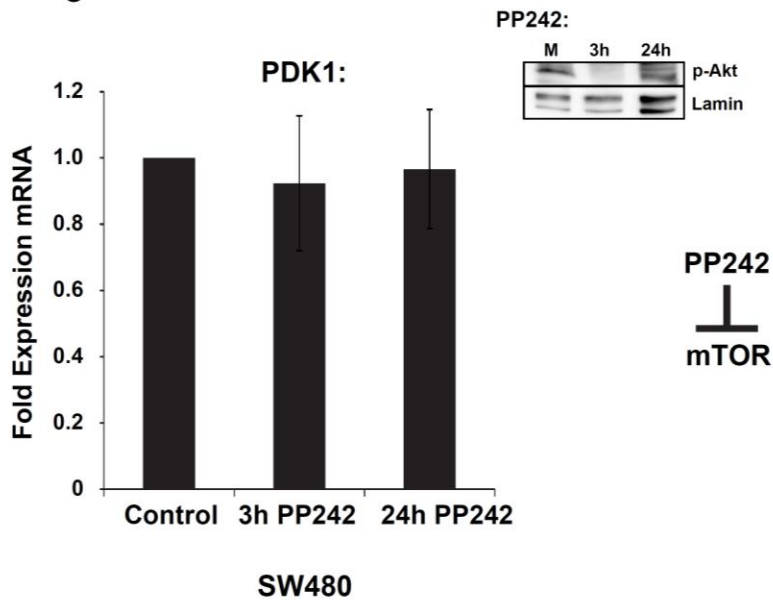


Figure 2.15. β -catenin-dependent Wnt signaling is not coupled to mTORC2 activity.

(A) Western blot analysis of DLD-1 cells treated with doxycycline for the indicated times, or of (B) SW480 cells with the Wnt inhibitor XAV939 (10 μ M) shows that short-term treatments do not change the level of phosphorylated AKT on residue serine 473. (C) RT-qPCR analysis was performed on RNA collected from SW480 cells harvested 3h and 24h after the addition of the active site mTOR inhibitor PP242 (250nM). Data in the bar graph represents the average of three independent trials with error bars representing the S.D. among the three biological replicates. Western blot inset of whole cell lysates from SW480 cells shows relative levels of phosphorylated AKT on residue serine 473 at matching timepoints. Blocking total cellular mTOR activity has no effect on PDK1 mRNA levels, a result that distinguishes the actions of Wnt/ β -catenin signaling from short term effects on mTORC2 (β -catenin-independent Wnt signaling). (*Figure adapted from Figure S9 of Pate, Stringari, Sprowl-Tanio et al., 2014*).

mode is of primary importance in cancers that harbor aberrant, chronic, elevated levels of Wnt signaling with or without Wnt ligands. Chronic Wnt signaling could transform the metabolic potential of cancer cells by elevating the overall levels of key components for glycolysis and thereby set the stage for robust Warburg metabolism in the face of whatever environment the transformed cells encounter.

PDK1 is a well known, key metabolic regulator of glycolysis. This kinase phosphorylates the pyruvate dehydrogenase (PDH) complex to inhibit the first step of converting pyruvate to acetyl-CoA⁹⁹ an important regulatory nexus between glycolysis and respiration. PDK1 phosphorylation of PDH suppresses entry of fuel into mitochondria and instead promotes glucose fermentation to lactate in the cytoplasm, an important activity for promoting the Warburg effect in cancer. Indeed, PDK1 is upregulated in numerous cancers, including colon cancer^{100–102}. Here we propose that cancer relevant levels of Wnt signaling uses LEF/TCFs for direct regulation of PDK1. *PDK1* mRNA was identified through microarray analysis as downregulated after blocking Wnt in colon cancer cells (Fig. 2.1). Our chromatin immunoprecipitation, 4-Thiouridine labeling, and transient transfection analyses show that this downregulation is direct (Fig. 2.7D-F, Fig. 2.8). Genome-wide ChIP-seq studies by others (ENCODE) also show the *PDK1* gene locus is occupied by TCF-4 (*TCF7L2*) in multiple cancer cell lines (Fig. 2.16). Interestingly, peaks of occupancy are also present in the promoter regions of the other PDK family members, especially for *PDK2* and *PDK4*. It is possible that multiple PDK isoforms have the capacity to respond to Wnt signaling, a possibility underscored by our observation of compensatory recovery of PDH phosphorylation when PDK1 was selectively targeted for knockdown by shRNAs.

In this chapter we identify a new link between Wnt signaling and tumor angiogenesis. Although Wnt has been connected to angiogenesis through direct regulation of VEGF

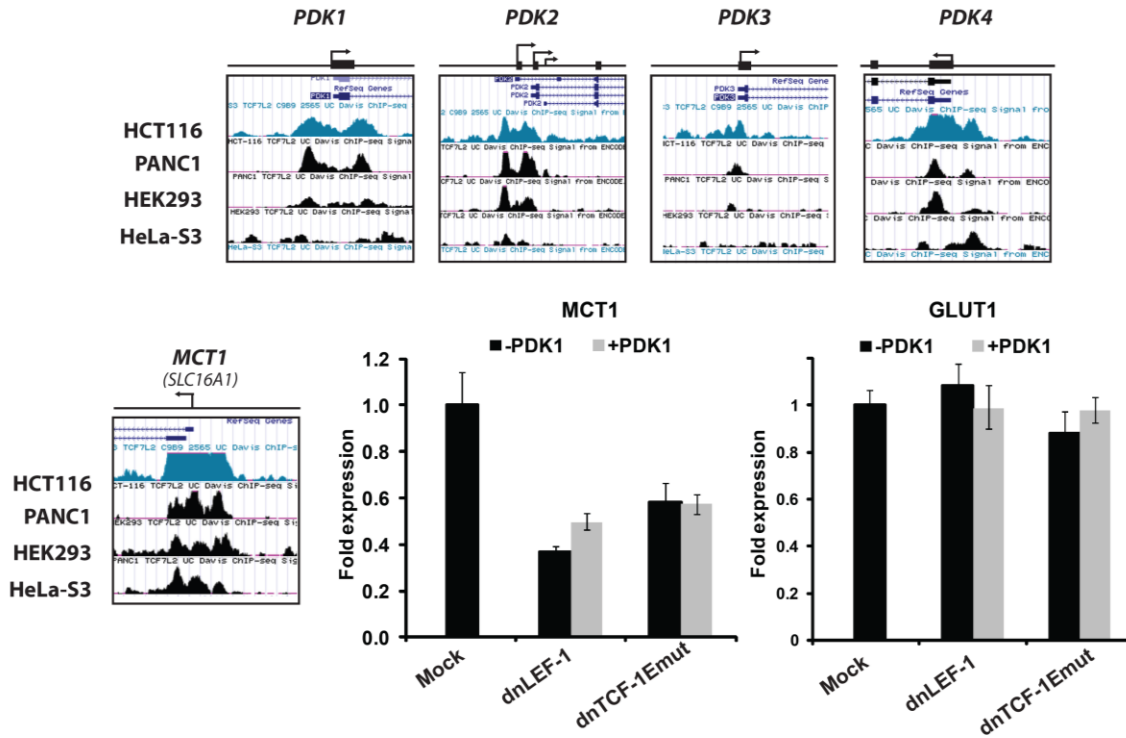


Figure 2.16. TCF-4 occupies the *PDK* and *MCT1* promoters.

ChIP-seq data compiled from the UCSC Genome Browser (assembly Feb. 2009, hg19; <http://genome.ucsc.edu> ¹²⁴), showing *TCF-4* occupancy in four different cell lines over the promoter regions of *PDK1*, *PDK2*, *PDK3*, *PDK4*, and *MCT1*. These data were generated and analyzed by the labs of Michael Snyder at Stanford University; Mark Gerstein and Sherman Weissman at Yale University; Peggy Farnham at University of Southern California; and Kevin Struhl at Harvard. RT-qPCR analysis of *MCT-1* and *GLUT1* was performed on RNA prepared from freshly-extracted xenograft tumors. RT-qPCR data shown are representative of two replicate tumor sets. Error bars represent the standard error between three internal replicates. (Figure adapted from Figure S8 of Pate, Stringari, Sprowl-Tanio et al., 2014).

expression¹¹⁶, we report for the first time the role of Wnt-directed PDK1 expression in this process. Indeed, PDK1 and PDK2 have recently been shown to enhance angiogenesis^{112,117}. We suggest that one mechanism for this phenomenon is increased lactate production because levels of this metabolite were increased in PDK1 rescue tumors (Fig. 2.14F). Lactate has been associated with increased angiogenesis via reduced ADP ribosylation and stabilization of HIF-1 α protein^{113,114,118}. Stabilized HIF-1 α could enhance angiogenesis at least partly through upregulation of VEGF^{119,120} and SDF-1 (stromal cell derived factor-1)¹²¹. While we observe changes in HIF1 α levels that correlate with tumor vessel density, we did not observe concomitant changes in VEGF levels, suggesting that other angiogenic factors such as SDF-1 might be relevant (Fig. 2.14C-E). Even though the exact mechanism linking Wnt and PDK1 to angiogenesis is not known, our discovery that PDK1 rescues vascularization highlights how the metabolic status of cancer cells communicates to the tumor microenvironment.

Consistent with our finding that oncogenic Wnt regulates PDK1, blocking Wnt mimics the effects of small molecule inhibition of the PDK family of kinases through DCA. DCA treatment reduces glycolysis, increases oxidative phosphorylation, decreases lactate production, increases cancer cell sensitivity to chemotherapy drugs, and reduces xenograft tumor mass and vascularity^{107,122}. A DCA trial in human glioblastoma patients resulted in promising tumor regression, as well as enhanced tumor apoptosis, and to note: decreased tumor vascularity¹²³. Collectively, results from multiple studies suggest that the effects of DCA are much more robust *in vivo* than *in vitro*¹²², mirroring our lack of growth phenotype when blocking Wnt in culture, as opposed to the drastic reduction in xenograft tumor size *in vivo*. This could be attributed to the excess nutrients available in *in vitro* culture which can mask dependencies on specific metabolic pathways. More intriguing is the possibility that DCA and dnLEF-1 expression are more

effective *in vivo* because blocking aerobic glycolysis has profound effects on the tumor microenvironment, such as reduced vascularity. Our study therefore has important implications for development of cancer therapies targeting the Wnt pathway and for testing Wnt inhibitors *in vivo*, as inhibitors that do not block proliferation or cell cycle progression in artificial culture conditions *in vitro*, may still be effective at limiting tumor growth *in vivo* via their effects on the more sensitive Wnt-metabolism program. In fact, partial interference with oncogenic Wnt signaling may be an effective treatment strategy as it might normalize metabolic activity in tumor cells while preserving essential Wnt signaling functions in normal cells such as cell cycle and cell differentiation programs.

CHAPTER THREE

Lactate Transporter MCT-1 is a Wnt Target Gene and Confers Sensitivity to 3-bromopyruvate in Colon Cancer

Introduction

Many groups have used overexpression of dominant negative isoforms of LEF/TCF transcription factors (dnLEF/TCFs) in multiple contexts and model systems to identify Wnt target genes^{56,125}. These shorter forms retain the capabilities of full length LEF/TCFs to occupy Wnt Response Elements (WREs) throughout the genome, but they lack the ability to recruit β -catenin. Interference by these dominant negative isoforms represses target gene transcription, and thus, genome-wide expression analysis of downregulated transcription can reveal candidate target genes and the gene programs with which they are associated. We used this type of analysis in Chapter 2 to discover that Wnt signaling promotes colon tumor cell preferences for aerobic glycolysis/ Warburg metabolism, with the Wnt target gene pyruvate dehydrogenase kinase 1 (PDK1) playing a significant role in this metabolic fate. We also observed additional metabolism-linked genes to be sensitive to dnLEF/TCF expression, suggesting that PDK1 is coordinately regulated by Wnt signaling within a larger gene program. One of these additional genes was monocarboxylate transporter 1 (*SLC16A1*, encoding the protein MCT-1), a known lactate transporter observed to be upregulated in many cancers^{126,127}. qRT-PCR analysis of xenograft tumors from a colon cancer cell line showed MCT-1 downregulation in the presence of dnLEF/TCFs, and Chip-Seq ENCODE data shows TCF-4 occupancy of *SLC16A1* in HCT116 colon cancer cells¹²⁸. These preliminary findings strongly implicated MCT-1 as a direct Wnt target gene that might be coordinately regulated with PDK1. In this chapter I show that MCT-1/

SLC16A1 is a direct target gene of β -catenin-LEF/TCF complexes and I define its transcriptional regulation by Wnt signaling in colon cancer cells.

MCT-1 is one of the fourteen members of the *SLC16* family of transporters¹²⁹. While the functions of many MCT family members remain uncharacterized, MCT-1 through MCT-4 are confirmed proton-linked monocarboxylic acid transporters¹³⁰. These four family members have been shown to transport monocarboxylates including acetoacetate, β -hydroxybutyrate, short chain fatty acids, pyruvate, and lactate. In a normal setting, MCTs are necessary for lactate efflux from highly glycolytic/ hypoxic muscle fibers during exercise, and reabsorption or uptake of monocarboxylates from the gut, liver and kidney for gluconeogenesis or lipogenesis– activities tightly linked to aerobic and anaerobic glycolysis¹³⁰. MCT-1 has a reasonably strong affinity for lactate compared to the other MCTs (K_m of 2.5-4.5 mM, compared to MCT-2: $K_m = 0.7$ mM; MCT-3: $K_m = 6$ mM; MCT-4: $K_m = 17$ -34 mM), and it is ubiquitously expressed, while other MCT family members are localized to specific regions of the body at varying levels of expression^{129,131}.

While the increased expression of MCT-1 in response to the physiological stresses of exercise and physical stimulation has been well defined, the precise mechanisms of how it is molecularly regulated are still poorly understood. At the transcriptional level, the *SLC16A1* promoter contains nuclear factor of activated T-cells (NFAT) binding sequences¹³⁰, but its significance is yet unknown. In rat skeletal muscle tissues, PGC α (a transcriptional co-activator linked to regulation of genes involved in energy metabolism) has been associated with MCT-1 upregulation in response to muscle activity¹³². However, no follow-up studies have been conducted to determine whether the *SLC16A1* promoter is subject to its activation. The ribonucleotide metabolite and AMP-activated protein kinase (AMPK) activator, 5-

AminoImidazole-4-CarboxAmide-1- β -D-Ribonucleoside (AICAR), has been shown to upregulate or downregulate *SLC16A1* promoter activity depending on the study and tissue context^{133,134}. Likewise, butyrate, another metabolite and energy source for the colon epithelium, has been identified to enhance transcription and transcript stability of *SLC16A1* mRNA¹³⁵, but the mechanisms and responsive genomic regions behind these effects are not known. Finally, hypoxia was shown to upregulate MCT-1 in human adipocytes¹³⁶, but not in other cell types (including HeLa, COS cells, and cardiac myocyte cell line HL-1¹³⁷). However, MCT-4 is generally considered to be the main transcriptional responder to hypoxia as multiple, high affinity HIF response elements (HREs) have been identified in its promoter¹³⁷.

The observation that MCT-1 expression is increased in cancer has led to studies focused on its regulation in a cancer cells. For example, the tumor suppressor p53 directly binds to the MCT-1 promoter for transcription repression, and therefore loss of p53 in cancer cells promotes MCT-1 mRNA production¹³⁸. c-Myc also directly regulates MCT-1 transcription, especially in cancer cells where high levels of c-Myc drive glycolysis and other metabolic pathways¹³⁹. A common theme among cancer cells is the use of elevated MCT-1 expression to support the glycolytic preference of the cells via its ability to export lactate. This export minimizes the cellular stresses from acid and maintains proper intracellular pH, an activity crucial to their survival¹⁴⁰. Alternatively, a recent study found that MCT-1 primarily exports pyruvate, where co-expressed MCT-4 plays the dominant role in exporting lactate¹⁴¹. Inhibition of MCT-1 transporter activity or downregulation of its protein levels leads to increased oxidative phosphorylation and decreased proliferation¹⁴¹. Taken together, no matter the precise actions of its transporter functions, MCT-1 appears to be a key player in cancer cell metabolism, survival, and proliferation, making it a potentially important candidate target in glycolytic cancer cells.

Recent findings highlight how MCT-1 overexpression may be an exploitable feature for cancer therapy. Birsoy *et al* have shown that breast cancer cells expressing MCT-1 are sensitive to 3-bromopyruvate (3-BP), a molecule that can have anti-proliferative effects by targeting glycolytic enzymes and other metabolic pathways¹⁴². Like its parent molecule pyruvate, 3-BP must be transported across the plasma membrane. Therefore, Birsoy *et al* used genome-wide screening to discover that 3-BP is imported into cells strictly through MCT-1 and no other transporter or alternative pathway. Whether this makes MCT-1 expression the single most important biomarker for determining tumor sensitivity to 3-BP is not yet known as its precise mode of action has not been defined, and only breast cancer cells were used in the study. Nevertheless, this compound is currently being studied in phase I clinical trials for cancer treatment, underscoring the importance of understanding how *SLC16A1* gene expression is regulated. Here we show that MCT-1/*SLC16A1* is a direct Wnt target gene coordinately regulated with other genes that promote glycolysis in colon cancer cells. We define a region in the upstream promoter with at least two WREs and show that the endogenous gene is sensitive to dnLEF/TCF inhibition in multiple colon cancer cell lines, and that transcriptional regulation of MCT-1 by β -catenin/LEF/TCFs is separate and independent from c-Myc action. We demonstrate that colon cancer cells are sensitive to 3-BP and that the sensitivity tracks partially, but not completely, with the strength of oncogenic Wnt signaling. Finally we show that Wnt inhibitors do not synergize with 3-BP to suppress proliferation, but instead interfere with the antiproliferative effects of 3-BP and provide a resistance mechanism for colon cancer cells.

Results

MCT-1 is regulated by Wnt signaling

Our recent discovery showing that Wnt signaling directs colon cancer cells to utilize glycolysis specifically focused on Wnt regulation of target gene pyruvate dehydrogenase kinase 1 (*PDK1*), a mitochondrial kinase that suppresses pyruvate uptake by mitochondria to favor conversion to lactate in the cytoplasm. We utilized a microarray analysis of dnLEF/TCF isoform induction in the colon cancer cell line DLD-1 to reveal novel roles of Wnt signaling in colon cancer. Ontology analysis of the entire gene expression dataset revealed that additional metabolic genes might be coordinately regulated with *PDK1* and contribute to the effect Wnt signaling has on tumor cell metabolism. In this study we focus on the lactate transporter *SLC16A1*/ MCT-1 because it lies downstream of *PDK1* and glycolysis to export lactate, and because it is the importer of 3-BP. We ask if it is directly regulated by β -catenin/LEF/TCF complexes and if this regulation is an important consideration for cancer therapies.

To validate the microarray results in DLD-1 cells and to expand the analysis to additional colon cancer cell lines, we used qRT-PCR analysis to measure how *SLC16A1* mRNA levels change in response to modulation of β -catenin and LEF/TCFs. *SLC16A1* mRNA was purified from SW480 cells (Fig. 3.1A) and SW620 cells (Fig. 3.1B) stably expressing dnLEF-1. In parallel cultures we interfered with canonical signaling by lentiviral transduction of dnLEF-1 to block recruitment of β -catenin to target genes. We found that dnLEF-1 expression reduced *SLC16A1* mRNA to 50% (SW480) and 70% (SW620) of parental levels, suggesting that endogenous LEF/TCF/ β -catenin complexes are contributing to *SLC16A1* transcription. *SLC16A1* mRNA levels were also determined for HCT116 cells with dnLEF-1 (Fig. 3.1C) and doxycycline- induced dnLEF-1 DLD-1 cells for comparison to the microarray analysis (Fig.

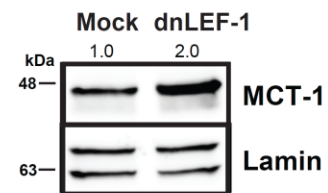
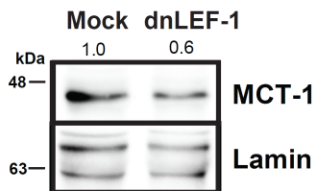
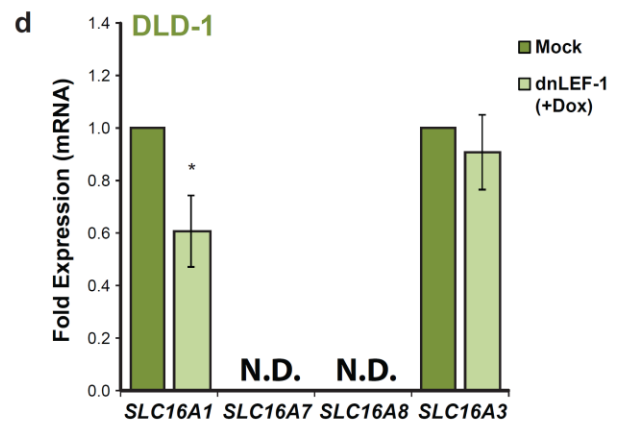
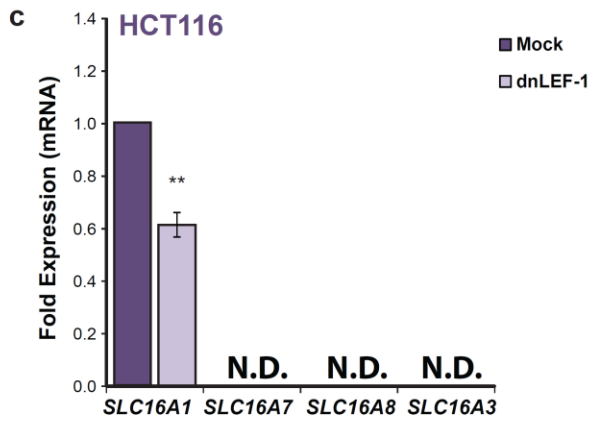
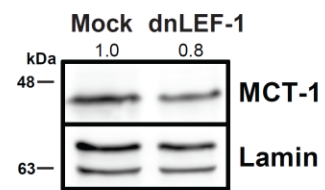
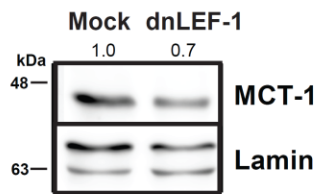
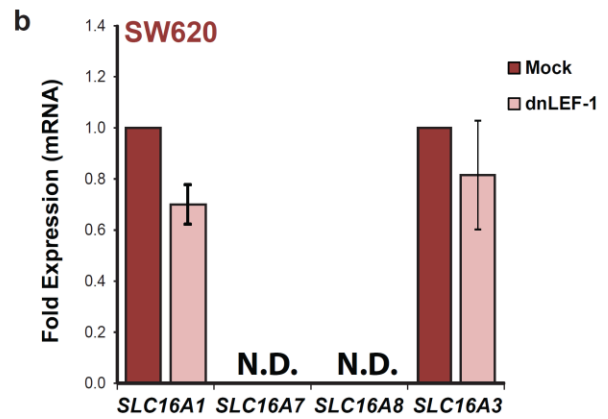
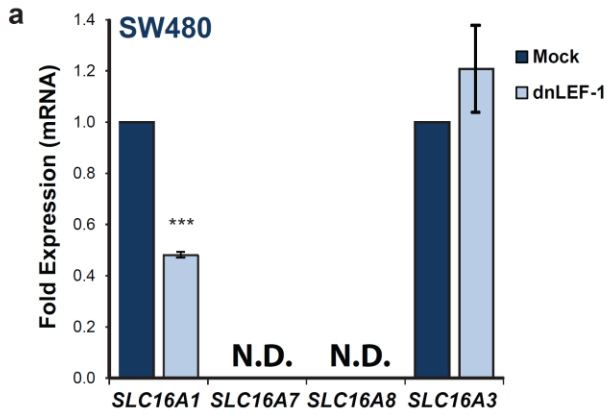


Figure 3.1. Blocking Wnt with dnLEF-1 reduces MCT-1 but not MCT-4 levels.

qRT-PCR analysis was performed on RNA collected from SW480 (A) and SW620 (B) cells stably expressing dnLEF-1. Analysis was also performed for HCT116 cells (C) 72 hours after lentiviral transduction of dnLEF-1 and DLD-1 dnLEF-1 cells (D) harvested 72 hours after the addition of doxycycline. Graphs shown represent the average of three trials (+/- S.E.M.). Whole cell lysates from each cell line (A-D) were harvested concurrently with RNA and were probed with the antibodies shown. (*p-value<0.05; **p-value<0.01; ***p-value<0.001) (*Figure adapted from Figure 1 of Sprowl-Tanio et al., Submitted*).

3.1D). In these latter two cases, we observed a reduction of *SLC16A1* mRNA to approximately 60% of Mock for each cell line.

Since there are four members in the *SLC16* family known to export lactate (MCT1-4), we asked whether any of the other members were also downregulated after inhibiting Wnt signaling. We then performed qRT-PCR analysis of these four genes (MCT-1, MCT-2, MCT-3, MCT-4) in SW480, SW620, HCT116 and DLD-1 cells under the previously mentioned conditions. We found that both *SLC16A7/MCT-2* and *SLC16A8/MCT-3* were undetectable in these four cell lines. As for *SLC16A3/MCT-4*, while the mRNA transcripts were detectable there were no statistically significant fold changes upon inhibition of Wnt signaling, with the exception of HCT116 cells where *SLC16A3* was not detected (Fig. 3.1A-D). We also tested for differences at the protein level using western blot analysis. MCT-1 levels were reduced to 60-80% for SW480, SW620 and HCT116 cells, similar to the reduction observed at the mRNA level (Fig. 3.1A-C). In contrast, DLD-1 cells showed a 2-fold increase in protein level with dnLEF-1 expression, suggesting that MCT-1 may be regulated differently in this cell line compared to the three others (Fig. 3.1D).

We next asked whether MCT-1 levels correlated with the level of Wnt signaling in each cell line. To test this we transfected SW480, SW620, HCT116, and DLD-1 cells with SuperTopflash, a luciferase reporter plasmid regulated by an array of seven WREs and a minimal promoter¹⁴³. Each cell line exhibited varying levels of Wnt signaling as reported by the SuperTopflash activity with SW480 cells showing the highest level of activity by far. SW620 cells had 35 fold less activity in comparison, and HCT116 and DLD-1 cells exhibited the lowest levels (Fig. 3.2A). We hypothesized that if *SLC16A1* is a direct target of Wnt signaling, the relative level of mRNA in each of the cell lines would correlate with the activity level of the

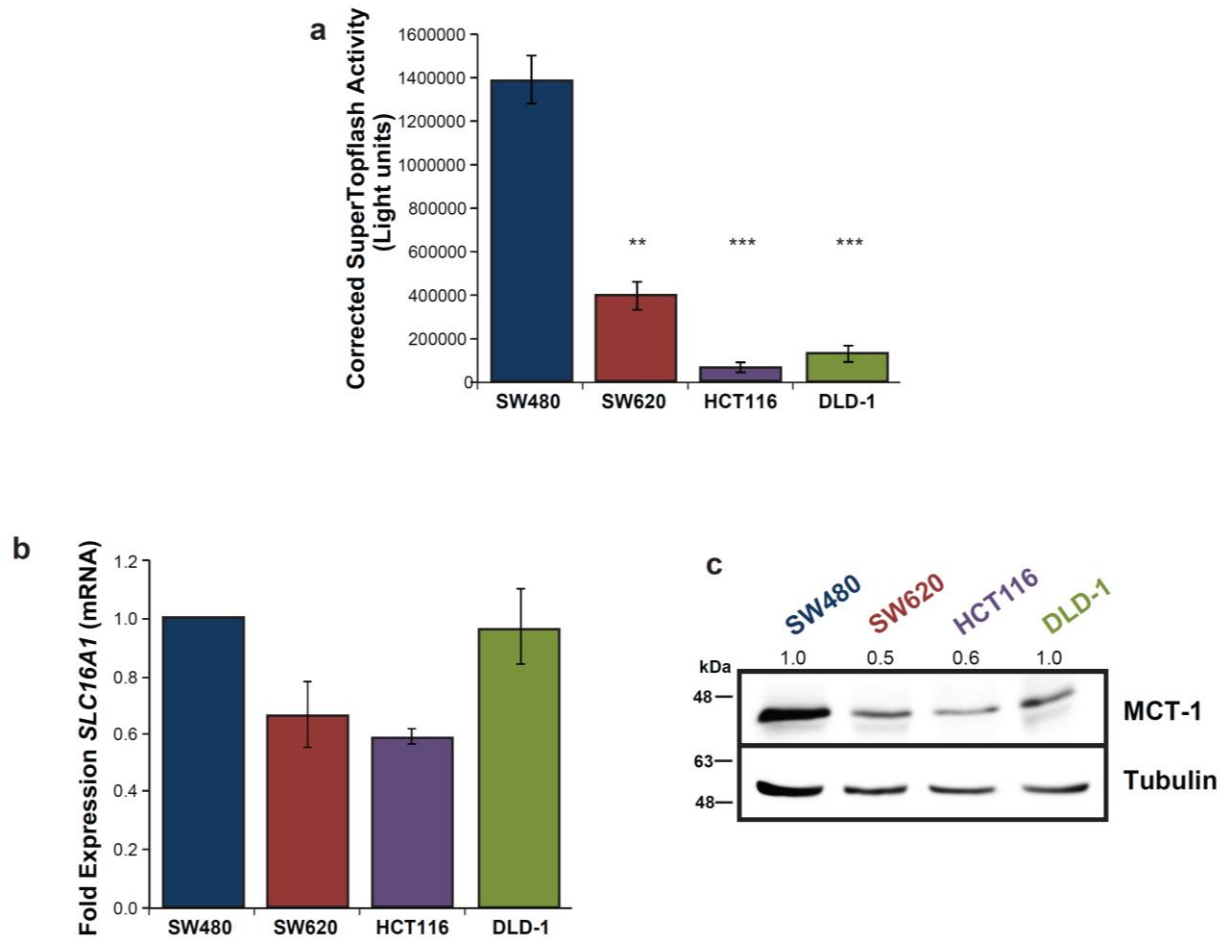


Figure 3.2. Wnt signaling levels and expression of MCT-1 in colon cancer cell lines

(A) Luciferase reporter activity in parental SW480, SW620, HCT116 and DLD-1 cells shows varying levels of Wnt signaling based on SuperTopflash activity. Graph represents the average of three trials (+/- S.E.M.). (*p-value<0.05; **p-value<0.01; ***p-value<0.001)

(B) qRT-PCR analysis was performed on RNA collected from parental SW480, SW620, HCT116 and DLD-1 cells. Graph represents the average of three trials with fold change over SW480 cells (+/- S.D.). (C) Whole cell lysates from each cell line were collected and probed with the antibodies shown. (Figure adapted from Figure 2 of Sprowl-Tanio et al., Submitted).

SuperTopflash reporter. To test this, we performed qRT-PCR analysis of *SLC16A1* mRNA for each cell line and normalized the results to SW480 levels (Fig. 3.2B). We observed that SW620 and HCT116 cells had lower *SLC16A1* mRNA transcripts compared to the Wnt^{Hi} SW480 cells. We also compared protein levels using western blot analysis, normalizing protein level to SW480 cells for comparison (Fig. 3.2C). MCT-1 levels were reduced to 50-60% for SW620 and HCT116 cells, similar to the reduction observed at the mRNA level for each individual cell line. DLD-1 cells differed from the correlation in that the mRNA and protein levels were similar to Wnt^{Hi} SW480 cells, even though the SuperTopflash activity was some of the lowest. Overall, these data suggest that MCT-1/*SLC16A1* is regulated by Wnt/ β -catenin signaling in colon cancer cells, and that with one exception (DLD-1), MCT-1/*SLC16A1* RNA and protein levels correlate with the relative levels of canonical Wnt activity.

MCT-1 is a direct target of Wnt signaling

To ask whether the apparent regulation of MCT-1/*SLC16A1* expression is direct, we mined a previously-performed genome-wide ChIP-seq data set of dnTCF-1 binding in DLD-1 cells¹⁰⁵, and discovered in the genome dataset that TCF-1 binds to a region in the *SLC16A1* locus (Fig. 3.3A). This region (486 nucleotides; “ChIP peak”) of occupancy contains two putative WREs (sequence, Fig. 3.4). To test whether the *SLC16A1* promoter confers transcription regulation in colon cancer cells, we subcloned a fragment of the genomic locus encompassing the ChIP peak and the transcription start site next to the luciferase open reading frame in the plasmid pGL2b. Using “Empty” pGL2b plasmid activity as a negative control and SuperTopflash activity as a positive control, the transient transfection assays showed that the promoter fragment increased reporter activity over empty vector in each of the four surveyed

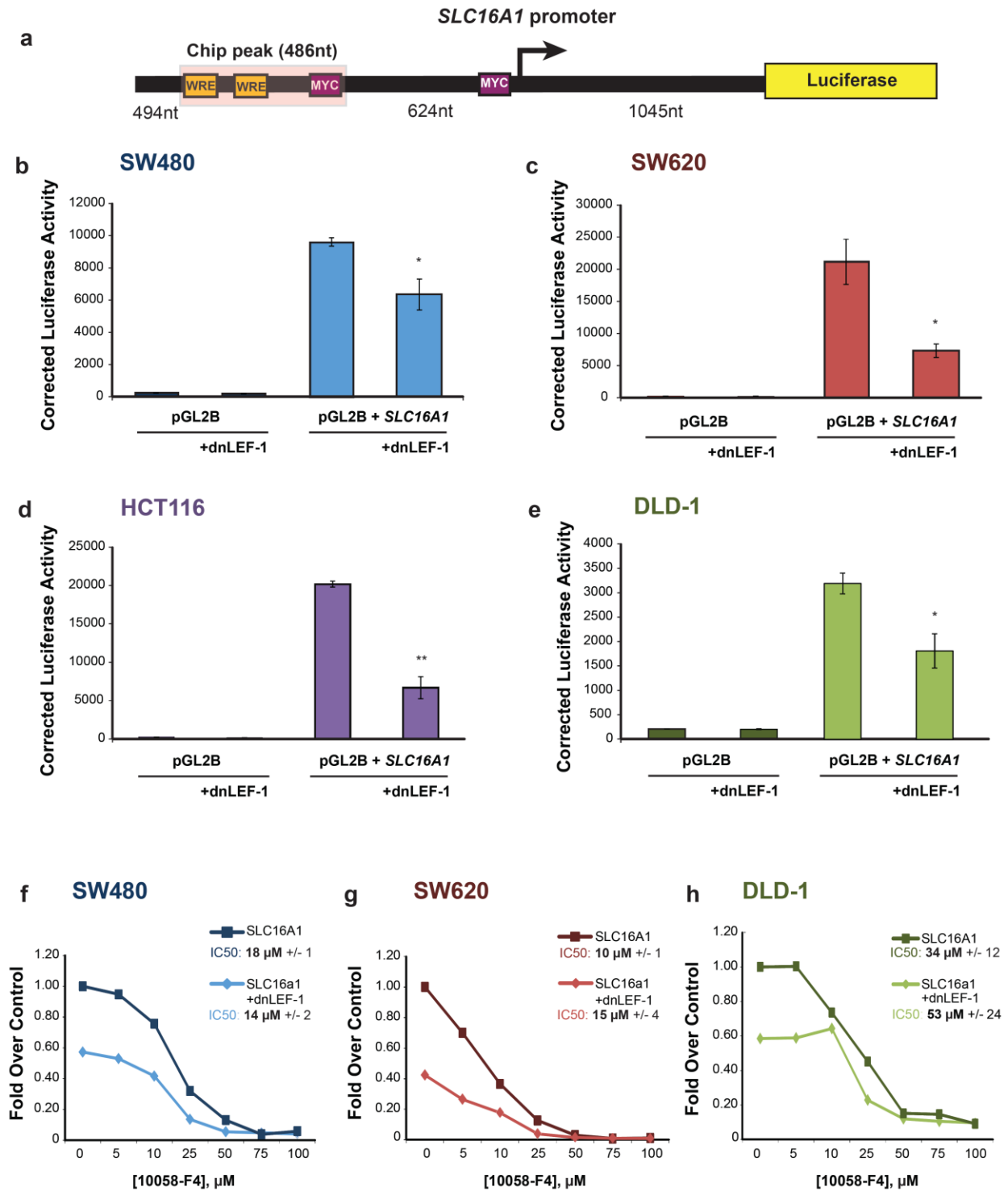


Figure 3.3. Wnt directly targets the MCT-1/ *SLC16A1* promoter for regulation

Schematic (A) representing a region of the endogenous *SLC16A1* promoter (-1604, +1045) subcloned 5' of a luciferase open reading frame. One regulatory region located approximately 624nt upstream from the *SLC16A1* transcription start site (+1) is occupied by dnTCF-1 and contains two putative Wnt Response Elements (highlighted in yellow). Previously identified c-Myc binding sites are also represented (in purple). Transient transfection analysis of three independent experiments in SW480 (B), SW620 (C), HCT116 (D) and DLD1 (E) cells show that the endogenous promoter fragment increases transcription, and that co-expression of dnLEF-1 reduces activity of this promoter construct. Graphs shown represent the average of three trials (+/- S.E.M.; *p-value<0.05; **p-value<0.01; ***p-value<0.001). Luciferase reporter activity in SW480 (F), SW620 (G), and DLD1 (H) cells shows that treatment with the Wnt inhibitor XAV939 (10 μ M) and increasing concentrations of c-Myc inhibitor 10058-F4 decrease transcription of the *SLC16A1* promoter additively, but not synergistically. A representative graph is shown of three replicates, with calculation of the IC₅₀ and S.E.M. from all three replicates for each cell line in the legend. (*Figure adapted from Figure 3 of Sprowl-Tanio et al., Submitted*).

Figure 3.4. *SLC16A1* transcription is directly regulated by LEF/TCFs and Wnt signaling

(A) Schematic of one regulatory region located approximately 624nt upstream from the *SLC16A1* transcription start site (+1) is occupied by dnTCF-1E and contains two putative Wnt Response Elements (WREs). Genomic location and sequence show putative WREs highlighted in red. (B) SuperTopflash reporter serves as a positive control for luciferase activity assays in parental SW480, SW620, HCT116 and DLD-1 cells. The SuperTopflash reporter is significantly sensitive to repression by dnLEF-1. (*Figure adapted from Figure S1 of Sprowl-Tanio et al., Submitted*).

lines (SW480: 44-fold; SW620: 98-fold; HCT116: 83-fold; DLD-1 16-fold), and that it was specifically sensitive to downregulation when dnLEF-1 was co-expressed (Fig. 3.3B-E, Fig. 3.4).

Two c-Myc binding sites have been previously identified within the promoter region of the gene (-624 to the transcription start site) and shown to regulate *SLC16A1* transcription¹³⁹. Since c-Myc is a well-established Wnt target gene, we asked whether c-Myc and LEF/TCFs synergize to activate transcription of *SLC16A1*. To examine this, we transfected the *SLC16A1* reporter into SW480, SW620 and DLD-1 cells and then treated the cultures with an increasing dose of the small molecule c-Myc inhibitor 10058-F4, which prevents c-Myc-Max interaction. The inhibitor reduced promoter activity in all lines at similar IC₅₀, with DLD-1 cultures showing a modest level of decrease in sensitivity. A parallel set of cultures in which dnLEF1 was expressed to partially lower Wnt signaling were treated with the same dose response drug regimen (Fig. 3.3F-H). While the combination clearly had additive effects, there was no significant difference in the IC₅₀ for 10058-F4 alone compared to combination with dnLEF-1. These data demonstrate that *SLC16A1* promoter is sensitive to Wnt inhibition in a manner additive, but not synergistic, with c-Myc.

To confirm that the putative Wnt response elements confer transcription regulation to a heterologous promoter in colon cancer cells, we subcloned the “ChIP peak” next to the thymidine kinase (TK) promoter and luciferase open reading frame (Fig. 3.5A). Luciferase activity assays were performed in the presence of dnLEF-1 or Wnt inhibitor XAV939. XAV939 acts by inhibiting Tankyrase 1/2, poly-ADP-ribosylating enzymes that de-stabilize the Destruction Complex via PARsylation-directed ubiquitination of Axin, a key scaffolding subunit⁸⁹. Transient transfection assays showed that the fragment increased promoter activity in SW480, SW620, HCT116 and DLD-1 colon cancer cells. Nevertheless, dnLEF-1 induction

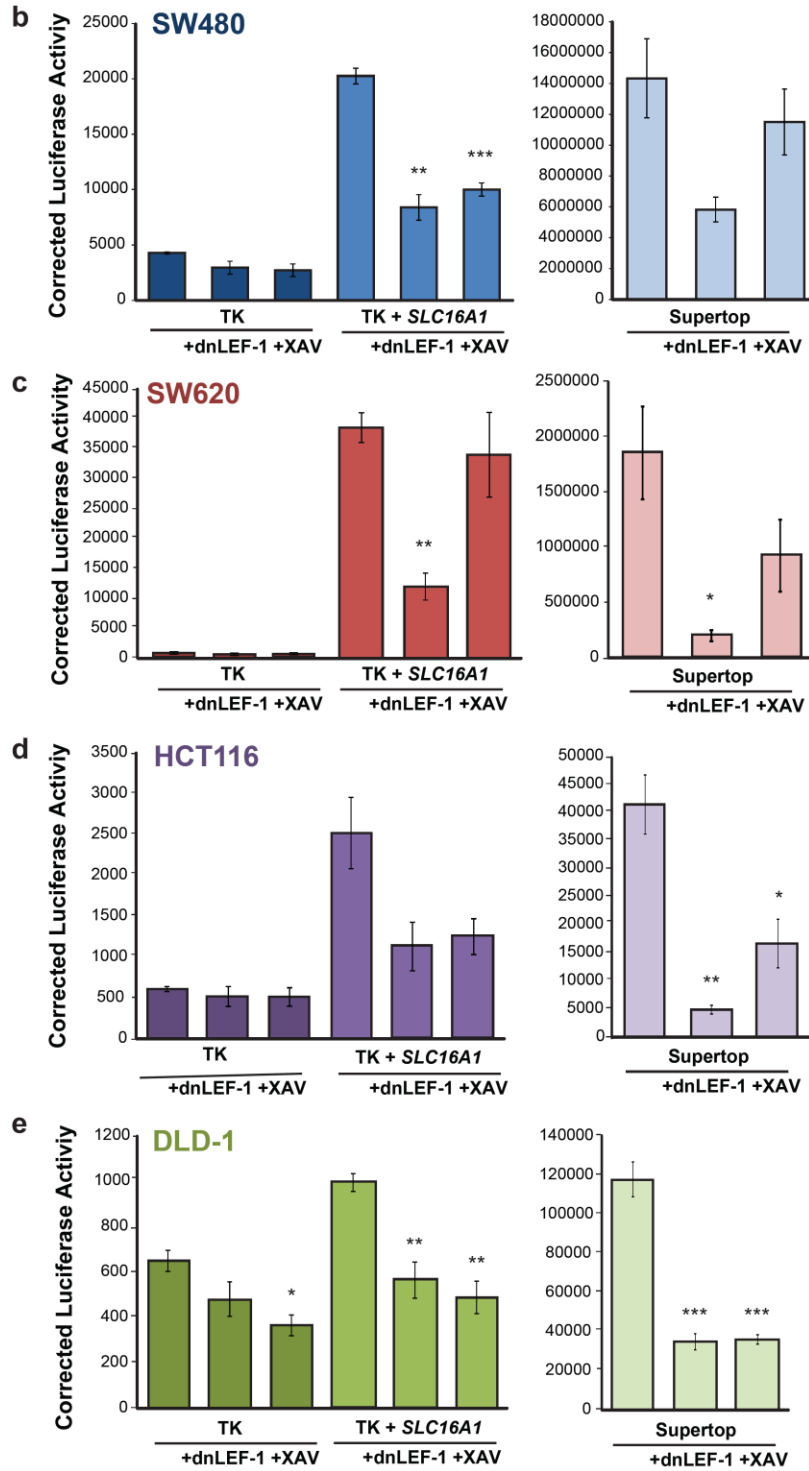
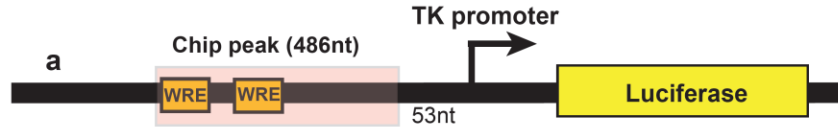


Figure 3.5. Identification of a Wnt responsive region in the *SLC16A1* promoter region
Schematic (A) representing the Chip peak region (486nt) occupied by dnTCF-1, subcloned 5' of a heterologous thymidine kinase (TK) promoter and luciferase open reading frame. Luciferase reporter activity in SW480 (B), SW620 (C), HCT116 (D) and DLD1 (E) cells shows that the Chip peak region confers elevated transcription activity to the heterologous TK promoter. Expression of transfected dnLEF-1, or treatment with the Wnt inhibitor XAV939 (10 μ M) reduces the regulatory activity of these fragments. Graphs shown represent the average of three independent replicates (\pm S.E.M.). (*p-value<0.05; **p-value<0.01; ***p-value<0.001) (Figure adapted from Figure 4 of Sprowl-Tanio et al., Submitted).

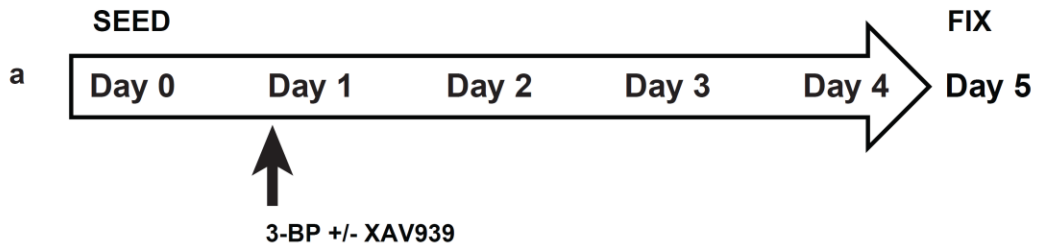
reduced luciferase expression to near baseline in all the cell lines. Treatment with Wnt inhibitor XAV939 also repressed reporter expression, but with more variability (Fig. 3.5B-E). The “ChIP peak” fragment exhibited more activity in SW480 cells and SW620 cells compared to HCT116 cells and DLD-1 cells, tracking better with the activity profile of the SuperTopflash reporter (Figure 3.2A). These results demonstrate that SLC16A1/MCT-1 is a direct Wnt target gene and that regulation occurs through sites within the promoter locus. Therefore MCT-1 is part of a metabolic/glycolytic gene program directed by Wnt signaling.

Wnt signaling inhibition increases colon cancer cell resistance to 3-bromopyruvate

The importance of MCT-1 to cancer cell survival has been well characterized in other cancer¹⁴⁴⁻¹⁴⁶, with a recent study identifying a potential glycolysis inhibitor which targets cells via import through MCT-1¹⁴². In fact, Birsoy *et al* used a genome wide siRNA knockdown screen to discover that MCT-1 and basigin (the transmembrane glycoprotein responsible for anchoring MCT-1 to the cell surface^{147,148}) are uniquely and sufficiently capable of importing the toxic molecule 3-BP into breast cancer cells. Breast cancer cell lines expressing high levels of MCT-1 were exquisitely sensitive to treatment with 3-BP, while cell lines that did not express MCT-1 survived similarly in the presence and absence of the molecule. Furthermore, knockdown or overexpression of MCT-1 in breast cancer cell lines prohibited or enhanced survival, respectively. Since that study focused exclusively on breast cancer cell lines, we asked what effect 3-BP would have in colon cancer. Given that Birsoy *et al* showed a direct correlation between MCT-1 levels and sensitivity to 3-BP, we asked whether there is a correlation between the level of Wnt signaling and 3-BP sensitivity. To assess tumor cell line sensitivity, we followed cell proliferation for four days in the presence of increasing concentrations of 3-BP. We

performed the analysis in the presence and absence of Wnt signaling inhibitors, asking whether reduction of β -catenin levels would enhance any negative effect of 3-BP on cell growth or whether it would produce complex effects by lowering MCT-1 expression. We subjected the cells to 96 hours of 3-BP treatment in the presence or absence of Wnt signaling inhibitor XAV939 (Fig. 3.6A). While XAV939 treatment provided additional inhibitory effects on growth in the presence of low concentrations of 3-BP, it appeared to be protective at higher doses (Fig. 3.6B-E). Analysis of the IC_{50} concentrations showed that XAV939 caused significant increases in survival for SW620 ($p = 0.02$) and DLD1 ($p = 8.5e-5$), but not for SW480 cells ($p = 0.11$) or HCT116 cultures ($p = 0.43$) compared to 3-BP alone. This data led us to ask whether the partial protection provided by XAV939 would be evident in the cultures even when the drug was removed, affecting the survival and recovery of colon cancer cells from toxic, high doses of 3-BP.

To elucidate the effect on survival of cancer cells in the presence of XAV939, the four surveyed cell lines were subjected to 200 μ M, 250 μ M, or 300 μ M 3-BP for 96 hours, followed by a “wash out” and recovery period over the course of five days (Fig. 3.7A). In SW480 cells treated with 200 μ M 3-BP there was no significant difference in the ability of the cells to recover in the absence or presence of XAV939. However, at 250 μ M, the cells survived significantly better when subjected to treatment with XAV939, and at 300 μ M 3-BP, Wnt signaling inhibition allowed the cells to recover where untreated cultures did not recover at all (Fig. 3.7B). Similarly in SW620 cultures, XAV939 treatment increased survival and recovery at 250 μ M 3-BP. The 300 μ M condition had a modest recovery compared to untreated (Fig. 3.7C). Wnt signaling-inhibited cells survived and recovered better at every experimental concentration of 3-BP in HCT116 cells (Fig. 3.7D), while DLD-1 cells did not recover at all. DLD-1 lack of recovery was



b

	IC50, μM	
	-XAV939	+XAV939
SW480	156 +/- 21	234 +/- 32
SW620	168 +/- 29	286* +/- 10
HCT116	161 +/- 47	204 +/- 16
DLD-1	59 +/- 3	89* +/- 2

* $p < 0.05$

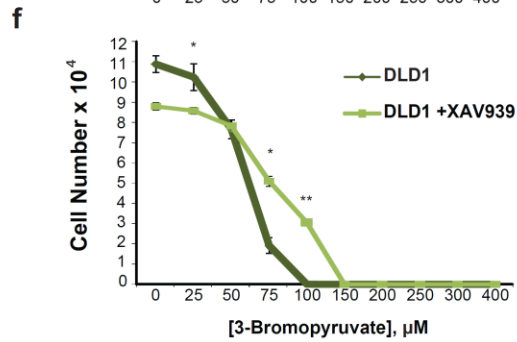
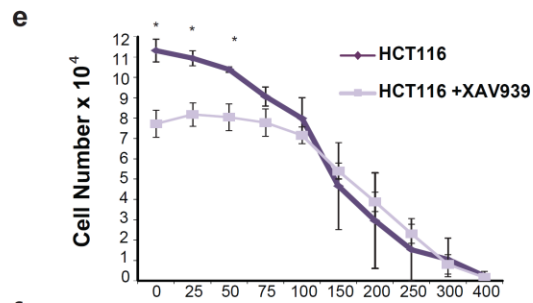
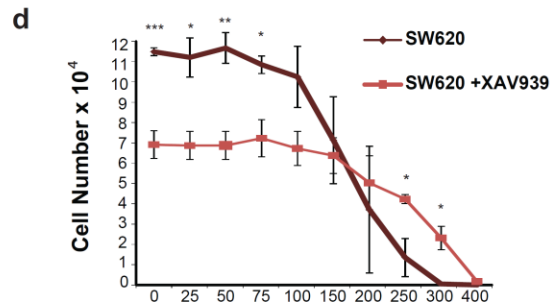
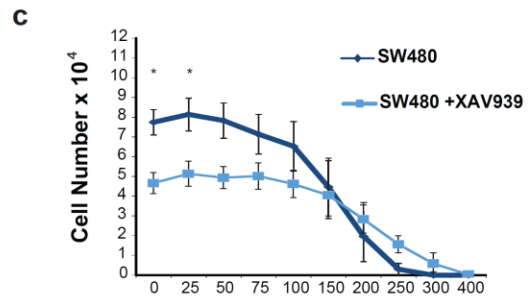


Figure 3.6. XAV939 affects colon cancer cell sensitivity to 3-bromopyruvate

(A) Experimental workflow for colorimetric-based kill curve assay. Individual cell lines were seeded on Day 0, treated after 24 hours (Day 1) with increasing concentrations of 3-bromopyruvate +/- the Wnt inhibitor XAV939 (10 μ M) and fixed 96 hours later on Day 5. SW480 (B), SW620 (C), HCT116 (D) and DLD1 (E) cells treated with the Wnt inhibitor XAV939 (10 μ M) reduces survival compared to without 3-bromopyruvate treatment, except at high concentrations. Graphs shown represent the average of three independent replicates with error bars depicting the standard error of the mean. (*p-value<0.05; **p-value<0.01; ***p-value<0.001) (*Figure adapted from Figure 5 of Sprowl-Tanio et al., Submitted*).

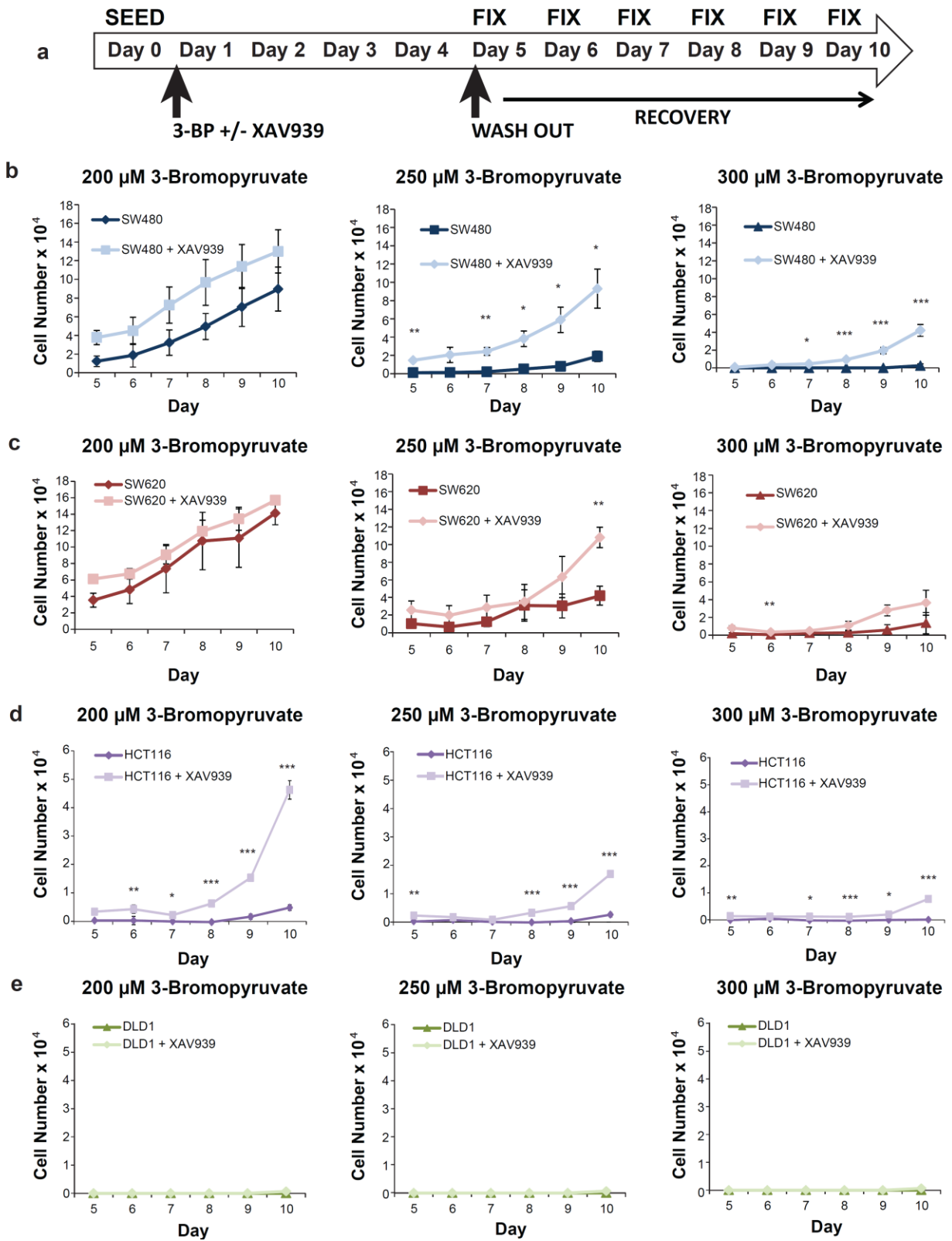


Figure 3.7. XAV939 promotes colon cancer cell recovery from 3-bromopyruvate

(A) Experimental workflow for colorimetric-based survival curve assay. Individual cell lines were seeded on Day 0 and treated after 24 hours (Day 1) with 200, 250, or 300 μM 3-bromopyruvate +/- the Wnt inhibitor XAV939 (10 μM) until Day 5. On Day 5 treatments were “washed out” and replaced with control medium. Cells were fixed Day 5, 6, 7, 8, 9, and 10 days post seeding to observe recovery over time. SW480 (B), HCT116 (D) cells treated with the Wnt inhibitor XAV939 (10 μM) survived and recovered compared to without treatment of 3-bromopyruvate. SW620 (C) cells recovered similarly +/- XAV939 treatment, and DLD1 cells (E) did not recover. Graphs shown represent the average of three independent replicates (+/- S.E.M.). (*p-value<0.05; **p-value<0.01; ***p-value<0.001) (Figure adapted from Figure 6 of Sprowl-Tanio et al., Submitted).

unsurprising, due to the lower IC_{50} and greater sensitivity of the cell line to 3-BP (Fig. 3.6E, Fig. 3.7E). These data demonstrate that colon cancer cells are sensitive to 3-BP, likely because MCT-1 transports 3-BP, and that co-treatment with Wnt signaling inhibitor XAV939, which lowers MCT-1 expression, allows cells to resist the anti-proliferative effects of 3-BP leading to increased survival and enhanced recovery. These results demonstrate an important drug interaction combination that should be avoided when trying to treat cancer cells with aberrant Wnt signaling and glycolytic metabolism.

Discussion

Here we report that *SLC16A1*/MCT-1 is a direct Wnt target gene within a program of glycolysis and angiogenesis we have defined for colon cancer¹²⁸. We have previously shown that colon cancer cells with high levels of oncogenic Wnt signaling (Wnt^{Hi}) have extremely strong signatures of aerobic glycolysis (Warburg metabolism) *in vitro* and *in vivo*¹²⁸. MCT-1 upregulation in cells with oncogenic Wnt signaling supports their adoption of a glycolytic phenotype, likely through lactate efflux to maintain intracellular pH, but possibly also through export of excess pyruvate which can enhance oxidative phosphorylation and reduce proliferation¹⁴¹. We show that colon cancer cells express at least one other monocarboxylate transporter (MCT-4), but it is MCT-1 that has optimal export kinetics for lactate, and therefore provides a sensitive and responsive avenue to help maintain pH homeostasis for the intracellular environment. While previous studies have shown c-Myc can activate *SLC16A1* transcription, we find that this action is independent of Wnt signaling. Furthermore, MCT-1 expression renders colon cancer cells sensitive to the uptake of the toxic molecule 3-bromopyruvate. Sensitivity to

3-BP is reduced by Wnt signaling inhibition, and in fact tumor cells survive and recover better from the toxic drug if they are simultaneously treated with Wnt signaling inhibitor XAV939.

3-bromopyruvate is a highly toxic small molecule that targets multiple enzymes in glycolysis, particularly cells exhibiting high rates of Warburg metabolism^{142,149}. Therefore, targeting metabolism is a promising avenue for treatment of colon cancer. High levels of aerobic glycolysis results in the accumulation of metabolic products that alter the intracellular pH, generating high levels of H⁺ that unless eliminated, will cause cell death. MCT proteins can rid cancer cells of H⁺ via proton-coupled export of lactate, the “waste” end product of glycolysis, providing an important survival function for cancer cells. Thus, cells that have high levels of glycolytic activity tend to exhibit strong expression of MCT-1 and MCT-4¹⁵⁰. Studies with breast cancer cell lines show that 3-BP enters cells specifically and only through MCT-1, not MCT-4, suggesting that signaling pathways that regulate MCT-1 expression are important for determining sensitivity to this promising anti-cancer agent¹⁴⁵.

Whether the level of Wnt signaling is the single, most important indicator for cell sensitivity to 3-BP depends on understanding whether alternative modes exist for regulation of MCT-1 and whether the toxic activities of 3-BP target different processes inside cells. Our studies show that MCT-1 mRNA and protein levels largely correlated with Wnt signaling but that DLD-1 cells were an exception. This cell line has low Wnt signaling but relatively high levels of MCT-1 mRNA and protein, levels that are similar to Wnt^{Hi} SW480 cells (Fig. 3.2). There were also differences in the way the *SLC16A1* promoter responded to c-Myc and dnLEF-1 inhibition in DLD-1 cells. The promoter had a slightly lower sensitivity to the c-Myc inhibitor (IC₅₀ of 34 μM compared to SW480 cells (18 μM) and SW620 cells (10 μM)). To note, dnLEF-1 expression only made a noticeable difference at the lowest concentration of c-Myc inhibitor (Fig.

3.3), suggesting that there are relative differences in the way β -catenin/LEF and c-Myc contribute to promoter activity in DLD-1 cells. In general, c-Myc regulates two different kinetic steps of transcription at promoters: an early step of polymerase recruitment and initiation complex assembly, and pause-release at a later, downstream step¹⁵¹. Perhaps the kinetics and contributions of these steps differ among the cells. Whatever the mechanistic differences at the promoter, MCT-1 expression and by implication, 3-BP import potential, may have more to do with c-Myc than Wnt signaling in these cells. It is also interesting to note that DLD-1 cells exhibit enhanced sensitivity to 3-BP, (IC_{50} of 59 μ M compared to SW480 cells (156 μ M) and SW620 cells (168 μ M); Fig. 3.6), suggesting that there are additional modes of regulation that contribute to 3-BP sensitivity.

Finally, our data highlight interesting patterns of colon cancer cell growth when Wnt signaling inhibitors are combined with 3-BP treatment. Our hypothesis was that, if MCT-1 is a target of Wnt signaling, and if MCT-1 transport is the mechanism by which 3-BP gains access to colon cancer cells, then Wnt signaling inhibition should reduce sensitivity to 3-BP. We confirmed this hypothesis in at least two of the cell lines, as the IC_{50} for 3-BP inhibition was significantly shifted to higher concentrations when XAV939 was included in the cultures. This was even true in the DLD-1 cell line where Wnt signaling appears to make less of a contribution to MCT-1 expression. Interestingly, using the highest concentration of 3-BP that reduced cell numbers to below the point of detection (300 μ M), we observed that XAV939 treated cultures recovered better and faster when the drugs were washed out. It is particularly notable, that even though XAV939 had no significant effect on protection in SW480 and HCT116 cells, its protective effects were more noticeable after the drug was removed. Meaning, even though there was no significant difference in the number of cells five days after 3-BP treatment, XAV939

treated cultures recovered better and faster. We speculate that XAV939 triggers adaptations that confer faster recovery and cell cycle progression. This possibility points to the caveats that can arise when two classes of drugs are combined. These data also suggest that the heterogeneous patterns of Wnt signaling that have been observed in different subtypes of primary human colon cancer, and within the tumor microenvironment, will directly affect the efficacy of 3-BP and its derivatives.

CHAPTER FOUR

A uniform human Wnt expression library reveals a shared secretory pathway and unique signaling activities

Introduction

The Wnt signaling pathways regulate key networks during both embryonic development and adult tissue homeostasis. Pivotal to the activation of these networks are Wnt ligands, a highly conserved family of cysteine-rich secreted morphogens. Wnt proteins are synthesized in the endoplasmic reticulum (ER) where the membrane bound O-acyltransferase porcupine (PORCN) catalyzes their palmitoylation^{152,153}. Modified Wnt ligands are chaperoned to the plasma membrane by binding to the carrier protein Wntless (WLS) and then released from this complex to allow secretion^{154,155}. In total, there are 19 human Wnts that regulate numerous biological processes via diverse signaling pathways. One important property of many Wnts is their ability to stabilize β -catenin, an activity referred to as ‘canonical’ signaling¹. β -catenin stabilization occurs when Wnt ligands bind to the Frizzled (Fz) and LRP5/6 (LDL-related protein) co-receptors, initiating a signaling cascade that releases the transcriptional co-activator β -catenin from a destruction complex. In the absence of Wnt ligands, this complex, which is composed of glycogen synthase kinase 3 (GSK3), Casein kinase 1 α (CK1 α), Adenomatous Polyposis Coli (APC) and Axin, among other factors, phosphorylates β -catenin, marking it for degradation through the proteasome pathway. The stabilization of β -catenin leads to its cytoplasmic accumulation. Additional events are required for the subsequent translocation of β -catenin into the nucleus, where it binds to Lymphoid Enhancer Factor/T-cell Factor (LEF/TCF) transcription factors and activates diverse, tissue specific Wnt target genes. Importantly, “non-canonical” Wnt signaling through both Frizzled and additional classes of cell surface receptors

including receptor tyrosine kinases, forgoes β -catenin stabilization in favor of the activation of β -catenin-independent pathways, such as the Planar Cell Polarity (PCP) pathway and the Wnt/Calcium pathway⁷.

Despite the many efforts to elucidate the dynamics of Wnt signaling, several questions remain unanswered. The classification of Wnts has been largely based on their signaling properties across different systems rather than direct comparison among Wnts of the same species in a single cell type. For example, WNT1 and 3A are traditionally considered to be potent activators of Wnt/ β -catenin signaling while other Wnts such as 5A and 11 are known to activate β -catenin independent pathways. However, recent reports have demonstrated that WNT5A can activate Wnt/ β -catenin signaling depending on the receptors expressed at the plasma membrane. Furthermore, both WNT5A and 11 have been shown to heterodimerize to activate the β -catenin dependent pathway^{2,156}. Similarly, WNT3A, a traditionally “canonical” Wnt has been shown to induce morphogenetic changes by activating Rho-associated kinase or c-Jun N-terminal kinase, depending on cell type^{157,158}. These data hint at a more complex scenario than that proposed by the traditional classification of Wnts. Moreover, the production, processing and secretion of Wnts 1, 3A, 5A and 11 have been extensively studied, but other Wnt ligands have not been characterized beyond expression patterns and general signaling and phenotype outcomes. Whether the post-translational modification and secretion of all Wnt ligands are regulated in a similar fashion has not been properly examined. These questions and the lack of understanding of Wnt signaling properties have emphasized the requirement for a full standardized set of Wnt expression plasmids. Such a set would allow for a direct side-by-side comparison of Wnt processing, secretion and signaling. For this reason, we started the “Open Source Wnt” plasmid depository and cloned open reading frame sequences for all 19 human

Wnts into the same expression plasmid backbone. Using this plasmid set, we have been able to analyze and compare the expression levels and the efficiency of secretion of all human Wnts in a defined set of cell lines, revealing valuable insight on their processing, their signaling potential and their accumulation in conditioned media. We show that, dependent on cell type, up to 14 out of the 19 Wnts are capable of signaling through the β -catenin-dependent pathway to activate the Super8XTOPflash reporter. Notably, Wnt/ β -catenin signaling is inhibited by C-terminal tagging in a different fashion for different Wnt ligands. Wnt/ β -catenin signaling is broadly reduced by the secreted Wnt inhibitors Dkk-1 and the SFRPs (Secreted Frizzled-Related Proteins). Activation of the Super8XTOPflash reporter, with a few exceptions, is more sensitive than, but tracks with, LRP6 phosphorylation and the stabilization of β -catenin. Finally, we find that PORCN and WLS are essential elements of a common Wnt secretion pathway, as all assessable Wnts require PORCN-dependent palmitoylation to bind to the carrier protein WLS and to signal through β -catenin-dependent and independent pathways.

Results

Human Wnt Cloning

In order to create a synchronized set of Wnt expression plasmids, cDNAs of all 19 human Wnt proteins (1, 2, 2B2, 3A, 3, 4, 5A, 5B, 6, 7A, 7B, 8A, 8B, 9A, 9B, 10A, 10B, 11 and 16) were cloned into the same backbone, thus allowing for direct comparisons to be made among the different Wnts. First, *WNT* cDNA was amplified using PCR with both *WNT*-specific “STOP” and “Non-STOP” reverse primers. “STOP” primers contained the TGA STOP codon, while “Non-STOP” primers contained the codon TGC rather than TGA. This one basepair difference in the two reverse primers also introduced an *EcoRI* restriction site that is unique to clones

amplified using the “STOP” primers (*TGA ATT CTG*), therefore allowing the excision of the *WNT* coding sequence using restriction digest techniques. For this reason, internal *EcoRI* sites were destroyed in *WNTs* 2, 8A and 9A while maintaining the integrity of the amino acid sequence. Following PCR amplification, the products were cloned using the TOPO cloning system into a Gateway entry vector, pENTR/D-TOPO. Finally, the *WNT* coding sequence was transferred, through the use of homologous recombination, into a Gateway destination vector, pcDNA3.2/V5-DEST, which contains a C-terminal V5 epitope tag. Consequently, clones that contain the STOP codon are expressed as untagged Wnt ligands, while those that do not are expressed as V5-tagged at the C-terminus (Figure 4.1). In a parallel cloning effort, all Wnts were cloned into a p3XFLAG-CMV-8 vector where the native signal peptide is replaced with the preprotrypsin signal peptide. These N-terminally tagged Wnts were expressed and secreted at 50-fold higher amounts than the Gateway clones, but also had a >1000-fold decrease in signaling activity (Fig. 4.2). We speculate that the N-terminal tag and use of the vector-supplied signal peptide accounts for both the increased protein production and also for the substantial decrease in activity. The N-tagged Wnts in p3XFLAG were not extensively studied.

Wnt ligand production and secretion profile

As a first step for validation of the Gateway Wnt clones, the expression and secretion levels of each Wnt were monitored in HEK293 cells (Fig. 4.3A), a human embryonic kidney cell line, and NIH3T3 cells (Fig. 4.3B), a mouse fibroblast cell line. Plasmids expressing C-terminal V5-tagged Wnts were transiently transfected and both lysates and media were probed with V5-tag antibody. Transient transfection of the “STOP” expression plasmid for untagged WNT1 was included in the analysis (Fig. 4.3A, last lane). For this sample, no WNT1-V5 was detected in

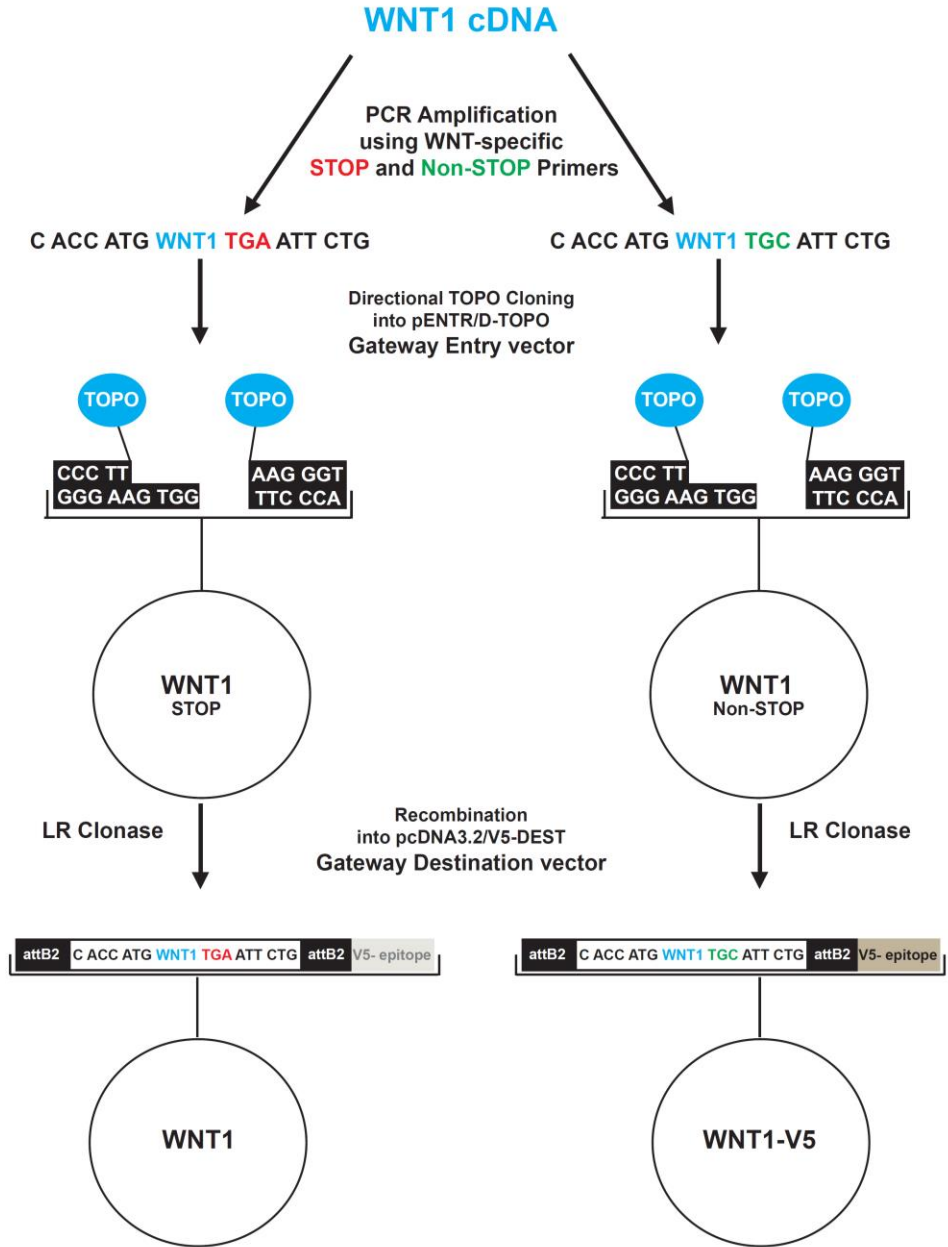


Figure 4.1. Wnt cloning scheme using WNT1 as an example.

WNT1 cDNA was amplified by PCR using *WNT1*-specific “STOP” and “Non-STOP” primers. The PCR product was then transferred, using TOPO cloning, into the pENTR/D-TOPO Gateway Entry vector, and subsequently shuttled, using recombination, into the pcDNA3.2/V5-DEST Gateway Destination vector. The outcome of the cloning process is 4 *WNT1* plasmids: 2 Entry vectors (*WNT1* STOP and *WNT1* Non-STOP) and 2 Destination vectors (*WNT1* and *WNT1*-V5). (Figure adapted from Figure 1 of Najdi, Proffitt, Sprowl et al., 2012).

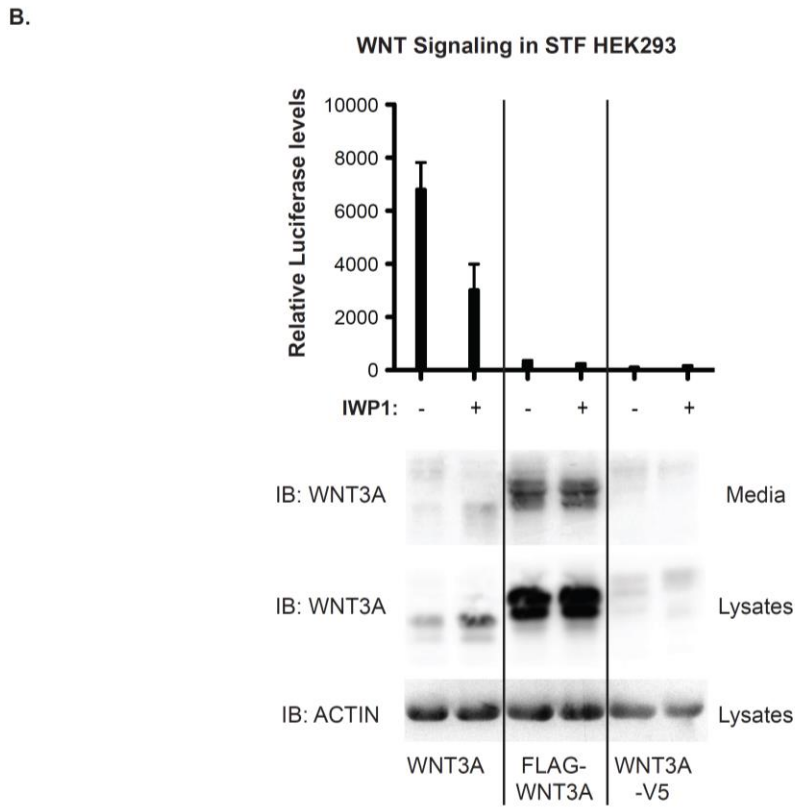
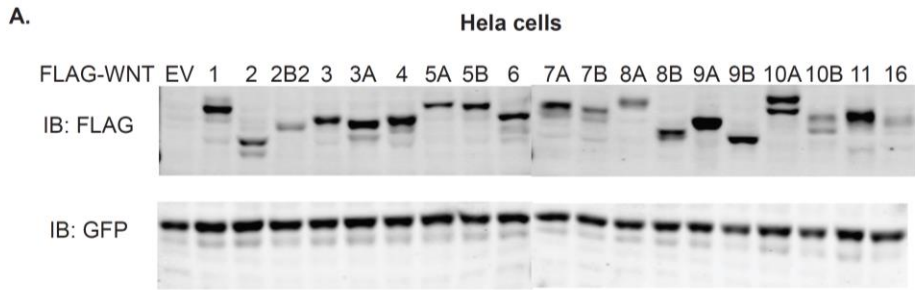


Figure 4.2. Analysis of FLAG-tagged Wnts

(A) N-terminal FLAG-tagged Wnts are well expressed. HeLa cells were transfected with 10 ng of the indicated FLAG-tagged Wnt plasmid in a 12-well dish. Lysates were analyzed by SDS-PAGE and immunoblotting with anti-FLAG antibody. (B) FLAG-tagged WNT3A is much less active than untagged Wnts and its robust secretion is insensitive to IWP. HEK293 cells with an integrated Super8XTopFlash reporter were transfected with 100 ng of the various WNT3A plasmids as indicated and treated with either DMSO or IWP1 (2 μ M) overnight. Lysates and conditioned media were analyzed by SDS-PAGE and immunoblotted with an anti-WNT3A monoclonal antibody. Based on protein abundance and TOPflash activity, the specific activity of the FLAG tagged WNT3A is approximately 2500-fold lower than that of the untagged WNT3A. Cell Lysates and media collected from NIH3T3 cells that had been transfected with V5-tagged Wnts were separated by SDS-PAGE on a 10% gel and then probed with a V5 antibody to determine expression (1st panels) and secretion levels (3rd panels). Cell lysates were also probed for β -Tubulin as a loading control (2nd panels). (*Figure adapted from Figure S1 of Najdi, Proffitt, Sprowl et al., 2012*).

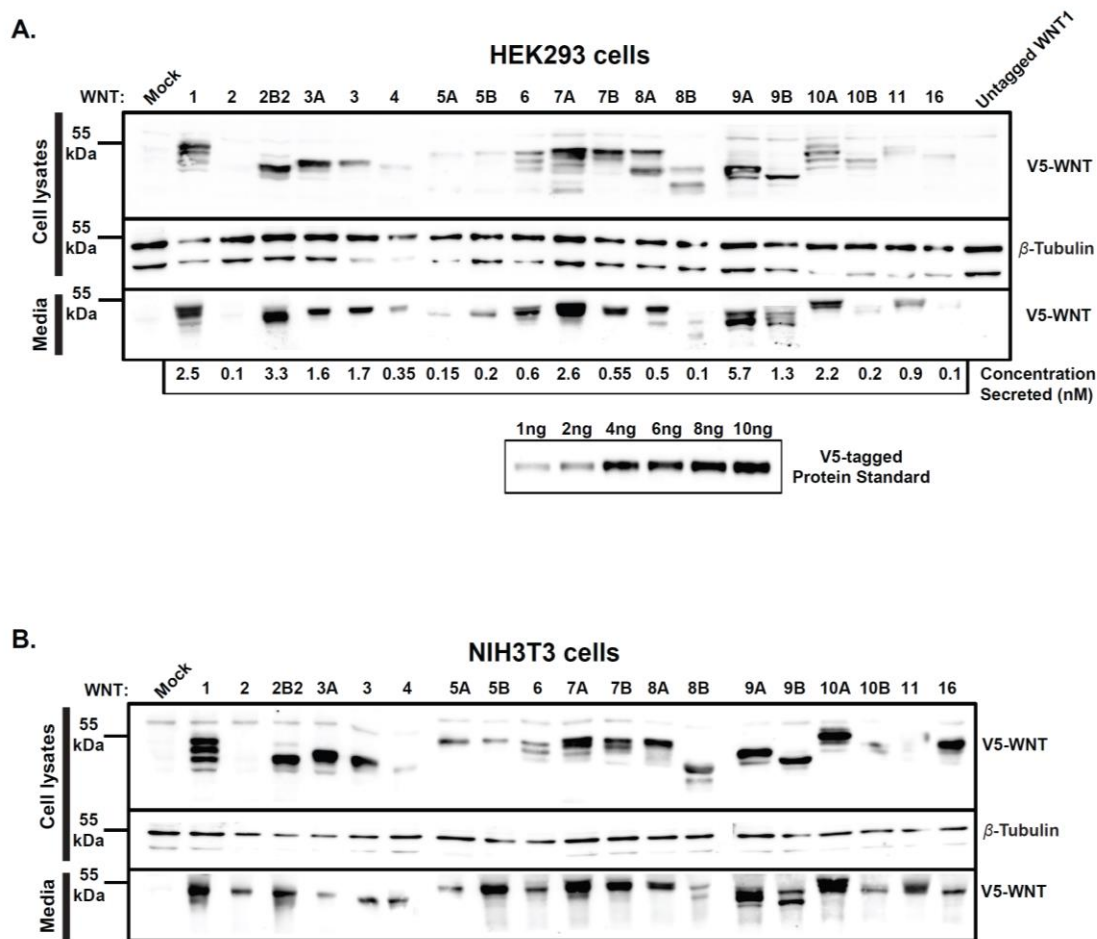


Figure 4.3. V5-tagged Wnt expression.

Cell Lysates and media collected from HEK293 (**A**) and NIH3T3 (**B**) cells that had been transfected with V5-tagged Wnts (and untagged WNT1 for HEK293 cells) were separated by SDS-PAGE on a 10% gel and then probed with a V5 antibody to determine expression (1st panels) and secretion levels (3rd panels). Cell lysates were also probed for β -Tubulin as a loading control (2nd panels). A V5-tagged protein standard (4.3A, 5th panel) was processed on a parallel immunoblot at the same time and used to calculate the amount of V5-tagged Wnts secreted into the media of HEK293 cells (4.3A, 4th panel). In HEK293 cells, WNT9A was the most secreted Wnt into the media (5.7 nM), while WNT2, 8B and 16 were the least secreted Wnts (0.1 nM). (Figure adapted from Figure 2 of Najdi, Proffitt, Sprowl et al., 2012).

lysates or media demonstrating that the single nucleotide difference that creates a translation stop codon for the untagged plasmids is effective. While all Wnt ligands were expressed in the lysates and secreted into the media of both cell lines, there was tremendous variation in both expression and secretion. The variation was particularly surprising since all clones share the same backbone plasmid and produce relatively similar amounts of mRNA transcripts in HEK293 cells (Fig. 4.4). This suggested that the amino acid sequence or protein structure of each Wnt ligand might dictate its abundance and the efficiency of its secretion. It might also be that the V5-tag differentially affects the stabilities of the various Wnts. To quantify the amount of Wnt protein secreted into the media of HEK293 cells, a purified V5-tagged protein of known concentration (Recombinant Yeast Calmodulin Kinase Array Control Protein, see Materials and Methods) was utilized as a V5-tag standard to calculate the different concentrations at which each Wnt is secreted (Fig. 4.3A; panel 6). WNT1, 2B2, 7A and 9A were among the most abundantly secreted Wnts in HEK293 cells, while WNT2, 5A, 8B and 16 were the least well secreted Wnts (Fig. 4.3A; panel 4). It is important to point out that there were more protein isoforms in lysates than in media for WNT1, 6, 7A and 10A. Another interesting observation is the relative consistency in expression, secretion and processing from one cell line to another, as the patterns observed in HEK293 cells are largely unchanged in NIH3T3 cells. However, WNT2 and 5B appear to be secreted more efficiently from NIH3T3 cells (Fig. 4.3B; panel 3).

Wnt activation of the β -catenin-dependent pathway

The ability of “non-canonical” Wnts such as 5A and 11 to activate Wnt/ β -catenin signaling suggested that in theory, all Wnt ligands might be capable of signaling via the β -catenin-dependent pathway or other β -catenin-independent pathways when provided with the

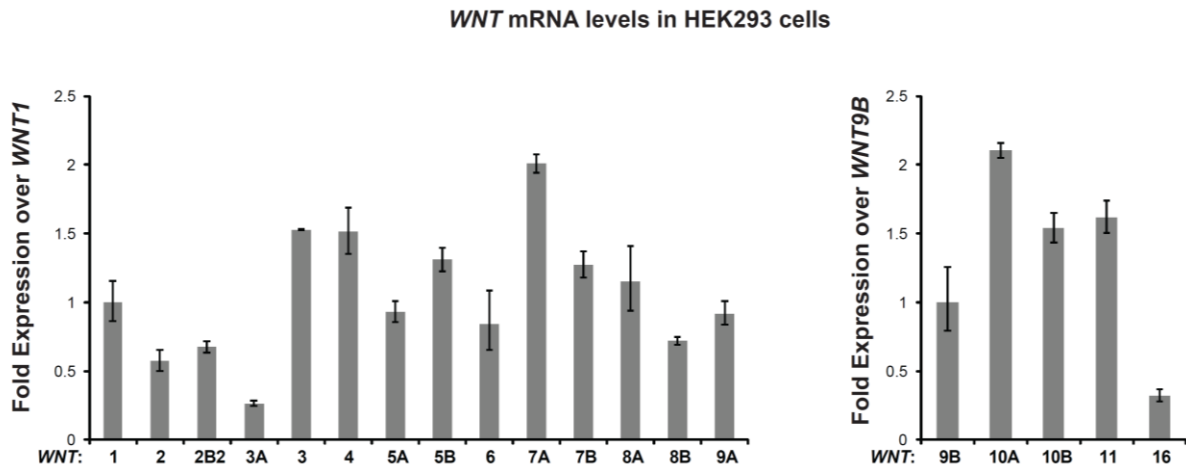


Figure 4.4. WNT mRNA levels in HEK293 cells.

293 cells were transfected with plasmids expressing V5-tagged Wnts and expression was monitored by qRT-PCR of isolated mRNA. All Wnts produce relatively similar amounts of mRNA transcripts with little variation. The experiment was performed in two different sets: The first set displays fold expression over *WNT1* mRNA, while the second set displays fold expression over *WNT9B* mRNA. mRNA levels were normalized to GAPDH. (Figure adapted from Figure S2 of Najdi, Proffitt, Sprowl et al., 2012).

right conditions (8-9). To test which Wnts can activate the Wnt/ β -catenin signaling in HEK293, NIH3T3 and HT1080 cells, plasmids expressing untagged Wnts were co-transfected with Super8XTOPflash (STF), a luciferase reporter plasmid with 8 multimerized Wnt response elements (Fig. 3A). Out of all 19 Wnts, WNT1 was the most active in HEK293 cells. Additionally, WNT2, 2B2, 3A, 3, 6, 7A, 7B, 8A, 9A, 9B and 10B also exhibited considerable activation of the STF reporter when compared to mock-transfected cells. Meanwhile, only WNT1, 3A and 3 significantly activated the β -catenin-dependent pathway in NIH3T3 cells (Fig. 4.5B). HT1080 cells were particularly responsive to Wnt/ β -catenin signaling, as Wnts 8B and 10A gained activity in HT1080 cells, and many other Wnts gave better than 10-fold activation of the STF reporter (Fig. 4.8A). Since the V5 tagged versions of each Wnt show that they are efficiently produced and secreted from NIH3T3 cells, as with HEK293 cells, the global decrease in reporter activity in mouse NIH3T3 cells may be due to decreased expression of Wnt receptors on the cell surface, or decreased activity of other downstream Wnt pathway components.

All Wnt/ β -catenin signaling is thought to require the LRRP5/6 co-receptors. Consistent with this, addition of Dkk-1, an inhibitor of Wnt signaling that binds to the LRP5/6 co-receptor at the plasma membrane, significantly reduced the activating potential of all Wnt proteins in both NIH3T3 and HEK293 cells (Fig. 4.5A and 4.5B)¹⁵⁹⁻¹⁶¹. In addition to Dkk-1, we also tested whether the soluble Frizzled-related proteins SFRP1-3 can negatively regulate Wnt-induced activation of Wnt/ β -catenin-signaling in HEK293 cells (Fig. 4.5C). SFRP proteins differ from Dkk-1 in that they directly bind to Wnt ligands to block their actions. Co-transfection of either SFRP1 or SFRP3 effectively reduced the activation of the STF reporter by WNT1, 2, 3A, 3, 6, 7A and 7B. Conversely, SFRP2 was globally a less effective inhibitor of Wnt/ β -catenin

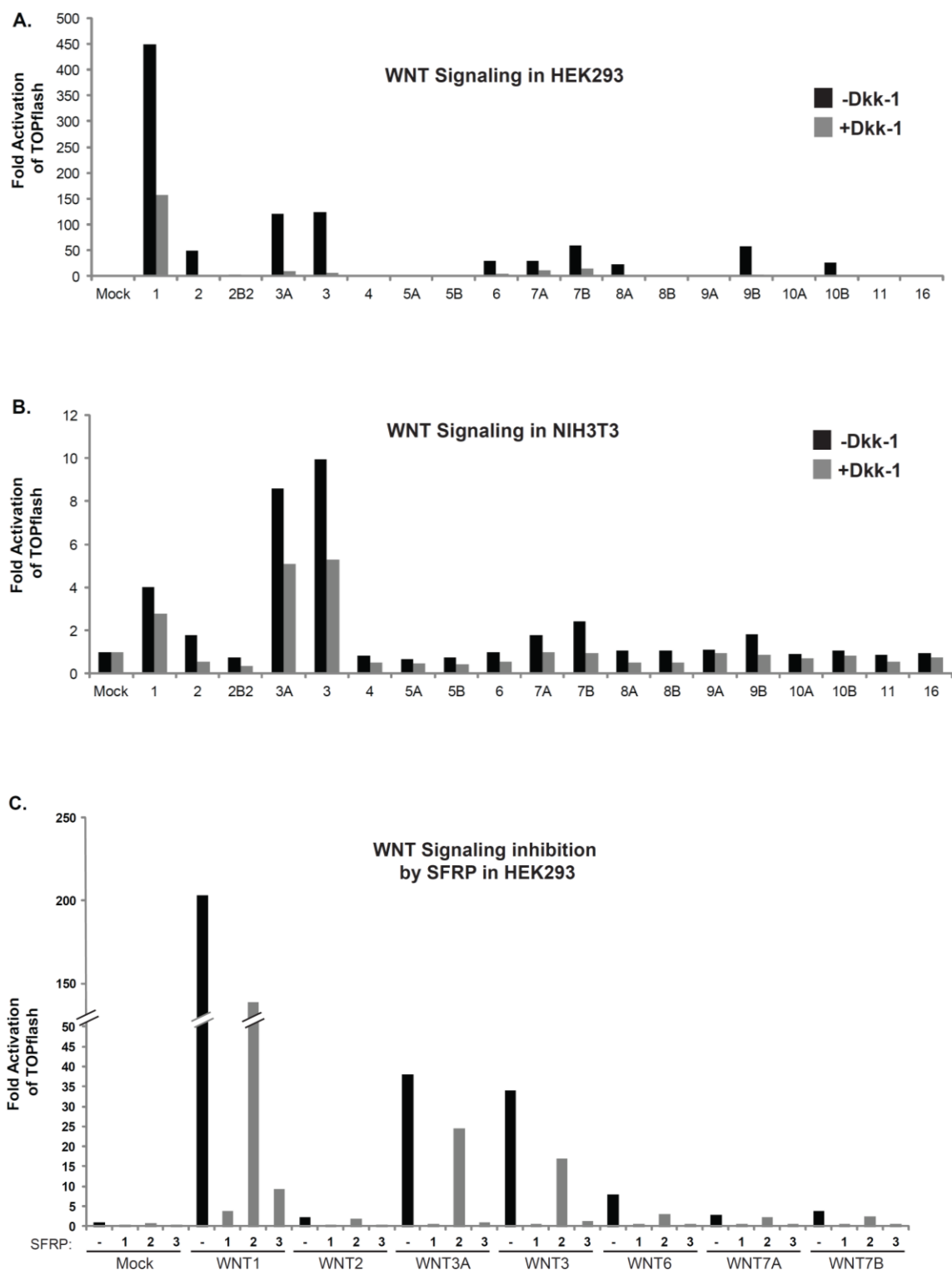


Figure 4.5. Wnt activation of the β -catenin-dependent pathway.

All 19 untagged Wnts (100 ng each plasmid) were compared for their ability to activate the Super8XTOPflash (STF) reporter in HEK293 (**A**) and NIH3T3 (**B**) cells in 6-well dishes. WNT1, 2, 3A, 3, 6, 7A, 7B, 8A, 9B and 10B were significantly active in HEK293 cells, while only WNT1, 3A, 3 and 7B were significantly active in NIH3T3 cells. Co-expression of the Wnt inhibitors Dkk-1 (400 ng plasmid) (**A** and **B**) and SFRPs 1 and 3, but not 2 (400 ng plasmid) (**C**) effectively reduced Wnt/ β -catenin signaling activity. (*Figure adapted from Figure 3 of Najdi, Proffitt, Sprowl et al., 2012*).

activation, although this could be due to expression levels rather than a decrease in binding efficiency.

We next asked whether C-terminal tagging of Wnt proteins affects their signaling properties. Plasmids expressing V5-tagged Wnts were co-transfected with the STF reporter into HEK293 cells (Fig. 4.6A). While the untagged versions of WNT1, 2, 3A, 3, 6, 7A and 7B were highly active (Fig. 4.5A and 4.6A), their C-terminal tagged counterparts could not activate the STF reporter, suggesting that C-terminal tagging interferes with their signaling potential. However, C-terminal tagging did not appear to affect expression or secretion of Wnt proteins (Fig. 4.3A, 2B and 4C). We therefore hypothesized that C-terminal tagging with the Gateway and V5 sequence might interfere with the ability of Wnt ligands to bind to their receptors at the plasma membrane. To test this hypothesis, untagged *WNT1* or *WNT3A* cDNAs were co-transfected with C-terminally tagged *WNT1-V5* or *WNT3A-V5* cDNAs respectively in HEK293 cells (Fig. 4.6B). If addition of the V5-tagged Wnt can interfere with the ability of the untagged Wnt to activate Wnt/ β -catenin signaling, it would suggest that C-terminally tagged Wnt ligands are still capable of binding to their receptors and competing with untagged Wnts, but that the tag affects signal relay to downstream components of the pathway. If addition of the V5-tagged Wnt has no effect, it would imply that C-terminal tagging interferes with the ability of Wnt ligands to bind their receptors. While WNT1-induced activation remained unchanged with increasing concentrations of *WNT1-V5* cDNA, introduction of *WNT3A-V5* cDNA blocked WNT3A-induced activation in a dose-dependent manner. To rule out the possibility that V5-tagging affects WNT1 accumulation in the media, HEK293 lysates and media were probed for the expression and accumulation of untagged Wnts 1 and 3A and their V5-tagged counterparts (Fig. 4.6C). Both versions of Wnts 1 and 3A were detected in cell lysates and media. Therefore, the inability of

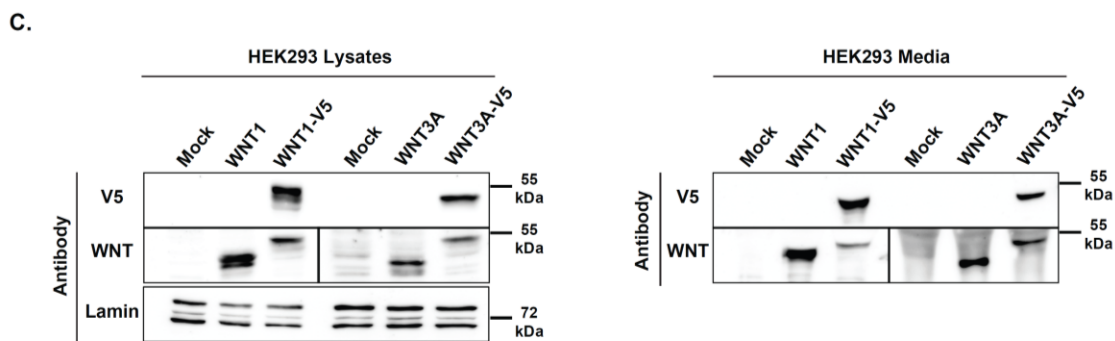
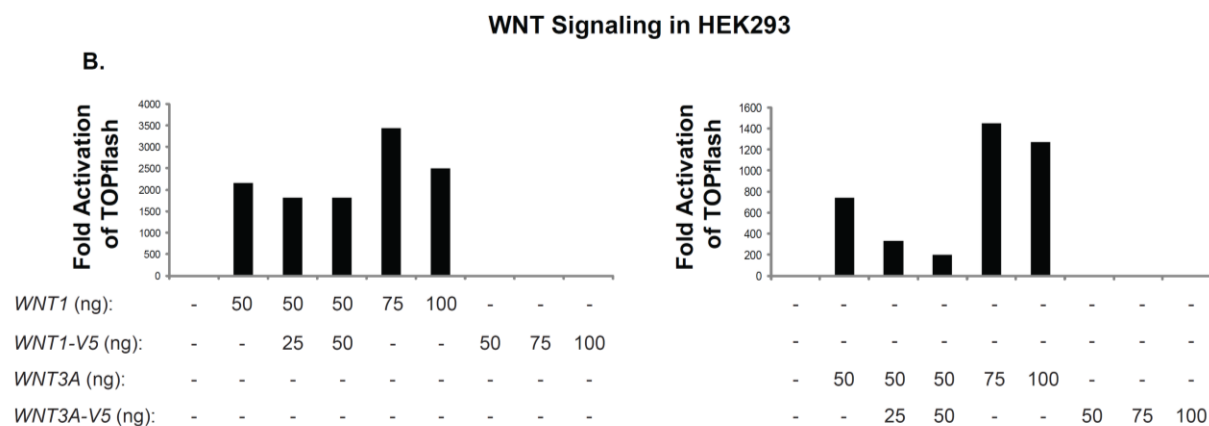
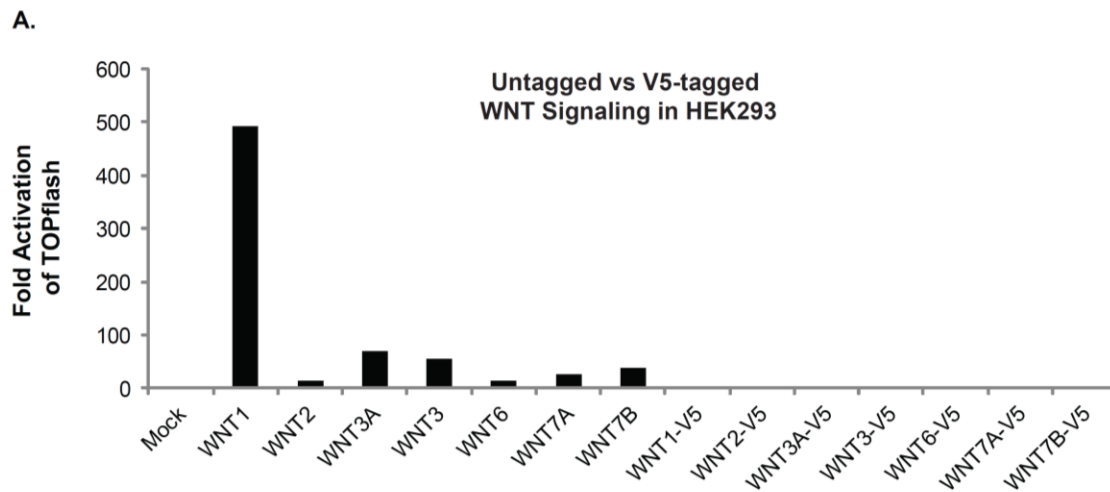


Figure 4.6. Effect of C-terminal tagging on Wnt activity, expression and accumulation.

(A) The indicated untagged and V5-tagged versions of the active Wnts were co-transfected with the STF reporter into HEK293 cells. The C-terminal V5 tag significantly reduced Wnt/ β -catenin signaling activity. (B) V5-tagged Wnts 1 and 3A were co-transfected with their untagged counterparts into HEK293 cells to determine whether they can compete for cell surface receptors. V5-tagging affects different Wnts in different manners; it interferes with the ability of WNT1-V5 to bind to cell-surface receptors, but does not do so with WNT3A-V5. (C) The expression levels of Wnts 1 and 3A in lysates (left panel) or their accumulation levels in media (right panel) are not significantly affected by C-terminal V5-tagging in HEK293 cells. Cell lysates were also probed for Lamin as a loading control. (*Figure adapted from Figure 4 of Najdi, Proffitt, Sprowl et al., 2012*).

WNT1-V5 to interfere with untagged WNT1-mediated signaling is not due to low levels of expression/secretion or its lack of accumulation in the media. These experiments suggested that C-terminal tagging might affect each Wnt ligand in a distinct manner; interfering with its binding to cell-surface receptors in the case of WNT1 or simply affecting its ability to induce activation once bound to its receptor(s) in the case of WNT3A. This is consistent with the recent finding that different Wnts might bind to different propeller domains of LRP6¹⁶².

Wnt-dependent phosphorylation of LRP6 and stabilization of β -catenin

The most readily measured effect of Wnt signaling is the activation of the β -catenin-dependent pathway. For that to occur, the LRP5/6 receptor at the cell surface must be phosphorylated at its PPPSP motif by GSK3 (Glycogen Synthase Kinase 3) and CK1 γ (Casein Kinase 1 gamma) in response to the binding of Wnt ligands¹⁶³⁻¹⁶⁵. Another hallmark of the activation of this pathway is the stabilization of the co-activator β -catenin once released from the destruction complex^{166,167}. We therefore monitored LRP6 phosphorylation and unphosphorylated β -catenin abundance by immunoblot analysis in HEK293 cells (Fig. 4.7A). While transfection of 100 ng of untagged *WNT* cDNA activated the STF reporter, this amount of Wnt plasmid had little effect on the levels of both phospho-LRP6 and non-phospho β -catenin (data not shown, Fig. 4.5A). However, transfection of a super-saturating amount, 1000 ng, of untagged *WNT* cDNA induced readily detectable changes in both phospho-LRP6 and non-phospho β -catenin abundance (Fig. 4.7A). In order to allow for accurate comparison with the activation of the STF reporter, 1000 ng of untagged *WNT* cDNA was transfected into HEK293 cells to assay for luciferase levels (Fig. 4.7B). While this saturating Wnt expression actually elicited less activity than lower expression levels, the patterns of activation remained the same (Fig. 4.5A and 4.7B). As expected, all

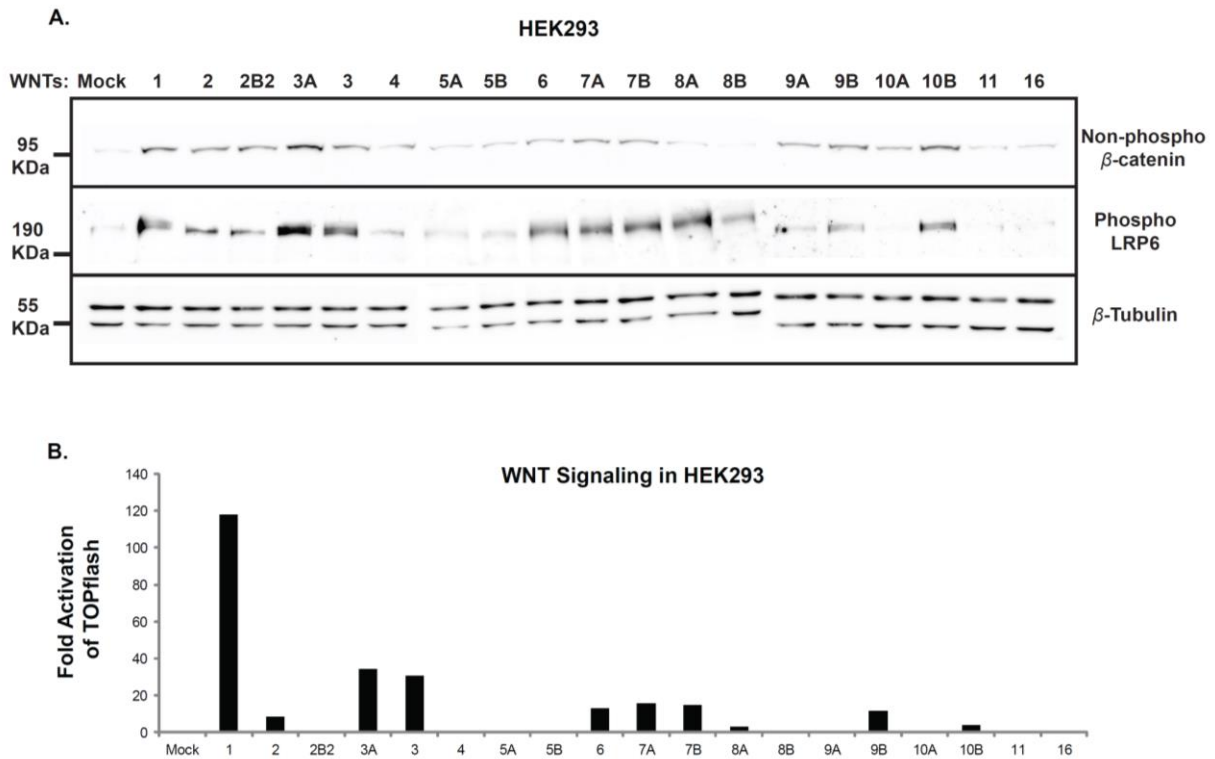


Figure 4.7. Wnt-dependent phosphorylation of LRP6 and stabilization of β -catenin. (A) The 19 untagged Wnts (1 μ g each) were tested for their ability to induce non-phosphorylated β -catenin (1st panel) and phosphorylation of LRP6 (2nd panel) in HEK293 cells. All the active Wnts (1, 2, 3A, 3, 6, 7A, 7B, 8A, 9B and 10B) were successful in inducing both, while a subset of the inactive Wnts displayed varying degrees of LRP6 phosphorylation and β -catenin dephosphorylation. β -Tubulin levels were monitored as a loading control (3rd panel). (B) Plasmid encoding untagged Wnts (1000 ng each) was transfected to determine their effect on the STF reporter in HEK293. The activation pattern is similar to that observed with 100ng of plasmid DNA (Fig. 4.5A). (Figure adapted from Figure 5 of Najdi, Proffitt, Sprowl et al., 2012).

Wnts that activated the STF reporter also induced phosphorylation of LRP6 and β -catenin stabilization to varying degrees (WNT1, 2, 3A, 3, 6, 7A, 7B, 8A, 9B and 10B). However, phospho-LRP6 and non-phospho β -catenin levels did not always track with activation of the STF reporter. For example, WNT2B2, 9A and 10A, which did not activate the β -catenin-dependent pathway in HEK293 cells, caused significant levels of β -catenin stabilization when compared to mock-transfected cells (Fig. 4.7A and 4.7B). This suggests that changes in β -catenin abundance and LRP6 phosphorylation are significantly less sensitive than the STF reporter to Wnt/ β -catenin signaling.

Analysis of the core Wnt modification and secretion pathway

One goal of the Open Source Wnt project is to test if the core Wnt synthesis and secretion pathway is common to all Wnt proteins. In the current model, all vertebrate and most metazoan Wnts are post-translationally modified by palmitoylation on one or two conserved Cysteine and Serine residues^{152,153}. Serine palmitoylation (with a mono-unsaturated palmitate) is required for several Wnts to bind to the integral membrane protein WLS, which then transports the Wnts to the plasma membrane¹⁶⁸. All but one *Drosophila wingless* protein requires WLS for activity^{169,170} suggesting a broad requirement for both PORCN and WLS proteins. Conversely, however, one study suggested that WLS is only required for a small subset of Wnts in *Xenopus* development¹⁷¹. The standardized Wnt expression library allows us to examine if there is variability in the mechanism by which human Wnts are secreted from cells.

To ask if all human Wnts require PORCN for activity, we created a human fibrosarcoma HT1080 cell line with a zinc-finger nuclease-mediated null mutation in the single copy PORCN gene (PORCN is on the X chromosome, and HT1080 cells are male)¹⁷². The activity of

transfected Wnts was tested in paired wildtype and PORCN null cells by STF reporter assays (Fig. 4.8A) and Dvl2 (Dishevelled 2) mobility shift (Fig. 4.8B). As Figure 6 shows, wildtype HT1080 cells were extremely responsive to Wnts. Fourteen of the nineteen Wnts were able to activate β -catenin-dependent signaling, ranging from 3- to 1000-fold. In all cases, the matched PORCN null cells had no measurable Wnt/ β -catenin signaling activity. This was not due to any secondary effect of the PORCN mutation, since the signaling activity of the null cells could be rescued by wildtype but not catalytically inactive PORCN plasmid co-transfection (Fig. 4.8B and data not shown). A subset of Wnts was not able to activate Wnt/ β -catenin signaling in HT1080 cells. These Wnts (and WNT3A) were assessed for their ability to activate the CK1-dependent phosphorylation of endogenous Dvl2. WNT3A and four of five additional Wnts were able to stimulate Dvl2 mobility shift in a PORCN-dependent manner (Fig. 4.8B), indicating that PORCN is also essential for β -catenin-independent Wnt signaling. Of the nineteen Wnts tested, PORCN (and hence Wnt palmitoylation) was essential for the function of eighteen while one Wnt, WNT5B, was unable to be assessed in these assays.

Palmitoylation can affect Wnt export, membrane association, and receptor binding. Palmitoylation is required for WNT3A and WNT5A to bind to WLS for proper transport to the cell membrane. However, whether all of the mammalian Wnts similarly bind to endogenous WLS in a palmitoylation-dependent manner is not known. To test this, we utilized the Wnt-V5 library and the PORCN inhibitor IWP1¹⁷³. Wnts that were expressed at sufficiently high levels to be clearly visualized were assessed in HeLa cells (HeLa cells were chosen because they have high endogenous WLS levels). In every evaluable case, Wnts co-immunoprecipitated with WLS, and this interaction was sensitive to the PORCN inhibitor IWP1 (Fig. 4.9). WNT5B, whose

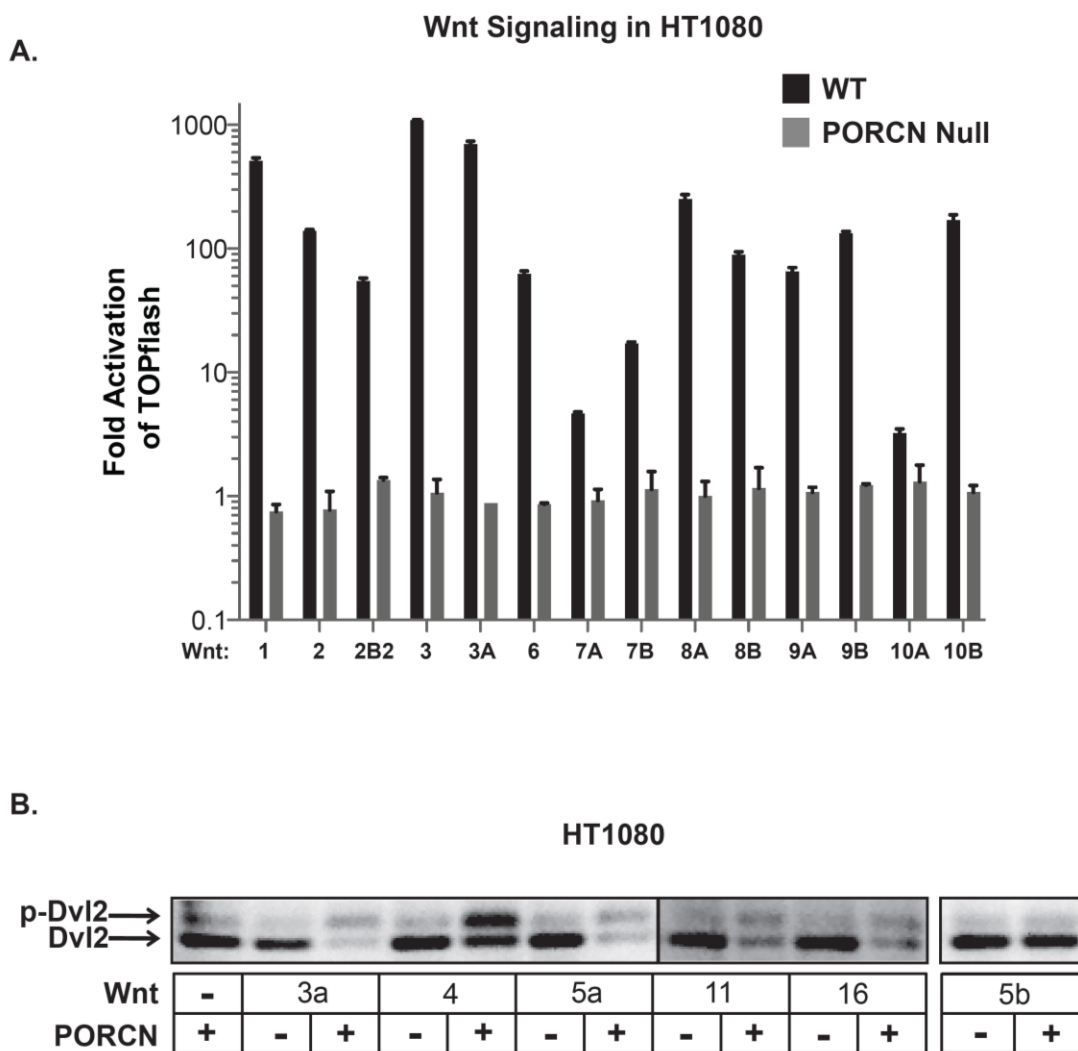


Figure 4.8. Wnts require PORCN for activity.

(A) WT and PORCN null HT1080 cells were transfected in parallel with untagged Wnts shown (50 ng per well in a 24-well dish) in combination with the STF reporter. Data is presented as fold activation over background signal with no transfected Wnt. Error bars represent SD. (B) PORCN null HT1080 cells were transfected with Wnts shown, in combination with mPORCN-D expression plasmid as indicated. Western blots were performed to analyze the Wnt and PORCN-dependent Dvl2 electrophoretic mobility shift. (Figure adapted from Figure 6 of Najdi, Proffitt, Sprowl et al., 2012).

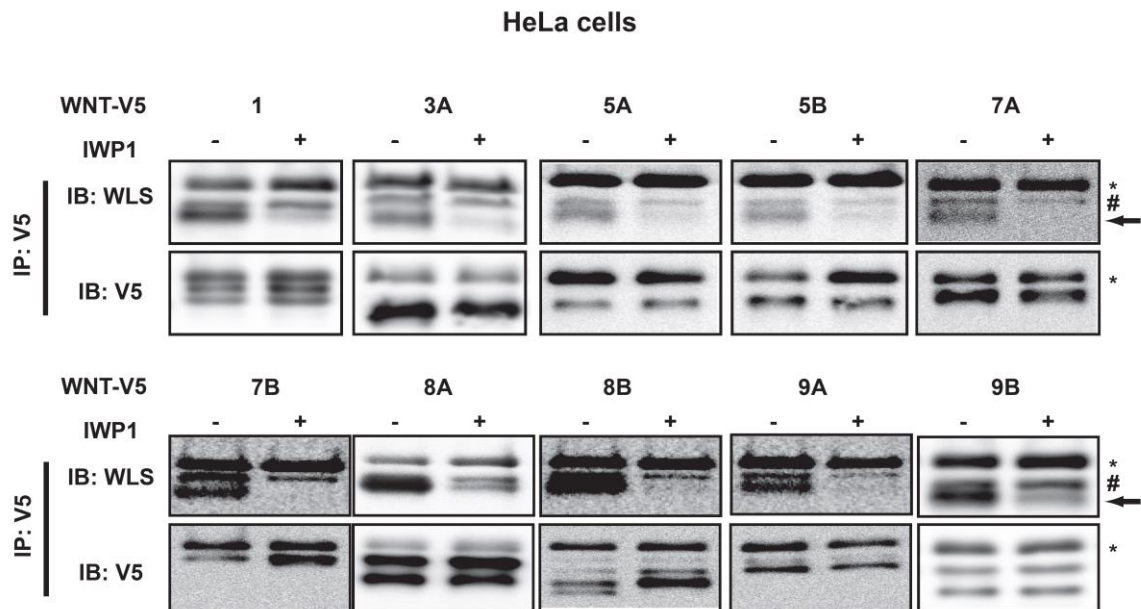


Figure 4.9. All tested Wnts bind WLS in a PORCN dependent manner. HeLa cells were transfected with C-terminal V5 tagged Wnts (1000 ng per 10 cm dish) and treated with either DMSO or the PORCN inhibitor IWP1 (2 μ M) overnight. 500 μ g of lysate was subject to immunoprecipitation with anti-V5 antibody and immunoblot carried out with anti-WLS and anti-V5 antibodies. Arrow indicates WLS, asterisk (*) indicates IgG heavy chain. Hex (#) indicates non-specific band. (Figure adapted from Figure 7 of Najdi, Proffitt, Sprowl et al., 2012).

WNT Signaling in HEK293

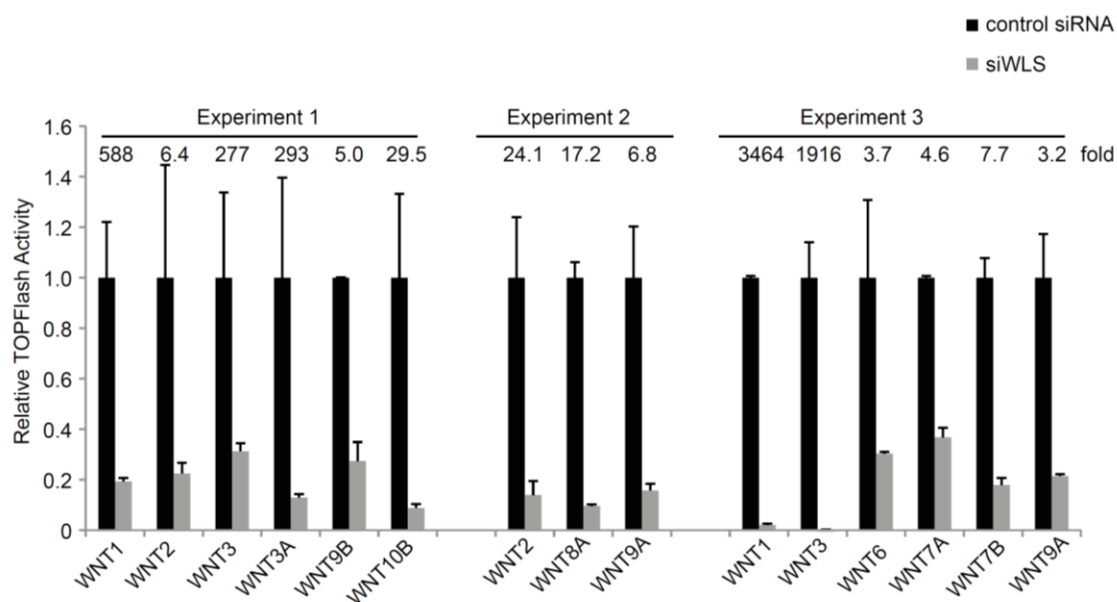


Figure 4.10. Wnt signaling requires WLS.

HEK293 cells with an integrated Super8XTopFlash reporter (STF cells (21)) were transfected with the indicated untagged Wnts together with either control or WLS siRNA. Fold activation by the Wnts in the presence of control siRNA is indicated above the columns, and the effect of WLS knockdown is presented as remaining Wnt/ β -catenin signaling activity in cells with WLS knockdown. (Figure adapted from Figure 8 of Najdi, Proffitt, Sprowl et al., 2012).

signaling activity we were unable to assess, nonetheless interacted with WLS in a palmitoylation-dependent manner. Thus, the palmitate-dependent interaction of Wnts with WLS is a general feature of human Wnt secretion. This suggested that WLS, like PORCN, would be essential for the signaling activity of all Wnts. To test this directly, WLS was knocked down by siRNA and Wnt/ β -catenin signaling activity of was assessed. As shown in figure 4.10, all evaluable Wnts (11 of 19) require WLS for full Wnt/ β -catenin signaling activity.

Discussion

Here we report the cloning of all 19 human Wnts and the subsequent analysis of their expression in cells, their secretion and accumulation in media, and their signaling properties through the Wnt/ β -catenin pathway. All V5-tagged Wnt proteins are produced in HEK293 cells and secreted into the media (Fig. 4.3). While some Wnts (1, 2B2, 3A, 7A and 9A) are highly expressed, others (2, 4, 5A, 5B and 16) are poorly produced. There are also major differences in the estimated concentrations at which Wnts are secreted into the media, and these largely correlate with the expression levels. Since Wnt mRNA levels are relatively similar, this variation could be due to several factors (Fig. 4.4). Some Wnts might contain seed sequences for miRNAs to target and therefore downregulate the translation of the message. Another possibility is that different protein structures or folding have varying effects on Wnt protein stability. This is supported by the fact that Wnt proteins are expressed and secreted in relatively similar patterns in two different cell lines, with the exception of WNT16, which is produced at higher levels in NIH3T3 cells. The variation in Wnt protein levels suggests that the use of conditioned media to survey Wnt activity might not be an accurate representation of the signaling potential of each Wnt since they are all expressed and secreted at different levels. Therefore, it is essential to

confirm whether Wnt proteins are efficiently secreted and can be detected in the media before reaching conclusions about their signaling properties, a task made easier by these matched untagged and V5-tagged Wnt expression constructs. The greater number of Wnt protein isoforms observed in cell lysates compared with culture media is likely due to the different stages of processing and protein modifications that these particular Wnts undergo inside cells prior to secretion. This could provide a glimpse into the post-translational modifications of Wnt proteins and how different this process is for each ligand. For example, WNT1 has four isoforms as it goes through several steps of processing while WNT3 has only one isoform. Curiously, out of the Wnts that have more than one isoform in HEK293 cells, only Wnts 1 and 8B exhibit a similar processing pattern in NIH3T3 cells, suggesting key differences between the two cell lines in the Wnt biogenesis pathway.

The use of the STF reporter has allowed us to assess and compare the ability of all Wnts to signal through the Wnt/ β -catenin pathway (Fig. 4.5 and 4.8A). Twelve Wnts are capable of significantly activating the β -catenin-dependent pathway in HEK293 cells, ranging from 2- to 450-fold above background. The inability of the other 7 Wnts to activate the STF reporter may not accurately reflect their potential, since it is possible that the cell-surface receptors required for these Wnts to signal through β -catenin are not expressed in HEK293 cells. Indeed, this has already been shown for WNT5A². In our system, WNT8B and Wnt10A were inactive in HEK293 and HeLa cells but activated the STF reporter in HT1080 cells, with WNT8B increasing signal nearly 100 fold above background. This is consistent with the model that the repertoire of cell surface receptors determines the nature of the response to the Wnts. For example, the inhibitory effects of WNT5A in HEK293 cells are typically mediated through the orphan tyrosine kinase receptor Ror2, but when Fz4 and LRP5 are available for binding,

WNT5A activates β -catenin signaling². A second hypothesis for the inactivity of some Wnts could be inability to interact with other Wnts. The clearest example is that of Wnts 5A and 11, which may heterodimerize together to activate β -catenin signaling¹⁵⁶. Since this interaction is dependent on tyrosyl sulfation of both interacting Wnts, defects in Wnt sulfation or the absence of the corresponding Wnt partner could all be reasons for the inability to activate the STF reporter. Overall, these data suggest that all Wnts might be capable of signaling through the β -catenin arm of the pathway as long as the right components are expressed. One might also argue that the expression/secretion profiles affect signaling potential; Wnts that are abundantly secreted might be expected to signal efficiently while those that are poorly produced may not signal at all. However, this is clearly not the case. WNT2, which is barely detectable in western blots (Fig. 4.3A), is one of the more potent activators of the β -catenin pathway (Fig. 4.5A). Meanwhile, highly expressed/secreted Wnts such as 2B2, 9A and 10A have little to no activity.

Activation of the β -catenin pathway can be effectively abrogated by the Wnt inhibitors Dkk-1, SFRP1 and SFRP3 (Fig. 4.5). Inhibition by Dkk-1 is not surprising considering that β -catenin signaling is mediated through the LRP5/6 co-receptor and that Dkk-1 blocks Wnt signaling by binding to LRP5/6. SFRP1 and SFRP3-mediated repression of Wnt activity suggests that those two members of the SFRP family can efficiently bind to all the Wnts that were tested. The ineffective inhibition by SFRP2, on the other hand, might be due to poor expression or to poor binding to Wnt ligands in HEK293 cells (Fig. 4.5C). However, in L cells, SFRP proteins 1 and 2, but not 3 are strong inhibitors of WNT3A-mediated signaling¹⁷⁴. It was previously reported that C-terminal tagging of Wnts can have negative effects on Wnt ligand activity (data not shown). Here we show that these Gateway-V5-tagged Wnts can no longer activate β -catenin signaling and that inactivity may be due to Wnt-specific variable causes (Fig.

4.6). This is demonstrated by the finding that the C-terminal tagging of WNT1 likely blocks its ability to bind to cell surface receptors, while our data suggest that WNT3A-V5 can bind to receptors, but does not induce activation of the pathway for other reasons. While the V5-tagged Wnts are inactive and appear to be secreted at a slightly lower concentration than their untagged counterparts, they have proven to be important for monitoring Wnt expression, secretion and accumulation in the media (Fig. 4.3 and 4.6C).

In addition to surveying Wnts for activation of the STF reporter, we also examined their ability to induce phosphorylation of LRP6 and stabilization of β -catenin in HEK293 cells (Fig. 4.7). All Wnts that activate the STF reporter are also capable of inducing LRP6 phosphorylation and β -catenin stabilization, two requirements for the activation of Wnt/ β -catenin signaling. Interestingly, some Wnts such as 2B2, 9A and 10A can trigger LRP6 phosphorylation and β -catenin stabilization despite not having any effect on STF activity. The same Wnts are also highly expressed and secreted into the media, suggesting that despite their abundance and stability, these Wnts are not potent enough to significantly affect the transcriptional output of the Wnt pathway. In this case, it is possible that the stabilized β -catenin is bound to E-cadherin complexes at the plasma membrane or not effectively transported into the nucleus¹⁷⁵. This is certainly true in cancer, where stabilized β -catenin is often predominantly cytosolic rather than nuclear. Alternatively, although stabilized, perhaps there is a threshold of β -catenin accumulation that needs to be reached before it can translocate to the nucleus and activate transcription. Even if β -catenin accumulates and translocates to the nucleus, activation of gene expression is not always guaranteed¹⁷⁶. In other cases, LRP6 phosphorylation and β -catenin stabilization do not go hand in hand. For example, WNT8B upregulates phospho-LRP6, but cannot stabilize β -catenin in HEK293 cells, suggesting that LRP6 phosphorylation may not always be sufficient to

inactivate the destruction complex. Whatever is missing in HEK293 cells is present in HT1080 cells because WNT8B is a strong activator of the STF reporter in that system (Fig. 4.8). On the other hand, WNT10A stabilizes β -catenin without detectable phospho-LRP6, again suggesting the phospho-LRP6 is an insensitive assay, or that there may be an alternative ligand-receptor combination. While Wnt-mediated transcriptional activation is always accompanied by either LRP6 phosphorylation or the accumulation of β -catenin, the inverse is not true: even when both LRP6 phosphorylation and β -catenin accumulation are observed, STF reporter activation is not guaranteed.

Finally, we investigated whether all Wnts require PORCN-mediated palmitoylation to signal and to bind to the transporter protein WLS. We find that all Wnts that signal through the β -catenin pathway in HT1080 cells are dependent on the presence of PORCN to activate the STF reporter (Fig. 4.8A). In addition, the Wnts that signal through β -catenin-independent pathways (4, 5A, 11 and 16) also require PORCN to induce the phosphorylation of Dvl2, a marker of both β -catenin-dependent and independent Wnt activity (Fig. 4.8B). WNT5B is the only Wnt that does not exhibit any signaling activity that we could measure, but it too required PORCN function to bind to WLS. We also find that WLS is required at least for the Wnt/ β -catenin signaling activity of all testable Wnts, since WLS knockdown inhibited the STF reporter activity of the 11 assessable Wnts (Fig 4.10). Since Wnts 5A and 5B have very similar amino acid sequences, it is possible that the few amino acid differences dictate the differences in their signaling activity. Thus, PORCN and WLS form an essential core Wnt production module. We also confirm that one key function of Wnt palmitoylation is to enable their binding to WLS. Finally, an implication of this work is that inhibition of either PORCN or WLS will block the

ability of cells to secrete any active Wnts, which makes them potential drug targets for diseases of excess Wnt activity.

The availability of this complete and standardized set of untagged and V5-tagged Wnt plasmids has made it possible to thoroughly compare and contrast the secretion and signaling profiles of all human Wnt ligands and will be useful to the scientific community to gain new understanding of the Wnt signaling pathway.

CHAPTER FIVE

Discussion

Functions of LEF/TCFs and Wnts in Colon Cancer

The presence of full-length LEF/TCF isoforms in colon cancer and the absence of their dominant negative counterparts provides a window of opportunity for probing functional outputs and gene programs regulated by the Wnt signaling pathway. Dominant negative LEF/TCFs, when expressed, compete with their full-length, β -catenin binding-counterparts for occupancy of Wnt Response Elements in target genes. Their competitive binding results in repression of transcription of target genes, and silencing of Wnt target gene programs^{33,34}. Previous studies in the Waterman lab used overexpression of dnTCF-1 or dnTCF4 isoforms that contain a C-terminal E-tail to reveal the role of the E-tail encoding C-clamp in regulation of the cell cycle (See *LEF/TCF Structure* in the Introduction for reference). Regulation of the cell cycle occurs in part through Wnt target gene *SP5* and its subsequent downregulation of the cell cycle inhibitor p21^{28,29,86}. Expression of dnTCF-4 with an N-tail restores epithelial cell polarity, suggesting that its full-length counterpart somehow interferes with this process and most likely favors activities such as epithelial-mesenchymal transition and cell movement⁶⁸. We expressed dnLEF-1 and an isoform of dnTCF-1E that was inactivated for the C-clamp (dnTCF-1Emut) in colon cancer cells as a tool to modulate Wnt signaling and discover additional roles that LEF/TCFs play in the cancer cell phenotype beyond cell cycle and cell polarity regulation. Through expression of these isoforms we identify Warburg metabolism as a novel Wnt-driven gene program in colon cancer. Furthermore, we identify pyruvate dehydrogenase kinase 1 (PDK1) and monocarboxylate transporter 1 (MCT-1) as direct target genes important for this program.

Our current understanding in the field of metabolism is that cancer cells adopt a preference for glycolysis over oxidative phosphorylation for two reasons: to optimize the production of biomass for rapidly proliferating cells and to limit ROS production^{71,177-180}. We propose that the Wnt signaling pathway plays a crucial role in directing Warburg metabolism, a form of glycolysis that can occur independent of oxygen tension. We propose that Wnt regulates at least two key steps in this pathway (Model, Fig. 5.1). Our experiments demonstrate that PDK1 is a pivotal mediator of Wnt signaling's effects on metabolism. Not only is it a direct Wnt target gene with at least two distal regions that regulate transcription of the PDK1 locus, but rescue of its protein expression in cancer cells with reduced Wnt signaling (expressing dnLEF/TCFs) restored the level of glycolysis that was apparent in the presence of full Wnt signaling. We hypothesized that PDK1 is only one target of a multi-gene program driven by Wnt to promote cancer-supporting metabolism. It is possible that knockdown of a single Wnt target gene out of the context of an entire gene program is not sufficient to shift metabolism and tumor proliferation phenotypes. Ontology analysis of our microarray study identified additional metabolism-linked genes that were downregulated by dnLEF/TCFs (Fig. 2.1), including genes that encode nutrient and small molecule transporter genes that affect metabolic pathways. We asked whether the gene *SLC16A1*/MCT-1 is a direct Wnt target as its known function is to transport lactate, the waste product of Warburg metabolism. Here we show that indeed, *SLC16A1* transcription is directly regulated by LEF/TCFs and β -catenin. This discovery places *SLC16A1* within a program of glycolysis that we have defined for colon cancer. We determine that *SLC16A1*/MCT-1 regulation is mediated directly through two Wnt Response Elements in the promoter (Fig. 3.5). *SLC16A1*/MCT-1 mRNA was downregulated via dnLEF/TCF expression, as evidenced both by microarray and RT-qPCR analysis of xenograft tumors (Fig. 2.16).

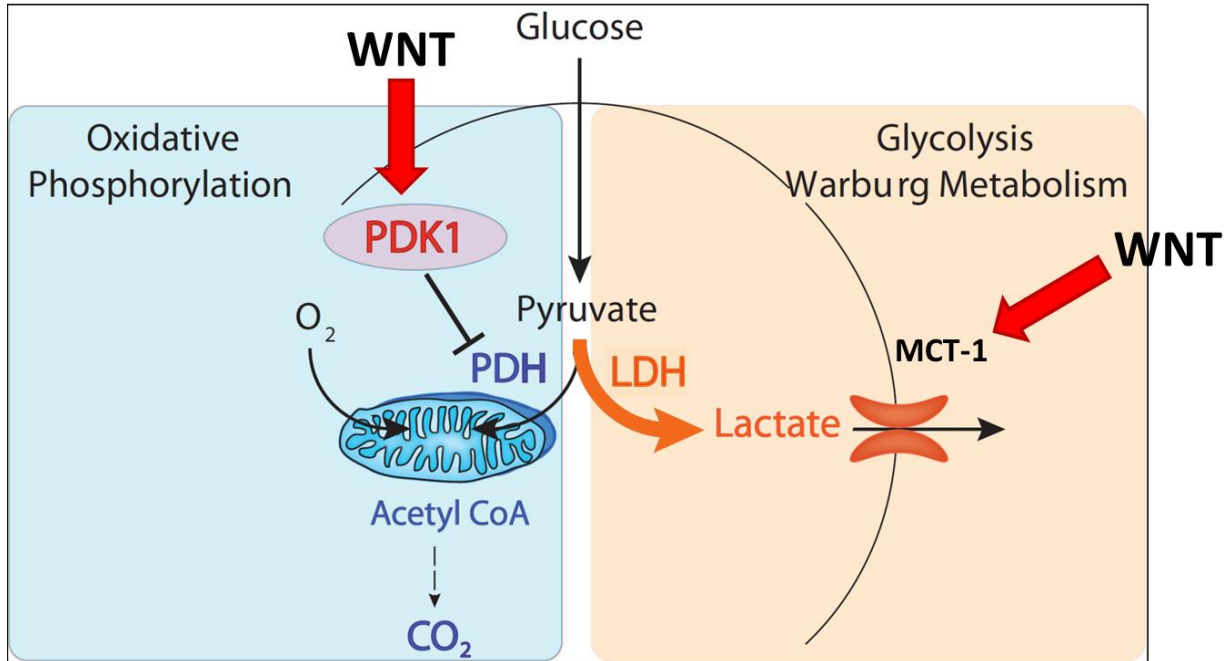


Figure 5.1. Wnt signaling influences cancer metabolism through regulation of PDK1 and *SLC16A1*/MCT-1 expression.

In the presence of oxygen in normal differentiated tissue, glucose is completely oxidized to CO₂ through glycolysis, the TCA cycle, and oxidative phosphorylation. In the absence of oxygen, glucose metabolism is limited to glycolysis and is fermented into lactate. Cancer cells have an altered metabolism characterized as the Warburg metabolism or aerobic glycolysis - even in the presence of oxygen, cells continue to limit their metabolism to glycolysis and convert pyruvate to lactate via Lactate Dehydrogenase (LDH). Wnt signaling regulates Warburg metabolism through the upregulation of Pyruvate Dehydrogenase Kinase 1 (PDK1), which phosphorylates and inhibits Pyruvate Dehydrogenase (PDH) in the mitochondria and Monocarboxylate Transporter 1 (MCT-1), a lactate transporter (*Figure adapted from Dr. Marian Waterman*).

Furthermore, we and others determined using ChiP-seq that the MCT-1 promoter is directly occupied by TCFs, in HCT116 and DLD-1 colon cancer cells (Fig. 2.16). MCT-1 is a critical player in tumor metabolism and is known to be upregulated in colon cancer¹⁸¹. We observe highly upregulated, heterogeneous levels of MCT-1 protein throughout a set of probed human colon adenocarcinoma samples, compared to weak expression in the normal mucosa surface (see Figure 5.2). Increased expression of MCT-1 in cancerous lesions aligns with an increased reliance of glycolytic cancer cells on lactate/ monocarboxylate transporters (such as MCT-1) to secrete lactate, a waste product of fermentation. Lactate is highly acidic and its export from cells helps maintain intracellular pH levels. Our studies also show that colon cancer cells express at least one other monocarboxylate transporter (MCT-4), but it is MCT-1 that has optimal export kinetics for lactate, and therefore provides a more sensitive and responsive avenue to maintain pH homeostasis for the intracellular environment. Interestingly, the glucose transporter GLUT-1 was also downregulated with dnLEF/TCF expression, both by microarray analysis and RT-qPCR analysis of xenograft tumors (Fig. 2.16). Since tumors with a strong glycolytic phenotype rely heavily on glucose uptake, GLUT-1 may be another example of a Wnt target gene that contributes to the Warburg metabolic program regulated by this pathway.

Previous studies have identified other metabolism-connected Wnt target genes. For example, the well-known Wnt target gene *MYC* plays pivotal roles in cancer metabolism, driving both aerobic glycolysis and accumulation of biomass through transcriptional activation of genes that drive nucleotide synthesis, lipid synthesis and glutaminolysis^{71,182-187}. In fact, c-Myc has been shown to enhance HIF-1 α -mediated regulation of PDK1¹⁰³. c-Myc was not required in the xenograft system to mediate changes in metabolism as its levels were not altered with expression of dnLEF-1 (supported by microarray, Western, and RT-qPCR analyses - Chapter 2, Figure 2.7).

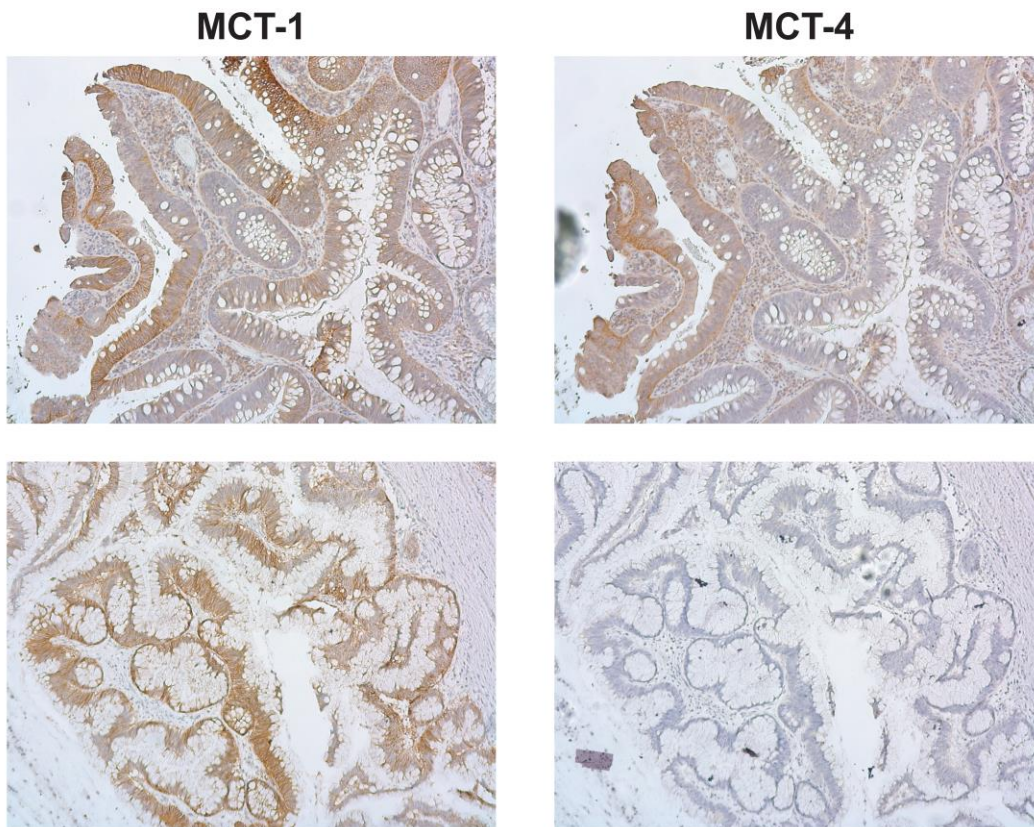


Figure 5.2. MCT-1 and MCT-4 expression in colon adenocarcinoma samples. Immunohistochemical staining of colon adenocarcinoma (MCT-1 and MCT-4) shows high, heterogeneous expression of MCT-1 consistent with Wnt signaling patterns of expression, and low levels of MCT-4. Images were taken at 10X magnification.

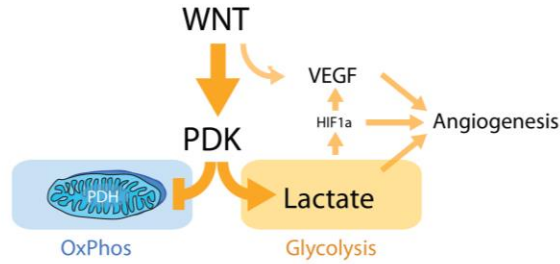
However, as Wnt/ β -catenin signaling is the main driver of colon cancer, it is likely that the Wnt target c-Myc should cooperate with the genes identified in our study to collectively drive strong, glycolytic signatures of Warburg metabolism. Additional Wnt target genes linked to glycolysis have also been identified in the liver. For example, Chafey, et al. show that Wnt augments LDH (lactate dehydrogenase) activity and downregulates two mitochondrial ATPase subunits in hepatocytes, thus driving glycolysis at the expense of oxidative phosphorylation¹⁸⁸. While it is not clear whether these effects are direct or indirect, this data along with the other evidence above suggests that Wnt signaling promotes a gene program that supports a cancer-promoting metabolic profile of enhanced aerobic glycolysis.

Most tumorigenic actions of signaling pathways like Wnt represent distorted use of normal functions crucial to cellular homeostasis. How might Wnt promotion of aerobic glycolysis be beneficial to normal tissues? One organ that illustrates this benefit is the liver where Wnt signaling regulates liver function, including functional and anatomical liver zonation, hepatocyte maturation and glycolytic metabolism^{189–192}. The pancreas is also central to whole-body glucose homeostasis, a tissue that exhibits important links between Wnt signaling and disease. The most relevant link to normal tissue from this study is that Wnt regulation of glycolysis is important to normal intestinal tissue. The Waterman and Gratton laboratories recently collaborated to use FLIM analysis to identify a metabolic gradient along the crypt-villus axis of the mouse small intestine⁸⁵. Consistent with our finding that Wnt signals drive a glycolytic phenotype, the strongest glycolytic signatures were observed at the base of the crypt and lowest at the top of the villi, correlating with high and low Wnt activity, respectively. Interestingly, immunofluorescence of the stem cell compartment staining for Lgr5⁺ stem cells and CD31⁺ vessels showed the vasculature hugging the base of the crypt where the stem cells

reside, suggesting that the stem cells are not hypoxic and perhaps choosing Warburg metabolism (Stringari and Waterman, unpublished). According to the model proposed here (Fig. 5.3), Wnt promotes a glycolytic signature through regulation of PDK1, which then promotes HIF1 α stabilization. Consistent with this model, high levels of PDK1 protein and its target, phosphoPDH, were detected at the bottom of human intestinal crypts (Fig. 5.3). Stabilized HIF1 α is also detected in crypt bases (in addition to the hypoxic region at the tops of crypts, which has been reported previously¹⁹³; Fig. 5.3). Wnt-stimulated HIF1 α stabilization could contribute to a positive feedback loop to support glycolysis in the intestinal stem cell niche as HIF1 α targets several components of glycolysis. Wnt also plays an important direct role in the maintenance of stem cells, which utilize aerobic glycolysis as a metabolic resource^{36,194–196}. The benefits of this type of metabolism in stem cells include support for proliferation as well as reduction in ROS (reactive oxygen species) production to protect the integrity of the genome^{197,198}.

Given the strong evidence for direct regulation of PDK1 and *SLC16A1*/MCT-1 transcription in colon cancer cells, we collaborated with Dr. Chad Garner (Dept. Epidemiology) to ask whether Wnt and glycolysis gene programs were correlated in primary human tumors. Publically available gene expression data from The Cancer Genome Atlas Data Portal was used to test for correlations between PDK1 expression and signatures of overactive Wnt signaling (TCGA, <https://tcga-data.nci.nih.gov/tcga/>). No correlation was identified. Nevertheless, a different method of analysis detected links between Wnt signaling and glycolysis in tumors (Fig. 5.4). In this analysis a comparison of the expression level of Wnt and glycolysis genes (defined by Kyoto Encyclopedia of Genes and Genomes (KEGG)) was used for unsupervised clustering of 238 human tumors into nine tumor groups with one group of 21 tumors strongly clustered (group 4, Fig. 5.4a). This same cluster was detected when gene

a



b

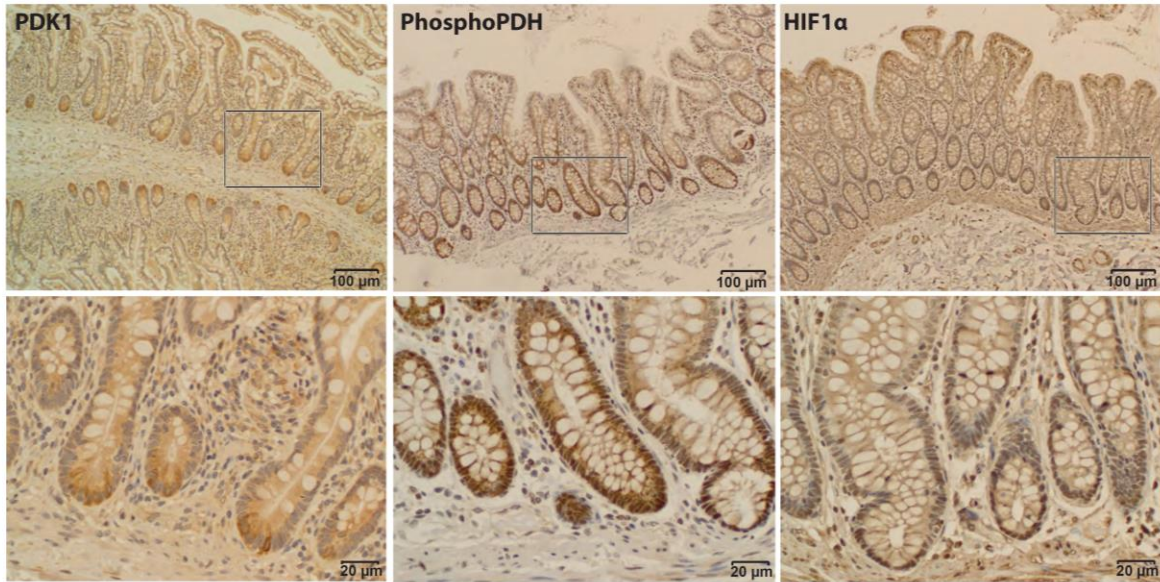


Figure 5.3. Wnt promotes aerobic glycolysis through PDK1.

(A) Model of Wnt regulation of cancer metabolism and angiogenesis through PDK1. (B) Immunohistochemical staining of normal human small intestine (PDK1) and normal human colon (PhosphoPDH and HIF1 α) shows correlations between high levels of Wnt signaling, PDK1 activity, and HIF1 α levels. Bottom row shows higher power images of boxed portions in the top row. (Figure adapted from Figure 8 of Pate, Stringari, Sprowl-Tanio et al., 2014).

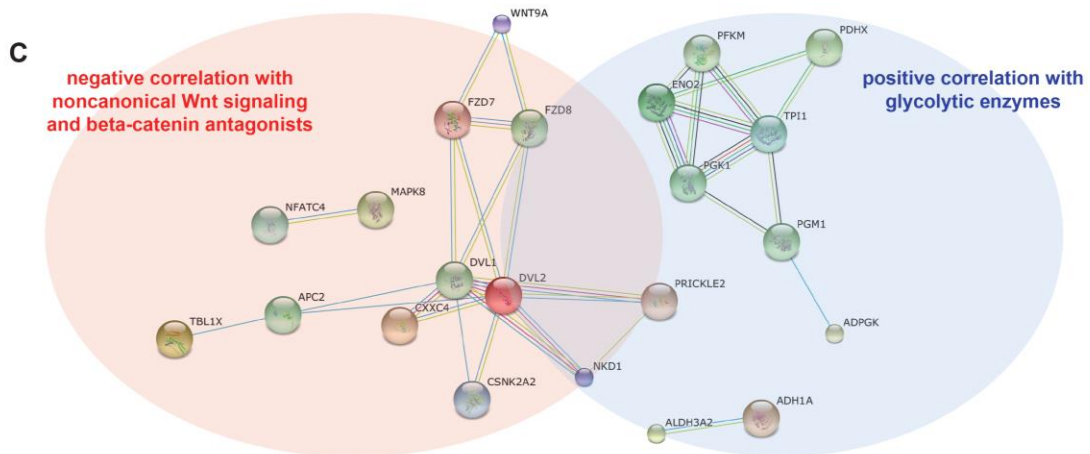
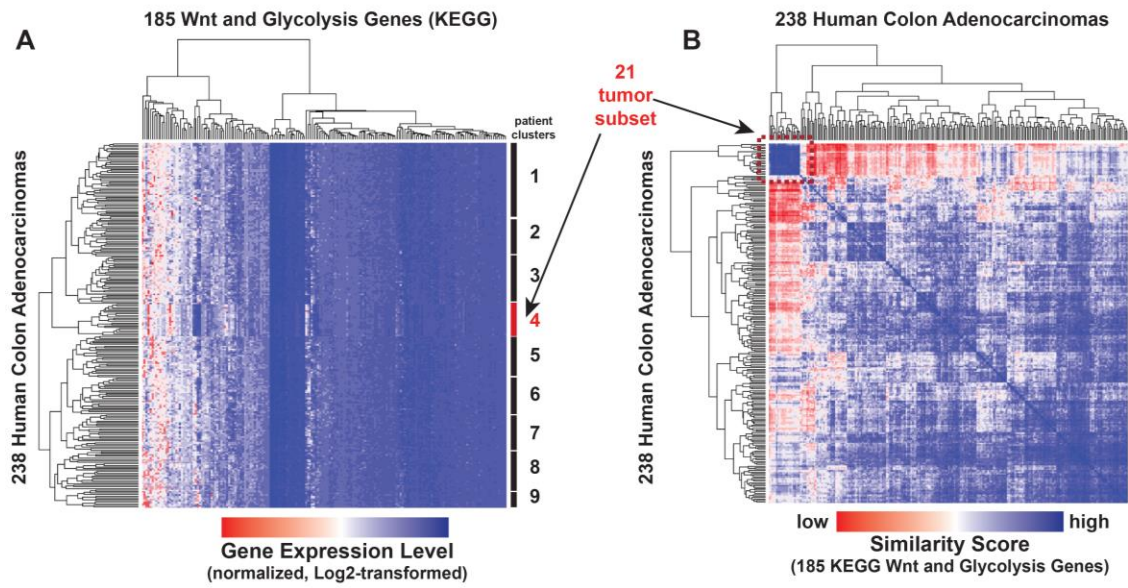


Figure 5.4. Bioinformatic analysis of colon adenocarcinoma tumors that segregate based on Wnt and Glycolysis gene signatures.

(A) Publically available data from The Cancer Genome Atlas (TCGA) Data Portal (<https://tcga-data.nci.nih.gov/tcga/>) was used to probe for correlations between PDK1 expression and signatures of overactive Wnt signaling. A simple comparison of the expression level of Wnt genes and Glycolysis genes (as defined by KEGG) enables unsupervised clustering of 238 human tumors into nine groups, with a single group of 21 tumors strongly clustered (#4). (B) This same group of tumors is detected as having a strong similarity (i.e. strong correlations (or anti-correlations)) and a distinct signature in the expression pattern of the KEGG-defined Wnt signaling and glycolysis genes when a distance measure is applied in a cross-comparison among the 238 tumors. PDK1 ranks as one of the most highly correlated genes in these 21 tumors with strong correlations to 16 Wnt and 9 glycolysis genes (see Supplemental Experimental Procedures for the list of genes and correlation scores). (C) The strongest correlations between PDK1 and Wnt signaling are negative correlations while most correlations with glycolysis genes are positive. Gene IDs of the 25 correlating genes was submitted for STRING analysis (http://string_db.org) which generates a network of known and predicted functional interactions from a user-defined gene list where each colored node is one gene. The Venn diagram overlay indicates that the majority of anti-correlating Wnt genes are either antagonists that reduce Wnt signaling, components of non-canonical Wnt signaling and/or interactors of the Wnt signaling component Dishevelled. (Figure adapted from Figure S10 of Pate, Stringari, Sprowl-Tanio et al., 2014).

signatures were compared via distance measures within the cluster versus the other eight tumor groups (Fig. 5.4b). Strong similarities (correlations and anti-correlations) between Wnt signaling components and glycolysis genes were detected within this group, relationships that distinguished the cluster from the remaining clusters. Importantly, PDK1 ranked as a highly correlated gene in the 21 tumors, its expression most often having negative, anti-correlations with Wnt components. The majority of anti-correlating genes encode antagonists of Wnt signaling or components of noncanonical Wnt signaling, and interestingly, the STRING algorithm for protein interaction networks revealed that most of these anti-correlating components engage in direct or indirect interactions with the Wnt component Dishevelled (Fig. 5.4c;¹⁹⁹). These data are compelling because any kind of clustering of colon tumors on the basis of gene expression suggests a promising approach to probe differences between tumors for diagnosis and/or prognosis, and they most certainly warrant further investigation and validation.

As mentioned above, Wnt and glycolysis gene programs were not correlated in primary human tumors. This finding is consistent with recent studies of large tumor datasets (> 2,500) that found confounding levels of heterogeneity for gene signatures of metabolism, and consistent with our observation of compensatory PDK activities in PDK1 shRNA knockdown lines²⁰⁰. Furthermore, there is no significant difference in relative levels of MCT-1 mRNA expression when comparing colon cancer cell lines to normal colon tissue¹⁴², contrary to clear upregulation of MCT-1 in colon tumor samples. It is possible that this lack of correlation may be attributed to heterogeneous expression, in both normal tissue and cancer. In normal mucosa, MCT-1 expression exists in a gradient, with highest expression found at the mucosal surface facing the lumen. This may be due to activating factors in the gut environment, such as microbiome-derived butyrate^{135,201}. While MCT-1 protein expression is upregulated in adenocarcinoma samples, the

expression is highly heterogeneous (Fig. 5.2). Heterogeneity in patient cancer lesions has previously been associated with dissimilarities in differentiation, vascularity and invasiveness potential²⁰². Intriguingly, our group has discovered heterogeneity in the form of patterns of metabolism in xenograft tumors. Immunohistochemical analysis of the xenograft colon cancer tumors produced from the study presented in chapter 2 was performed with antisera specific for phosphorylated PDH (indicative of active PDK1 and glycolysis). The staining revealed an interesting, specific “spotted” pattern consisting of regularly spaced foci of approximately five-to-ten cells with high levels of phosphoPDH, surrounded by cells with reduced positive staining (Figure 5.5). Xenograft tumors consisting of dnLEF-1 expressing colon cancer cells were also examined for pPDH (PDK1 activity). In this case, the overall staining intensity was weaker but the spots were larger. That these intriguing patterns are truly connected to PDK1 was confirmed by staining xenograft tumors consisting of colon cancer cells in which PDK1 was overexpressed in every cell. In this case, there was a uniform level of elevated staining for pPDH. Although it is not clear by what means these foci are generated, it is possible that lactate excreted from phosphoPDH-high cells (cells that are glycolytic) signals to neighboring cells, perhaps enhancing their preference for consuming lactate as an energy source for oxidative phosphorylation. If lactate secretion plays a role in the spotted pattern, does MCT-1 expression play an important role in setting up this pattern? This question remains to be answered. To determine if this spotted pattern represents communication between neighboring cells through modulation of metabolism and possibly Wnt signaling, current members of the Waterman laboratory are collaborating with the Lowengrub group in the Mathematics department at UC Irvine to develop a reaction-diffusion model that incorporates Wnt signaling and different modes of metabolism. The model predicts that high levels of Wnt signaling correspond with high levels of phosphoPDH, and that

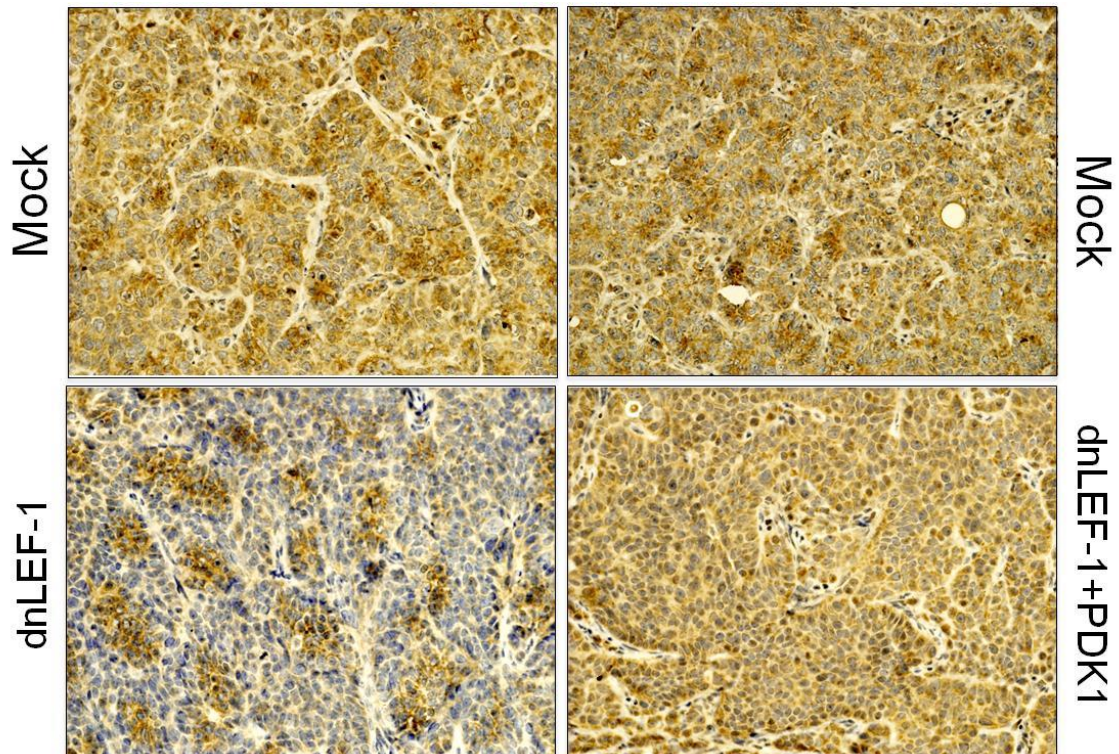


Figure 5.5. Phosphorylated pyruvate dehydrogenase staining in xenograft tumors. Immunohistochemical staining of phosphoPDH (phosphorylated pyruvate dehydrogenase) in sections of xenograft tumors developed from subcutaneous injection of SW480 cells (expressing empty vector (Mock), dnLEF-1, or dnLEF-1 and PDK1) in immunodeficient NOG (NOD/Shi-*scid*/IL-2R γ null) mice. Images were taken at 20X magnification. (Figure adapted Dr.Kira Pate).

inhibition of Wnt will alter the size and intensity of the spotted pattern. These predictions were validated using xenograft tumors (Chen and Lee, *in preparation*). Going forward, it will be important to determine if lactate levels, MCT-1 expression and/or other metabolic signatures correspond with these patterns of phosphoPDH staining and Wnt signaling. New experimental approaches may provide avenues to explore these experimental unknowns in depth. For example, single cell RNA Sequencing (RNA-Seq) has recently been used to probe heterogeneity in cancer cell settings such as melanoma, primary glioblastoma, circulating tumor cells and even human colon tumors^{203–206}. If Wnt signaling is heterogeneous at the single cell level, then one might expect that gene expression patterns of glycolysis to correlate with that heterogeneity. One major caveat of single cell RNA-Seq is that cells are removed from their original context and cellular environment, and therefore any spatial pattern such as “spotting” or other patterns will be destroyed²⁰⁷. Exciting new methods using RNA sequencing and mass spectrometry *in situ* are emerging^{208–211}, however, with technical improvements and increased sensitivity, these methods show great promise in application for studying tumor heterogeneity without disrupting spatial heterogeneities.

In addition to studying the role of Wnt signaling through LEF/TCF expression, this thesis also examined the role of the Wnt ligands themselves. The most common mutations of the Wnt signaling pathway are loss-of-function mutations in destruction complex-associated APC, and gain-of-function, stabilizing mutations in β -catenin. However, aberrant Wnt signaling activities involve not only β -catenin and the destruction complex, but also upstream signaling components of the pathway. This is important because Wnt ligands are capable of circumventing the destruction complex, and modulating the pathway at the level of LEF/TCFs and β -catenin. Notably, Wnt ligand expression levels are modified in cancer²¹². For example, WNT2 and

WNT5A expression are elevated in colon cancer compared to normal colon especially during the progression from adenoma to carcinoma^{43,213,214}. In contrast, the expression of other Wnts including WNT2B2, WNT4, WNT7B and WNT10B does not change, they remain strongly expressed in both normal colon and colon cancer²¹⁵. WNT5A has been shown in various studies to either inhibit or activate canonical Wnt signaling, depending on cell and receptor context. For example, WNT5A inhibits β -catenin dependent Wnt signaling through Ror2 receptor binding and subsequent pathway activation. In contrast, WNT5A activates β -catenin dependent signaling through interaction with co-receptors Fz4 and LRP5⁶⁵. What is the overall effect of Wnt ligands in the tumor microenvironment? Are there tumor-promoting and tumor-suppressing actions? Since drugs that prevent secretion of Wnt ligands are already in phase I clinical trials (see *Considerations for Clinical Therapeutics of Colon Cancer* below), answering these questions for colon cancer is important.

Our group recently showed that a kinase signaling cascade triggered by Wnt ligand activation regulates TCF-1 export in colon cancer cells³⁵. This pathway was shown to be stimulated by either WNT1 or WNT5A, reducing β -catenin-dependent signaling by triggering the nuclear export of TCF-1 and in doing so, reducing the overall concentration of LEF/TCFs in the nucleus. At the time the study was conducted, however, only a subset of Wnt ligands were available to test for their ability to activate this non-canonical kinase cascade. Are other ligands capable of triggering this export response? To answer that question, we created the “Open Source Wnt” plasmid depository, a library comprised of cDNA clones encoding all 19 human Wnt ligands, in multiple plasmid backbones, including those appropriate for expression in mammalian cells. Using this library, we find that WNT1 and WNT5A can also trigger export in

SW480 cells (Figure 5.6). In RKO cells expressing the various Wnt ligands, we find that WNT1, WNT2 and WNT5A each trigger high levels of TCF-1 export, while WNT7B, WNT9A, WNT11 and WNT16 trigger moderate levels of TCF-1 export. The remaining Wnt ligands do not trigger export (Figure 5.7 and 5.8). Whether TCF-1 export is a phenomenon specific to colon cancer is unknown, but LEF-1 and TCF-4 do not export from nuclei and their expression levels are not modified³⁵. While this data suggests that expression of specific Wnt ligands might act to inhibit canonical signaling, whether they do so in colon tumors may depend on the receptor context and cell setting. Taken together, the Wnt expression library can be used to continue probing the complexities of non-canonical Wnt signaling in a more comprehensive manner to better understand how various Wnt-ligand-based signals may modify colon cancer, even with a disrupted destruction complex.

Considerations for Clinical Therapeutics of Colon Cancer

Based on our findings, MCT-1 expression renders colon cancer cells sensitive to the uptake of the toxic molecule 3-bromopyruvate (3-BP). Our hypothesis was that, if MCT-1 is a target of Wnt signaling, and if MCT-1 transport is the mechanism by which 3-BP gains access to colon cancer cells, then Wnt signaling inhibition should reduce sensitivity to 3-BP. The results are consistent with this hypothesis, as sensitivity to 3-BP is reduced when Wnt signaling is inhibited. In fact, tumor cells survive and recover better from the toxic drug if they are simultaneously treated with Wnt signaling inhibitor XAV939. It is possible that XAV939 triggers adaptations that confer faster recovery and cell cycle progression. This possibility serves as a good illustration of the caveats that can arise when two classes of drugs are combined (Model, 5.9). These data also suggest that the heterogeneous patterns of Wnt signaling that have been observed in different subtypes of primary human colon cancer, and within the tumor

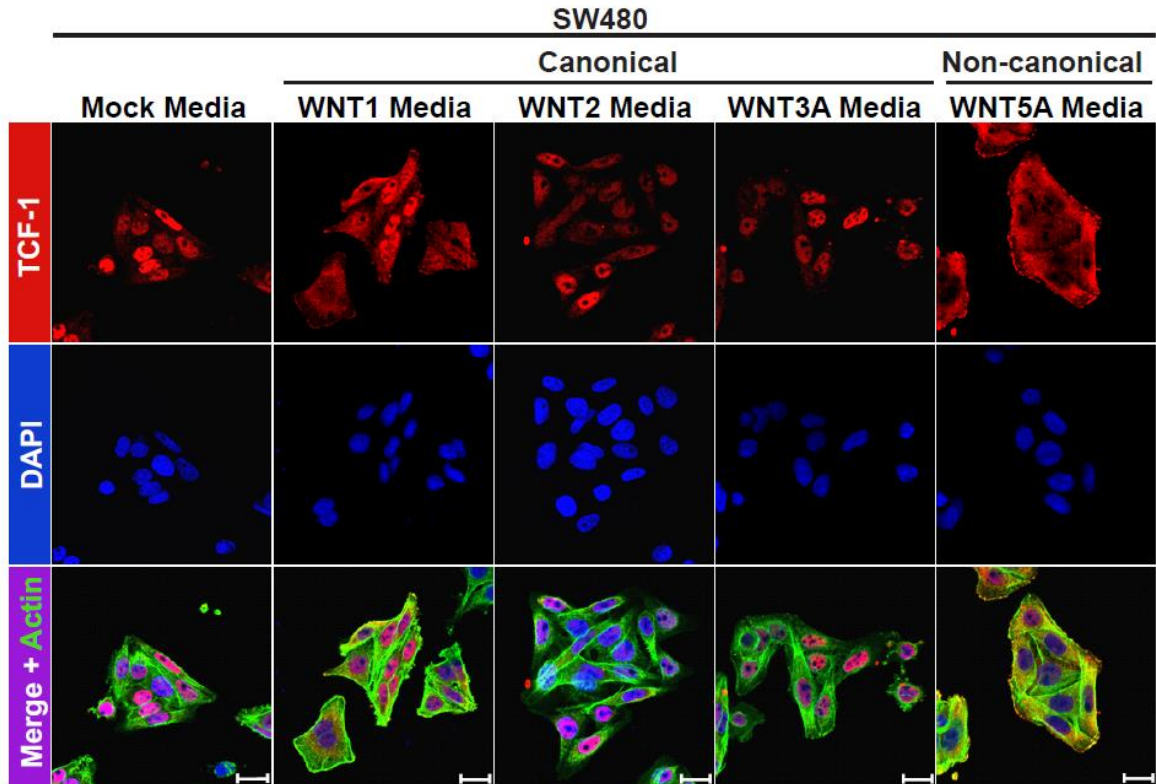
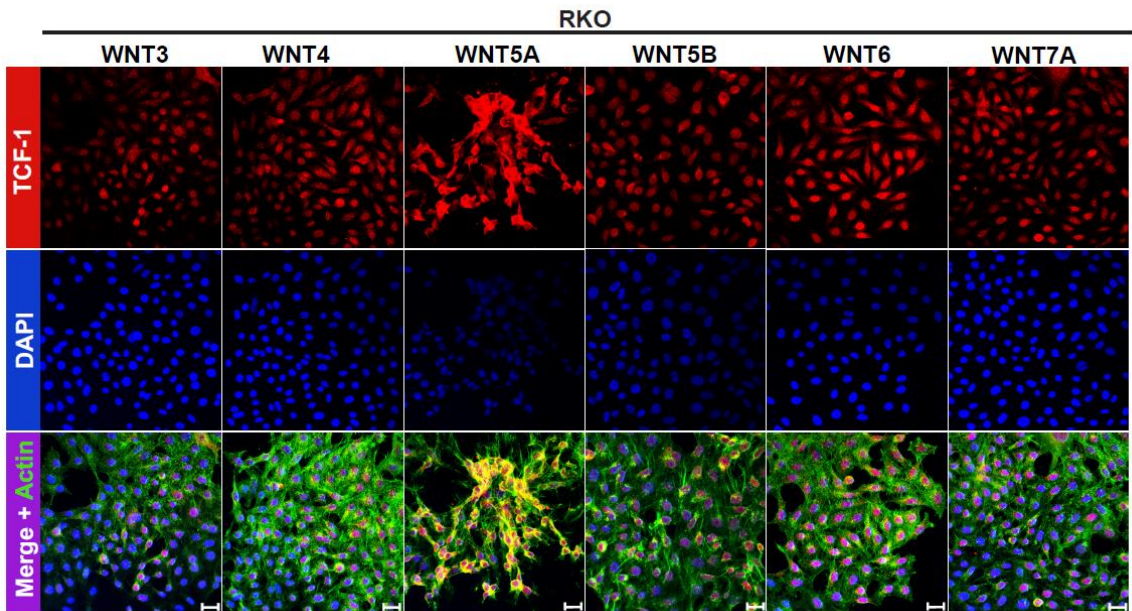
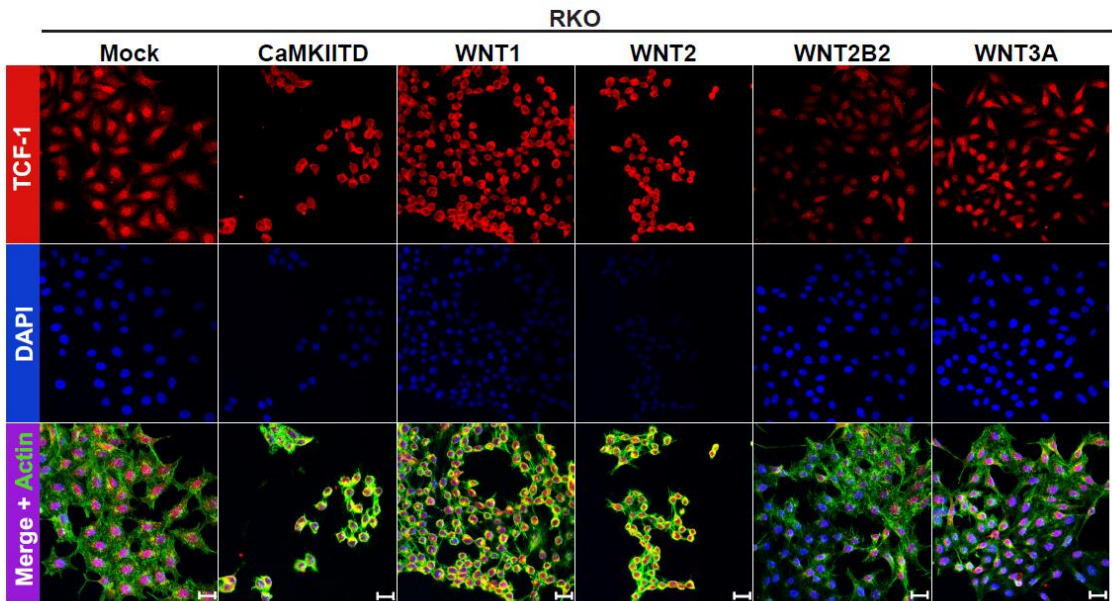


Figure 5.6. WNT1 and WNT5A induce TCF-1 export in SW480 cells. Media from NIH3T3 mouse fibroblasts that had been transfected with WNT1, WNT2, WNT3A or WNT5A was transferred to SW480 cells for 24 hr and TCF-1 was stained red. F-Actin staining is green and nuclear staining is blue. Scale bar is 20 μ m. WNT1 and WNT5A can both induce the export of TCF-1 in SW480 cells. (*Figure adapted from Dr. Rani Najdi*).



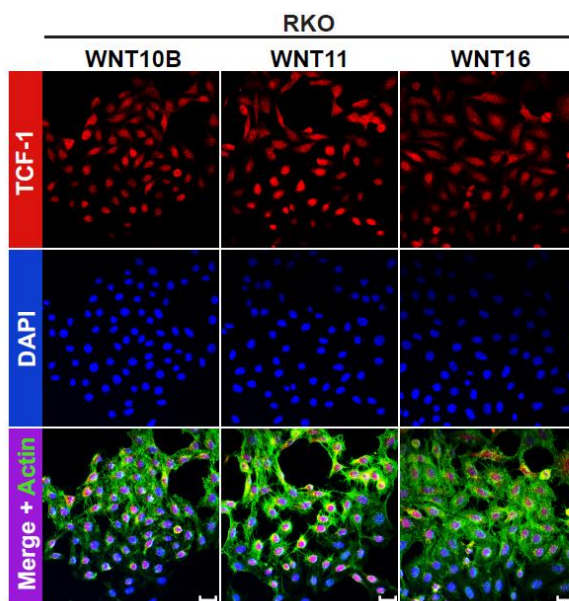
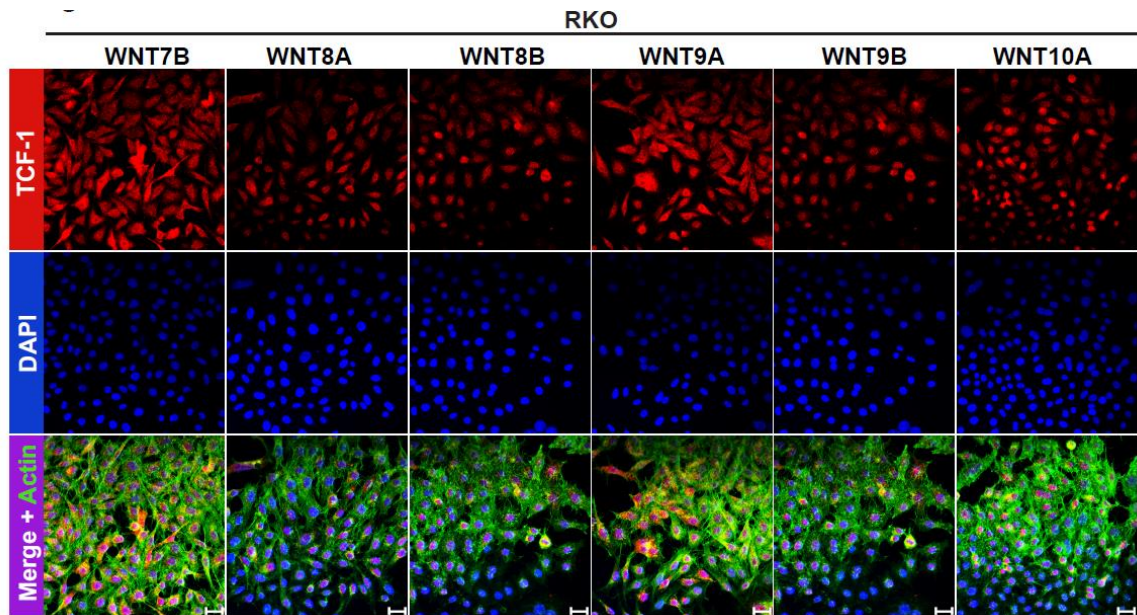


Figure 5.7. WNT1, 2 and WNT5A induce TCF-1 export in RKO cells. RKO cells were transfected with plasmids expressing all 19 human Wnts (1000ng) for 48 hr and TCF-1 was stained red. F-Actin staining is green and nuclear staining is blue. Scale bar is 20µm. WNT1, 2, and WNT5A can all trigger high levels of TCF-1 export in cells, while WNT7B, 9A, 11 and 16 trigger moderate levels of export. (*Figure adapted from Dr. Rani Najdi*).

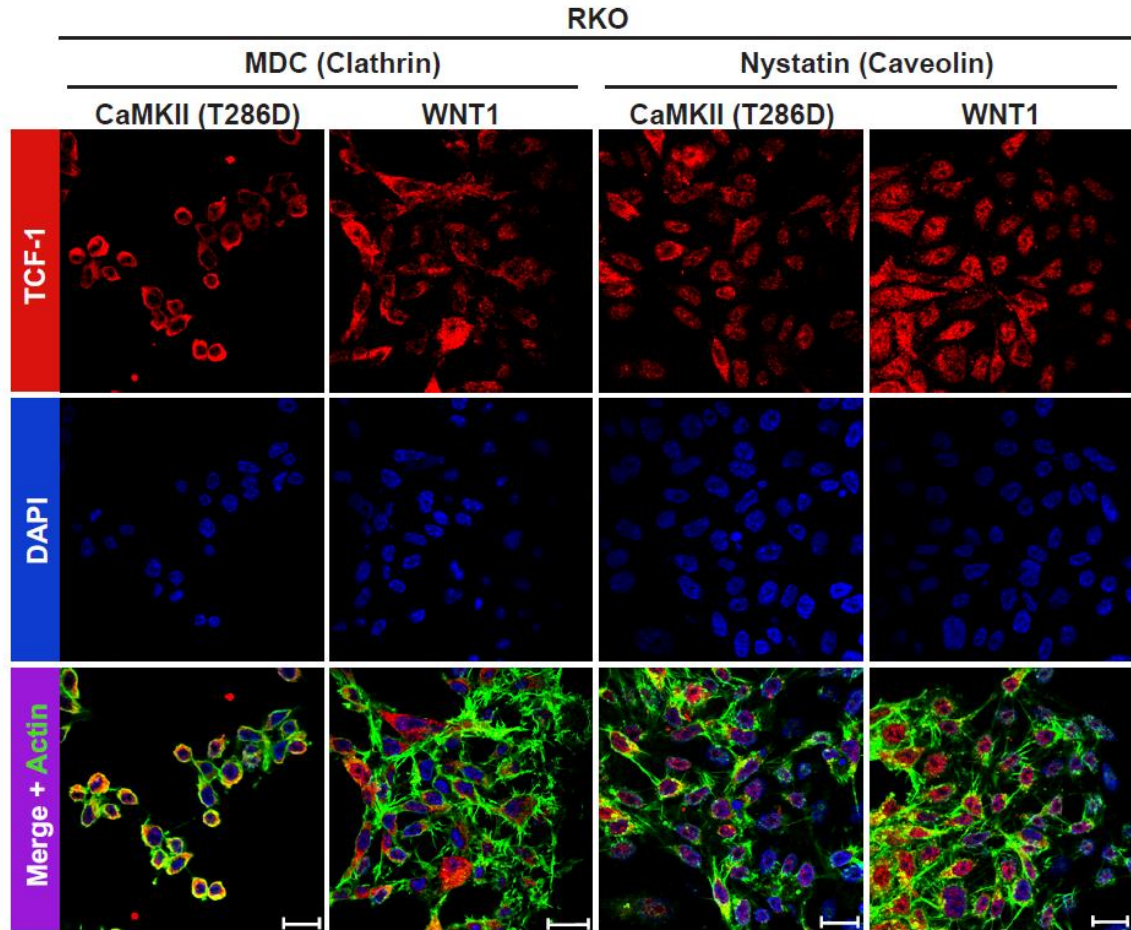


Figure 5.8. The role of endocytosis in TCF-1 export. RKO cells that had been transfected with plasmids expressing CaMKII (T286D) or WNT1 were treated with MDC (30 minutes; 50 μ M) to block clathrin-mediated endocytosis of Nystatin (30 minutes; 25 μ g/mL) to block caveolin-mediated endocytosis, and then stained for TCF-1 (red). F-Actin staining is in green and nuclear staining is blue. Scale bar is 20 μ m. Treatment of cells with MDC has no effect on TCF-1 localization as it remains cytoplasmic in response to activated CaMKII or WNT1. Nystatin treatment blocks the export of TCF-1 and is exported to the cytoplasm in response to activated CaMKII and WNT1 in RKO cells. (Figure adapted from Dr. Rani Najdi).

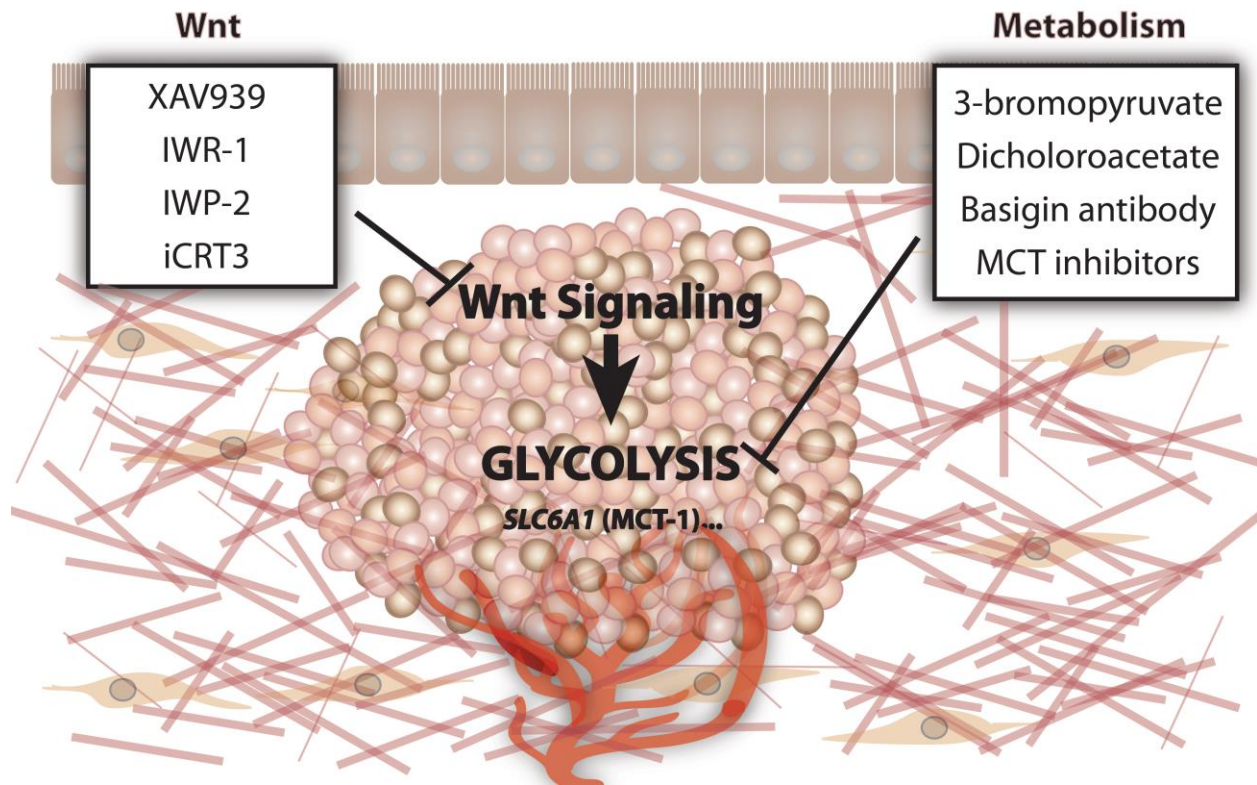


Figure 5.9. Wnt signaling influences cancer metabolism through regulation of *SLC16A1*/MCT-1 expression

Model of a colorectal tumor with Wnt regulating cancer metabolism through target genes including *SLC16A1*/MCT-1. Examples of Wnt and metabolic inhibitors currently under clinical development shown in boxed regions. (Figure adapted from Figure 7 of Sprowl-Tanio et al., Submitted).

microenvironment, will directly affect the efficacy of 3-BP and its derivatives. Below is a summary of two classes of drugs under pre-clinical development for the treatment of colon cancer: Wnt pathway inhibitors and inhibitors of cancer cell metabolism.

The discovery that Wnt signaling drives oncogenesis in many tumor types has inspired the development of small molecule inhibitors to target the pathway. Even though there is concern that Wnt signaling is necessary for stem cell compartments in normal tissues and therefore inhibitors will be deleterious and not tolerated, therapeutic windows have been demonstrated in animal experiments where Wnt-driven oncogenesis has been suppressed without general toxicity^{216,217}. Thus, the therapeutic relevance of the Wnt pathway to human cancer and an interest in developing an effective inhibitor for the pathway remains. Furthermore, since Wnt signaling drives cancer cell preference for glycolysis, Wnt inhibition may provide an alternative approach to manipulate cancer cell metabolism. Multiple drugs that inhibit Wnt signaling are showing promise for clinical application (e.g. inhibitors of Wnt secretion, tankyrase 1/2 inhibitors, and inhibitors of β -catenin interactions²¹⁸). In the study presented here, XAV939 (a tankyrase inhibitor that promotes Axin stabilization) was used to reduce Wnt signaling in the presence or absence of an inhibitor of metabolism. XAV939, as well as a compound called IWR-1, inhibits Wnt signaling downstream of ligand-receptor interaction at the level of the Destruction Complex. XAV939 treatment therefore acts to stabilize the Destruction Complex and promote β -catenin degradation. Both XAV939 and IWR-1 are currently in pre-clinical development, though the low potency of these specific molecules has prompted the development of second generation drugs that target Axin stabilization²¹⁸. For example, more specific tankyrase inhibitors are in the pipeline such as GM244-LM, a XAV939 analogue, and G007-LK, both with greater specificity to tankyrase 1 and 2^{218,219}. Interestingly, XAV939 has been shown

to increase sensitivity to chemotherapeutic drugs 5-fluorouracil and cisplatin in SW480 and SW620 cells, suggesting that Wnt inhibitors might be good candidates for combination with standard-of-care therapies²²⁰. Whether Wnt inhibitors might also be candidates for combination with new therapies that target tumor metabolism such as 3-bromopyruvate, was a question addressed in the studies presented here. Another promising set of Wnt inhibitors that are currently in clinical trials act upstream of the Destruction Complex. One class acts to prevent the production of Wnt ligands through inhibition of the enzyme Porcupine. Porcupine is an enzyme in the endoplasmic reticulum that adds a palmitoyl tail (a lipid modification) to Wnt ligands, permitting their subsequent secretion¹⁵³. Porcupine inhibitor LGK974 is currently in Phase One clinical trials (NCT01351103), suggesting that Wnt secretion may provide a promising avenue for Wnt inhibition *in vivo*²²¹. An alternative class of inhibitors works downstream of the Destruction Complex, preventing β -catenin interaction with its co-activators. One example is iCRT3, a small molecule that inhibits β -catenin and LEF/TCF interactions²²². While iCRT3 is under pre-clinical development²²³, we find that concentrations of 50-100 μ M are required to reach IC50 in our colon cancer cell lines (Habowski, *unpublished observation*). Other more promising candidates include ICG-001, which prevents β -catenin interaction with transcriptional co-activator CBP, and PRI-724, currently in clinical trials for both solid tumors (NCT01302405) and acute myeloid leukemia (NCT01606579)²²⁴.

While our work adds a note of caution to combining inhibitors of Wnt signaling and glycolysis, it does not negate the potential and promise of glycolysis inhibitors that are currently undergoing clinical development. We used 3-bromopyruvate in our studies to inhibit colon cancer cell metabolism because of its reliance on MCT-1 expression for import¹⁴². 3-bromopyruvate is a mimetic of pyruvate, very similar in structure apart from a bromine side

group. Due to its similarity, it is logical that 3-BP would compete and complicate interactions with molecules that normally partner with pyruvate; because of this, 3-bromopyruvate has multiple metabolic targets, including Hexokinase II and Glyceraldehyde 3-phosphate dehydrogenase (GAPDH)²²⁵. Another concern with using 3-BP as a cancer therapeutic is its stability. With a half-life of only 77 minutes, efforts are underway to increase stability of the drug, and structural modifications will be necessary for 3-bromopyruvate to have a future in the clinical setting²²⁶.

In contrast to exploitation of MCT-1 for import of toxic molecules, another treatment strategy involves inhibition of MCT-1 protein, confining lethal levels of intracellular H⁺ within the cell. MCT inhibitors (such as AZD3965; binds and directly inhibits) and Basigin/CD147 antibodies (indirectly inhibits localization of MCT-1 to the cell surface) are both clinically viable options^{227,228}. Knockdown of Basigin (the transmembrane glycoprotein responsible for anchoring MCT-1 and 4 to the cell surface^{147,148}) and MCT-4 via zinc finger nuclease in colon cancer and glioblastoma cell lines while simultaneously treating cells with AZD3965 redirected cells toward oxidative phosphorylation; as a result, cells became sensitive to the OXPHOS inhibitor phenformin²²⁹. In breast cancer cells, butyrate increases 3-BP uptake through upregulation of MCT-1²³⁰. In the colon, where butyrate increases expression of MCT-1 at the lumen surface, modulation of butyrate should also be considered¹³⁵. Dichloroacetate (DCA), a pan-pyruvate dehydrogenase (PDK) inhibitor, directs cells away from glycolysis toward cellular respiration and shows great promise as a chemotherapeutic. A DCA trial in human glioblastoma patients resulted in tumor regression, as well as enhanced tumor apoptosis¹²³. Collectively, glycolysis inhibitors may drive cells toward a more OXPHOS phenotype, potentially sensitizing cells to drugs like metformin and phenformin. Further understanding of Wnt signaling and metabolic

networks will be essential to guide the development of successful therapeutic interventions and to understand potential and outcomes of combination therapy using multiple drug classes.

REFERENCES

1. van Amerongen, R. & Nusse, R. Towards an integrated view of Wnt signaling in development. *Development* **136**, 3205–3214 (2009).
2. Mikels, A. J. & Nusse, R. Purified Wnt5a protein activates or inhibits beta-catenin-TCF signaling depending on receptor context. *PLoS Biol.* **4**, e115 (2006).
3. Huber, O. *et al.* Nuclear localization of beta-catenin by interaction with transcription factor LEF-1. *Mech. Dev.* **59**, 3–10 (1996).
4. Molenaar, M. *et al.* XTcf-3 transcription factor mediates beta-catenin-induced axis formation in *Xenopus* embryos. *Cell* **86**, 391–399 (1996).
5. Papkoff, J., Rubinfeld, B., Schryver, B. & Polakis, P. Wnt-1 regulates free pools of catenins and stabilizes APC-catenin complexes. *Mol Cell Biol* **16**, 2128–2134 (1996).
6. Porfiri, E. *et al.* Induction of a beta-catenin-LEF-1 complex by wnt-1 and transforming mutants of beta-catenin. *Oncogene* **15**, 2833–2839 (1997).
7. Najdi, R., Holcombe, R. F. & Waterman, M. L. Wnt signaling and colon carcinogenesis: beyond APC. *J. Carcinog.* **10**, 5 (2011).
8. van Amerongen, R., Mikels, A. & Nusse, R. Alternative wnt signaling is initiated by distinct receptors. *Sci. Signal.* **1**, re9 (2008).
9. Dabdoub, A. & Kelley, M. W. Planar cell polarity and a potential role for a Wnt morphogen gradient in stereociliary bundle orientation in the mammalian inner ear. *J. Neurobiol.* **64**, 446–457 (2005).
10. Dabdoub, A. *et al.* Wnt signaling mediates reorientation of outer hair cell stereociliary bundles in the mammalian cochlea. *Development* **130**, 2375–84 (2003).
11. Qian, D. *et al.* Wnt5a functions in planar cell polarity regulation in mice. *Dev. Biol.* **306**, 121–133 (2007).
12. Wallingford, J. B., Vogeli, K. M. & Harland, R. M. Regulation of convergent extension in *Xenopus* by Wnt5a and Frizzled-8 is independent of the canonical Wnt pathway. *Int. J. Dev. Biol.* **45**, 225–227 (2001).
13. Kilian, B. *et al.* The role of Ppt/Wnt5 in regulating cell shape and movement during zebrafish gastrulation. *Mech. Dev.* **120**, 467–476 (2003).
14. Heisenberg, C. P. *et al.* Silberblick/Wnt11 mediates convergent extension movements during zebrafish gastrulation. *Nature* **405**, 76–81 (2000).
15. Veeman, M. T., Axelrod, J. D. & Moon, R. T. A second canon: Functions and mechanisms of β -catenin-independent Wnt signaling. *Dev. Cell* **5**, 367–377 (2003).
16. Yoshikawa, S., McKinnon, R. D., Kokel, M. & Thomas, J. B. Wnt-mediated axon guidance via the *Drosophila* Derailed receptor. *Nature* **422**, 583–588 (2003).
17. Harris, K. E. & Beckendorf, S. K. Different Wnt signals act through the Frizzled and RYK receptors during *Drosophila* salivary gland migration. *Development* **134**, 2017–2025 (2007).

18. Oishi, I. *et al.* The receptor tyrosine kinase Ror2 is involved in non-canonical Wnt5a/JNK signalling pathway. *Genes to Cells* **8**, 645–654 (2003).
19. Yamamoto, S. *et al.* Cthrc1 Selectively Activates the Planar Cell Polarity Pathway of Wnt Signaling by Stabilizing the Wnt-Receptor Complex. *Dev. Cell* **15**, 23–36 (2008).
20. Clevers, H. & van de Wetering, M. TCF/LEF factor earn their wings. *Trends Genet* **13**, 485–489 (1997).
21. Eastman, Q. & Grosschedl, R. Regulation of LEF-1/TCF transcription factors by Wnt and other signals. *Curr. Opin. Cell Biol.* **11**, 233–240 (1999).
22. van de Wetering, M. & Clevers, H. Sequence-specific interaction of the HMG box proteins TCF-1 and SRY occurs within the minor groove of a Watson-Crick double helix. *EMBO J.* **11**, 3039–3044 (1992).
23. van Beest, M. *et al.* Sequence-specific high mobility group box factors recognize 10-12-base pair minor groove motifs. *J Biol Chem* **275**, 27266–27273 (2000).
24. Behrens, J. *et al.* Functional interaction of beta-catenin with the transcription factor LEF-1. *Nature* **382**, 638–642 (1996).
25. Arce, L., Pate, K. T. & Waterman, M. L. Groucho binds two conserved regions of LEF-1 for HDAC-dependent repression. *BMC Cancer* **9**, 159 (2009).
26. Arce, L., Yokoyama, N. N. & Waterman, M. L. Diversity of LEF/TCF action in development and disease. *Oncogene* **25**, 7492–504 (2006).
27. Cadigan, K. M. & Waterman, M. L. TCF / LEFs and Wnt Signaling in the Nucleus. *Cold Spring Harb Symp Quant Biol* 1–22 (2012). doi:10.1101/cshperspect.a007906
28. Atcha, F. *et al.* A unique DNA binding domain converts T-cell factors into strong Wnt effectors. *Mol. Cell. Biol.* **27**, 8352–63 (2007).
29. Hoverter, N. P., Ting, J.-H., Sundaresh, S., Baldi, P. & Waterman, M. L. A WNT/p21 circuit directed by the C-clamp, a sequence-specific DNA binding domain in TCFs. *Mol. Cell. Biol.* **32**, 3648–3662 (2012).
30. Van de Wetering, M., Castrop, J., Korinek, V. & Clevers, H. Extensive alternative splicing and dual promoter usage generate Tcf-1 protein isoforms with differential transcription control properties. *Mol Cell Biol* **16**, 745–752 (1996).
31. Hovanes, K. *et al.* Beta-catenin-sensitive isoforms of lymphoid enhancer factor-1 are selectively expressed in colon cancer. *Nat. Genet.* **28**, 53–7 (2001).
32. Vacik, T. & Lemke, G. Dominant-negative isoforms of Tcf/Lef proteins in development and disease. *Cell cycle* **10**, 4199–200 (2011).
33. Brantjes, H., Roose, J., van De Wetering, M. & Clevers, H. All Tcf HMG box transcription factors interact with Groucho-related co-repressors. *Nucleic Acids Res* **29**, 1410–1419 (2001).
34. Daniels, D. L. & Weis, W. I. Beta-catenin directly displaces Groucho/TLE repressors from Tcf/Lef in Wnt-mediated transcription activation. *Nat Struct Mol Biol* **12**, 364–371 (2005).
35. Najdi, R. *et al.* A Wnt kinase network alters nuclear localization of TCF-1 in colon cancer.

- Oncogene* **28**, 4133–46 (2009).
36. Korinek, V. *et al.* Depletion of epithelial stem-cell compartments in the small intestine of mice lacking Tcf-4. *Nat. Genet.* **19**, 379–83 (1998).
 37. Roose, J. *et al.* Synergy between tumor suppressor APC and the beta-catenin-Tcf4 target Tcf1. *Science (80-.)*. **285**, 1923–1926 (1999).
 38. Fuchs, E. The tortoise and the hair: slow-cycling cells in the stem cell race. *Cell* **137**, 811–9 (2009).
 39. Clevers, H. Wnt/Beta-Catenin Signaling in Development and Disease. *Cell* **127**, 469–480 (2006).
 40. Sato, T. *et al.* Paneth cells constitute the niche for Lgr5 stem cells in intestinal crypts. *Nature* **469**, 415–8 (2011).
 41. ten Berge, D. *et al.* Embryonic stem cells require Wnt proteins to prevent differentiation to epiblast stem cells. *Nat. Cell Biol.* **13**, 1070–5 (2011).
 42. Clevers, H. & Nusse, R. Wnt/ β -catenin signaling and disease. *Cell* **149**, 1192–1205 (2012).
 43. Holcombe, R. F. *et al.* Expression of Wnt ligands and Frizzled receptors in colonic mucosa and in colon carcinoma. *Mol. Pathol.* **55**, 220–226 (2002).
 44. Klaus, A. & Birchmeier, W. Wnt signalling and its impact on development and cancer. *Nat Rev Cancer* **8**, 387–398 (2008).
 45. Polakis, P. Wnt signaling and cancer. *Genes Dev* **14**, 1837–51 (2000).
 46. Brown, A. M. Wnt signaling in breast cancer: have we come full circle? *Breast Cancer Res.* **3**, 351–355 (2001).
 47. Rubinfeld, B. *et al.* Stabilization of b-catenin by genetic defects in melanoma cell lines. *Science (80-.)*. **275**, 1790–1792 (1997).
 48. Li, X. *et al.* Oncogenic transformation of diverse gastrointestinal tissues in primary organoid culture. *Nat. Med.* **20**, 769–77 (2014).
 49. Fearon, E. R. & Vogelstein, B. A genetic model for colorectal tumorigenesis. *Cell* **61**, 759–767 (1990).
 50. Phelps, R. A. *et al.* A Two-Step Model for Colon Adenoma Initiation and Progression Caused by APC Loss. *Cell* **137**, 623–634 (2009).
 51. Miyoshi, Y. *et al.* Somatic mutations of the APC gene in colorectal tumors : mutation cluster region in the APC gene. *Hum. Mol. Genet.* **1**, 229–233 (1992).
 52. Stamos, J. L. & Weis, W. I. The β -catenin destruction complex. *Cold Spring Harb. Perspect. Biol.* **5**, (2013).
 53. Dow, L. E. *et al.* Apc Restoration Promotes Cellular Differentiation and Reestablishes Crypt Homeostasis in Colorectal Cancer. *Cell* **161**, 1539–1552 (2015).
 54. He, T. C. *et al.* Identification of c-MYC as a target of the APC pathway. *Science (80-.)*. **281**, 1509–1512 (1998).
 55. Tetsu, O. & McCormick, F. Beta-catenin regulates expression of cyclin D1 in colon

- carcinoma cells. *Nature* **398**, 422–426 (1999).
56. Hoverter, N. P., Ting, J.-H., Sundaresh, S., Baldi, P. & Waterman, M. L. A WNT/p21 circuit directed by the C-clamp, a sequence-specific DNA binding domain in TCFs. *Mol. Cell. Biol.* **32**, 3648–62 (2012).
 57. Hovanes, K. *et al.* Beta-catenin-sensitive isoforms of lymphoid enhancer factor-1 are selectively expressed in colon cancer. *Nat. Genet.* **28**, 53–57 (2001).
 58. Roose, J. *et al.* Synergy between tumor suppressor APC and the beta-catenin-Tcf4 target Tcf1. *Science* **285**, 1923–1926 (1999).
 59. He, T. *et al.* Identification of c- MYC as a Target of the APC Pathway. *Science (80-.)*. **281**, 1509–1512 (1998).
 60. Tetsu, O. & McCormick, F. Beta-catenin regulates expression of cyclin D1 in colon carcinoma cells. *Nature* **398**, 422–426 (1999).
 61. Zhang, X., Gaspard, J. P. & Chung, D. C. Regulation of vascular endothelial growth factor by the Wnt and K-ras pathways in colonic neoplasia. *Cancer Res.* **61**, 6050–6054 (2001).
 62. Shimokawa, T. *et al.* Involvement of the FGF18 gene in colorectal carcinogenesis, as a novel downstream target of the β -catenin/T-cell factor complex. *Cancer Res.* **63**, 6116–6120 (2003).
 63. Vermeulen, L. *et al.* Wnt activity defines colon cancer stem cells and is regulated by the microenvironment. *Nat. Cell Biol.* **12**, 468–76 (2010).
 64. Huang, F.-I., Chen, Y.-L., Chang, C.-N., Yuan, R.-H. & Jeng, Y.-M. Hepatocyte growth factor activates Wnt pathway by transcriptional activation of LEF1 to facilitate tumor invasion. *Carcinogenesis* **0**, 1–7 (2012).
 65. Mikels, A. J. & Nusse, R. Purified Wnt5a protein activates or inhibits β -catenin-TCF signaling depending on receptor context. *PLoS Biol.* **4**, 570–582 (2006).
 66. Yokoyama, N. N., Pate, K. T. & Waterman, M. L. A role for YY1 in repression of dominant negative LEF-1 expression in colon cancer- before review. *Nucleic Acids Res.* 0–36
 67. Mayer, K., Hieronymus, T., Castrop, J., Clevers, H. & Ballhausen, W. G. Ectopic activation of lymphoid high mobility group-box transcription factor TCF-1 and overexpression in colorectal cancer cells. *Int J Cancer* **72**, 625–630 (1997).
 68. Naishiro, Y. *et al.* Restoration of epithelial cell polarity in a colorectal cancer cell line by suppression of beta-catenin / T-cell factor 4-mediated gene transactivation. *Cancer Res.* **61**, 2751–2758 (2001).
 69. Warburg, O., Wind, F. & Negelein, E. The Metabolism of Tumors in the body. *J. Gen. Physiol.* **8**, 519–30 (1927).
 70. Warburg, O. On the origin of cancer cells. *Science (80-.)*. **123**, 309–14 (1956).
 71. Vander Heiden, M. G., Cantley, L. C., Thompson, C. B. & Heiden, M. G. Vander. Understanding the Warburg effect: the metabolic requirements of cell proliferation. *Science (80-.)*. **324**, 1029–1033 (2009).
 72. DeBerardinis, R. J., Lum, J. J., Hatzivassiliou, G. & Thompson, C. B. The biology of

- cancer: metabolic reprogramming fuels cell growth and proliferation. *Cell Metab.* **7**, 11–20 (2008).
73. DeBerardinis, R. J. *et al.* Beyond aerobic glycolysis: transformed cells can engage in glutamine metabolism that exceeds the requirement for protein and nucleotide synthesis. *Proc Natl Acad Sci U S A* **104**, 19345–19350 (2007).
 74. Ward, P. S. & Thompson, C. B. Metabolic reprogramming: a cancer hallmark even Warburg did not anticipate. *Cancer Cell* **21**, 297–308 (2012).
 75. Buzzai, M. *et al.* The glucose dependence of Akt-transformed cells can be reversed by pharmacologic activation of fatty acid beta-oxidation. *Oncogene* **24**, 4165–73 (2005).
 76. Elstrom, R. L. *et al.* Akt stimulates aerobic glycolysis in cancer cells. *Cancer Res.* **64**, 3892–9 (2004).
 77. Shackelford, D. B. & Shaw, R. J. The LKB1-AMPK pathway: metabolism and growth control in tumour suppression. *Nat. Rev. Cancer* **9**, 563–75 (2009).
 78. Cairns, R. a, Harris, I. S. & Mak, T. W. Regulation of cancer cell metabolism. *Nat. Rev. Cancer* **11**, 85–95 (2011).
 79. Liu, H. *et al.* Wnt signaling regulates hepatic metabolism. *Sci. Signal.* **4**, ra6 (2011).
 80. Sethi, J. K. & Vidal-Puig, A. Wnt signalling and the control of cellular metabolism. *Biochem. J.* **427**, 1–17 (2010).
 81. Esen, E. *et al.* WNT-LRP5 signaling induces warburg effect through mTORC2 activation during osteoblast differentiation. *Cell Metab.* **17**, 745–755 (2013).
 82. Semenza, G. L. HIF-1 : upstream and downstream of cancer metabolism. *Curr. Opin. Genet. Dev.* **20**, 51–6 (2010).
 83. Stringari, C. *et al.* Phasor approach to fluorescence lifetime microscopy distinguishes different metabolic states of germ cells in a live tissue. *Proc. Natl. Acad. Sci. U. S. A.* **108**, 13582–7 (2011).
 84. Digman, M. A., Caiolfa, V. R., Zamai, M. & Gratton, E. The phasor approach to fluorescence lifetime imaging analysis. *Biophys. J.* **94**, L14–6 (2008).
 85. Stringari, C. *et al.* Metabolic trajectory of cellular differentiation in small intestine by Phasor Fluorescence Lifetime Microscopy of NADH. *Sci. Rep.* **2**, 568 (2012).
 86. van de Wetering, M. *et al.* The beta-catenin / TCF-4 complex imposes a crypt progenitor phenotype on colorectal cancer cells. *Cell* **111**, 241–250 (2002).
 87. Thomas, P. D. PANTHER: a browsable database of gene products organized by biological function, using curated protein family and subfamily classification. *Nucleic Acids Res.* **31**, 334–341 (2003).
 88. Thomas, P. D. *et al.* Applications for protein sequence-function evolution data: mRNA/protein expression analysis and coding SNP scoring tools. *Nucleic Acids Res.* **34**, W645–W650 (2006).
 89. Huang, S.-M. a *et al.* Tankyrase inhibition stabilizes axin and antagonizes Wnt signalling. *Nature* **461**, 614–620 (2009).

90. Lakowicz, J. R., Szmajdzinski, H., Nowaczyk, K. & Johnson, M. L. Fluorescence lifetime imaging of free and protein-bound NADH. *Proc. Natl. Acad. Sci. U. S. A.* **89**, 1271–5 (1992).
91. Croce, A. C. *et al.* Autofluorescence properties of isolated rat hepatocytes under different metabolic conditions. *Photochem. Photobiol. Sci.* **3**, 920–926 (2004).
92. Monici, M. *et al.* Dependence of leukemic cell autofluorescence patterns on the degree of differentiation. *Photochem. Photobiol. Sci.* **2**, 981 (2003).
93. Becker, W. *et al.* Fluorescence lifetime imaging by time-correlated single-photon counting. *Microsc. Res. Tech.* **63**, 58–66 (2004).
94. Colyer, R. A., Lee, C. & Gratton, E. A novel fluorescence lifetime imaging system that optimizes photon efficiency. *Microsc. Res. Tech.* **71**, 201–13 (2008).
95. Bird, D. K. *et al.* Metabolic mapping of MCF10A human breast cells via multiphoton fluorescence lifetime imaging of the coenzyme NADH. *Cancer Res.* **65**, 8766–73 (2005).
96. Skala, M. C. *et al.* In vivo multiphoton microscopy of NADH and FAD redox states, fluorescence lifetimes, and cellular morphology in precancerous epithelia. *Proc. Natl. Acad. Sci. U. S. A.* **104**, 19494–9 (2007).
97. Yu, Q. & Heikal, A. A. Two-photon autofluorescence dynamics imaging reveals sensitivity of intracellular NADH concentration and conformation to cell physiology at the single-cell level. *J. Photochem. Photobiol. B Biol.* **95**, 46–57 (2009).
98. Yuan, Y., Li, Y., Cameron, B. D. & Relue, P. Fluorescence anisotropy of cellular NADH as a tool to study different metabolic properties of human melanocytes and melanoma cells. *IEEE J. Sel. Top. Quantum Electron.* **13**, 1671–1679 (2007).
99. Roche, T. E. *et al.* Distinct regulatory properties of pyruvate dehydrogenase kinase and phosphatase isoforms. *Prog. Nucleic Acid Res. Mol. Biol.* **70**, 33–75 (2001).
100. Baumunk, D. *et al.* Expression parameters of the metabolic pathway genes pyruvate dehydrogenase kinase-1 (PDK-1) and DJ-1/PARK7 in renal cell carcinoma (RCC). *World J. Urol.* (2012). doi:10.1007/s00345-012-0874-5
101. Koukourakis, M. I., Giatromanolaki, A., Harris, A. L. & Sivridis, E. Comparison of metabolic pathways between cancer cells and stromal cells in colorectal carcinomas: a metabolic survival role for tumor-associated stroma. *Cancer Res.* **66**, 632–7 (2006).
102. Wigfield, S. M. *et al.* PDK-1 regulates lactate production in hypoxia and is associated with poor prognosis in head and neck squamous cancer. *Br. J. Cancer* **98**, 1975–84 (2008).
103. Kim, J., Gao, P., Liu, Y.-C., Semenza, G. L. & Dang, C. V. Hypoxia-inducible factor 1 and dysregulated c-Myc cooperatively induce vascular endothelial growth factor and metabolic switches hexokinase 2 and pyruvate dehydrogenase kinase 1. *Mol. Cell. Biol.* **27**, 7381–93 (2007).
104. Dölken, L. *et al.* High-resolution gene expression profiling for simultaneous kinetic parameter analysis of RNA synthesis and decay. *RNA* **14**, 1959–72 (2008).
105. Hoverter, N. P. *et al.* The TCF C-clamp DNA binding domain expands the Wnt transcriptome via alternative target recognition. *Nucleic Acids Res.* **42**, 13615–13632

- (2014).
106. Whitehouse, S., Cooper, R. H. & Randle, P. J. Mechanism of activation of pyruvate dehydrogenase by dichloroacetate and other halogenated carboxylic acids. *Biochem. J.* **141**, 761–74 (1974).
 107. Bonnet, S. *et al.* A mitochondria-K⁺ channel axis is suppressed in cancer and its normalization promotes apoptosis and inhibits cancer growth. *Cancer Cell* **11**, 37–51 (2007).
 108. Sun, R. C., Board, P. G. & Blackburn, A. C. Targeting metabolism with arsenic trioxide and dichloroacetate in breast cancer cells. *Mol. Cancer* **10**, 142 (2011).
 109. Cairns, R. A., Papandreou, I., Sutphin, P. D. & Denko, N. C. Metabolic targeting of hypoxia and HIF1 in solid tumors can enhance cytotoxic chemotherapy. *Proc. Natl. Acad. Sci. U. S. A.* **104**, 9445–50 (2007).
 110. Stockwin, L. H. *et al.* Sodium dichloroacetate selectively targets cells with defects in the mitochondrial ETC. *Int. J. cancer.* **127**, 2510–9 (2010).
 111. Tong, J. *et al.* Synergistic antitumor effect of dichloroacetate in combination with 5-fluorouracil in colorectal cancer. *J. Biomed. Biotechnol.* **2011**, 740564 (2011).
 112. Sutendra, G. *et al.* Mitochondrial activation by inhibition of PDKII suppresses HIF1a signaling and angiogenesis in cancer. *Oncogene* 1–13 (2012). doi:10.1038/onc.2012.198
 113. Hunt, T. K. *et al.* Aerobically derived lactate stimulates revascularization and tissue repair via redox mechanisms. *Antioxid. Redox Signal.* **9**, 1115–24 (2007).
 114. Milovanova, T. N. *et al.* Lactate stimulates vasculogenic stem cells via the thioredoxin system and engages an autocrine activation loop involving hypoxia-inducible factor 1. *Mol. Cell. Biol.* **28**, 6248–61 (2008).
 115. Lee, S. Y. *et al.* Wnt/Snail signaling regulates cytochrome c oxidase and glucose metabolism. *Cancer Res.* **72**, 3607–17 (2012).
 116. Zhang, X., Gaspard, J. P. & Chung, D. C. Regulation of vascular endothelial growth factor by the Wnt and K-ras pathways in colonic neoplasia. *Cancer Res.* **61**, 6050–6054 (2001).
 117. McFate, T. *et al.* Pyruvate dehydrogenase complex activity controls metabolic and malignant phenotype in cancer cells. *J. Biol. Chem.* **283**, 22700–8 (2008).
 118. Lu, H., Forbes, R. A. & Verma, A. Hypoxia-inducible factor 1 activation by aerobic glycolysis implicates the Warburg effect in carcinogenesis. *J. Biol. Chem.* **277**, 23111–5 (2002).
 119. Forsythe, J. A. *et al.* Activation of vascular endothelial growth factor gene transcription by hypoxia-inducible factor 1. *Mol. Cell. Biol.* **16**, 4604–13 (1996).
 120. Pugh, C. W. & Ratcliffe, P. J. Regulation of angiogenesis by hypoxia: role of the HIF system. *Nat. Med.* **9**, 677–84 (2003).
 121. Karshovska, E. *et al.* Expression of HIF-1alpha in injured arteries controls SDF-1alpha mediated neointima formation in apolipoprotein E deficient mice. *Arterioscler. Thromb. Vasc. Biol.* **27**, 2540–7 (2007).
 122. Papandreou, I., Golasova, T. & Denko, N. C. Anticancer drugs that target metabolism: Is

- dichloroacetate the new paradigm? *Int. J. cancer.* **128**, 1001–8 (2011).
123. Michelakis, E. D. *et al.* Metabolic modulation of glioblastoma with dichloroacetate. *Sci. Transl. Med.* **2**, 31ra34 (2010).
 124. Kent, W. J. *et al.* The human genome browser at UCSC. *Genome Res.* **12**, 996–1006 (2002).
 125. Schuijers, J., Mokry, M., Hatzis, P., Cuppen, E. & Clevers, H. Wnt-induced transcriptional activation is exclusively mediated by TCF/LEF. *EMBO J.* **33**, 146–156 (2014).
 126. Izumi, H. *et al.* Monocarboxylate transporters 1 and 4 are involved in the invasion activity of human lung cancer cells. *Cancer Sci.* **102**, 1007–1013 (2011).
 127. Pinheiro, C. *et al.* Role of monocarboxylate transporters in human cancers: state of the art. *J. Bioenerg. Biomembr.* **44**, 127–139 (2012).
 128. Pate, K. T. *et al.* Wnt signaling directs a metabolic program of glycolysis and angiogenesis in colon cancer. *EMBO J.* **33**, 1454–73 (2014).
 129. Halestrap, A. P. Monocarboxylic Acid Transport. *Compr. Physiol.* **3**, 1611–1643 (2013).
 130. Halestrap, A. P. & Wilson, M. C. The monocarboxylate transporter family--role and regulation. *IUBMB Life* **64**, 109–19 (2012).
 131. Majumdar, S., Gunda, S., Pal, D. & Mitra, A. K. Functional activity of a monocarboxylate transporter, MCT1, in the human retinal pigmented epithelium cell line, ARPE-19. *Mol. Pharm.* **2**, 109–117 (2005).
 132. Benton, C. R. *et al.* PGC-1alpha increases skeletal muscle lactate uptake by increasing the expression of MCT1 but not MCT2 or MCT4. *Physiol. Genomics* **35**, 45–54 (2008).
 133. Galardo, M. N., Riera, M. F., Pellizzari, E. H., Cigorruga, S. B. & Meroni, S. B. The AMP-activated protein kinase activator, 5-aminoimidazole-4-carboxamide-1- β -D-ribose nucleoside, regulates lactate production in rat Sertoli cells. *J. Mol. Endocrinol.* **39**, 279–288 (2007).
 134. Halestrap, A. P. & Wilson, M. C. The monocarboxylate transporter family-Role and regulation. *IUBMB Life* **64**, 109–119 (2012).
 135. Cuff, M. a, Lambert, D. W. & Shirazi-Beechey, S. P. Substrate-induced regulation of the human colonic monocarboxylate transporter, MCT1. *J. Physiol.* **539**, 361–371 (2002).
 136. Perez de Heredia, F., Wood, I. S. & Trayhurn, P. Hypoxia stimulates lactate release and modulates monocarboxylate transporter (MCT1, MCT2, and MCT4) expression in human adipocytes. *Pflugers Arch* **459**, 509–518 (2010).
 137. Ullah, M. S., Davies, A. J. & Halestrap, A. P. The plasma membrane lactate transporter MCT4, but not MCT1, is up-regulated by hypoxia through a HIF-1alpha-dependent mechanism. *J. Biol. Chem.* **281**, 9030–9037 (2006).
 138. Boidot, R. *et al.* Regulation of monocarboxylate transporter MCT1 expression by p53 mediates inward and outward lactate fluxes in tumors. *Cancer Res.* **72**, 939–948 (2012).
 139. Doherty, J. R. *et al.* Blocking lactate export by inhibiting the Myc target MCT1 Disables glycolysis and glutathione synthesis. *Cancer Res.* **74**, 908–20 (2014).

140. Dhup, S., Dadhich, R. K., Porporato, P. E. & Sonveaux, P. Multiple biological activities of lactic acid in cancer: influences on tumor growth, angiogenesis and metastasis. *Curr. Pharm. Des* **18**, 1319–30 (2012).
141. Hong, C. S. *et al.* MCT1 Modulates Cancer Cell Pyruvate Export and Growth of Tumors that Co-express MCT1 and MCT4. *Cell Rep.* **14**, 1590–1601 (2016).
142. Birsoy, K. *et al.* MCT1-mediated transport of a toxic molecule is an effective strategy for targeting glycolytic tumors. *Nat. Genet.* **45**, 104–8 (2013).
143. Veeman, M. T., Slusarski, D. C., Kaykas, A., Louie, S. H. & Moon, R. T. Zebrafish prickles, a modulator of noncanonical Wnt/Fz signaling, regulates gastrulation movements. *Curr. Biol.* **13**, 680–685 (2003).
144. Baltazar, F. *et al.* Monocarboxylate transporters as targets and mediators in cancer therapy response. *Histol. Histopathol.* **29**, 1511–1524 (2014).
145. Morais-Santos, F. *et al.* Targeting lactate transport suppresses in vivo breast tumour growth. *Oncotarget* (2015). at <<http://www.ncbi.nlm.nih.gov/pubmed/26203664>>
146. Sonveaux, P. *et al.* Targeting lactate-fueled respiration selectively kills hypoxic tumor cells in mice. *J. Clin. Invest.* **118**, 3930–42 (2008).
147. Baba, M., Inoue, M., Itoh, K. & Nishizawa, Y. Blocking CD147 induces cell death in cancer cells through impairment of glycolytic energy metabolism. *Biochem. Biophys. Res. Commun.* **374**, 111–116 (2008).
148. Kirk, P. *et al.* CD147 is tightly associated with lactate transporters MCT1 and MCT4 and facilitates their cell surface expression. *EMBO J.* **19**, 3896–3904 (2000).
149. Nilsson, H. *et al.* Primary clear cell renal carcinoma cells display minimal mitochondrial respiratory capacity resulting in pronounced sensitivity to glycolytic inhibition by 3-Bromopyruvate. *Cell Death Dis.* **6**, e1585 (2015).
150. Parks, S. K., Chiche, J. & Pouyssegur, J. pH control mechanisms of tumor survival and growth. *J. Cell. Physiol.* **226**, 299–308 (2011).
151. Rahl, P. B. *et al.* C-Myc regulates transcriptional pause release. *Cell* **141**, 432–445 (2010).
152. Takada, R. *et al.* Monounsaturated Fatty Acid Modification of Wnt Protein: Its Role in Wnt Secretion. *Dev. Cell* **11**, 791–801 (2006).
153. Willert, K., Brown, J., Danenberg, E. & Duncan, A. Wnt proteins are lipid-modified and can act as stem cell growth factors. *Nature* **423**, 448–452 (2003).
154. Bänziger, C. *et al.* Wntless, a Conserved Membrane Protein Dedicated to the Secretion of Wnt Proteins from Signaling Cells. *Cell* **125**, 509–522 (2006).
155. Bartscherer, K., Pelte, N., Ingelfinger, D. & Boutros, M. Secretion of Wnt Ligands Requires Evi, a Conserved Transmembrane Protein. *Cell* **125**, 523–533 (2006).
156. Cha, S. W. *et al.* Wnt11/5a Complex Formation Caused by Tyrosine Sulfation Increases Canonical Signaling Activity. *Curr. Biol.* **19**, 1573–1580 (2009).
157. Endo, Y. *et al.* Wnt-3a and Dickkopf-1 stimulate neurite outgrowth in Ewing tumor cells via a Frizzled3- and c-Jun N-terminal kinase-dependent mechanism. *Mol. Cell. Biol.* **28**, 2368–2379 (2008).

158. Kishida, S., Yamamoto, H. & Kikuchi, A. Wnt-3a and Dvl induce neurite retraction by activating Rho-associated kinase. *Mol. Cell. Biol.* **24**, 4487–501 (2004).
159. Glinka, a *et al.* Dickkopf-1 is a member of a new family of secreted proteins and functions in head induction. *Nature* **391**, 357–362 (1998).
160. Mao, B. *et al.* LDL-receptor-related protein 6 is a receptor for Dickkopf proteins. *Nature* **411**, 321–325 (2001).
161. Li, X. *et al.* Sclerostin binds to LRP5/6 and antagonizes canonical Wnt signaling. *J. Biol. Chem.* **280**, 19883–19887 (2005).
162. Bourhis, E. *et al.* Reconstitution of a Frizzled8 □ Wnt3a □ LRP6 Signaling Complex Reveals Multiple Wnt and Dkk1 Binding Sites on LRP6 □. *J. Biol. Chem.* **285**, 9172–9179 (2010).
163. Tamai, K. *et al.* A Mechanism for Wnt Coreceptor Activation. *Mol. Cell* **13**, 149–156 (2004).
164. Zeng, X. *et al.* A dual-kinase mechanism for Wnt co-receptor phosphorylation and activation. *Nature* **438**, 873–877 (2005).
165. Davidson, G. *et al.* Casein kinase 1 gamma couples Wnt receptor activation to cytoplasmic signal transduction. *Nature* **438**, 867–872 (2005).
166. Yost, C. *et al.* The axis-inducing activity, stability, and subcellular distribution of beta-catenin is regulated in *Xenopus* embryos by glycogen synthase kinase 3. *Genes Dev.* **10**, 1443–1454 (1996).
167. Liu, C. *et al.* Control of β -catenin phosphorylation/degradation by a dual-kinase mechanism. *Cell* **108**, 837–847 (2002).
168. Coombs, G. S. *et al.* WLS-dependent secretion of WNT3A requires Ser209 acylation and vacuolar acidification. *J. Cell Sci.* **123**, 3357–3367 (2010).
169. Ching, W., Hang, H. C. & Nusse, R. Lipid-independent secretion of a *Drosophila* Wnt protein. *J. Biol. Chem.* **283**, 17092–17098 (2008).
170. Herr, P. & Basler, K. Porcupine-mediated lipidation is required for Wnt recognition by Wls. *Dev. Biol.* **361**, 392–402 (2012).
171. Kim, H. *et al.* *Xenopus* Wntless and the retromer complex cooperate to regulate XWnt4 secretion. *Mol. Cell. Biol.* **29**, 2118–28 (2009).
172. Proffitt, K. D. *et al.* Pharmacological inhibition of the Wnt acyltransferase PORCN prevents growth of WNT-driven mammary cancer. *Cancer Res.* **73**, 502–507 (2013).
173. Chen, B. *et al.* Small molecule-mediated disruption of Wnt-dependent signaling in tissue regeneration and cancer. *Nat. Chem. Biol.* **5**, 100–7 (2009).
174. Galli, L. M. *et al.* Differential inhibition of Wnt-3a by Sfrp-1, Sfrp-2, and Sfrp-3. *Dev. Dyn.* **235**, 681–690 (2006).
175. Orsulic, S., Huber, O., Aberle, H., Arnold, S. & Kemler, R. E-cadherin binding prevents beta-catenin nuclear localization and beta-catenin/LEF-1-mediated transactivation. *J. Cell Sci.* **112** (Pt 8, 1237–1245 (1999).

176. Prieve, M. G. & Waterman, M. L. Nuclear localization and formation of beta-catenin-lymphoid enhancer factor 1 complexes are not sufficient for activation of gene expression. *Mol. Cell. Biol.* **19**, 4503–15 (1999).
177. Bayley, J.-P. & Devilee, P. The Warburg effect in 2012. *Curr. Opin. Oncol.* **24**, 62–7 (2012).
178. Hamanaka, R. B. & Chandel, N. S. Warburg effect and redox balance. *Science* (80-.). **334**, 1219–1220 (2011).
179. Bensinger, S. J. & Christofk, H. R. New aspects of the Warburg effect in cancer cell biology. *Semin. Cell Dev. Biol.* **23**, 352–61 (2012).
180. Ferreira, L. M. R. Cancer metabolism: the Warburg effect today. *Exp. Mol. Pathol.* **89**, 372–80 (2010).
181. Pinheiro, C. *et al.* Increased expression of monocarboxylate transporters 1, 2, and 4 in colorectal carcinomas. *Virchows Arch.* **452**, 139–46 (2008).
182. Sherwood, V. WNT Signaling: an Emerging Mediator of Cancer Cell Metabolism? *Mol. Cell. Biol.* **35**, 2–10 (2015).
183. Gordan, J. D., Thompson, C. B. & Simon, M. C. HIF and c-Myc: Sibling Rivals for Control of Cancer Cell Metabolism and Proliferation. *Cancer Cell* **12**, 108–113 (2007).
184. Dang, C. V., Le, A. & Gao, P. MYC-induced cancer cell energy metabolism and therapeutic opportunities. *Clin. Cancer Res.* **15**, 6479–6483 (2009).
185. Dang, C. V. Rethinking the Warburg effect with Myc micromanaging glutamine metabolism. *Cancer Res.* **70**, 859–62 (2010).
186. Osthus, R. C. *et al.* Deregulation of glucose transporter 1 and glycolytic gene expression by c-Myc. *J. Biol. Chem.* **275**, 21797–800 (2000).
187. Wise, D. R. *et al.* Myc regulates a transcriptional program that stimulates mitochondrial glutaminolysis and leads to glutamine addiction. *Proc. Natl. Acad. Sci. U. S. A.* **105**, 18782–7 (2008).
188. Chafey, P. *et al.* Proteomic analysis of beta-catenin activation in mouse liver by DIGE analysis identifies glucose metabolism as a new target of the Wnt pathway. *Proteomics* **9**, 3889–900 (2009).
189. Colletti, M. *et al.* Convergence of Wnt signaling on the HNF4alpha-driven transcription in controlling liver zonation. *Gastroenterology* **137**, 660–72 (2009).
190. Gebhardt, R. & Hovhannisyan, A. Organ patterning in the adult stage: the role of Wnt/beta-catenin signaling in liver zonation and beyond. *Dev. Dyn.* **239**, 45–55 (2010).
191. Tan, X., Behari, J., Cieply, B., Michalopoulos, G. K. & Monga, S. P. S. Conditional deletion of beta-catenin reveals its role in liver growth and regeneration. *Gastroenterology* **131**, 1561–72 (2006).
192. Thompson, M. D. & Monga, S. P. S. WNT/beta-catenin signaling in liver health and disease. *Hepatology* **45**, 1298–305 (2007).
193. Giles, R. H. *et al.* Interplay between VHL/HIF1alpha and Wnt/beta-catenin pathways during colorectal tumorigenesis. *Oncogene* **25**, 3065–70 (2006).

194. Nusse, R. Wnt signaling and stem cell control. *Cell Res.* **18**, 523–7 (2008).
195. Suda, T., Takubo, K. & Semenza, G. L. Metabolic regulation of hematopoietic stem cells in the hypoxic niche. *Cell Stem Cell* **9**, 298–310 (2011).
196. Zhou, W. *et al.* HIF1 α induced switch from bivalent to exclusively glycolytic metabolism during ESC-to-EpiSC/hESC transition. *EMBO J.* **31**, 2103–16 (2012).
197. Prigione, A., Fauler, B., Lurz, R., Lehrach, H. & Adjaye, J. The senescence-related mitochondrial/oxidative stress pathway is repressed in human induced pluripotent stem cells. *Stem Cells* **28**, 721–33 (2010).
198. Kondoh, H. *et al.* A high glycolytic flux supports the proliferative potential of murine embryonic stem cells. *Antioxid. Redox Signal.* **9**, 293–299 (2007).
199. Szklarczyk, D. *et al.* The STRING database in 2011: functional interaction networks of proteins, globally integrated and scored. *Nucleic Acids Res.* **39**, D561–8 (2011).
200. Hu, J. *et al.* Heterogeneity of tumor-induced gene expression changes in the human metabolic network. *Nat. Biotechnol.* **31**, 522–9 (2013).
201. Cuff, M. a & Shirazi-Beechey, S. P. The human monocarboxylate transporter, MCT1: genomic organization and promoter analysis. *Biochem. Biophys. Res. Commun.* **292**, 1048–56 (2002).
202. Hanahan, D. & Weinberg, R. A. Hallmarks of cancer: The next generation. *Cell* **144**, 646–674 (2011).
203. Tirosh, I. *et al.* Dissecting the multicellular ecosystem of metastatic melanoma by single-cell RNA-seq. *Science (80-.).* **352**, 189–196 (2016).
204. Patel, A. P. *et al.* Single-cell RNA-seq highlights intratumoral heterogeneity in primary glioblastoma. *Science* **344**, 1396–401 (2014).
205. Dalerba, P. *et al.* Single-cell dissection of transcriptional heterogeneity in human colon tumors. *Nat. Biotechnol.* **29**, 1120–1127 (2011).
206. Ramsköld, D. *et al.* Full-length mRNA-Seq from single-cell levels of RNA and individual circulating tumor cells. *Nat. Biotechnol.* **30**, 777–82 (2012).
207. Liu, S. & Trapnell, C. Single-cell transcriptome sequencing: recent advances and remaining challenges. *F1000Research* **5**, (2016).
208. Balluff, B. *et al.* De novo discovery of phenotypic intratumour heterogeneity using imaging mass spectrometry. *J. Pathol.* **235**, 3–13 (2015).
209. Lee, J. H. *et al.* Highly Multiplexed Subcellular RNA Sequencing in Situ. *Science (80-.).* **343**, 1360–1363 (2014).
210. Tata, A. *et al.* Contrast Agent Mass Spectrometry Imaging Reveals Tumor Heterogeneity. *Anal. Chem.* **87**, 7683–7689 (2015).
211. Zhang, K. *et al.* In situ sequencing for RNA analysis in preserved tissue and cells. *Nat. Methods* **45**, 618–630 (2013).
212. Bafico, A., Liu, G., Goldin, L., Harris, V. & Aaronson, S. A. An autocrine mechanism for constitutive Wnt pathway activation in human cancer cells. *Cancer Cell* **6**, 497–506

- (2004).
213. Smith, K. *et al.* Up-regulation of macrophage wnt gene expression in adenoma-carcinoma progression of human colorectal cancer. *Br. J. Cancer* **81**, 496–502 (1999).
 214. Park, J. K. *et al.* Overexpression of Wnt-2 in colorectal cancers. *Neoplasma* **56**, 119–123 (2009).
 215. Suzuki, H. *et al.* Epigenetic inactivation of SFRP genes allows constitutive WNT signaling in colorectal cancer. *Nat. Genet.* **36**, 417–22 (2004).
 216. Yu, J. & Virshup, D. M. Updating the Wnt pathways. *Biosci. Rep.* **34**, 593–607 (2014).
 217. Cong, F., Cheung, A. K. & Huang, S.-M. a. Chemical genetics-based target identification in drug discovery. *Annu. Rev. Pharmacol. Toxicol.* **52**, 57–78 (2012).
 218. Kahn, M. Can we safely target the WNT pathway? *Nat. Rev. Drug Discov.* **13**, 513–32 (2014).
 219. Lau, T. *et al.* A novel tankyrase small-molecule inhibitor suppresses APC mutation-driven colorectal tumor growth. *Cancer Res.* **73**, 3132–3144 (2013).
 220. Wu, X., Luo, F., Li, J., Zhong, X. & Liu, K. Tankyrase 1 inhibitor XAV939 increases chemosensitivity in colon cancer cell lines via inhibition of the Wnt signaling pathway. *Int. J. Oncol.* 1–8 (2016). doi:10.3892/ijo.2016.3360
 221. Liu, J. *et al.* Targeting Wnt-driven cancer through the inhibition of Porcupine by LGK974. *Proc. Natl. Acad. Sci. U. S. A.* **110**, 20224–9 (2013).
 222. Gonsalves, F. C. *et al.* An RNAi-based chemical genetic screen identifies three small-molecule inhibitors of the Wnt / wingless signaling pathway. *Proc. Natl. Acad. Sci. U. S. A.* **108**, 5954–5963 (2011).
 223. Kahn, M. Can we safely target the WNT pathway? *Nat. Rev. Drug Discov.* **13**, 513–32 (2014).
 224. Lenz, H. J. & Kahn, M. Safely targeting cancer stem cells via selective catenin coactivator antagonism. *Cancer Sci.* **105**, 1087–1092 (2014).
 225. Ganapathy-Kanniappan, S., Kunjithapatham, R. & Geschwind, J. F. Anticancer efficacy of the metabolic blocker 3-bromopyruvate: Specific molecular targeting. *Anticancer Res.* **33**, 13–20 (2013).
 226. Glick, M., Biddle, P., Jantzi, J., Weaver, S. & Schirch, D. The antitumor agent 3-bromopyruvate has a short half-life at physiological conditions. *Biochem. Biophys. Res. Commun.* **452**, 170–3 (2014).
 227. Baltazar, F. *et al.* Monocarboxylate transporters as targets and mediators in cancer therapy response. *Histol. Histopathol.* **29**, 1511–1524 (2014).
 228. Xiong, L., Edwards, C. K. & Zhou, L. The biological function and clinical utilization of CD147 in human diseases: A review of the current scientific literature. *Int. J. Mol. Sci.* **15**, 17411–17441 (2014).
 229. Marchiq, I., Le Floch, R., Roux, D., Simon, M.-P. & Pouyssegur, J. Genetic Disruption of Lactate/H⁺ Symporters (MCTs) and Their Subunit CD147/BASIGIN Sensitizes Glycolytic Tumor Cells to Phenformin. *Cancer Res.* **75**, 171–180 (2015).

230. Azevedo-Silva, J. *et al.* The cytotoxicity of 3-bromopyruvate in breast cancer cells depends on extracellular pH. *Biochem. J.* **467**, 247–58 (2015).
231. He, Y., Vogelstein, B., Velculescu, V. E., Papadopoulos, N. & Kinzler, K. W. The antisense transcriptomes of human cells. *Science (80-.)*. **322**, 1855–1857 (2008).
232. Core, L. J., Waterfall, J. J. & Lis, J. T. Nascent RNA sequencing reveals widespread pausing and divergent initiation at human promoters. *Science (80-.)*. **322**, 1845–1848 (2008).
233. Lin, J. M. *et al.* Transcription factor binding and modified histones in human bidirectional promoters. *Genome Res.* **17**, 818–27 (2007).
234. Pang, K. C. *et al.* Genome-wide identification of long noncoding RNAs in CD8+ T cells. *J Immunol* **182**, 7738–7748 (2009).
235. Fong, N., Ohman, M. & Bentley, D. L. Fast ribozyme cleavage releases transcripts from RNA polymerase II and aborts co-transcriptional pre-mRNA processing. *Nat. Struct. Mol. Biol.* **16**, 916–22 (2009).
236. Yokoyama, N. N., Pate, K. T., Sprowl, S. & Waterman, M. L. A role for YY1 in repression of dominant negative LEF-1 expression in colon cancer. *Nucleic Acids Res* **38**, 6375–6388 (2010).
237. Boehm, J. S. *et al.* Integrative genomic approaches identify IKBKE as a breast cancer oncogene. *Cell* **129**, 1065–79 (2007).
238. Skehan, P. *et al.* New colorimetric cytotoxicity assay for anticancer-drug screening. *J. Natl. Cancer Inst.* **82**, 1107–12 (1990).
239. Zhang, J. *et al.* Measuring energy metabolism in cultured cells, including human pluripotent stem cells and differentiated cells. *Nat. Protoc.* **7**, 1068–85 (2012).

APPENDIX A

Predicting mechanism of biphasic growth factor action on tumor growth using a multi-species model with feedback control

Introduction

In development and tissue regeneration post-injury, a large number of growth factors have been found to elicit a biphasic response from the tissue: at lower concentrations the growth factor exerts a mitogenic or cell size growth effect, and at higher concentrations this effect is abrogated and cells quiesce or differentiate.^(1, 2) For example, a long list of endogenous and exogenous agents display a biphasic dose-response curve with respect to neurite outgrowth both *in vitro* and *in vivo*, including Nerve Growth Factor (NGF), Fibroblast Growth Factor (FGF), Vascular Endothelial Growth Factor (VEGF), and adrenocorticotrophic hormone (ACTH).^(3, 4) Purported mechanisms for the biphasic dose response include presence of a high affinity and a low affinity receptor,^(5–8) receptor internalization at high growth factor concentration,⁽⁹⁾ and/or concentration-dependent biphasic receptor response via activation of opposing pathways.⁽¹⁰⁾

During skeletal muscle injury, dormant satellite myogenic stem cells are activated to enter the cell cycle by low concentrations of Hepatocyte Growth Factor, HGF, which is released from extracellular stores (as well as produced by spleen, liver, and the satellite cells themselves) after injury.^(11, 12) But, at concentrations of greater than 10 ng/ml, HGF inhibits satellite cell division,^(13, 14) and it was shown that this inhibition is due to increased myostatin (a TGF β family member) production at higher levels of HGF.⁽¹⁰⁾ As with the growth factors involved in neurite outgrowth, while the mitogenic action of HGF is well understood (HGF binds to its cognate c-Met receptor, whose activation results in translocation of β -catenin into the nucleus,

where it acts as a transcription factor of canonical Wnt gene products⁽¹⁵⁾, the molecular nature of the inhibitory effect of HGF at high concentrations has not yet been established. Yamada et al. provided two hypotheses: that differential activation of c-Met is the cause of proliferation arrest, as evidenced by requirement of phosphatase SHP2 for the arrest, which is recruited by activated c-Met, and/or the presence of as yet unidentified low affinity receptors for HGF.^(10, 13, 16)

We have recently found that culture of tumor spheroids derived from Colon Cancer Initiating Cells (CCICs), a primary colon cancer cell line,^(17, 18) in presence of increasing concentrations of HGF, also has a biphasic effect on tumor growth.⁽¹⁹⁾ Based on the research from Yamada et al. as well as findings that addition of HGF at a concentration of 40 ng/ml induces expression of several members of the TGF β family in an *in vitro* liver organoid culture,⁽²⁰⁾ we have developed a simple model of biphasic HGF action on tumor growth where HGF stimulates canonical Wnt signal at low concentrations and TGF β signal at higher doses. We show that the shape of the resulting dose-response curve of the model is dependent on the assumption of linearity (or non-linearity) of the effect of HGF on TGF β production, hence demonstrating that the shape of the dose-response curve can give insight into the molecular nature of the biphasic response.

Mathematical Model

The mathematical model is specific to our experimental system, namely of HGF action on tumor cells, in order to optimize parametrization. Nevertheless, the model is simple enough that it can represent a more general system of a growth factor action on a tissue in a non-monotonic fashion. In this study, we develop a single-scale, spatially homogeneous model of HGF action on a multi-species tumor which consists of a coupled system of nonlinear ordinary

differential equations representing changes in stem and terminal cell tumor species, as well as positive regulators (W) and negative regulators of tumor growth (T), as summarized in Figure 1 and discussed in the remainder of the section.

Tumor Cell Species

We characterize tumor cell dynamics using the cell lineage hypothesis.^(21, 22) It has been shown that tumor cells progress through lineage stages where the ability to self-renew is gradually lost.^(23, 24) We consider a simplified lineage with cancer stem cell (S) and terminal cell (TC) species that make up the viable fraction of the tumor. Stem cells self-renew, i.e., form new stem cells upon division, with a probability P . We note that in our continuum model, results from asymmetric or symmetric stem cell division are identical, thus we do not make a distinction between these mechanisms of self-renewal. Change in species concentration is a function of the fraction of daughter cells that either remain after division ($2P - 1$) in the case of stem cells, with the factor of ‘2’ accounting for the production of two daughter cells from each parent cell at each cell division, or the fraction of cells that differentiate, $2(1 - P)$, in the case of terminal cells, and the cell division rate of each species,

$$\frac{\partial S}{\partial t} = (2P - 1)K_S S \quad (1)$$

$$\frac{\partial TC}{\partial t} = 2(1 - P)K_S S + K_{TC} TC \quad (2)$$

where K_S , K_{TC} are the stem and differentiated cell division rates, respectively. We discuss the dependence of K_S on various growth factors below, and assume K_{TC} to be constant, since

terminal cells have less variable and lower division rates than CSCs.⁽²⁵⁾ We set $K_{TC} = 0.1$, as it falls below the lowest observed CCIC division rate of 0.13, which was observed in a mixed (i.e., CSC and TC) population of CCICs.⁽¹⁹⁾ Moreover, we assume that nutrient and oxygen concentrations are not limiting, which is applicable to an experimental cell culture system with proper media, and hence necrosis and apoptosis are negligible.

Stem Cell Self-Renewal Rate and Division Rate

It has been shown that microenvironmental feedback on self-renewal in a tissue cell lineage is necessary for robust control of lineage progression.⁽²¹⁾ Current data shows that elements of such a control system are also present in cancer cell lineages, although often in a dysregulated manner. Indeed, the Wnt/ β -catenin system, which involves stem cell-produced glycoproteins from the Wnt family which cause nuclear translocation and activation of transcription factor β -catenin, and is associated with increased cell proliferation and self-renewal in normal tissues, has been shown to be overactivated in several types of tumors, including glioma, meduloblastoma, colon cancer, and hepatocellular carcinoma.^(26–28) These factors are represented by W in the model. Moreover, it has been shown across several tissues and in both normal and early cancerous tissue that growth factors, most notably those from the TGF β superfamily, are produced that feedback on to the stem cells to reduce rates of cell proliferation and self-renewal.^(29–31) We model the effect of this class of factors using T . Hence, P and K_S are modeled as follows,

$$P = P_{\min} + (P_{\max} - P_{\min})M_P \quad (3)$$

$$K_S = K_{S_{\min}} + (K_{S_{\max}} - K_{S_{\min}})M_{K_S} \quad (4)$$

$$M_{P, K_S} = \left(\frac{\xi_{P, K_S} W}{1 + \xi_{P, K_S} W} \right) \left(\frac{1}{1 + \psi_{P, K_S} T} \right) \quad (5)$$

where P_{\min} and P_{\max} are minimum and maximum rates of self-renewal, respectively, and $K_{S_{\min}}$ and $K_{S_{\max}}$ are the minimum and maximum rates of stem cell division, respectively. The functions M_P and M_{K_S} represent the feedback of W and T on P and K_S , respectively. We set $P_{\min} = 0.2$ and $P_{\max} = 1.0$ to represent the possible extremes of P , and $K_{S_{\min}} = 0.1$ and $K_{S_{\max}} = 1.0$ as we have found that CCICs have division rates of approximately 0.15 to 0.5 in culture.⁽¹⁹⁾ The upper limit is set to 1.0 since our findings were based on growth rates of CCICs that may have been differentiating, hence the division rates of the stem cells would have to be slightly greater than the aggregated division rate. ξ_P , K_S represent the positive effect of W on P and K_S , respectively, and ψ_P , K_S represent the inhibitory effect of T on P and K_S , respectively. We set $\xi_P = 1.0$ and $\psi_P = 0.5$. These values were derived by Youssefpour et al. in a model of this system that includes, in addition to Eqs. (1)–(5), generalized diffusion and convection terms for the cell species.⁽²²⁾ We set $\xi_{K_S} = 0.01$ and $\Phi_{K_S} = 0.5$, which were derived using an extension of the Youssefpour model to parametrize growing CCICs in culture.⁽¹⁹⁾

Growth Factor Concentration

A hallmark of colorectal cancer is disruption and over-activation of the Wnt/ β -catenin signaling pathway, often through inactivation of the cytoplasmic β -catenin binding protein APC, or through activating mutations in β -catenin itself.⁽³²⁾ Moreover, it has been shown that several distinct downstream factors of the β -catenin signal, including Phospholipase D and BMI1, act as activators of the Wnt/ β -catenin pathway, creating a positive feedback loop that is nonlinear due to the multiple feedback mechanisms on the pathway.^(33–35) We model this aspect of the W auto regulation using a modified Michaelis–Menten equation, in order to account for signal saturation. Additionally, HGF, acting through its CSC-expressed cognate receptor c-Met, results in translocation of β -catenin to the nucleus, and hence also potentiates Wnt signal. Moreover, as discussed in the introduction, there is evidence that HGF also acts on T at high concentrations,^(10, 20) although the mechanism by which it does so is currently unknown. Therefore, we model changes to W and T as follows,

$$\frac{\partial W}{\partial t} = (\lambda_H H + \frac{\lambda_{PW1} W^2}{1 + \lambda_{PW2} W^2}) S - \nu_{DW} W \quad (6)$$

$$\frac{\partial T}{\partial t} = g_i(H)(S + TC) - \nu_{DT} T \quad i=1, 2, 3 \quad (7)$$

where $s\lambda_H$ represents the feedback response of W on H , λ_{PW1} is the strength of the autocrine positive feedback response of W , λ_{PW2} is the Michaelis–Menton constant for W , ν_{DW} , DT are the decay rates for W and T , respectively, and $g_i(H)$ is the positive feedback function of H on T ,

which becomes increasingly nonlinear with increasing i (see below). λ_H , λ_{PW1} , and λ_{PW2} are estimated to fit a maximum peak of the dose response curve to approximately 1000%. The value of 1000% is derived from the following observation: in the original experiments with CCICs, the observed maximum growth rate was found to be approximately 2000%,⁽¹⁹⁾ but we have found that this growth rate was dependent on initial spheroid size, and when normalized for average spheroid size, the predicted maximum growth rate is approximately 1000% (unpublished observations). Currently, *in vitro* decay rates for W and T are unavailable, and hence we set, as a first approximation, $v_{DW} = v_{DT} = 1.0$ and note that since calculation of λ_H , $\lambda_{PW1, 2}$ are dependent on ambient W and T , a change in v_{DW} or v_{DT} would necessitate a change in λ_H and $\lambda_{PW1, 2}$ to match the tumor growth rate, hence the output in S and TC would be similar to the results for $v_{DW} = v_{DT} = 1.0$.

The effect of H on T is modeled using three different functions, each which differ by (1) the degree of the nonlinearity of H and (2) the modulating factor, which is set to allow the maximum peak growth to be similar between the different functions. We note that, in nature, i need not be an integer, but nevertheless, as i increases, we will show that the post-peak curvature of the dose-response curve will increase, hence while it may not be possible to determine the specific i of the growth factor from the dose-response curve alone, it will be possible to determine the qualitative degree of nonlinearity of action of the negative growth regulator. Therefore, our choice of i act as representative values of the (non-)linear effect of the negative growth regulator. For this study, we set $g_1(H) = 5^{-3}H$, $g_2(H) = 3^{-4}H^2$, and $g_3(H) = 2^{-5}H^3$. We summarize all parameter values in Table I.

Quasi-Steady State Growth Factor Concentration

In order to analyze the dynamics, we reduced the system by assuming quasi-steady state concentrations for W and T . Setting the time derivatives to 0 in Eqs. (6) and (7) allowed us to solve for W in terms of S and H , and for T in terms of H , S and TC . In the case of W , we obtained the cubic function $0 = -W^3 + W_2S(2H + 1) - W + 2H$, and in the case of T , we have $0 = g(H)(CS + TC) - T$. The real solution to the first equation was calculated using the MATLAB symbolic solver,

$$\begin{aligned}
 W = & S/3 + (H - S/6 + (S + 2HS))^{3/27} \\
 & + (H - S/6 + (S + 2HS))^{3/27} \\
 & - ((HS)/3)^2 \\
 & - (1/9(S + 2HS)^2 - 1/3)^{1/2} \\
 & - ((HS)/3)^{1/3} \\
 & + (S + 2HS)^{2/9} \\
 & - 1/3 / (H - S/6 + (S + 2HS))^{3/27} + ((H - S/6 + (S + 2HS))^{3/27} - (HS)/3)^2 - (1/9(S + 2HS)^2 - 1/3)^{1/2} - (HS)/3
 \end{aligned}$$

For the second equation, we obtain:

$$T = g(H)(S + TC) \quad (9)$$

Results

The equations were numerically solved in MATLAB using MATLAB's standard solver for ordinary differential equations, ode45. Initial conditions were set to model a CCIC culture system. Since CCICs are composed of stem cells derived from primary colon tumors,⁽¹⁷⁾ we set $S = 1$ and $TC = 0$, where 1 simulation cell corresponds to 10 biological cells, which is the average number of cells initially in each experiment.⁽¹⁹⁾ Since stem cells produce W but not T ,

we set $2.0=W \gg T=0.01$ as initial conditions, with units for all growth factors in ng/ml. We chose the specific value of 2.0 for W as double to the decay rate so that it does not artificially decay to zero, and 0.01 for T to account for any background levels of the growth factor. The simulation was run over various H values (H is assumed to be constant throughout the simulation). The simulation was run from $t = 0$ to $t = 9$, where t represents the number of days of the simulation. The dose-response curve for % tumor growth at day 9 in increasing concentrations of HGF for the full system is found in Figure 2 and for the quasi-steady state system in Figure 3. Note that growth curves for the original and quasi-steady state model are not identical, indeed at very low, but non-zero, concentrations of H , the curve for nonlinear g overestimates cellular growth. This is because if $g(H) = 2^{-5}H^3$, then $T = g(H)(S+TC)$ is very small at low H , and its effect is negligible on P and K_S , resulting in increased growth and proliferation of stem cells, and thus rapid production of W (Fig. 4 (ii)), therefore the assumption that W is in a quasi-steady state at this concentration of H is not accurate.

Nevertheless, the stem cell, terminal cell, W , and T dynamics are very similar between the two models at both $H = 0$ and higher values of H (Fig. 5). The peak of both curves occurs at approximately $H = 20$, and at this HGF concentration, stem cell concentrations increase throughout the simulation in both models. Therefore, since our analysis is concentrated on curve behavior in control conditions and after the growth peak is attained, we assume that the quasi-steady state system provides a good approximation of the cell numbers.

A phase plane analysis of stem and terminal cell dynamics shows that at a concentration of $H = 100$, stem cell concentrations tend to 0 over time while terminal cell concentrations increase, whereas at $H = 20$, both stem and terminal cell concentrations increase independent of initial conditions (Figs. 6(b), (c)). Interestingly, there is a divergence of stem cell

response for $H = 0$, at initial concentrations of less than 2, the stem cell concentration tends to 0, whereas at higher initial concentrations, stem cell concentrations also increase over time. This occurs due to a higher production of W at the initial time points that potentiates the stem cell populations. Therefore, if initial concentrations of stem cells is high, the growth peak would move left on the dose-response curve due to the increase in stem cell growth.

To investigate whether a different choice of g resulted in different relative fractions of stem versus terminal cells at concentrations of H after the peak growth phase, we plotted the stem cell fraction at linear and cubic g at the final time point over concentrations of H ranging from 20–100. Indeed, a cubic g resulted in a nonlinear decrease in stem cell fraction after the peak growth phase, whereas a linear g resulted in a more linear decrease in the stem cell fraction, consistent with the the action of T on stem cell self-renewal (Fig. 7).

Discussion

In this study, we analyze the relationship between the mechanism of growth factor-mediated activation of a growth inhibitor at high concentrations and the shape of a biphasic dose-response curve of tissue growth in response to increasing concentrations of growth factor. Since the molecular nature of the inhibitor activation is often unknown, the shape of an experimental growth curve can serve as an aid in generating hypotheses of growth factor action. For example, if the curve post-peak segment (CPPS) displays low curvature (i.e., is near linear), then most likely there is no synergy of inhibitor activation by the growth factor. For example, in the Yamada et al. study on HGF effect on muscle satellite cell proliferation, the CPPS is linear (Fig. 8). Therefore, we hypothesize that either HGF acts via biphasic activation of c-Met, or via a low-affinity growth receptor to stimulate myostatin production. On the other hand, if the CPPS shows

high curvature, then we hypothesize that the growth factor increases expression of the growth inhibitor in a non-linear fashion. Experimental examples of such growth curves include NGF action on neurite outgrowth and copper chloride action on bacterial colony formation (Fig. 9). In biological signaling, a nonlinear signal is often indicative of activation of multiple downstream effectors.^(36, 38) Hence, a nonlinear CPPS may be indicative of pleiotropic action of the growth factor on growth inhibition.

Moreover, we also show that nonlinear activation of an inhibitor results in a nonlinear decline in the stem cell fraction in the cell population with increasing H after the peak growth concentration (Fig. 7). Experimental establishment of this relationship requires use of a CSC marker such as CD133, which is specific to colon CSCs,⁽⁴⁰⁾ and can serve to provide evidence that the growth antagonist acts on P and K_S , hence further substantiating details of the mathematical model. Additionally, use of a CSC marker can give insight into the predictions of the phase plane analysis, specifically that peak growth is dependent on the steady state of CSCs: peak growth occurs at H concentration where CSC populations increase during the entire time course of the experiments (i.e., do not tend towards the alternative steady state of 0) (Fig. 6). A simplification of the current model to make it amenable to analytical analysis may also be used to confirm the stability results.

Conclusions

Our simple model of HGF action on cell proliferation in a multi-species colon cancer models serves to establish the hypothesis that a shape analysis of a dose-response curve can inform molecular mechanism of growth factor action. Moreover, the model can be extended to include different hypotheses on activator induction by the growth factor, or in cases where the

growth curve is monotonic, the shape analysis can be performed on the pre-peak curve segment or the entire curve, respectively. Generation of experimental dose-response curves and subsequent curve shape analysis using a system where the molecular mechanism of action of a growth factor on the phenotypic output is known can be used to test the model predictions.

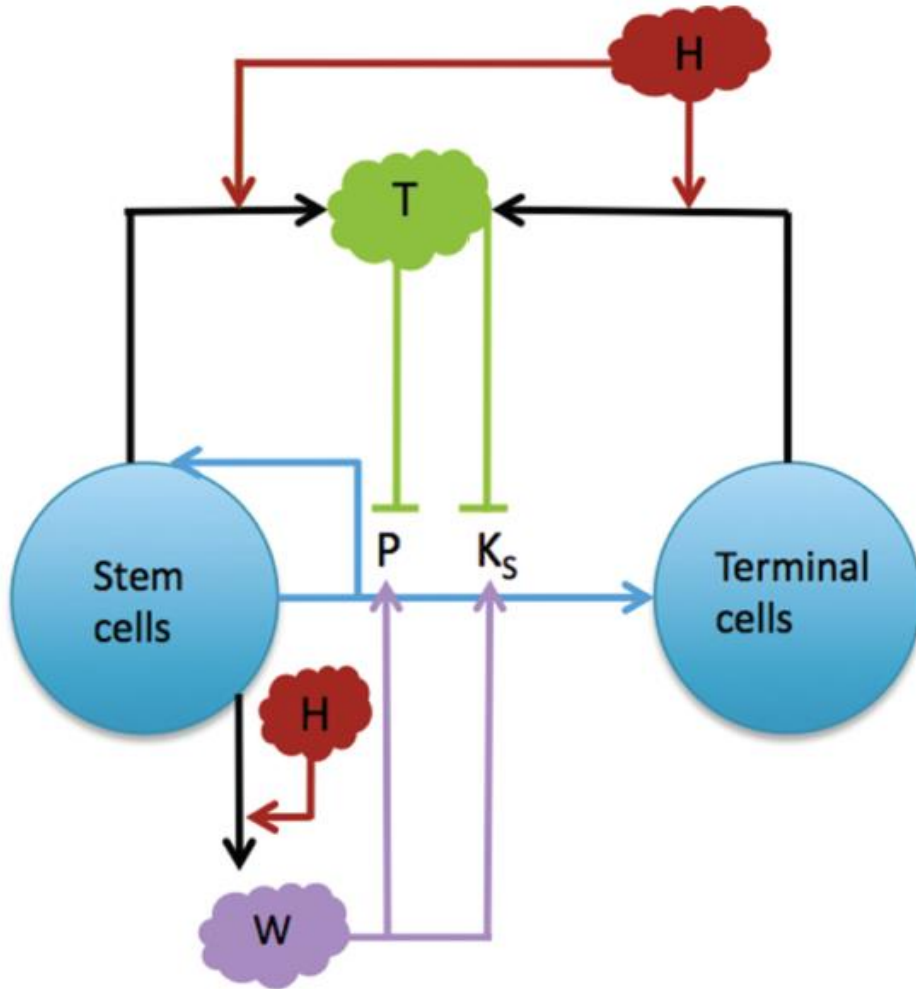


Figure A1. A multispecies model of tumor signaling.

Tumor tissue is composed of two cell types: cancer stem cells (S), and terminally differentiated cells (TC). Stem cells have a probability of self renewal P , differentiate into TCs with probability $1-P$, and divide at a rate K_S . P and K_S are promoted by W signals produced by the stem cells and inhibited by T , which are produced by S and TCs in response to high H , which represents HGF. H acts by both increasing production of W (at low concentrations) and T (at high concentrations). (Adapted from [22], H. Youssefpour, et al.; *J. Theor. Biol.* 304, 39 (2011)).

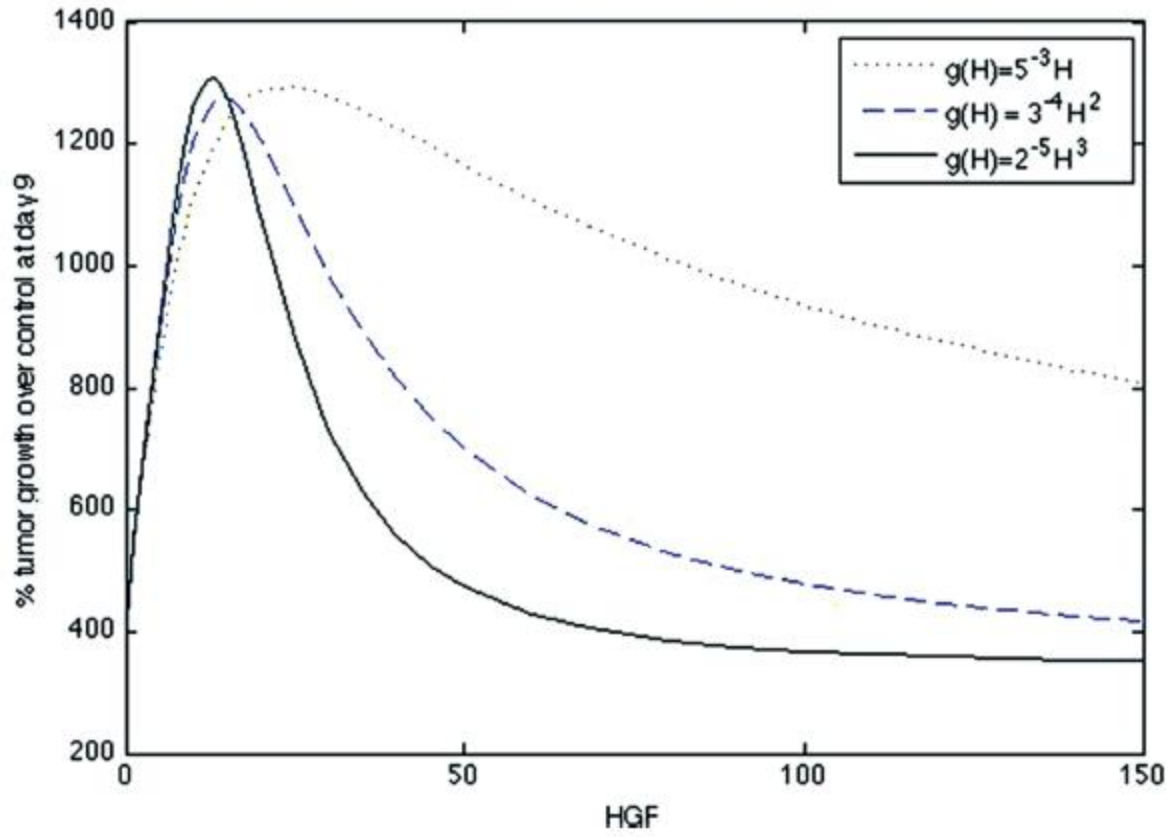


Fig. A2. Dose-response curve of original system.

(Eqs. (1)–(7)) for a linear $g(H) = 5^{-3}H$, quadratic $g(H) = 3^{-4}H^2$, and cubic $g(H) = 2^{-5}H^3$.

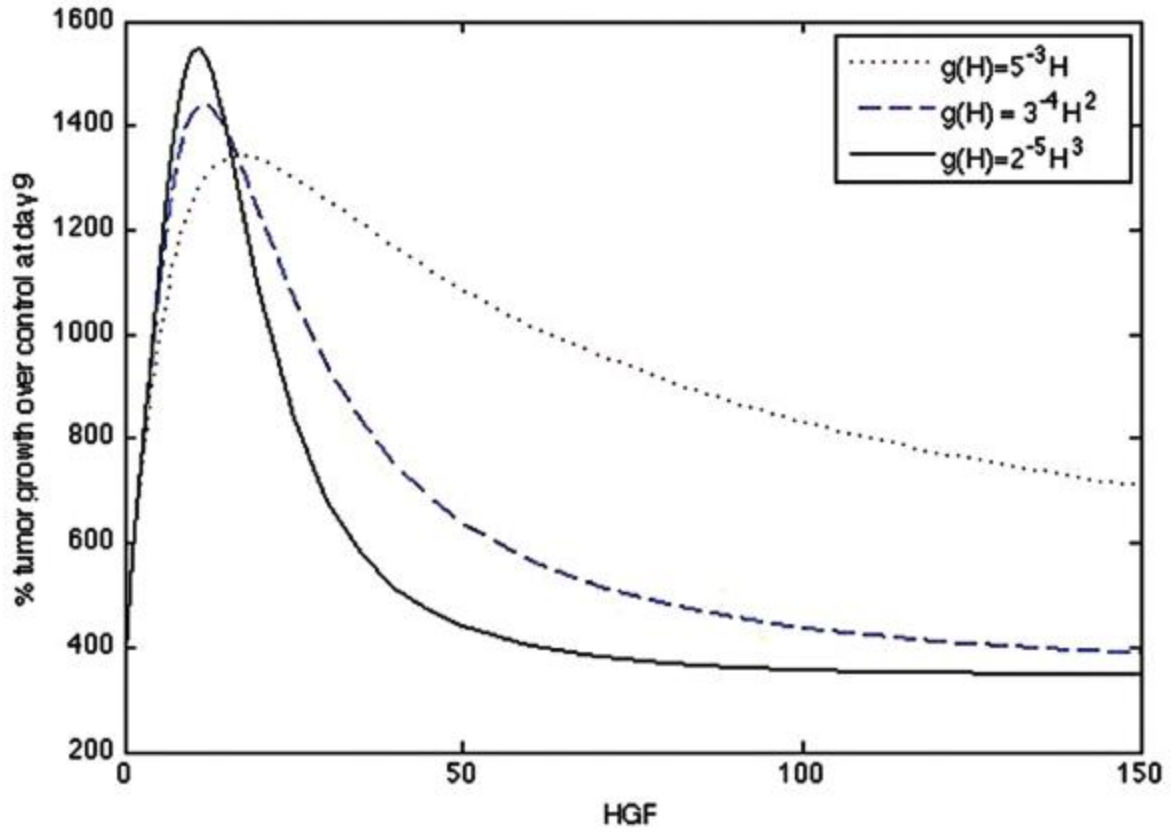
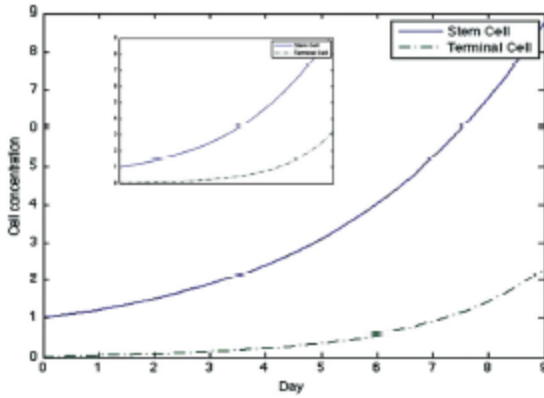


Fig. A3. Dose-response curve of quasi-steady state system.

(Eqs. (1)– (5), (8), (9)) for a linear $g(H) = 5^{-3}H$, quadratic $g(H) = 3^{-4}H^2$, and cubic $g(H) = 2^{-5}H^3$.

$H=10$

(i) $g(H) = 5^{-3}H$



(ii) $g(H) = 2^{-5}H^3$

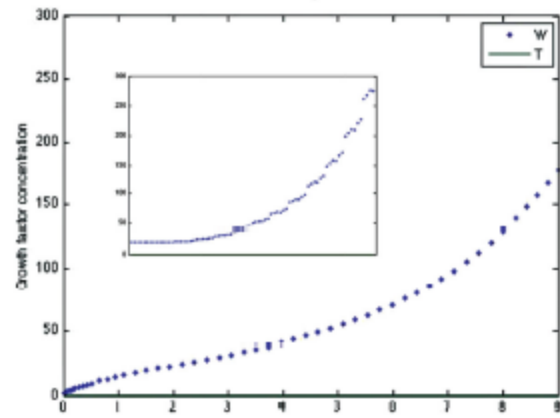
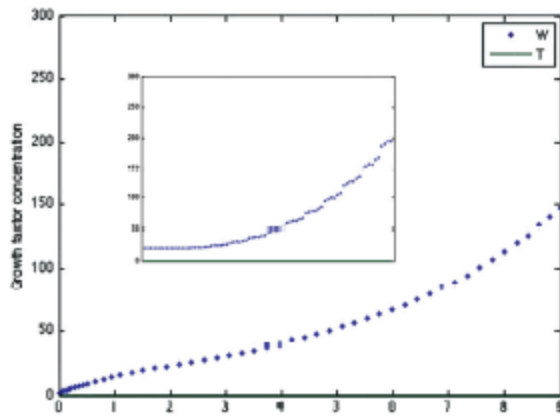
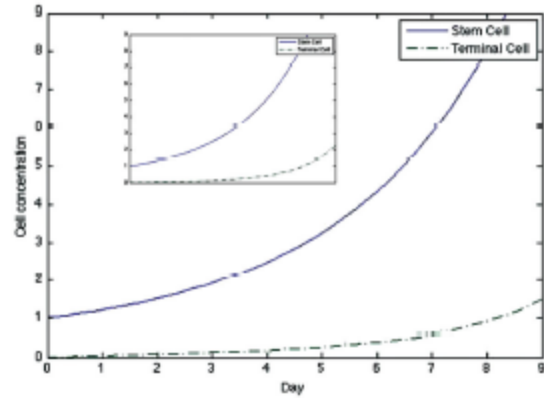


Fig. A4. Dynamics of stem cell, terminal cell, W , and T concentrations in the original model for linear and cubic g and at $H = 10$.

The graph insets for each simulation are the dynamics of the same factor in the quasi-steady state model.

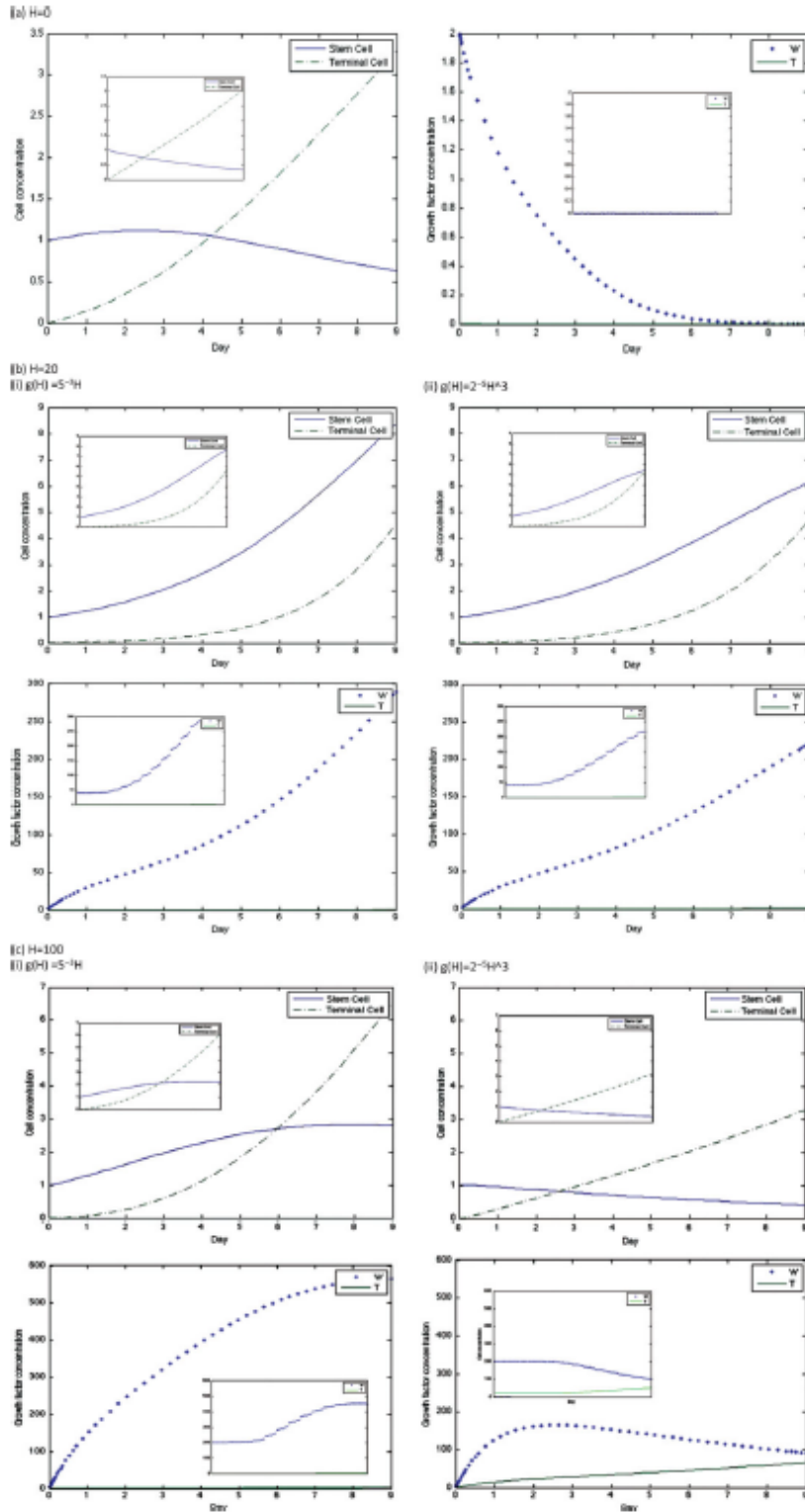


Fig. A5. Dynamics of stem cell, terminal cell, W , and T concentrations in the original model for linear and cubic g and at concentrations of (a) $H = 0$, (b) $H = 20$, and (c) $H = 100$. The graph insets for each simulation are the dynamics of the same factor in the quasi-steady state model.

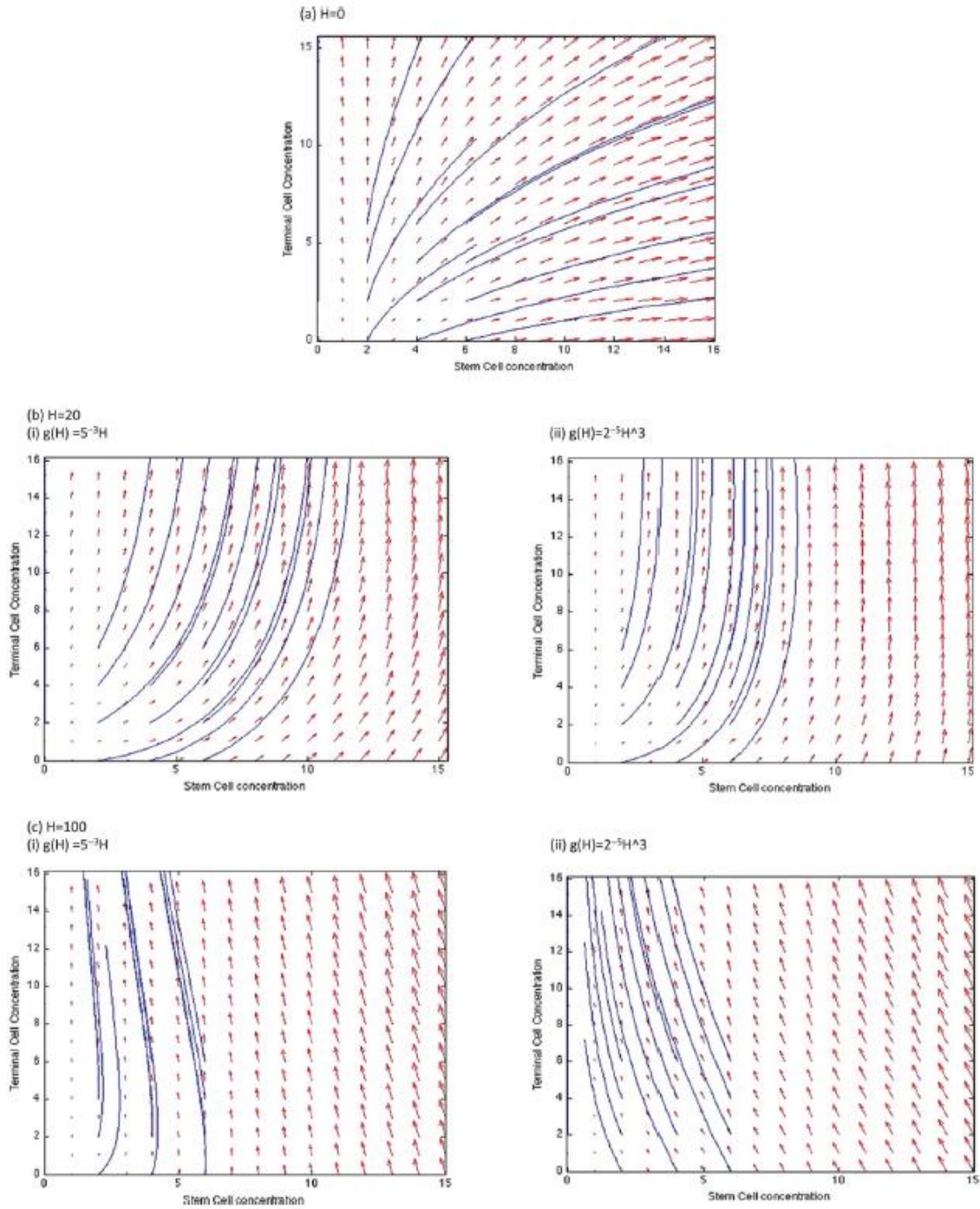


Fig. A6. Phase planes of stem and terminal cell dynamics for the quasi-steady state system at (a) $H = 0$, (b) $H = 20$, with linear and cubic $g(H)$, and (c) $H = 100$, with linear and cubic $g(H)$.

Solutions are plotted for initial conditions ranging from 0–6 stem and terminal cells (each).

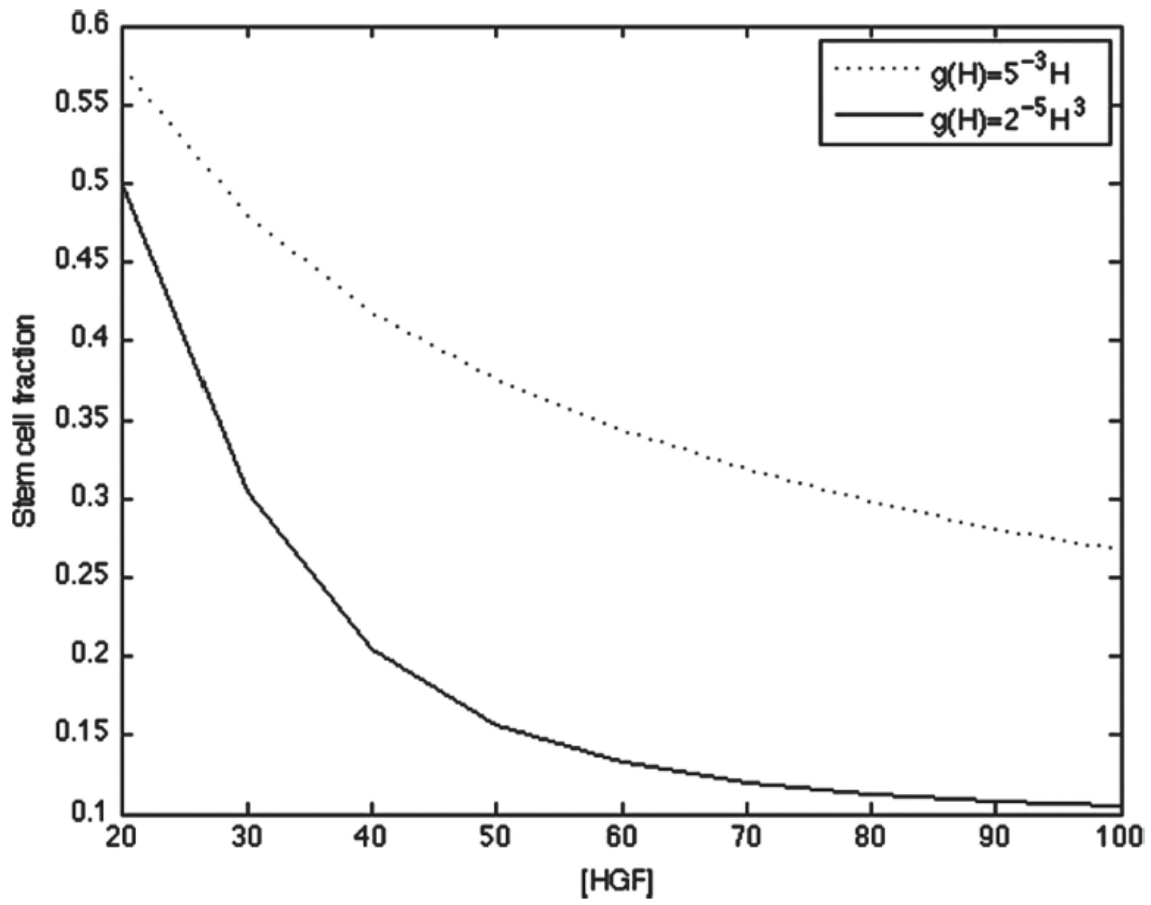


Fig. A7. Stem cell fraction at $t = 9$ and $20 \leq H \leq 100$ for the quasisteady state system at linear and cubic $g(H)$.

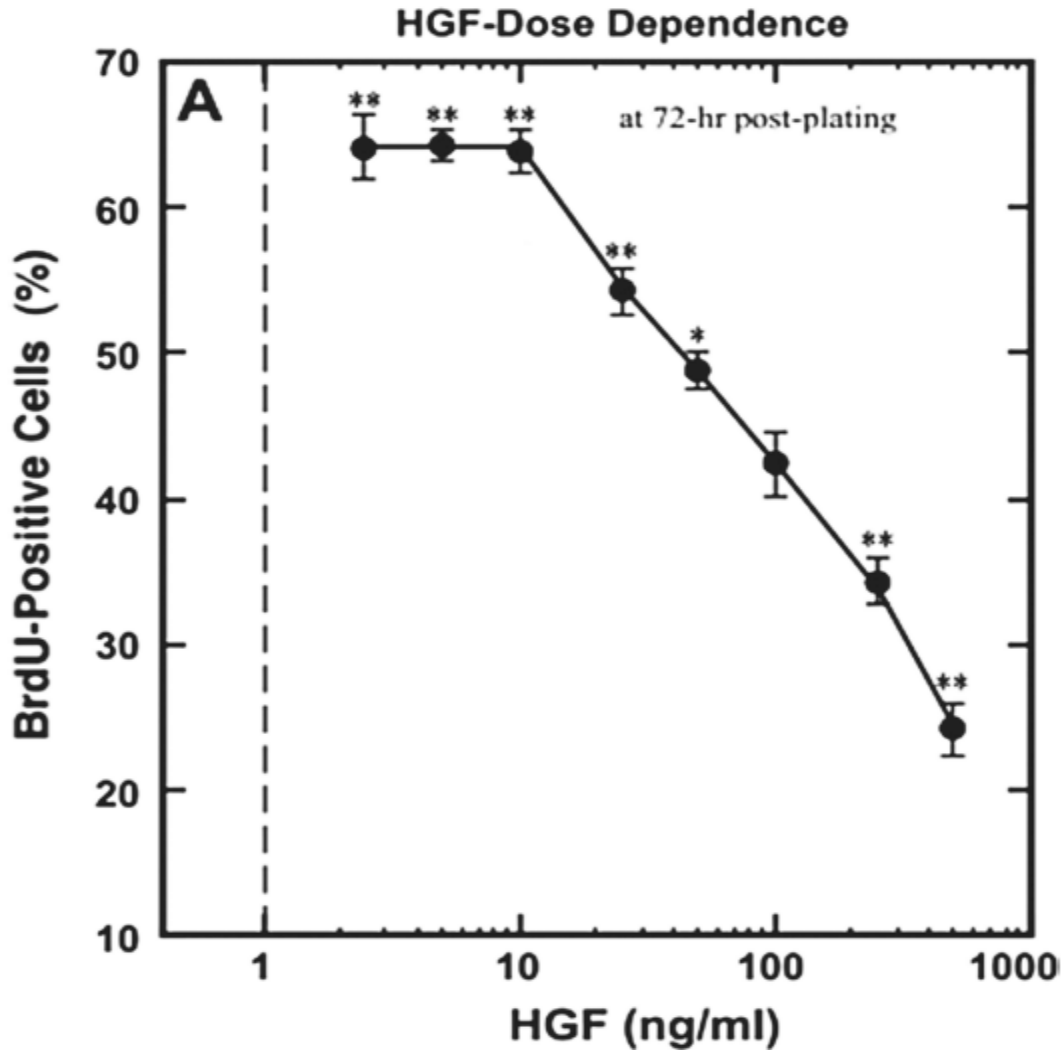


Fig. A8. Example of a linear dose-response curve.

BrdU, a thymidine analogue, is incorporated into newly synthesized DNA of replicating cells, and can be detected using anti-BrdU antibodies. Hence, it acts as a marker of cell proliferation. The dose-response curve of BrdU uptake by satellite muscle cells in response to increasing HGF shows a linear post-peak decline in BrdU-positive cells with increasing HGF. (*Reprinted with permission from [10], M. Yamada, et al.; Am. J. Physiol. Cell Physiol. 298, C465 (2010).*)

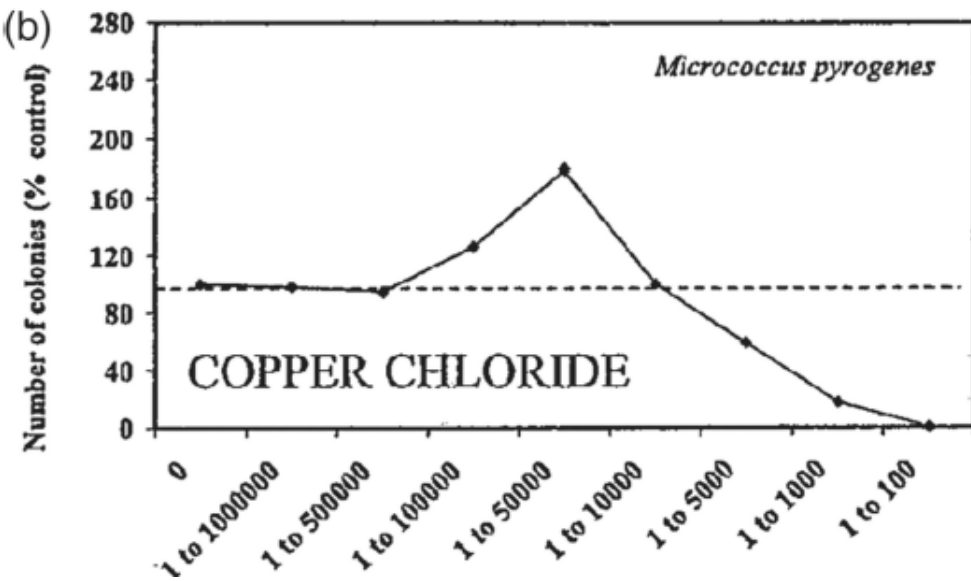
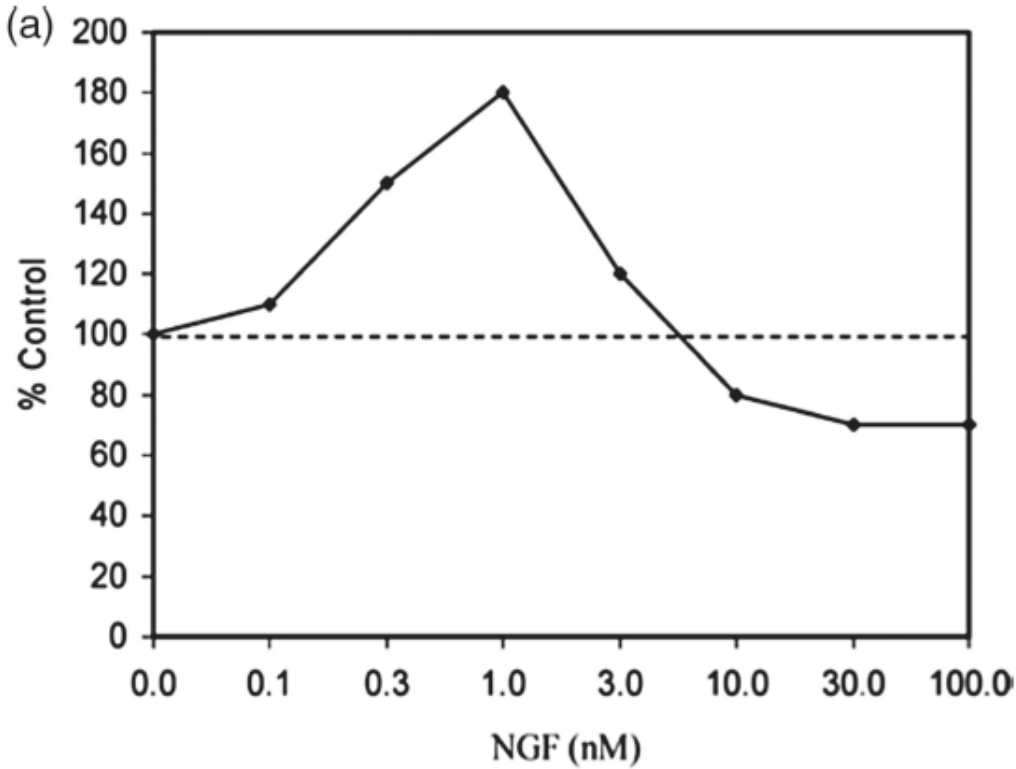


Fig. A9. Examples of non-linear dose-response curves

(A) effect of NGF on neuronal outgrowth in dorsal root ganglion neurons of rat lumbar region. (Reprinted with permission from [3], E. J. Calabrese; *Crit. Rev. Toxicol.* 38, 391 (2008)). (B) effect of copper chloride on growth of *Micrococcus Pyrogenes* bacterial cultures. (Reprinted with permission from [39], E. J. Calabrese and L. A. Baldwin; *Crit. Rev. Toxicol.* 31, 353 (2001)).

Summary of parameter values for Eqs. (1)–(7).

Parameter	Description	Value
K_{TC}	TC mitosis rate	0.1
P_{\min}	Min. CSC self-renewal rate	0.2
P_{\max}	Max. CSC self-renewal rate	1.0
$K_{S_{\min}}$	Min. CSC mitosis rate	0.1
$K_{S_{\max}}$	Max. CSC mitosis rate	1.0
ξ_P	Pos. feedback response of P	1.0
ψ_P	Neg. feedback response of P	0.5
ξ_{K_S}	Pos. feedback response of K_S	0.01
ψ_{K_S}	Neg. feedback response of K_S	0.5
λ_{PW1}	Pos. feedback response of W	1
λ_{PW2}	M–M constant for W	1
λ_H	H feedback response of W	2
$\nu_{D(W, T)}$	Decay rates for W and T , respectively	1

Fig. A10. Summary of parameter values for Eqs. (1)–(7).

REFERENCES

1. Calabrese EJ. *Environ. Pollut.* 2005; 138:378.
2. Saunier EF, Akhurst RJ. *Curr. Cancer Drug Targets.* 2006; 6:565. [PubMed: 17100564]
3. Calabrese EJ. *Crit. Rev. Toxicol.* 2008; 38:391. [PubMed: 18432421]
4. Zhang L, Jiang H, Hu Z. *Stem Cells Dev.* 2011; 20:1723. [PubMed: 21219132]
5. Hol EM, Gispén WH, Bar PR. *Peptides.* 1995; 16:979. [PubMed: 7479345]
6. Krall JA, Beyer EM, MacBeath G. *PLoS One.* 2011; 6:e15945. [PubMed: 21264347]
7. Xu X, Thomas ML. *Endocrine.* 1995; 3:661. [PubMed: 21153224]
8. Calabrese EJ. *Crit. Rev. Toxicol.* 2013; 43:580. [PubMed: 23875765]
9. Sondell M, Lundborg G, Kanje M. *J Neurosci.* 1999; 19:5731. [PubMed: 10407014]
10. Yamada M, Tatsumi R, Yamanouchi K, Hosoyama T, Shiratsuchi S, Sato A, Mizunoya W, Ikeuchi Y, Furuse M, Allen RE. *Am. J. Physiol. Cell Physiol.* 2010; 298:C465. [PubMed: 20007454]
11. Sheehan SM, Tatsumi R, Temm-Grove CJ, Allen RE. *Muscle Nerve.* 2000; 23:239. [PubMed:10639617]
12. Suzuki S, Yamanouchi K, Soeta C, Katakai Y, Harada R, Naito K, Tojo H. *Biochem. Biophys. Res. Commun.* 2002; 292:709. [PubMed: 11922624]
13. Li J, Reed SA, Johnson SE. *Exp. Cell Res.* 2009; 315:2284. [PubMed: 19393645]
14. Tatsumi R, Hattori A, Ikeuchi Y, Anderson JE, Allen RE. *Mol. Biol. Cell.* 2002; 13
15. Banumathy G, Cairns P. *Cancer Biol. Ther.* 2010; 10:658.
16. Tatsumi R, Sankoda Y, Anderson JE, Sato Y, Mizunoya W, Shimizu N, Suzuki T, Yamada M, Rhoads RP Jr, Ikeuchi Y, Allen RE. *Am. J. Physiol. Cell Physiol.* 2009; 297:C238. [PubMed:19515904]
17. Ricci-Vitiani L, Lombardi DG, Pilozzi E, Biffoni M, Todaro M, Peschle C, De Maria R. *Nature.*2007; 445:1111.
18. Shaheen SS, Pate KT, Anderson S, Dizon D, Edwards RA, Waterman ML, Lipkin SM. *Cancer Res.* 2010; 70:1469. [PubMed: 20145124]
19. Konstorum A, Sprowl SA, Lander AD, Waterman ML, Lowengrub JS. *Proc. ICAND.* 2014; 2012:295.
20. Michalopoulos GK, Bowen WC, Mule K, Luo J. *Gene Expr.* 2003; 11:55. [PubMed: 12837037]
21. Lander AD, Gokoffski KK, Wan FY, Nie Q, Calof AL. *PLoS Biol.* 2009; 7:e15. [PubMed:19166268]
22. Youssefpour H, Li X, Lander AD, Lowengrub JS. *J. Theor. Biol.* 2011; 304:39. [PubMed:22554945]
23. Reya T, Morrison SJ, Clarke MF, Weissman IL. *Nature.* 2001; 414:105. [PubMed: 11689955]
24. Blainpain C, Simons BD. *Nat. Rev. Mol. Cell Biol.* 2013; 14:489. [PubMed: 23860235]
25. Yamashita T, Wang XW. *Clin Invest.* 2013; 123:1911.
26. Gong A, Huang S. *Cancer Res.* 2012; 72:5658. [PubMed: 23139209]

27. Anastas JN, Moon RT. *Nat Rev. Cancer.* 2013; 13:11. [PubMed: 23258168]
28. Holland JD, Klaus A, Garratt AN, Birchmeier W. *Curr. Opin Cell Biol.* 2013; 25:254. [PubMed:23347562]
29. Haramis AP, Begthel H, van den Born M, van Es J, Jonkheer S, Offerhaus GJ, Clevers H. *Science.*2004; 303:1684. [PubMed: 15017003]
30. Skeen VR, Paterson I, Paraskeva C, Williams AC. *Curr. Pharm Des.* 2012; 18:3874. [PubMed:22632753]
31. Massague J. *Cell.* 2012; 134:215. [PubMed: 18662538]
32. Pinto D, Clevers H. *Biol. Cell.* 2005; 97:185. [PubMed: 15715524]
33. Kang DW, Lee SH, Yoon JW, Park WS, Choi KY, Min Do S. *Cancer Res.* 2010; 70:4233. [PubMed: 20442281]
34. Kim D, Rath O, Kolch W, Cho KH. *Oncogene.* 2007; 26:4571. [PubMed: 17237813]
35. Cho JH, Dimri M, Dimri GP. *J. Biol. Chem.* 2012; 288:3406. [PubMed: 23239878]
36. Bottinger EP, Bitzer M. *J. Am. Soc. Nephrol.* 2002; 13:2600. [PubMed: 12239251]
37. van Amerongen R, Nusse R. *Development.* 2009; 136:3205. [PubMed: 19736321]
38. Nadji R, Holcombe RF, Waterman ML. *J. Carcinog.* 2011; 10:5. [PubMed: 21483657]
39. Calabrese EJ, Baldwin LA. *Crit. Rev. Toxicol.* 2001; 31:353. [PubMed: 11504172]
40. Catalano V, Di Franco S, Lovino F, Dieli F, Stassi G, Todaro M. *Expert Opin Ther Targets.* 2012;16:259. [PubMed: 22385077]

APPENDIX B

Materials and Methods

Chapter 2:

Cell Lines/constructs

Colon cancer cell lines, SW480 and DLD-1, were cultured in either Dulbecco's modified Eagle's medium (DMEM; Gibco 11960) or RPMI-1640 medium (Cellgro 15-040), supplemented with 10% Fetal Bovine Serum (FBS) and 2 mM Glutamine. Unless otherwise stated, experiments were performed in the same media. DLD-1 dnLEF-1 and dnTCF-1Emut stable cells were created by transfecting Tet-inducible dnLEF-1N or dnTCF-1Emut into DLD-1 TR7 cells (a generous gift from M. van de Wetering and H. Clevers) as previously described^{29,236}. Cells were maintained in 500 µg/ml Zeocin and 10 µg/ml Blasticidin. However, it was found that dnLEF/TCF expression in the presence of Zeocin reduces cell proliferation (²³⁶ and data not shown). Therefore, in order to avoid any contribution from Zeocin, all experiments were performed in the absence of antibiotics. Induction of dnLEF-1 or dnTCF1-Emut was achieved through addition of 0.01 µg/ml or 1.0 µg/ml doxycycline to the media, respectively. Lentiviral constructs were cloned via Cold Fusion (System Biosciences) by inserting coding sequences for Flag-tagged dnLEF-1N, Flag-tagged dnTCF-1Emut²⁸, or Flag-tagged PDK1 [a gift of Jean Zhao²³⁷; Addgene plasmid #20564] into pCDH lentivector (System Biosciences; SBI #CD533A-2). See Supplemental Experimental Methods for cloning information regarding TK and PDK1 reporters.

Lentiviral Preparation and Infection

Lentivirus was prepared and target cells were transduced using System Biosciences lentivirus technology according to their specifications (see Supplemental Experimental Procedures for

details). Cells were harvested for subsequent assays 72h post-transduction unless otherwise stated.

Lactate Assay

Lactate measurements were performed on media collected from both cells grown in suspension (soft agar) and cells grown on solid support (plastic). SW480 cells were embedded in soft agar 72 h post transduction at a concentration of 1000 cells in 2.5 ml of 0.3% agar (in DMEM with 20% FBS). Fresh media was added once a week. After 22 days of growth (5 days since last media change), images of wells were taken and media was collected. For cells grown on plastic, SW480 cells (72 h post transduction) were seeded in a 96-well plate at 5000 cells per well. Media was changed after 72h and then left unchanged until media was collected after seven days. Media was collected from three triplicate wells, while the number of cells in three wells was determined using the SRB assay (described below). SW480 cells treated with XAV939 (Sigma X3004), were treated with either 10 μ m XAV939 or DMSO for at least four days prior to media collection. For lactate measurements of xenograft tumors, pre-weighed flash frozen xenograft tumors were homogenized in a Precellys 24 homogenizer in the presence of 10 μ L HBSS (Hank's Balanced Salt Solution) per mg tissue at 6000 rpm, twice, for 15 sec each. Tissue extraction and Lactate assay were performed according to L-Lactate Assay Kit (Eton Bioscience #1200011002). All measurements were performed in triplicate.

Sulforhodamine B cell growth (SRB) assay

Cells were seeded in 96-well plates at 5,000 cells per well with eight replicates for each condition and time point. Media was refreshed every day (with or without 0.01 μ g/ml

doxycycline, 2.5 μ M Irinotecan, or 20 mM DCA as needed). Cells were fixed and stained according to published protocols²³⁸ for a 10-day period. Optical density readings were performed at 450 nm.

ATP Assay

SW480 cells were seeded at 125,000 cells per well (12-well plate) 72 h post transduction and harvested 96 h after seeding. ATP measurements were performed according to the ENLITEN ATP Assay System (Promega #FF2000). All measurements were performed in triplicate.

Glucose Consumption Assay

Cells were seeded at 5000 cells per well in a 96-well plate and media was harvested 6 d later. Low glucose media (DMEM or RPMI with 5.5 mM glucose) was added 24h (SW480) or 12h (DLD-1) prior to harvest. XAV939 (10 μ M) treatment was performed for four days, while doxycycline was added throughout the experiment to induce dnLEF-1 in DLD-1 cells. Glucose concentration in the media was determined according to Glucose (HK) Kit (Sigma GAHK20).

XF24 Extracellular Flux Analyser

Metabolic rates of oxygen consumption (OCR) and extracellular acidification (ECAR) were measured using an XF24 Extracellular Flux Analyser (Seahorse Bioscience) as described previously²³⁹. Cells were plated at a density of 100,000 cells per well in a XF24 Cell Culture Microplate (Seahorse #100777-004). One hour before the assay, growth media was replaced by XF Assay Medium (Seahorse #102365-100) supplemented with 5.5mM glucose and adjusted to pH 7.4. Oligomycin, rotenone, and antimycin A were prepared for final concentrations of 1 μ M, and FCCP was prepared for a final concentration of 200nM. Inhibitors were injected during the

measurements: 2 minutes of mixing, 2 minutes incubate, and 4 minutes of measurement. After the assay, protein was collected and measured with BCA Protein Assay Reagent (Thermo # 23225) for data normalization. XAV939 and DCA and were added 16 hours before assay at concentrations of 10 μ M and 10 mM respectively and were maintained in the XF Assay Medium during the measurements. To exclude non-mitochondrial oxygen consumption, OCR values were calculated by taking the difference of the OCR before addition of inhibitors and the OCR after addition of rotenone and antimycin A.

Fluorescence Lifetime Imaging Microscopy (FLIM) of cells in vitro

Cells were seeded at 150,000 cells per plate (35 mm glass bottom dishes). Infection with lentivirus was performed 72 h prior to seeding. Treatment with 0.01 μ g/ml doxycycline was performed starting at the time of seeding. FLIM imaging was performed five days after seeding (under confluent conditions). Both XAV939 (10 μ M) and DCA (50 mM) were added 48 h prior to imaging. For KCN treatment, cells were treated with 4 mM KCN 24 h after seeding. Cells were imaged by FLIM before addition of KCN, as well as 1 min after treatment. Fluorescence lifetime images were acquired with a two-photon microscope coupled with a Becker and Hickl 830 card (Becker and Hickl, Berlin). See Supplemental Experimental Procedures for additional description of FLIM hardware, software, and analysis.

Western Blot Analysis

Thirty micrograms of lysate were analyzed by Western blot using the following antibodies: Flag (1:1000; Cell Signaling #2368), Lamin (1:1000 Cell Signaling #2032), PDHK1 (1:1000 Cell Signaling #3820), c-Myc (1:1000 Cell Signaling #5605), PDHpSer293 (1:1000 Calbiochem

#AP1062), HIF1 α (1:1000 Genetex #GTX127309), AKT (1:1000 Cell Signaling #9272), Phospho-Akt (Ser473; 1:1000 Cell Signaling #9271), and secondary antibody (1:15,000 anti-rabbit IgG-horseradish peroxidase; Amersham). Blots were imaged on the Fugifilm LAS4000 Imaging System. For preparation of xenograft lysates, tumors were homogenized in a Precellys 24 homogenizer in the presence of lysis buffer at 6000 rpm, twice, for 15 sec each.

Real-time PCR

Total RNA was isolated with Trizol from DLD-1 cells after treatment with doxycycline for either 24 h or 120 h. Xenograft tumors were homogenized in a Precellys 24 homogenizer in the presence of Trizol at 6000 rpm, twice, for 15 sec each. A total of 2 μ g of RNA were reverse transcribed using random primers according to the High Capacity cDNA Reverse Transcription Kit (Invitrogen #4374966). Real-time quantitative PCR (RT-qPCR) was performed with Maxima SYBR Green/ROX qPCR Master Mix (Fermentas #K0222). Relative change in gene expression was calculated using the $\Delta\Delta$ Ct method using GAPDH expression for normalization. See Supplemental Experimental Procedures for a list of primer sequences.

4' Thiouridine-labelling and isolation of nascent RNA

4' Thiouridine-labelling was performed in duplicate following two hours of Mock (no doxycycline) or 1.0 μ g/ml doxycycline treatment of DLD-1 colon cancer cells. 500 μ M 4' Thiouridine (Sigma) was added to cells for 30 minutes at 37°C. Collected cells were resuspended in 4 mL Trizol reagent and total RNA purified. Labeled RNA was chemically biotinylated and purified using streptavidin-coated magnetic beads as described¹⁰⁴. Briefly 4'Thiouridine-labelled RNA was biotinylated with 2 μ l biotin-HPDP [Pierce: 1 mg/mL dissolved in

dimethylformamide]/1 µg RNA added to 1 µl 10x Biotinylation buffer [100 mM Tris pH 7.4, 10 mM EDTA] and 7 µl water) for 1.5 hours at room temperature with rotation followed by RNA precipitation. Biotinylated RNA was separated from bulk, unlabelled RNA using streptavidin-coated magnetic beads (µMacs Streptavidin Kit).

Chromatin Immunoprecipitation (ChIP)

DLD-1 cells with or without 2 h doxycycline treatment (to induce expression of FLAG-dnTCF-1Emut) were crosslinked with 1% formaldehyde in 1X PBS for 12 minutes at room temperature. Crosslinking was quenched with 125mM glycine, 5 minutes and recovered cells washed with 1X PBS. Cellular lysates were balanced for immunoprecipitation by Bradford assay (500 Arbitrary Units (AU) per sample) and precleared with 30 µl His-magnetic beads (Invitrogen 10103D) for 30 minutes prior to addition of 50 µl of FLAG-antibody-conjugated magnetic beads (Sigma A2220). FLAG-antibody beads were pre-blocked by 3 washes with 1 mL 1X PBS/BSA solution (5 mg/mL BSA Fraction V in 1X PBS). Immunoprecipitations were carried out overnight at 4°C followed by magnetic separation and two, 5 minute washes with 1 mL LiCL buffer (100 mM Tris pH 7.5, 500 mM LiCl, 1% NP-40, 1% sodium deoxycholate). Beads were washed twice with cold 1X TBS before suspension in Proteinase K buffer (30mM Tris-HCl pH 8.0; 5 µl of Proteinase K (20mg/mL)) and 300mM NaCl for an overnight incubation at 65°C. ChIP DNA was recovered with the Fermentas GeneJET PCR Purification Kit in preparation for PCR. Real-time PCR (RT-PCR) was used to quantify enrichment of *PDK1* gene locus regions. Primers specific to the genomic regions are provide in Supplemental Experimental Procedures.

Luciferase Assay

Cells were seeded at 2.5×10^5 per 6-well 24 h prior to transfection. Each well was transfected with 0.1 μg Super8xTopflash (kind gift from Dr RT Moon) or TK or PDK1 luciferase reporters and 0.1 μg thymidine kinase β -galactosidase plasmid using BioT transfection reagent (Bioland Scientific). Cells were treated with 0.01 $\mu\text{g}/\text{ml}$ doxycycline or 10 μM XAV939 at the time of transfection where indicated. Cells were harvested 24 h post transfection and assayed for luciferase activity and β -galactosidase activity (for normalization).

Xenograft Tumors

SW480 stable transductants for xenograft injection were prepared through lentiviral infection with pCDH vector alone, dnLEF-1 or dnTCF-1Emut, with or without PDK1, followed by selection with 500 $\mu\text{g}/\text{ml}$ G418. Cells (2.5×10^6) were injected subcutaneously into immune deficient NOG mice. Tumors were removed and measured four weeks after injection. Xenograft tumors for FLIM analysis were injected at 5×10^6 cells per tumor and allowed to grow for three weeks.

Fluorescence Lifetime Imaging Microscopy (FLIM) of in vivo Xenograft Tumors

All animal procedures were approved by the UC Irvine IACUC. Nine week old NOG mice (Jackson Labs) with three-week old xenograft tumors were anesthetized with 100 mg/kg ketamine/10 mg/kg xylazine. FITC or TRITC Dextran (155 kDa; 12.5 mg/ml) was injected into the tail vein to label the tumor vasculature. Xenografts were exposed via a skin flap cut so as to avoid severing the xenografts' feeder vessels. The mice were positioned on the stage in an environment chamber maintained at a constant 27°C. Images were acquired at an average depth

of 50-200 μm , using FITC/TRITC-labeling of vessels to distinguish tumor cells from metabolically-distinct endothelial and blood cells. At least three 78 μm fields of view were imaged for each tumor. Tumors were examined from eight mice. Fluorescence lifetime images were acquired with a Zeiss 710 microscope (see Supplemental Experimental Procedures for additional description of FLIM hardware, software, and analysis).

Immunohistochemistry

For Ki67 staining, deparaffinized 3.5 μm sections of formalin-fixed paraffin-embedded (FFPE) tumor xenografts were stained for Ki67 (Dako #M7240, 1:400 dilution) using a Ventana Benchmark Ultra autostainer with peroxidase-based detection. For each section, the number of positive nuclei per 8-10 fields (at a 20X magnification) was manually enumerated and the mean \pm SEM was calculated. For CD31 staining, sections of FFPE tumor xenografts were blocked in avidin-biotin and a Mouse-On-Mouse kit (Vector Labs, Burlingame, CA) and subjected to antigen retrieval (citrate buffer pH 6.0 with steaming) and then incubated in a 1:50 dilution of anti-mouse CD31 (Dianova rat anti-mouse CD-31, #DIA-310), followed by peroxidase development. Enumeration of vessel density was done by counting vessels in every cross section within the subcapsular region of each tumor sample and calculating mean \pm SEM. For PDK staining in small intestine and phospho-PDH and HIF-1 α staining in colon, following pressure cooker antigen retrieval in citrate buffer, sections were blocked in 3% H₂O₂, goat serum, and avidin-biotin blocking reagent (Vector Labs). Sections were incubated in primary antibodies included anti-PDK (Santa Cruz sc-28783, 1:1000), anti-PDHpSer293 (Calbiochem #AP1062, 1:200), and anti-HIF-1 α (Thermo PA1-16601, 1:500), followed by biotinylated secondary

antibodies and visualization using a peroxidase-conjugated avidin-based Vectastain protocol. Slides were then counterstained with hematoxylin and mounted.

Bioinformatic Analysis of Human Adenocarcinoma Gene Expression

Analysis of Wnt signaling and glycolysis pathway gene expression in human colon cancer used the publicly available colon adenocarcinoma (COAD) mRNA expression data from The Cancer Genome Atlas (TCGA) Data Portal (<https://tcga-data.nci.nih.gov/tcga/>). Gene memberships of the Wnt signaling and glycolysis pathways were used as defined by Kyoto Encyclopedia of Genes and Genomes (KEGG). Hierarchical clustering of log₂ transformed normalized expression of 238 tumors was used to identify groups of tumor samples showing similar expression profiles for the 185 analyzed genes as well as direct tumor-to-tumor correlations for expression of pathway components. STRING analysis ([http://string-db.org](http://string-db.org;);¹⁹⁹) was used to display interactions amongst the PDK1 correlating genes. For additional details see Supplemental Experimental Procedures.

Statistical Analysis

Statistical evaluation was performed by Student's unpaired t test. $p < 0.05$ was considered statistically significant.

Chapter 3:

Cell Lines/constructs

Colon cancer cell lines were grown under the following conditions: SW480 and SW620 were cultured in Dulbecco's modified Eagle's medium (DMEM; Fisher SH3008102) supplemented

with 10% Fetal Bovine Serum (FBS; Atlas FP-0500-A) and 2 mM Glutamine (Fisher MT-25-005-CI). HCT116 and DLD-1 were cultured in RPMI-1640 medium (Fisher MT15040CM) supplemented with 10% Fetal Bovine Serum (FBS) and 2 mM Glutamine. Doxycycline-inducible DLD-1 cells were created by transfecting Tet-inducible dnLEF-1N into DLD-1 TR7 cells (a generous gift from M. van de Wetering and H. Clevers) as previously described¹²⁸. Induction of dnLEF-1 was achieved through addition of 0.01 µg/ml Doxycycline to the media. Lentiviral constructs were cloned via Cold Fusion (System Biosciences) by inserting the coding sequence for Flag-tagged dnLEF-1N into pCDH lentivector (System Biosciences; SBI #CD533A-2). See “Luciferase Reporter Plasmid Cloning” for details regarding TK and *SLC16A1* reporters.

Lentiviral Preparation and Infection

Lentiviruses were prepared using System Biosciences lentivirus technology. 293 TN cells (System Biosciences (SBI) LV900A-1) were seeded in 150 mm plates at 7.5×10^6 cells per plate with 20 mL DMEM without antibiotics for 24 hours. Cells were then transfected with 22.5 µg pPACKH1 HIV packaging mix (SBI LV500A-1) and 4.5 µg of pCDH lentiviral vector using BioT transfection reagent. Viral supernatant was collected 48 hours and 72 hours post-transfection. After centrifugation for 15 min at 3000 x g to remove debris, 1X PEG-it (SBI LV810A-1) was added to precipitate virus. After incubation at 4 °C for at least 16 hours, centrifugation (30 min at 1500 x g) was used to collect viral particles. Virus was resuspended in a small volume (300-500 µL) 1X PBS (phosphate buffered saline) and titered using the Global UltraRapid Lentiviral Titer Kit (SBI LV961A-1). Transduction of target cells was performed according to manufacturer’s protocol (SBI). Briefly, cells were seeded at 1.0×10^5 cells per 12-

well or 2.5×10^5 cells per 6-well plate. After 24 hours, cells were treated with fresh media, 1X TransDux (SBI LV850A-1), and lentivirus at a Multiplicity of Infection (MOI) of 10. MOI was determined using previously published methods (cite Kira's paper). Infected cells were collected for subsequent assays after 72 hours.

Real-time PCR

Total RNA was isolated with Trizol from SW480 and SW620 expressing dnLEF-1. HCT116 cells were lentivirally transduced with dnLEF-1, and total RNA was isolated with Trizol 72 hours post transduction. Total RNA was isolated with Trizol from DLD-1 cells after treatment with doxycycline for 72 hours. A total of 2 μ g of RNA were reverse transcribed using random primers according to the High Capacity cDNA Reverse Transcription Kit (Invitrogen 4374966). Real-time quantitative PCR (qRT-PCR) was performed with Maxima SYBR Green/ROX qPCR Master Mix (Fisher K0223). Relative change in gene expression was calculated using the $\Delta\Delta C_t$ method using GAPDH expression for normalization. Statistical evaluation was performed by Student's unpaired t test. $p < 0.05$ was considered statistically significant.

Primer pairs used for real-time PCR analysis include: human *GAPDH* (5'-TCGACAGTCAGCCGCATCTTCTT-3') and reverse (5'-GCGCCCAATACGACCAAATCC-3'), human *MCT-1* forward (5'-CACCGTACAGCAACTATACG-3') and reverse (5'-CAATGGTCGCCTCTTGTAGA-3'), human *MCT-2* forward (5'-GGCTGGTTCCCTCATGAGAC-3') and reverse (5'-GCTACCACAATAGCCCCAC-3'), human *MCT-3* forward (5'-TCGTGGGCTTCGTGGACAT-3') and reverse (5'-GCACAACGCAGGCAGCAGTT-3'), human *MCT-4* forward (5'-ATTGGCCTGGTGCTGCTGATG-3') and reverse (5'-CGAGTCTGCAGGAGGCTTGTG-3')

Western Blot Analysis

Cell lysates were prepared according to previously published methods¹²⁸. Forty micrograms (40 µg) of lysate were analyzed by Western blot using the following antibodies: Lamin A/C (1:1000 Cell Signaling #2032), β-Tubulin (1:1000 GeneTex GTX107175), MCT-1 (1:1000 Santa Cruz SC-50324) and secondary antibody (1:5,000 anti-rabbit IgG-horseradish peroxidase; Genesee 84-852). Blots were exposed to SuperSignal West Dura (Fisher PIA34075) and imaged on the Syngene GBox XL1.4 Imaging System.

Luciferase Reporter Plasmid Cloning

To create a luciferase reporter plasmid driven by the human *SLC16A1* or herpes virus thymidine kinase promoter, 5' flanking sequences of the primers (lower case) were designed for complementarity to the pGL2 or tkLUC vector backbone for use with a Cold Fusion cloning schema (Cold Fusion Cloning; System Biosciences). Human placental DNA was used as template for PCR amplification of the *SLC16A1* gene core promoter using Pfu Turbo polymerase. The PCR fragment and SmaI digested pGL2 vector was purified following the manufacturer's protocol (GeneJET Gel Extraction Kit, Fisher K0691) and ligations were performed with an insert:plasmid ratio of 1:2 with Cold Fusion reagents. Clones were verified by sequencing. The following PCR primers were used:

Forward primer (-1604), upper case sequence is genomic, lower case sequence is complementary to pGL2): 5'- gag cta aca taa ccc TCC TGG GAT TCA TCT TAT TT - 3'

Reverse primer (+1045), upper case sequence is genomic, lower case sequence is complementary to pGL2): 5'- agc tcg gta cct ccc tAT CCT CCA GAT TTC TCT CA - 3'

The following PCR primer sequences were used to amplify a region identified as occupied by TCF-1, for cloning 5' of the heterologous herpes virus tk promoter (tkLUC):

Primers designed for amplification and insertion into a plasmid backbone containing a minimal Herpes Virus thymidine kinase reporter (at BamHI):

“ChIP Peak” (486nt; Chromosome 1 113499604-113500089)

Forward primer (upper case sequence is genomic, lower case is complementary to tkLUC):

5'- atc tta tca tgt ctg TCC TGG CAA GCA GCA - 3'

Reverse primer (upper case sequence is genomic, lower case is complementary to tkLUC):

5'- ctc gga ccc cgg atc GTG GGT TGG GGT GTG - 3'

Luciferase Assay

Cells were seeded at 2.5×10^5 per 6-well 24 hours prior to transfection. Each well was transfected with 0.5 μ g M50 Super 8xTOPflash (a gift from Dr. RT Moon; Addgene plasmid #12456), TK, or PDK1 luciferase reporters and 0.1 μ g thymidine kinase β -galactosidase plasmid using BioT transfection reagent (Bioland Scientific B01-02). Cells were transfected with 0.01 μ g/ml dnLEF-1 and/ or treated with 10 μ M XAV939 at the time of reporter transfection where indicated. Cells were harvested 24 hours post transfection and assayed for luciferase activity and β -galactosidase activity (used for normalization). Statistical evaluation was performed by Student's unpaired t test. $p < 0.05$ was considered statistically significant.

Sulforhodamine B cell growth (SRB) assay

For 3-bromopyruvate kill curves, SW480, SW620 and HCT116 cells were seeded in 96-well plates at 5,000 cells per well with eight replicates for each condition. The density of DLD-1 cells

was optimized to obtain confluent cultures around Day 5 of each experiment. Twenty-four hours after seeding, cells were treated with 3-BPr for a period of 96 hours. Cells were then fixed on Day 5 and stained with Sulforhodamine B according to published protocols⁹² with optical density readings performed at 492 nm.

For survival assays, cells were seeded in 96-well plates at 5,000 cells per well with eight replicates for each condition. 24 hours after seeding, cells were treated for a period of 96 hours (4 days). On Day 5, media containing treatment was removed and replaced with media containing no treatment to begin “recovery” period. Cells were fixed on Day 5, Day 6, Day 7, Day 8, Day 9, and Day 10 (Days 0-6 post wash-out) and stained according to published protocols⁹². Optical density readings were performed at 492 nm.

Statistical evaluation was performed by Student’s unpaired t test. $p < 0.05$ was considered statistically significant.

Chapter 4:

Wnt Cloning

Human *WNT* cDNAs were PCR-amplified twice: one reaction using *WNT*-specific sense primers and “STOP” antisense primers, and another reaction using “Non-STOP” antisense primers (Refer to Table S1 for cDNA source, primer sequence and PCR conditions). 4 μ L of each PCR reaction were TOPO-cloned into the pENTR/D-TOPO Gateway Entry vector following the manufacturer’s protocol (pENTR Directional TOPO Cloning Kits, Invitrogen). Entry clones were then recombined into the pcDNA3.2/V5-DEST Gateway Destination vector at a 1:1 ratio using LR clonase II for 1 hour at 25°C (Gateway LR Clonase II Enzyme Mix, Invitrogen). All clones were sequence-validated at every step of the cloning process.

qRT-PCR analysis

Isolated RNA was reverse transcribed into cDNA using the High Capacity cDNA kit (Applied Biosystems). cDNA was amplified for 40 cycles with the Maxima SYBR Green/ROX qPCR Master Mix (2X) (Fermentas) using primers specific to the backbone destination vector for all of the Wnts. Primers used were destVect16F1 sense primer (5'- CGCGCCGACCCAGCTTTCTTG -3') and destVect121R1 antisense primer (5'- CGGTACGCGTAGAATCGAGACCG -3'). Melting and annealing temperatures were 95°C and 60°C.

Western Analysis

For detection of WNT expression and secretion, HEK293 or NIH3T3 cells were cultured in DMEM media with 10% FBS (Cellgro) and plated at a density of 1,000,000 cells per plate in 10 cm dishes. Cells were transfected using Bio T transfection reagent (Bioland Scientific) 24 hours post plating with plasmids containing V5-tagged Wnts (pcDNA3.2/V5-DEST; 5 µg) or untagged WNT 1 and 3A (pcDNA3.2/V5-DEST; 5 µg). Conditioned media and cell lysates were harvested 48 hours post transfection. The conditioned media was concentrated using StrataClean resin (Agilent Technologies). Media, lysates and a V5 protein standard (Recombinant Yeast Calmodulin Kinase Array Control Protein, Invitrogen) were separated by 10% SDS-PAGE and transferred to a nitrocellulose membrane (Whatman). For non-phospho β -catenin and phospho-LRP6 detection, HEK293 cells were plated at a density of 200,000 cells per well in 6-well plates and transfected using Bio T 24 hours later with plasmids containing untagged Wnts (pcDNA3.2/V5-DEST; 1 µg). Cell lysates were harvested 24 hours post transfection, separated by 10% SDS-PAGE and transferred to a nitrocellulose membrane (Amersham Biosciences). Blots were blocked in 5% milk for 30 min and hybridized with primary antibodies against V5

(1:5000 dilution, Invitrogen), Actin (I-19, 1:500, Santa Cruz), Lamin A/C (1:5000, Cell Signaling), WNT1 (N2C3, 1:1300, GeneTex), WNT3A (1:250, R&D Systems), non-phospho β -catenin (Ser33/37/Thr41, 1:500, Cell Signaling), phospho-LRP6 (Ser1490, 1:1000, Cell Signaling), or β -Tubulin (TUBB1, 1:1000, GeneTex) overnight at 4°C. After hybridization, the blots were washed and hybridized with anti-rabbit IgG-HRP (1:5000, Amersham Biosciences), anti-mouse IgG-HRP (1:5000, Amersham Biosciences), anti-rat IgG-HRP (1:50000, Jackson ImmunoResearch) or Bovine anti-goat IgG-HRP (1:15000, Santa Cruz) for 2 hours at RT. The ECL reaction was performed according to the manufacturer's protocol (Thermo Scientific) and blots were visualized using the LAS-4000 Fujifilm imaging system.

Luciferase Assays

HEK293 or NIH3T3 cells were cultured in DMEM media with 10% FBS and plated at a density of 200,000 cells per well in 6-well plates. Cells were transfected 24 hours post plating, using BioT, with Super8XTOPflash reporter plasmid (0.1 μ g; kind gift from Dr. R.T. Moon), thymidine kinase β -galactosidase plasmid (0.1 μ g), Wnt plasmids (pcDNA3.2/V5-DEST; 0.1 μ g), Dkk-1 expression plasmid (pcDNA3; 0.4 μ g) (Kind gift from Dr. B. Hoang) and expression plasmids containing SFRP1 (pcDNA3.1; 0.4 μ g), SFRP2 (pBABE; 0.4 μ g) or SFRP3 (pcDNA3.1; 0.5 μ g). For the competition experiment, the amount of Wnt plasmid transfected is indicated on the figure (Fig. 4B). For figure 5B, 1 μ g of Wnt DNA plasmid was transfected. Cells were harvested 24 hours post transfection and then luciferase activity was measured and normalized using β -galactosidase levels. For figure 8 (knockdown of WLS), three independent experiments were performed using HEK293 cells with an integrated Super8XTOPflash reporter. 100-200 ng of untagged Wnt plasmids were transfected into cells plated in 24-well plates using

lipofectamine 2000 (Life Technologies). siRNA targeting WLS (targeting sequences: ACGAATCCCTTCTACAGTA) was transfected into the cells using Dharmafect transfection reagent (Dharmacon). Cell lysates were assayed for luciferase activity 48 hours post transfection. Duplicate samples were assayed for each condition.

Porcupine-Deleted HT1080 Cells

Porcupine was functionally deleted from HT1080 cells (ATCC) using a zinc finger nuclease (Sigma-Aldrich) targeting exon 9 of the human PORCN gene (KP and DMV, manuscript in preparation). For luciferase assays in these lines, cells were seeded at 80,000 per well in 24-well culture dishes one day prior to transfection. 50 ng of untagged Wnt plasmid was transfected along with mCherry transfection control, Super8XTOPflash reporter, and 100 ng of HA-tagged mPORCN construct as indicated, all by lipofectamine 2000 (Life Technologies). Cell lysates were assayed for luciferase activity 24 hours post transfection.

Dvl-2 Mobility Shift

To test for Wnt-induced Dvl2 mobility shift, HT1080 PORCN null cells, seeded in 24-well dishes as in luciferase assays, were transfected with 400 ng of untagged Wnts indicated, in the presence or absence of 100 ng HA-PORCN expression plasmid. 24 hours following transfection, cell lysates were prepared (100 mM sodium phosphate, pH 7.5, 150 mM NaCl, 1% IGEPAL-CA630, complete protease inhibitor cocktail (Roche)) and separated by SDS-PAGE. After transfer to PVDF membranes and blocking with 3% BSA in TBS-T, blots were incubated overnight with Dvl2 antibodies (1:500, Santa Cruz #13974) followed by HRP-conjugated secondary antibodies and visualized by ECL.

FLAG Wnt Cloning

Human Wnt cDNAs, without their putative signal sequences, were cloned into p3XFLAG-CMV-8 (Sigma) using the Cold Fusion Cloning Kit (System Biosciences). p3XFLAG-CMV-8 was linearized with HindIII and XbaI. Design of PCR primers for cDNA amplification and cloning into the linearized vector were both carried out according to manufacturer's recommendations. HindIII and BglII restriction sites were incorporated into the forward and reverse primers respectively to provide unique sites to allow for linearization or excision of cDNA from this library. (Refer to Table S2 for primers used for cloning).

Co-Immunoprecipitation

HeLa cells were transfected (Invitrogen Lipofectamine 2000) with C-terminal V5 tagged Wnts (1000 ng per 10 cm dish) and treated with either DMSO or 2 uM IWP1 (MolPort) overnight. 500 ug of lysate was subject to immunoprecipitation with anti-V5 antibody (Invitrogen), separated by SDS-PAGE and immunoblot carried out with anti-WLS (YJ5, Millipore MABS87 (21)) and anti-V5 antibodies.